10-21-2014 12:00 AM

Contribution of Gypsum-board Sheathing to the Compressive Resistance of Wood Studs Subjected to Gravitational Loads

Daniel J. Grenier
The University of Western Ontario

Supervisor
Dr. F. Michael Bartlett
The University of Western Ontario

Graduate Program in Civil and Environmental Engineering
A thesis submitted in partial fulfillment of the requirements for the degree in Doctor of Philosophy

CONTRIBUTION OF GYPSUM-BOARD SHEATHING TO THE COMPRESSIVE RESISTANCE OF WOOD STUDS SUBJECTED TO GRAVITATIONAL LOADS

(Thesis format: Integrated-Article)

by

Daniel J. Grenier

Graduate Program in Civil and Environmental Engineering

A thesis submitted in partial fulfillment
of the requirements for the degree of
Doctor of Philosophy

The School of Graduate and Postdoctoral Studies
The University of Western Ontario
London, Ontario, Canada

Abstract

Gypsum board is the most commonly used sheathing material in Canadian residential construction. Current Canadian standards recognize the role of gypsum-board sheathing in bracing studs to prevent weak-axis buckling and in resisting in-plane shear, but do not recognize its potential contribution to axial compressive resistance of a sheathed wall. The research in this thesis, therefore, investigates this contribution for light-frame wood stud walls sheathed with gypsum-board on both sides of the stud. The axial compressive resistance of bare and gypsum-board sheathed studs were computed using new finite element models that account for the nonlinear wood stress-strain relationship and nonlinear shear load-slip response of gypsum-board-to-stud fastener connections. These models were validated using full-scale test data for 100 bare and 19 sheathed studs, and with an idealized responses of fastener connections derived using test data from 283 monotonic and 15 load-reversal tests. The strength distributions of the axial capacities of bare and sheathed studs were quantified by conducting Monte Carlo simulations using these models. As a result, it was determined that gypsum-board sheathing increases the axial compressive resistance of wood studs by a factor of 1.05 to 1.56, depending on the stud size, stud length, gypsum-board thickness, and fastener spacing. A modification factor that conforms to the current CAN/CSA-086-09 equations (CSA, 2009) to account for the strength increment provided by the gypsum-board sheathing was then derived as a function modulus of elasticity of the wood for various stud sizes and lengths, gypsum-board thicknesses, and fastener spacings. The revised equation was used to compute the factored axial compressive resistance of 2400 and 3600 mm long gypsum-board-sheathed 38x89 and 38x140 mm wood studs. A total of 15 additional stud designs are recommended to be included in Part 9 “Housing and Small Buildings” of National Building Code of Canada (NRC, 2010) when the extra strength provided by 12.7 mm or 15.9 mm gypsum-board sheathing, with a maximum fastener spacing of 300 mm, is accounted for.

Keywords

Axial compressive resistance, Fastener connections, Finite-element analysis, Gypsum-board sheathing, Initial out-of-straightness, Light-frame wood construction, Monte-Carlo simulation, Resistance Factor, Shear load-slip Response, Slenderness Ratio, Spruce-Pine-Fir, Studs.

Co-Authorship

All of the work presented was performed by Daniel J. Grenier. Chapters 2 to 6 of the thesis will be submitted to scholarly journals as manuscripts co-authored by Daniel J. Grenier and F. Michael Bartlett.

Acknowledgments

I would like to first acknowledge scholarship support provided by the Alexander Graham Bell Canada Graduate Scholarship through the Natural Sciences and Engineering Research Council of Canada, the Ontario Graduate Scholarship, the Queen Elizabeth II scholarship, and the Western Graduate Research Scholarship.

I would also like to acknowledge Stephanie Laurence and Whitney Barrett for their guidance through the technical requirements of my doctoral studies, Wilbert Logan who tirelessly guided me through my testing in the laboratories, Jared Harnish for his help conducting experiments, and Adam Van Bruinessen who provided me with unpublished experimental data.

I would like to provide my sincere appreciation to Dr. F. Michael Bartlett for his lessons and continuous positive criticism that have guided this investigation from the very beginning. His wisdom, patience, honesty, fairness, and passion for finding the truth will not be forgotten.

Finally, I am very thankful for the love and support from my wife Amy and son Patrick who have been my inspiration to complete this journey.

Table of Contents

List of Tables

List of Figures

List of Appendices

Notation

a	Distance from lateral load to end support *(mm)*
A_s	Cross-sectional area of wood stud *(mm^2)*
a'	Dimensionless parameter used to calculate X_L
b	Stud width *(mm)*
b_{GB}	Gypsum-board width *(mm)*
b'	Dimensionless parameter used to calculate X_L
c	Parameter defining the shape of the stress-strain relationship of wood
C_b	Basic snow-load roof factor
C_c	Slenderness factor
d	Stud depth *(mm)*
d'	Sensitivity index
e	End eccentricity *(mm)*
E	Modulus of Elasticity *(MPa)*
e_{GB}	Distance between gypsum-board force resultants *(mm)*
E_{GB}	Modulus of elasticity of gypsum board *(MPa)*
e_n	End distance of fastener connection to the edge of the gypsum board perpendicular to the applied load *(mm)*
e_s	Side distance of fastener connection to the edge of the gypsum board parallel to the applied load *(mm)*

E_s Modulus of elasticity of wood *(MPa)*

F Cumulative probability

f_c Crushing stress of wood *(MPa)*

F_c Compressive strength of wood parallel to the grain *(MPa)*

f_t Tensile fracture stress *(MPa)*

i Dummy variable

I_c Second moment of area of gypsum-board-sheathed wood stud *(mm^4)*

I_s Second moment of area of the wood stud *(mm^4)*

k Effective length factor

K Dimensionless parameter to compute X_L

k_c Stiffness of gypsum-board-sheathed wood stud *(kN/mm)*

K_c Slenderness factor

K_D Load-duration factor

k_f Stiffness of fastener connection *(kN/mm)*

k_{GB} Stiffness of gypsum board *(kN/mm)*

K_H System factor

k_L Length effect parameter

k_o Combined stiffness of gypsum-board sheathing and fastener connection *(kN/mm)*

k_s Stiffness of bare wood stud *(kN/mm)*

K_{Sc} Service condition factor for compression parallel to the grain

K_{SE} Service condition factor for modulus of elasticity

K_{SH} Gypsum-board sheathing factor

K_T Treatment factor

k_w Shape parameter for Weibull distribution

K_{Zc} Size factor fo compression parallel to the grain

L Stud length *(mm)*

L_f Distance from the face of the stud to the centroid of the gypsum board *(mm)*

L_T Tributary length *(m)*

M Applied moment *(N·mm)*

M_s Moment resisted by the wood stud *(N·mm)*

n Sample size

N_{GB} Axial load in the gypsum board *(N)*

P Axial compressive load *(kN)*

P_c Axial compressive resistance of gypsum-board-sheathed wood stud *(kN)*

P_e Euler buckling load *(kN)*

P_f Factored axial compressive load *(kN)*

P_{max} Axial capacity *(kN)*

P_r Factored compressive resistance of light-frame wood studs *(kN)*

P_s Axial compressive resistance of bare stud *(kN)*

P_1 Inverse of the tangent slope of the Southwell Plot *(kN)*

Q Axial compressive load per unit width of wall *(kN/m)*

r Radius of gyration *(mm)*

r_c Correlation coefficient

r_n Index of nonlinearity for stress-strain relationship of wood

R^2 Coefficient of determination

s Fastener spacing *(mm)*

S Specified load effects

S_r Rain load associated with specified ground snow load *(kPa)*

S_s Specified ground snow load *(kPa)*

$\bar{S}$ Mean load effects

t Gypsum-board thickness *(mm)*

v Initial mid-height out-of-straightness *(mm)*

V Shear load through fastener connection *(N)*

V_{R_c} Coefficient of variation of the resistance of gypsum-board-sheathed wood studs

V_{R_s} Coefficient of variation of the resistance of bare studs

V_S Coefficient of variation of the load effect

$V_{1.0}$ Shear resistance of fastener connection at a slip of 1.0 mm *(N)*

V_{δ_f} Shear resistance of fastener connection at specified slip *(N)*

w Distributed load *(kN/m)*

w_1 Distance from support to where a change in modulus of elasticity occurs *(mm)*

x Random variable

$\bar{x}$ Sample mean

X_L Lower-bound tolerance limit

x_o Location parameter for Weibull distribution

y_s Distance from the elastic neutral-axis of the stud to the face of the stud *(mm)*

z Standard score

Z Indicator variable

α Factor for load effects

α_w Scale parameter for Weilbull distribution

β Parameter determined from linear regression

$\hat{\beta}$ Parameter estimate determined from linear regression

β' Reliability index

γ Confidence level

δ_f Slip at gypsum-board-to-stud interface *(mm)*

δ_{GB} Axial deformation of the gypsum board *(mm)*

δ_{R_c} Bias coefficient of the resistance of gypsum-board-sheathed wood studs

δ_{R_S} Bias coefficient of the resistance of bare studs

δ_s Extreme-fibre deformation of the wood stud *(mm)*

δ^* Portion of fastener slip due to rotation of the wood stud *(mm)*

Δ Lateral mid-height deflection *(mm)*

ε Strain

ε_o Compressive strain at elastic failure

ε_r Inherent error from linear regression

ε_1 Compressive strain at crushing stress of wood

θ End rotation *(rad)*

ρ Percentile

σ Stress *(MPa)*

σ_a Standard deviation of sample

σ_s Stress at extreme fibre of wood stud *(MPa)*

σ_x Standard deviation of the random variable

φ_c Factor for resistance of gypsum-board-sheathed wood studs

φ_s Factor for resistance of wood studs

Chapter 1 Introduction

1.1 Background

Gypsum board is the most commonly used sheathing material in Canadian residential construction because of its "speed of installation, low cost, consistent result and fire resistance" (CMHC, 2013). Its primary purpose is to provide even surfaces for interior walls, as shown for example in Figure 1.1. Part 9 "Housing and Small Buildings" of the National Building Code of Canada (NBCC) (NRC, 2010) and the Engineering Guide for Wood-frame Construction (CWC, 2009) recognize the structural benefits of gypsum board, permitting it to brace the stud about its weak axis and to provide up to 80% of the required strength of shear walls in light-frame construction. However, both documents are mute in addressing the possible increase in axial compressive resistance of wood studs subjected to gravitational loads.

Figure 1.1: Typical Application of Gypsum-Board Sheathing

The structural adequacy of interior stud walls is commonly checked using the prescriptive provisions of Table 9.23.10.1 in Part 9 of the NBCC, as reproduced in Table 1.1. The

purpose of this table is to simplify the design process by indicating the limiting combinations of stud size, spacing, and height that, through a history of satisfactory performance, have been shown to be sufficient for the specified supported load categories. The accuracy of these table provisions is, however, questionable. For example, the load categories are somewhat ambiguous, with no explicit limitation of the tributary area supported by each wall. Therefore, research is needed to address the accuracy of the provisions of this table. In addition, the prescriptive provisions are based on the assumption that weak-axis of the studs are braced with appropriate sheathing material or with solid bridging (NRC, 2010), but do not appear to account for any possible increase in axial compressive capacity due to gypsum-board sheathing. Therefore, research is needed to quantify recommendations to account for the possible increase in axial resistance due to gypsum-board sheathing.

Table 1.1: NBCC Table 9.23.10.1 (NRC, 2010): Size and Spacing of Studs

Supported load case	Min. stud size *(mm)*	Max. stud spacing *(mm)*	Max. unsupported height *(mm)*
Interior walls			
Attic not accessible by stairway	38x89	600	3600
Attic accessible by stairway & 1 floor	38x89	400	3600
Roof load plus one floor	38x89	400	3600
Attic not accessible by stairway & 2 floors	38x89	400	3600
Roof load	38x64	400	2400
Attic accessible by stairway	38x64	400	2400
Attic not accessible by stairway & 1 floor	38x89	600	3600
Attic accessible by stairway & 2 floors	38x89	300	3600
	38x140	400	4200
Attic accessible by stairway & 3 floors	38x140	300	4200
Exterior walls			
Roof with or without attic storage	38x64	400	2400
	38x89	600	3000
Roof with or without attic storage & 1 floor	38x89	400	3000
	38x140	600	3000
Roof with or without attic storage & 2 floors	38x89	300	3000
	64x89	400	3000
	38x140	400	3000
Roof with or without attic storage & 3 floors	38x140	300	1800

CAN/CSA-086-09 “Engineering Design in Wood” (CSA, 2009) provisions can be used to compute the axial compressive resistance of wood studs. The resistance equations

specifically account for the type and duration of load, the number of studs in the structural system, the wood moisture content, and the presence of chemical preservative treatment. These equations are very appropriate tools for investigating the adequacy of NBCC Table 9.23.10.1. However, they do not account for the possible increase in axial compressive resistance of gypsum-board sheathed studs. Therefore, research is needed to quantify the contribution of the sheathing to include in the current CAN/CSA-086-09 equations. The bias and variability of the compressive strength of a sheathed stud have also not been quantified, which is necessary to derive appropriate associated resistance factors.

1.2 Quantification of the Axial Compressive Resistance

The axial compressive resistance of gypsum-board-sheathed wood studs is dependent on deterministic and random parameters for the wood stud, gypsum board, and fastener connections presented in Table 1.2. The deterministic parameters are generally guided by provisions in the NBCC (NRC, 2010) and values commonly used in practice are reported by CMHC (2013). The random parameters include the material properties of the wood and gypsum board and the mechanical properties of fasteners, and also the initial out-of-straightness of the studs, which can greatly affect the axial capacity of compressive members (Southwell, 1931). Most statistical parameters that define these random parameters are readily obtained from the literature. However, the statistical parameters that define the mechanical properties of fasteners, in particular, the shear load-slip relationship, are not readily available.

Table 1.2: Parameters that Influence the Axial Compressive Resistance of Gypsum-Board-Sheathed Wood Studs

Component	Deterministic parameter	Sources	Random parameter	Sources
Wood Stud	Species, grade, and dimensions	NRC 2010 CMHC 2013	Material properties Initial out-of-straightness	Bleau 1984 Buchanan 1984 Yanaga et al. 2003
Gypsum board	Type, thickness, and density	CMHC 2013	Material Properties	Groom 1992
Fastener	Type, size, location, and spacing	NRC 2010 CMHC 2013	Mechanical properties	NONE

Kamiya (1987 and 1988) and Srikanth (1992) developed analytical models to compute the stiffness and axial compressive resistance of wood studs sheathed with various materials. However, these models were only validated for wood sheathing and for specific stud sizes and lengths. They did not address all of the deterministic parameters for gypsum-board sheathed stud. Also, the material properties of the wood and sheathing were assumed linear elastic, and the mechanical properties of the fasteners were not specific to gypsum-board-to-wood-stud connections.

No published experimental investigation is available to validate numerical models for the axial capacities of gypsum-board sheathed studs. Marxhausen and Stalnaker (2006) presented the only experimental study on gypsum-board-sheathed studs subjected to axial compressive loads, but investigated specifically the ability of the gypsum board to brace the weak axis of the stud. They did not thoroughly investigate its axial compressive resistance. Therefore, an investigation is needed to quantify experimentally the axial compressive resistance of gypsum-board-sheathed wood studs.

To quantify the strength contribution of gypsum-board sheathing, the axial compressive resistance of sheathed studs needs to be compared to that of bare (i.e., unsheathed) studs with identical deterministic and random wood stud parameters. Maholtra and Mazur (1970) and Buchanan (1984) present numerical models for the axial compressive resistance of bare wood studs. The model presented by Maholtra and Mazur (1970) ignores any initial out-of-straightness of the stud. Buchanan (1984) provides a single model to compute the capacity of wood studs for various slenderness ratios that does not seem to be accurate for the specific cross-sections and lengths in NBCC Table 9.23.10.1. Therefore, a validated numerical model for bare wood studs is not available to accurately predict the axial capacity of bare studs. Experimental data reported by Buchanan (1984) can be used to validate a numerical model for similar stud dimensions provided in NBCC Table 9.23.10.1, thus no experimental investigation is needed.

Table 1.2 indicates that the mechanical properties of fasteners are not quantified in the literature. Gromala (1985), Gad (1997), and Liew et al. (2006) studied the shear strength of gypsum-board fastener connections. However, their results are at best incomplete or obtained from poorly controlled experiments: Gromala (1985) studied only one fastener

type and location without controlling the orientation of the gypsum-board; Gad (1997) studied the fasteners in steel studs; and Liew et al. (2006) studied only one fastener type at limited fastener locations using a type of gypsum-board sheathing not used in Canada. Both Gad (1997) and Liew et al. (2006) do not report mechanical properties for fasteners subjected to shear loads. Therefore, experimental research is still needed to quantify the mechanical properties of fastener connections.

The strength contribution of gypsum-board sheathing to the axial compressive resistance of wood studs varies depending on the deterministic and random parameters shown in Table 1.2. A sensitivity analysis is necessary to identify ranges of these parameters where the strength increase attributable to gypsum-board sheathing is sufficiently great to warrant its consideration in design practice. No experimental or analytical studies, however, have reported a sensitivity analysis on the parameters listed in Table 1.2 for sheathed studs subjected to axial compressive loads, let alone for gypsum-board sheathed studs.

The 5^{th} percentile strength is conventionally specified in wood design (CWC, 1994). The strength contribution of gypsum-board sheathing can be quantified by comparing the 5^{th} percentile axial capacity of the bare and sheathed stud. Therefore, a statistical distribution for the axial capacity of bare and sheathed studs needs to be quantified for each significant deterministic conditions. No such distributions for the bare or sheathed studs have been presented in the literature.

Once the strength contribution of gypsum-board sheathing is quantified, revisions can be recommended for CAN/CSA-086-09 equations to account for its contribution to the increase in axial capacity. The revised equations will then allow for the axial compressive resistance of gypsum-board sheathed studs to be quantified for the stud sizes and lengths specified in NBCC Table 9.23.10.1, and the accuracy of the provisions in that table assessed.

1.3 Objectives

The main objectives of this thesis are as follows:

1. Quantify experimentally the response of gypsum-board sheathed studs subjected to axial compressive loads. This requires exploration of the impact that the material properties of wood and gypsum board and the mechanical properties of fasteners have on the axial capacity of the sheathed studs. The results of such an experimental investigation can be used to validate new sophisticated numerical modeling.

2. Quantify the response of gypsum-board-to-wood-stud fastener connections. Idealization of the response would facilitate its input into new sophisticated numerical models

3. Develop new sophisticated numerical models and quantify numerically the axial compressive resistance of bare and gypsum-board-sheathed wood studs.

4. Identify deterministic conditions where the strength contribution of gypsum-board sheathing to the axial compressive resistance of wood studs is significant, and random parameters that have a significant influence. A companion objective is to quantify the strength distribution of bare and gypsum-board-sheathed wood studs for realistic ranges of the random parameters. The strength contribution of gypsum-board sheathing can be quantified by comparing the strength distribution for the bare and sheathed studs.

5. Determine a means to account for the strength contribution of gypsum-board sheathing in the current CAN/CSA-086-09 equations. This will provide an equation that can be used to quantify the axial compressive resistance of the bare and sheathed studs for the stud size and lengths specified in NBCC Table 9.23.10.1.

6. Investigate the adequacy of provisions in Table 9.23.10.1 of NBCC, and present recommended revisions to account for the contribution of gypsum-board sheathing. This investigation and the recommended revisions will ensure the provisions in this table are suitable for design of load-bearing stud walls in light-frame wood construction.

1.4 Scope of Thesis

This thesis concentrates on interior load-bearing walls with gypsum-board sheathing on both sides of the stud. This section summarizes the deterministic parameters that will be investigated in this thesis.

This thesis concentrates on No. 2 or better grade SPF wood studs, which are used most often for light-frame construction purposes (CMHC, 2013), with most stud sizes and lengths shown in NBCC Table 9.23.10.1. Studs with 38x64 mm cross-sections are not investigated because they are not commonly used to frame load-bearing walls (CMHC, 2013).

This thesis investigates the strength contribution of regular and ultra-light 12.7 and 15.9 mm gypsum boards only. On projects where fire resistance, sound insulation, and mold and mildew resistance are not of special concern, 12.7 mm thick regular gypsum board is the least expensive and so is generally used (CMHC, 2013). In 2011, manufacturers developed an ultra-light gypsum board that is less expensive and so has replaced regular gypsum board in light-frame construction. Gypsum board of 15.9 mm thickness is often used if more stringent fire resistance is required (Rousseau, 2011).

This thesis investigates coarse threaded 32 mm or 41 mm screw fasteners for 12.7 or 15.9 mm gypsum board, respectively, spaced not more than 300 mm apart and located not less than 10 mm from the board edge. Screws are the primary choice of contractors to fasten gypsum boards to wood studs because they can be easily installed and removed without causing excessive damage to the gypsum board, have a greater pull-out strength, and are less likely to project out from the surface when the wood shrinks (Rousseau, 2011). Fastener length, spacing, and distance from edge of gypsum-board are guided from provisions in Part 9 of the NBCC (NRC, 2010)

1.5 Organization of Thesis

This thesis is presented in Integrated-Article Format in accordance with format specifications defined by the University of Western Ontario Society of Graduate and

Postdoctoral Studies. All chapters except Chapter 1 and 7 are written in publication format, without an abstract, and with references at the end. The nomenclature presented is consistent throughout. Peripheral work is included in the form of appendices following the last chapter. Measurements in wood construction are still commonly expressed in Imperial Units (e.g., feet, inches) (CMHC, 2013), whereas measurements in the NBCC (NRC, 2010) are expressed in the International System of Units (SI). SI units are used consistently throughout this thesis.

Figure 1.2 shows the organization of the chapters in this thesis.

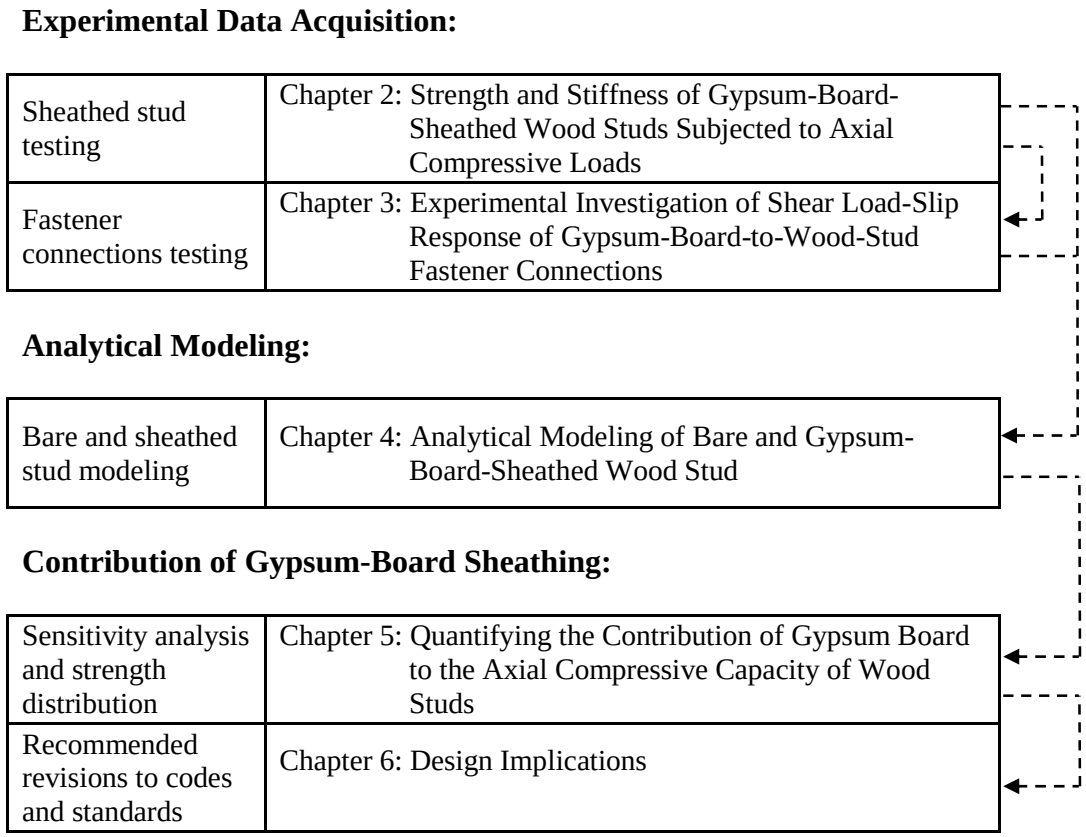

Figure 1.2: Organization of Thesis Chapters

Objected 1 is achieved in Chapter 2, where an experimental investigation on the response of gypsum-board sheathed studs subjected to axial compression is presented. Objective 2 is achieved in Chapter 3, where an experimental investigation on the response of gypsum-board-to-wood-stud fastener connection is summarized. Objective 3 is achieved in Chapter

4, where analytical models for the bare and sheathed studs are developed and validated using experimental data obtained from Chapters 2 and 3. Objective 4 is achieved in Chapter 5, where a sensitivity analysis is conducted for realistic ranges of deterministic and random parameters, and the associated strength distributions are quantified for the significant deterministic conditions using the significant random parameters. Objectives 5 and 6 are achieved in Chapter 6, where revisions to CAN/CSA-086-09 and NBCC Table 9.23.10.1 to account for the strength contribution of gypsum-board sheathing are presented.

1.6 References

Bleau, R., 1984. Comportement des Poutre-Colonnes en Bois. M.Sc.A. Thesis, Department of Civil Engineering, University of Sherbrooke, QC.

Buchanan, A.H., 1984. Strength Member and Design Methods for Bending and Axial Load Interaction in Timber Members. Ph.D. Thesis, Department of Civil Engineering, University of British Columbia, BC. 298 p.

Canadian Standards Association (CSA), 2009. CAN/CSA-086-09: Engineering Design in Wood. Canadian Wood Council, Ottawa, ON.

CMHC, 2013. Canadian Wood-Frame House Construction. Canadian Mortgage and Housing Corporation, Ottawa, ON, 315 p.

Canadian Wood Council (CWC), 1994. Canadian Lumber Properties. Canadian Wood Council, Ottawa, ON.

Canadian Wood Council (CWC), 2009. Engineering Guide for Wood Frame Construction. Canadian Wood Council, Ottawa, ON.

Gad, E. F. 1997. Performance of Brick-Veneer Cold-Formed Steel-Framed Domestic Structures when Subjected to Earthquake Loading", Ph.D. Thesis, Department of Civil and Environmental Engineering, The University of Melbourne, Australia. 360 p.

Gromala, D.S. 1985. Lateral Nail Resistance for Ten Common Sheathing Materials. Forest Products Journal, 35(9): 61-68.

Groom, K. M., 1992. Nonlinear Finite-Element Modeling of Intercomponent Connections in Light-Frame Wood Structures. M.Sc. Thesis, Department of Civil Engineering, Oregon State University, Corvallis, OR, USA. 167 p.

Kamiya, F., 1987. Buckling Theory of Sheathed Walls: Linear Analysis. Journal of Structural Engineering, Vol. 114, No. 9, pp. 625-641.

Kamiya, F., 1988. Buckling of Sheathed Walls: Nonlinear Analysis. Journal of Structural Engineering, Vol. 113, No. 3, pp. 2009-2022.

Liew, Y. L., Gad, E. F., and Duffield, C. F. 2006. Experimental and Analytical Validation of a Fastener Bearing Test as a Means of Evaluating the Bracing Characteristics of Plasterboard. Advances in Structural Engineering, 9(3): 421-432.

Marxhausen, P. D. and Stalnaker, J. J., 2006. Buckling of Conventionally Sheathed Stud Walls. Journal of Structural Engineering, Vol. 132, No. 5, pp. 745-750.

Maholtra, S. K. and Mazur, S. J., 1970. Buckling Strength of Solid Timber Columns. Transactions of the Engineering Institute of Canada, Vol. 13, No. A-4, pp. I-VII.

NRC. 2010. National Building Code of Canada - Part 9: Housing and Small Buildings. Institute for Research in Construction, National Research Council of Canada, Ottawa, ON.

Rousseau, J. 2011. Personal conversation with professional contractor on Sep. 8, 2011.

Southwell, R.V. 1931. On the Analysis of Experimental Observations in Problems of Elastic Stability. Proceedings of the Royal Society of London. Series A, Containing Papers of a Mathematical and Physical Character, Vol. 135, No. 828, pp. 601-616.

Srikanth, T. S. 1992. Structural Reliability of Light-Frame Wood Systems with Composite Action and Load Sharing. Ph.D. Thesis, Department of Forest Products, Oregon State University, Corvallis, OR, USA. 218 p.

Yagana, K., Mochida, T., Sasaki, Y., and Hirai, T., 2003. Reduction of Effective Resistance of Nailed Shear Walls caused by Misnailing III. Reduction of Effective Resistance caused by Bows of Frame Members. Journal of the Japan Wood Research Society, Vol. 49, No. 3, pp. 220-226.

Chapter 2 Strength and Stiffness of Gypsum-Board-Sheathed Wood Studs Subjected to Axial Compressive Loads

2.1 Introduction

Gypsum board is a common stud wall sheathing material that may provide additional strength and stiffness to a wood-frame structure. Part 9 of the National Building Code of Canada (NRC, 2010) permits the use of gypsum-board sheathing to provide bracing and lateral support for wood-stud shear walls subjected to lateral loads. The Engineering Guide for Wood-frame Construction (CWC, 2009) permits gypsum board to provide up to 80% of the required strength of shear walls in light-frame construction. However, both documents are mute in addressing any potential increase of the compressive resistance of sheathed stud walls subjected to gravitational loads.

Analytical models are available in the literature to predict the axial capacity of individual wood studs with wood sheathing (e.g., Kamiya, 1987; Kamiya, 1988; and Srikanth, 1992), but have shortcomings. For examples, all models assume a linear stress-strain relationship for the wood stud and the model by Srikanth (1992) ignores any initial out-of-straightness. Kamiya (1988) is the only study to consider nonlinear fastener response. These models can accommodate variable member length and stud cross-section. Their assumptions, however, have consequences that have not been validated for gypsum-board-sheathed wood studs, especially a 38 mm x 89 mm cross-section, and length of 2440 mm, which is typical in residential construction.

Marxhausen and Stalnaker (2005) is the only study on the axial compressive capacity of gypsum-board-sheathed studs. They subjected 2440 mm high wall specimens comprising four 38x89 mm wood studs to axial compressive loads to failure due to strong-axis buckling. However, the load-deformation response of the sheathed studs was not studied, and the effects of nonlinear wood stress-strain relationship and fastener load-slip response were not investigated. Therefore, the experimental data needed to quantify realistic load-

deformation responses of gypsum-board-sheathed-wood studs under axial compressive loads are not available in the literature.

This chapter concentrates on the contribution of gypsum board to the strength and stiffness of 2440 mm long 38x89 mm spruce-pine-fir (SPF) studs. Gypsum-board sheathing on both sides of the stud is studied to simulate interior load-bearing walls supporting spans on both sides, i.e., where axial compressive loads are greatest.

2.1.1 Objectives and Methodology

The objectives of this chapter are as follows:

1. Explore the consequences of the assumptions made to create available analytical models in literature, and determine if the assumptions are suitable for gypsum-board-sheathed-wood studs.
2. Design an experimental program to determine the load-deformation response and axial capacity of gypsum-board-sheathed-wood studs subjected to axial compressive loads.
3. Obtain the axial load and lateral mid-height-deflection responses of sheathed studs for various stud strengths, gypsum-board widths, and fastener stiffnesses.
4. Provide a preliminary quantification of the influence of nonlinear wood stress-strain relationship, initial out-of-straightness of the stud, and nonlinear load-slip response of fastener connections on the axial compressive capacity of sheathed studs.
5. Provide a preliminary quantification of the contribution of gypsum-board sheathing to the axial compressive resistance of wood studs.

The consequences of the assumptions made in other models will be determined by investigating the influence they have on the predicted axial load vs. mid-height deflection response of a sheathed stud when subjected to axial compression loads. It is by comparing the predicted responses to experimentally observed responses that the suitability of each

model can be determined. Therefore, the following section will present the design of a test program to produce experimentally observed axial load versus mid-height deflection responses. An analysis of the experimental test results will then follow, providing a preliminary quantification of the effects of nonlinear wood stress-strain relationship and nonlinear fastener load-slip response, and providing a preliminary quantification of the contribution of gypsum-board sheathing.

2.2 Predicted Load-Deformation Response

Figure 2.1 shows the deformation of sheathed studs subjected to concentric axial loads. Figure 2.1(a) shows a stud with an initial mid-height out-of-straightness, v, subjected to an axial compressive load, P, causing an additional lateral mid-height deflection, Δ, and the formation of convex and concave surfaces. In this chapter, the load-deformation response of a sheathed stud subjected to axial compression loads is referred to as the axial load versus mid-height deflection response, or P-Δ response. Partial-composite action occurs when connections fastening sheathing to the stud are not completely rigid, thus rotation at the top of the deformed stud causes slip, δ_f, at the gypsum-board-to-stud interface, as shown in Figure 2.1(b). This slip is associated with a shear load, V, through the fastener connections that transfers the applied axial load from the stud into the gypsum board and also increase the flexural stiffness of the member.

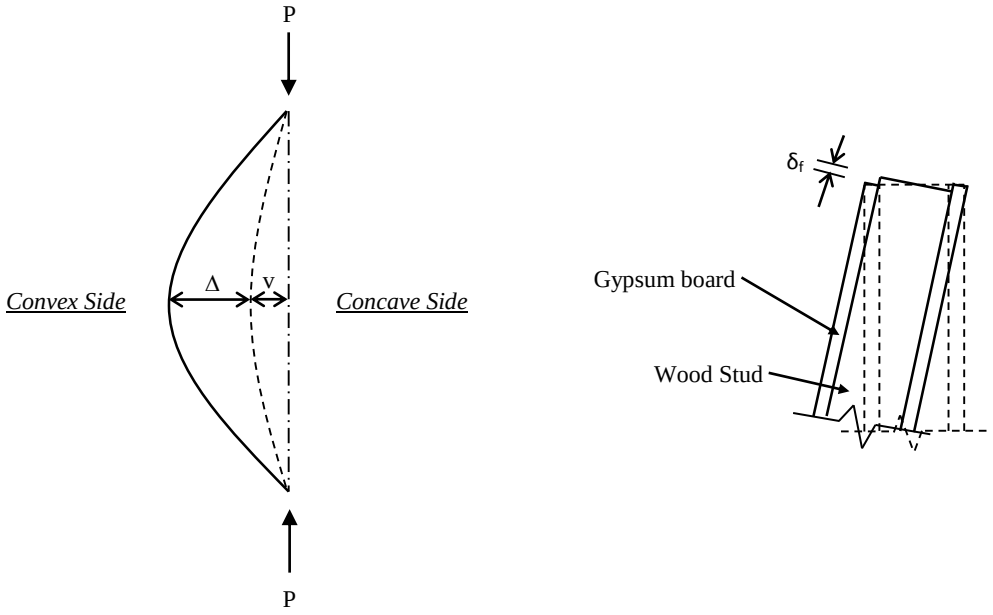

(a) Axial Load vs. Lateral Mid-Height Deflection (b) Slip at Gypsum-Board-to-Stud Interface

Figure 2.1: Buckling Behaviour of Sheathed Stud

Table 2.1 presents the constitutive models for wood stud, gypsum board, and fastener connections as reported by others. The stress-strain relationship of the wood in compression is conventionally assumed to be strain-softening with an initial slope equivalent to its modulus of elasticity, E_s, and a crushing stress, f_c, at a strain ε_1 greater than ε_0 where $\varepsilon_0 = f_c / E_s$. In tension, the wood is linear-elastic having the same slope, E_s, as for wood in compression and a fracture stress, f_t. These wood properties have been used by Bleau (1984), Buchanan (1984), and Song and Lam (2009) to simulate the results of buckling tests of wood studs. No studies have reported a stress-strain relationship of gypsum board in compression or tension. Groom (1992) tested 12.7 mm gypsum board in bending and reported a near-linear-elastic perfectly plastic lateral load versus mid-height deflection response, with an elastic stress limit that can be approximately estimated as 2 MPa. If the stress in the gypsum board does not exceed this limit, a linear-elastic stress-strain relationship can be assumed with a slope equivalent to its modulus of elasticity, E_{GB}. This assumption was made by Lee (1999) to predict the compressive capacity of gypsum-board-sheathed metal studs. The shear load-slip response of the fastener connections is

nonlinear with an initial elastic stiffness, k_f, typically followed by a significant plastic response, i.e., unrecoverable slip upon unloading. However, no clear idealization of the load-slip response was presented in or can be inferred from the literature.

Table 2.1: Constitutive Models of Individual Components of a Gypsum-Board-Sheathed Wood Stud

Component	Response	Source
Wood in compression	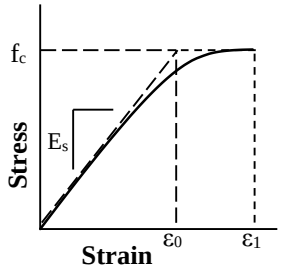	Ylinen 1956 O'Halloran 1973 Glos 1978 Song and Lam 2009
Wood in tension	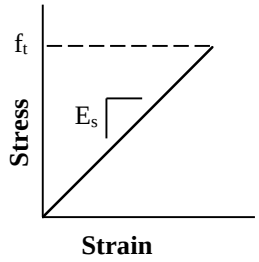	Buchanan 1984 Song and Lam 2009
Gypsum board in tension and compression	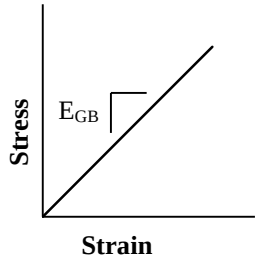	Groom 1992
Fastener connections	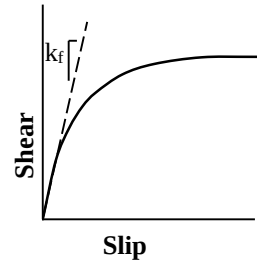	Gromala 1985 Gad 1997 Liew et al. 2006

The P-Δ response and axial compressive capacity of a sheathed stud, P_c, depend greatly on the material properties of the wood and gypsum board, the load-slip response of the fastener connections, and the presence of an initial out-of-straightness. Response A in Figure 2.2 is

the perfect Euler buckling response obtained when the wood stress-strain relationship and fastener load-slip response are linear-elastic and v equal to 0. The resulting P_c is independent of Δ and is equal to the Euler buckling load, P_e, given by:

[2.1] $P_e = \pi^2 EI_c / (kL)^2$

where EI_c is the flexural rigidity of the sheathed stud, and kL is its effective length. For v greater than 0, the stud response is represented by Response B, where P_c is still equal to P_e from Equation [2.1] (Southwell, 1931) but is reached only when Δ approaches ∞. Response C is similar to Response B but accounts for a nonlinear load-slip response of fastener connections. In this instance, the fastener connections are more flexible, thus EI_c is reduced and so is P_c. Finally, Response D accounts for: v greater than 0; a nonlinear load-slip response of fastener connections; and, a nonlinear wood stress-strain relationship in compression with a finite crushing stress, f_c. In this case, EI_c is further reduced as the applied load increases, and P_c corresponds to a finite mid-height deflection, thus is less than P_e.

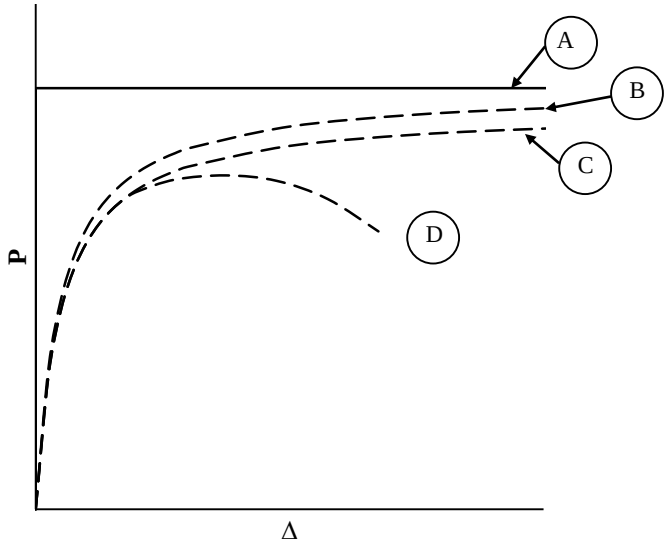

Figure 2.2: Possible P-Δ Response of Isolated and Sheathed Studs

2.2.1 Analytical Models

Others have reported equations, based on assumptions that are summarized in Table 2.2, to calculate EI_c and P_c of sheathed studs. Srikanth (1992) reported an equation to calculate EI_c accounting for linear-elastic wood stress-strain relationship and fastener load-slip response and v equal to 0. The value of P_c is thus equal to P_e irrespective of Δ, which corresponds to Response A in Figure 2.2. Kamiya (1987) reported an equation accounting for linear-elastic wood stress-strain relationship and fastener load-slip response with v greater than 0. The value of P_c is thus equal to P_e when Δ approaches ∞, which corresponds to Response B. Kamiya (1988) reported an improved equation to account for nonlinear load-slip response of fastener connections, which corresponds to Response C. No equations have yet been reported to also account for a nonlinear wood stress-strain relationship with a finite crushing stress, which, along with a nonlinear load-slip response of fastener connections with v greater than 0, corresponds to Response D.

Table 2.2: Properties Considered in Sets of Equations Reported by Others

Author	Nonlinear Stress-strain relationship of wood	Crushing of wood	Nonlinear Shear load-slip response of fastener	Initial mid-height out-of-straightness
Kamiya, 1987	Linear	No	No	Yes
Kamiya, 1988	Linear	No	Yes	Yes
Srikanth, 1992	Linear	No	No	No

The studies summarized in Table 2.2 can be augmented using finite element analysis that consider nonlinear wood stress-strain relationships. For example, Lau (2000) modeled bare stud beam-columns and Song and Lam (2009) modeled perfectly straight studs subjected to eccentric compression loads. The best predictions of the stud behaviour in both studies were obtained using similar nonlinear stress-strain relationships. However, no finite element models have been reported by others to predict the axial compressive capacity of sheathed studs considering a nonlinear wood stress-strain relationship with a crushing stress.

2.2.2 Summary

Others have reported equations to calculate the axial compressive capacity of sheathed studs by making assumptions that have consequences on the P-Δ response of sheathed studs and thus P_c. No analytical model has been reported to account for a nonlinear wood stress-strain relationship with a crushing stress, corresponding to a distinctive P-Δ response of sheathed studs and reduced value of P_c. Comparing the predicted P-Δ responses described in this section with experimentally observed P-Δ responses can determine the appropriate model for gypsum-board-sheathed wood studs. However, if it is necessary to consider a nonlinear wood stress-strain relationship with a crushing stress, a new analytical model must be developed.

2.3 Design of Testing Program; Specimen and Apparatus

The sheathed-stud specimens investigated in this chapter consist of individual studs to eliminate possible load-sharing between studs in multiple-stud specimens. Individual sheathed studs may fail by buckling about their weak axes, whereas stud walls do not exhibit this failure mode (e.g., Marxhausen and Stalnaker, 2006; CWC, 2009; NRC, 2010). Therefore, what gypsum-board width is required to ensure strong-axis buckling of the individual sheathed stud? An analytical study will first be presented to determine the minimum sheathing width necessary so that experimental tests can ensure a strong-axis buckling failure of the sheathed studs, considering full and partial-composite-action between the gypsum board and wood stud.

The testing program is designed to vary the stiffness of the wood stud, gypsum board, and fastener connections. The stiffness of the gypsum board and fastener connections can be readily varied by selection of the gypsum-board width and quantity of fasteners, respectively. However, the stud stiffness can only be quantified using a non-destructive testing methodology. Non-destructive bending tests will therefore be presented to determine the modulus of elasticity of the wood prior to conducting destructive buckling tests of sheathed studs.

The remainder of this section will summarize the design of the experimental buckling tests, which includes specimen designs, a test matrix, the testing apparatus, and finally the testing procedures.

2.3.1 Ensuring Strong-Axis Buckling of Isolated Stud

Figure 2.3 shows the cross section of a sheathed wood stud, with the width and depth of the stud represented by b and d, respectively, and the width and thickness of the gypsum-board sheathing represented by b_{GB} and t, respectively. The strong-axis moment of inertia is about the x-x axis, whereas the weak-axis moment of inertia is about the y-y axis.

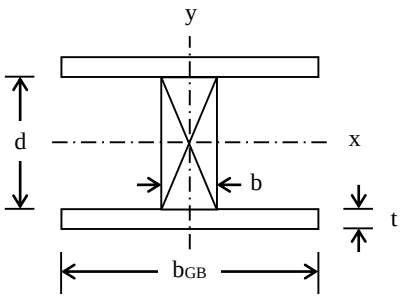

Figure 2.3: Cross Section of Sheathed Stud

The weak-axis flexural rigidity of a sheathed stud, $EI_{c(y)}$, does not depend on the stiffness of the fastener connections because they are sufficient to brace the weak axis of 38 x 89 mm studs (e.g., Marxhausen and Stalnaker, 2006). Therefore, $EI_{c(y)}$ can be computed assuming perfectly rigid fastener connections, yielding:

[2.2] $$EI_{c(y)} = E_s\, db^3 \,/\, 12 + E_{GB}\, tb_{GB}^{\,3} \,/\, 6$$

where E_s and E_{GB} are Young's Modulus of the stud and gypsum board, respectively.

Conversely, it is appropriate to assume non-rigid fastener connections when computing the strong-axis flexural rigidity of the sheathed stud, $EI_{c(x)}$ (e.g. Kamiya, 1987). Although fastener response may be nonlinear, it is conservative, when determining a value for b_{GB} to ensure strong-axis buckling, to assume a non-rigid linear-elastic fastener response.

Equations presented in literature to predict $EI_{c(x)}$ assuming linear-elastic fastener response account for sheathing on one side of the stud only (e.g., Kamiya, 1987, and Srikanth, 1992). Therefore, an analytical model is needed to account for sheathing on both sides of the stud.

Figure 2.4 shows the deformed shape of the sheathed stud due to equal first-order applied end moments causing single curvature. The deformed shape is symmetric about the stud mid-height, so only the top half of the stud is shown, with a free end at the top and a fixed support at mid-height. The length of the stud shown is half of the actual length, L, with fasteners spaced at a distance s. The moment, M, is applied about the strong axis, causing an end-rotation of the stud, θ, and a lateral deflection, Δ. The latter is the equivalent of a lateral mid-height deflection for full length studs with pinned ends subjected to similar end moments. The strong-axis flexural rigidity of the sheathed stud with non-rigid fastener connections can thus be calculated from the maximum deflection as (e.g., CISC 2004):

[2.3] $EI_{c(x)} = ML^2 / 8\Delta$

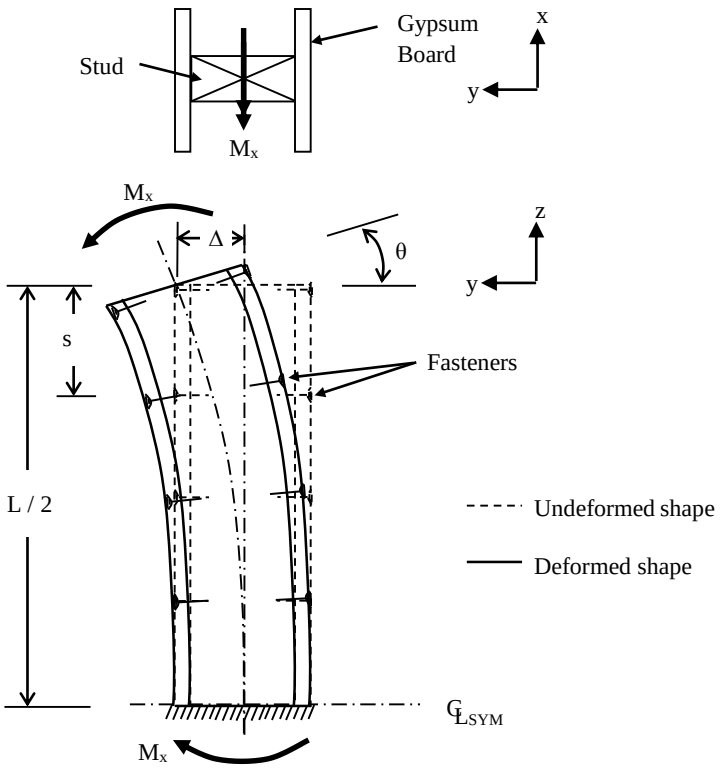

Figure 2.4: Deformed Shape of Sheathed Stud due to Applied End Moments

Figure 2.5 shows a free-body diagram of the sheathed stud between the upper two fasteners. A fictitious gap is shown between the wood stud and gypsum board to facilitate visualization of the deformed shape at the fastener connections. The relative deformations are shown at Fastener Lines 1 and 2 where each variable is defined by a subscript indicating its location with regards to the fastener lines. For example, at Fastener Line 1, $\theta_{(1)}$ is the rotation of the stud, $\delta_{s(1)}$ is the extreme-fibre deformation of the stud, $\delta_{GB(1)}$ is the axial deformation of the gypsum board, $\delta_{f(1)}$ is the fastener slip, and $\delta^*_{(1)}$ is the portion of fastener slip due to rotation of the stud needed for plane sections to remain plane. The variables shown in grey represent internal load effects, where $N_{GB(1)}$ is the axial load in the gypsum board between Fastener Lines 1 and 2, and $\sigma_{s(1)}$ is the extreme fibre stress of the stud between these fastener lines. Finally, additional dimensional parameters are needed: e_{GB} is the distance between the gypsum-board force resultants, y_s is the distance from the elastic neutral-axis in the stud to the face of the stud, and L_f is the distance from the face of the stud to the centroid of the gypsum board.

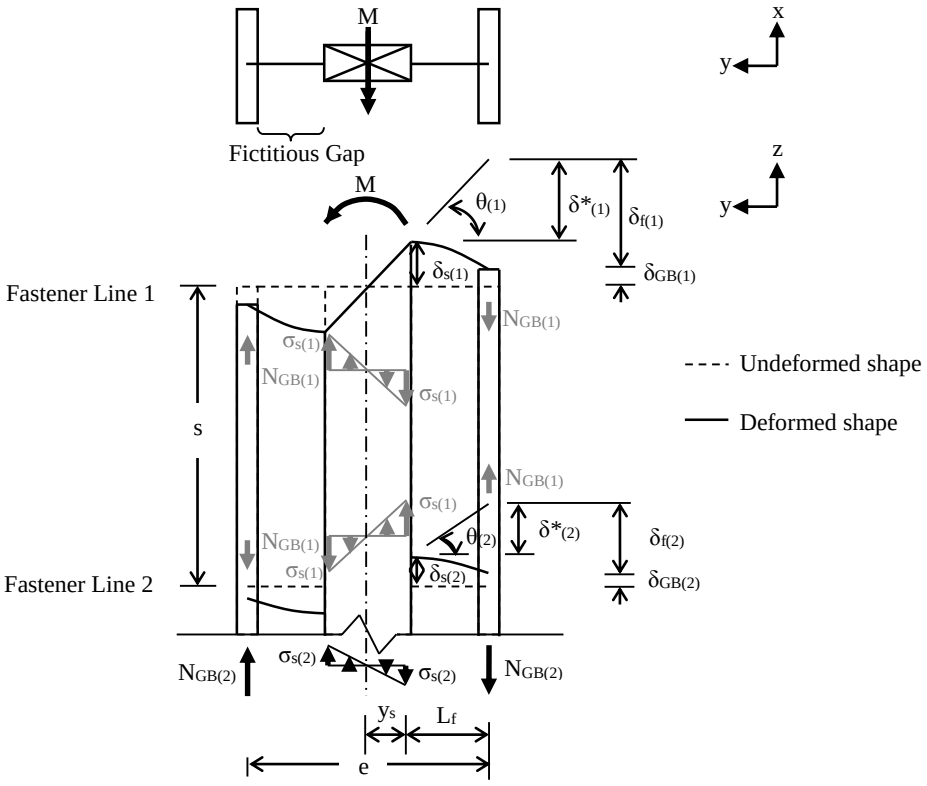

Figure 2.5: Free-body-diagram of Sheathed Stud

Equilibrium equations can be derived at each fastener elevation using a subscript, i, that represents the fastener line number from the top of the stud. Variables with a subscript number less than 1 or greater than the total number of fastener lines in the top half of the stud, n, are equal to zero. Moment equilibrium requires that:

[2.4] $M = N_{GB(i)}e_{GB} + \sigma_{s(i)}I_s / y_s$

Compatibility of the extreme-fibre deformations requires that:

[2.5] $\delta_{s(i)} = \delta_{GB(i)} + \delta_{f(i)} - \delta^*_{(i)}$

At the extreme fiber of the stud, the strain immediately below fastener line i, $\varepsilon_{s(i)}$, is given by:

[2.6] $\varepsilon_{s(i)} = \left(\delta_{s(i)} - \delta_{s(i+1)}\right) / s$

Similarly, the strain in the gypsum board immediately below fastener line i, $\varepsilon_{GB(i)}$, is

[2.7] $\varepsilon_{GB(i)} = \left(\delta_{GB(i)} - \delta_{GB(i+1)}\right) / s$

Compatibility of the rotation of the wood stud from one fastener line to the next requires that:

[2.8] $\theta_{(i)} = \theta_{(i+1)} + \varepsilon_{s(i)}s / y_s$

The portion of fastener slip due to rotation of the stud needed for plane sections to remain plane is given by:

[2.9] $\delta^*_{(i)} = \theta_{(i)}L_f$

For the assumed linear-elastic material response, the extreme fibre stress in the stud, $\sigma_{s(i)}$, is

[2.10] $\sigma_{s(i)} = \varepsilon_{s(i)} E_s$

and the axial force in the gypsum board is

[2.11] $N_{GB(i)} = \varepsilon_{GB(i)} E_{GB} b_{GB} t$

For the assumed linear-elastic fastener response, the shear load transferred through the fastener at a given fastener line is

[2.12] $N_{GB(i)} - N_{GB(i-1)} = \delta_{f(i)} k_f$

Equations [2.4] to [2.12] are used to derive $\varepsilon_{s(i)}$, which is used to calculate the moment resisted by the stud, $M_{s(i)}$, given by:

[2.13] $M_{s(i)} = \varepsilon_{s(i)} E_s I_s / y_s$

The lateral deflection at the top the bare stud, Δ, obtained by calculating the moment of the M_s/E_sI_s diagram about the end of the stud, is given by:

[2.14] $\Delta = \sum_{i=1}^{n} [i - 0.5] M_{s(i)} s^2 / E_s I_s$

The strong-axis flexural rigidity of the sheathed stud is obtained by inserting Δ into Equation [2.3]. A spreadsheet was programmed using these equations to do a preliminary sensitivity analysis to determine the gypsum-board width required to ensure strong-axis buckling of a gypsum-board sheathed stud.

Table 2.3 presents the input dimensions for a typical 38 x 89 mm stud sheathed with 12.7 mm thick gypsum board. Gypsum-board widths of 300 and 400 mm, i.e., typical spacing between 2x4 studs in a load-bearing wall (NRC, 2010), are considered in the analysis to capture the influence of the gypsum-board stiffness.

Table 2.3: Typical Dimension of a Sheathed Stud

Parameter	Definition	Dimension
d	Depth of stud	89 mm
b	Width of stud	38 mm
t	Thickness of gypsum board	12.7 mm
b_{GB}	Width of gypsum board	300 to 400 mm
y_s	Distance from elastic neutral-axis to face of stud	44.5 mm
L_f	Distance from face of stud to centroid of gypsum board	6.35 mm
e_{GB}	Distance between gypsum-board force resultants	101.7 mm
s	Fastener spacing	305 mm
L	Stud length	2440 mm

2.3.1.1 Influence of Flexural Rigidity on Buckling Direction

The 5th and 95th percentile values for E_s and E_{GB} and the lower and upper bound values for k_f are provided in Table 2.4. The values for E_s are for SPF wood studs of No. 2 grade or better. Values for E_{GB} are computed assuming normal distribution with a mean of 1780 MPa and coefficient of variation (CoV) of 0.08, as reported by Lee (1999). Values for k_f are based on data available in Appendix 3A for various types of gypsum-board-to-stud fastener connections from the experimental investigation reported in Chapter 3.

Table 2.4: Input Values for E_s, E_{GB}, and k_f

	5th percentile	95th percentile	Source
E_s	6700 MPa	12400 MPa	Bleau (1984)
E_{GB}	1560 MPa	2000 MPa	Lee (1999)
	Lower	Upper	
k_f	350 N/mm	2000 N/mm	Appendix 3A

Figure 2.6 shows the variation of the ratio of $EI_{c(y)}$ obtained using Equation [2.2] to $EI_{c(x)}$ obtained using Equations [2.3] through [2.14] vs. b_{GB}. Because Equation [2.2] assumes rigid fasteners when determining the weak-axis rigidity, yet Equations [2.3] through [2.14] assume non-rigid fasteners when determining the strong-axis rigidity, an increase in E_{GB} primarily increases $EI_{c(y)}$. Conversely, an increase in E_s and k_f primarily increase $EI_{c(x)}$. Therefore, the ratios shown are for cases of the 5th percentiles of E_s and k_f with the 95th percentile of E_{GB}, and the 95th percentiles E_s and k_f with the 5th percentile of E_{GB}. Clearly,

$EI_{c(y)}$ exceeds $EI_{c(x)}$ when b_{GB} exceeds 150 to 215 mm, depending on the elastic moduli and fastener stiffness parameters assumed.

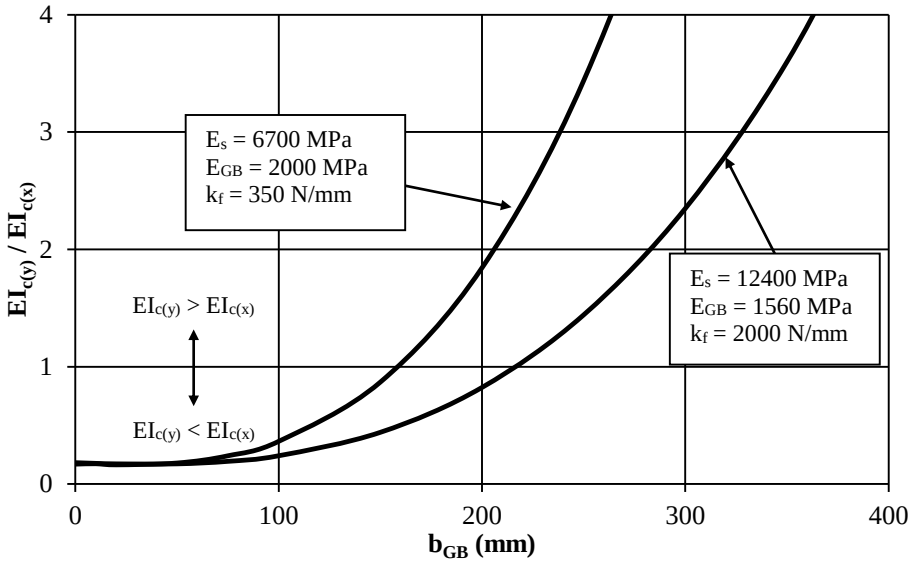

Figure 2.6: Variation of Flexural Rigidity of Stud with Variable Sheathing Width

2.3.1.2 Influence of Initial Out-of-Straightness on Buckling Direction

The buckling capacity of slender sheathed studs can be calculated using Equation [2.1], requiring only the flexural rigidity. For intermediate columns, however, the initial mid-height out-of-straightness must be considered. For example, Southwell (1931) reported that the linear-elastic buckling response of a column follows:

[2.15] $\Delta / P = \Delta / P_e + v / P_e$

where P_e is the Euler buckling load from Equation [2.1]. Rearranging Equation [2.15] to isolate the axial load normalized by P_e:

[2.16] $P / P_e = \Delta / (\Delta + v)$

This equation is used to create Figure 2.7 where Δ and v are normalized by the length of the stud, L. The flexibility of the member is indicated by the magnitude of Δ for a given P,

so members with larger v are always more flexible than members with smaller v. Therefore, for cases where the nominal flexural rigidities are equal about both axes, the axis with greater initial mid-height out-of-straightness will buckle first. Results in Appendix 2A, from a sample of 12 bare studs, present a mean value for v of 1.5 mm about the strong axis and, from a sample of 25 bare studs, 4.2 mm about the weak axis. At a length of 2440 mm, this corresponds to v/L equal to 0.00061 and 0.0017, respectively. The installation of gypsum-board sheathing is assumed not to reduce the initial out-of-straightness of the stud. Thus, for equal flexural rigidities about both axes, a typical sheathed stud is likely more susceptible to weak-axis buckling due to the greater relative out-of-straightness. Consequently, a gypsum-board width of 215 mm may not necessarily ensure strong-axis buckling of a sheathed stud with non-rigid linear-elastic fastener connections.

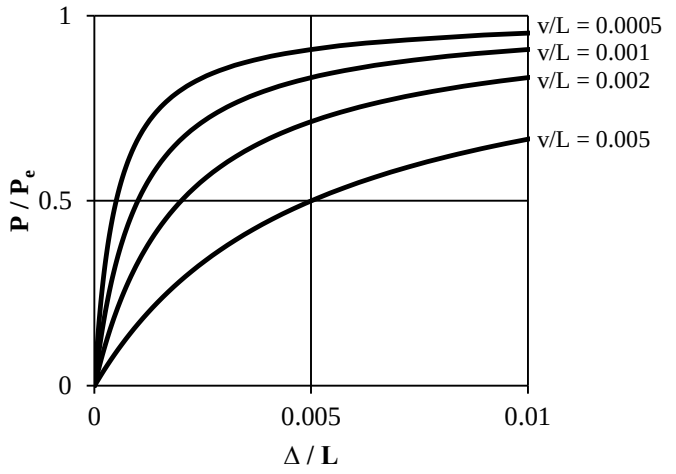

Figure 2.7: Influence of Initial Mid-Height Out-of-Straightness

The minimum gypsum-board width required to ensure strong-axis buckling can be determined by considering the most critical case: v of 12 mm about the weak axis, i.e., the approximate 95th percentile value observed in tests, and 0.5 mm about the strong axis, i.e., the approximate 5th percentile value observed in tests, with E_s of 12400 MPa, k_f of 2000 N/mm, and E_{GB} of 1500 MPa. Figure 2.8 shows the predicted P-Δ response of the sheathed studs for b_{GB} of 215, 250, and 300 mm. The corresponding computed P_e for the strong axis are 61.8, 62.9, and 64.1 kN, respectively, and for the weak axis, 60.6, 90.6, and 150 kN, respectively. These are the loads resisted when Δ approaches infinity, whereas the

maximum axial load in experimental testing occurred on average at $\Delta \approx 20$ mm, as will be shown later in Table 2.6, for both strong- and weak-axis buckling cases. Therefore, the gypsum-board width is considered sufficient to ensure strong-axis buckling when the strong-axis capacity is weaker than the weak-axis capacity at Δ equal to 20 mm. For b_{GB} of 215 mm, the strong-axis capacity at Δ equal 20 mm is markedly greater than the weak-axis capacity at this deflection, so this width is not satisfactory. For b_{GB} of 250 mm, similar strong- and weak-axis capacities are predicted when Δ equals 20 mm, so this width is also not satisfactory. For b_{GB} of 300 mm, the strong-axis capacity when Δ equals 20 mm is markedly smaller than the weak-axis capacity at this deflection, thus strong-axis buckling would likely occur. To ensure strong-axis buckling in sheathed single-stud specimens, the gypsum-board width should therefore be at least 300 mm.

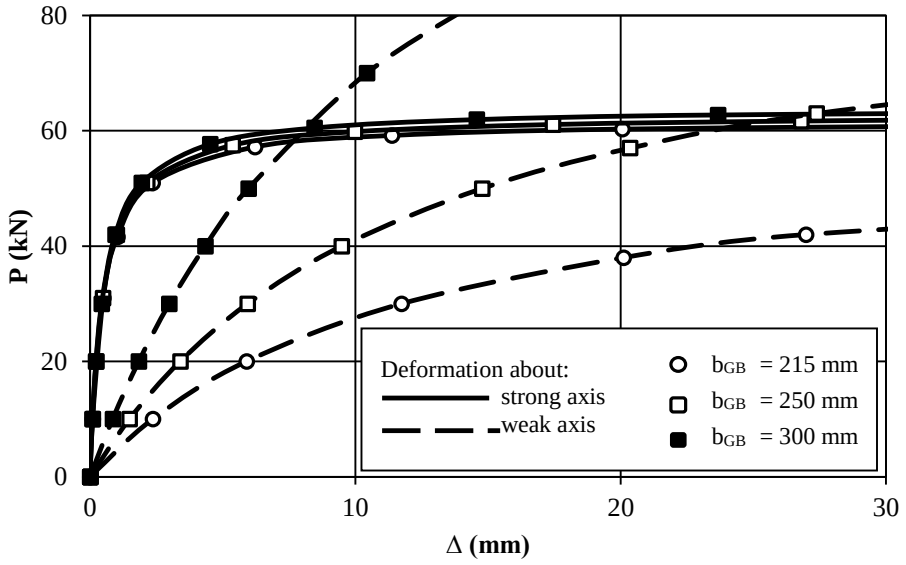

Figure 2.8: Flexibility of Sheathed Stud about Strong and Weak Axis

2.3.1.3 Summary

This section has considered analytically the influence of gypsum-board width on the possible buckling modes of individual 38 mm x 89 mm studs sheathed with 12.7 mm gypsum board on both sides, with an effective length for both axes of 2440 mm. It is possible for strong-axis buckling to occur with a gypsum-board width as little as 150 mm.

However, a minimum width of 300 mm is suggested to ensure strong-axis buckling given expected variations of fastener rigidities, material Young's moduli, and member out-of-straightness.

2.3.2 Non-Destructive Testing of Modulus of Elasticity of Wood

To capture the influence of E_s, the buckling test program included studs from each of the five stiffness categories shown in Figure 2.9. The Weibull 3-parameter cumulative distribution function with a mean of 9780 MPa and a standard deviation of 1730 MPa reported by Bleau (1984) was used to derive boundaries of each stiffness category as shown. The 20th percentile values for E_s are termed "very flexible", the 20th to 40th percentile values are "flexible", the 40th to 60th percentile values are "average", the 60th to 80th percentile values are "stiff", and the 80th to 100th percentile values are "very stiff".

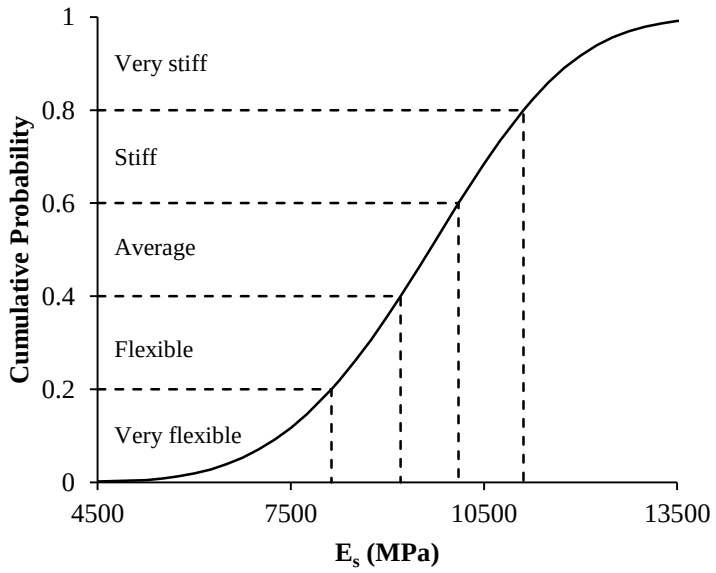

Figure 2.9: Distribution of E_s for 38 x 89 mm SPF Studs (Bleau, 1984)

However, before conducting buckling tests on sheathed studs, numerous studs needed to be subjected to non-destructive bending tests to determine E_s, and so classifying them by stiffness category. This allowed an even quantity of studs from each stiffness category to be used in the experimental buckling test program.

Bleau (1984) and Buchanan (1984) measured the flexural rigidity of the wood stud by conducting a four-point bending test with loads at the third-points, as shown in Figure 2.10. For this testing arrangement, E_s can be back-calculated using (e.g. CISC, 2004):

[2.17] $E_s = Pa\left(3L^2 - 4a^2\right) / 24\Delta I_s$

where a is the distance from the applied load to the adjacent support and I_s computed for the 38 x 89 mm finished cross-section dimensions. For a/L = 0.33,

[2.18] $E_s = 0.035\ PL^3 / \Delta I_s$

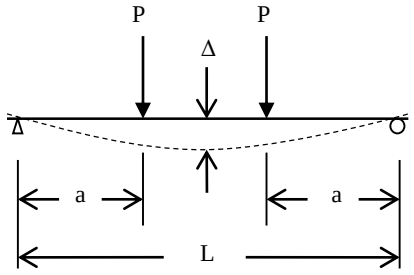

Figure 2.10: Four-point Bending Test Parameters

The modulus of elasticity of the studs in this chapter was obtained using a similar four-point bending test, with supports located 25 mm from each end, I_s computed for the 38 x 89 mm finished cross-section dimensions, and a/L = 0.22, as shown in Figure 2.11. For this load location:

[2.19] $E_s = 0.026\ PL^3 / \Delta I_s$

This shear span is different from that adopted by Bleau and Buchanan, and was selected to minimize the difference between the flexural rigidities obtained from flexural and buckling tests for a stud with variable Young's modulus along its length, as reported in Appendix 2B.

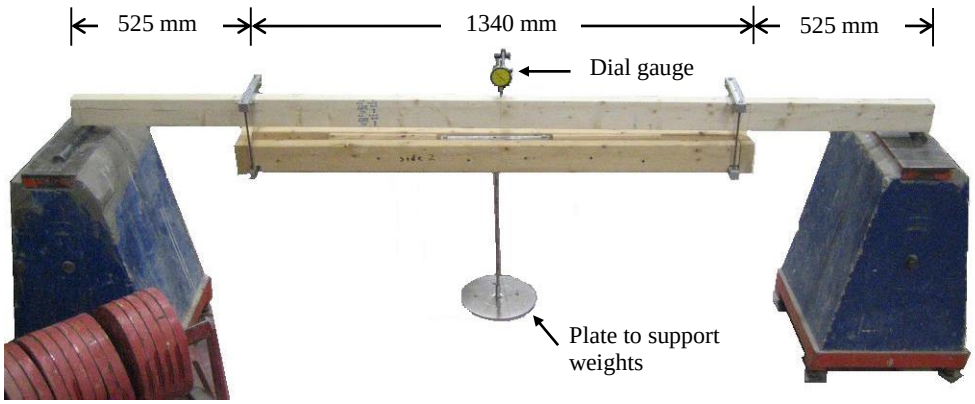

Figure 2.11: Four-point Bending Test in Western Engineering Structures Lab

Loads were applied in five increments of 49 N (5 kg) at each load point, and so generated a maximum extreme-fibre stress of only 2.6 MPa. At such low stress levels, no damage to the stud occurred. An interval of approximately 20 seconds occurred between each load increment, although each load increment required only between 0.5 and 1.0 second to be applied. This created an average rate-of-loading (ROL) of approximately 2.5 N/sec (0.026 MPa/sec) and an instantaneous ROL of 50 to 100 N/sec (0.52 to 1.0 MPa/sec). Displacement readings were obtained between load increments using a 30 mm dial gauge at the centre span, as shown in Figure 2.11. All studs tested had moisture contents below 10%. Each stud was tested twice, and inverted between tests to obtain an average modulus of elasticity.

2.3.3 Buckling Test Program

The buckling test program is presented in two sections. The first presents the specimen design and test matrix, and the second presents the testing apparatus and procedure.

2.3.3.1 Specimen Design and Test Matrix

Figure 2.12 shows a typical specimen with 12.7 mm gypsum board, in accordance with ASTM C1396-11 (ASTM, 2011), sheathing both sides of the 2440 mm long 2x4 SPF stud and fastened using 32 mm coarse gypsum-board screws, in accordance with ASTM C1002-

07 (ASTM, 2007), spaced at 300 mm starting 19 mm from the horizontal edges of the gypsum board. Two specimen types were tested with different fastener schedules to capture the influence of varying the fastener stiffness. Type A specimens were constructed with no seam in the gypsum board and a single line of fasteners along the middle of the stud board as shown. Type B specimens were constructed from pairs of gypsum board, creating a seam along the length of the stud fastened along the manufactured tapered edge of each gypsum-board sheet at a side distance of 10 mm. This fastening schedule meets the minimum requirements from Part 9 of the NBCC (NRC, 2010) so that fasteners on both sides of the seam can engage the 38 mm width of the stud. The influence of the axial rigidity of the gypsum board was captured by using b_{GB} for Type A specimens of 150, 200, 300 and 400 mm. Widths of 150 and 200 mm were recognized to be potentially insufficient to ensure strong-axis buckling, but were included to validate the analytical predictions presented in Section 2.3.1 for minimum gypsum-board width required to ensure strong-axis buckling of sheathed studs. The gypsum-board width for Type B specimens was maintained constant at 300 mm to ensure strong-axis buckling. The axial compressive load was applied concentrically to the stud only and not the gypsum board, as shown.

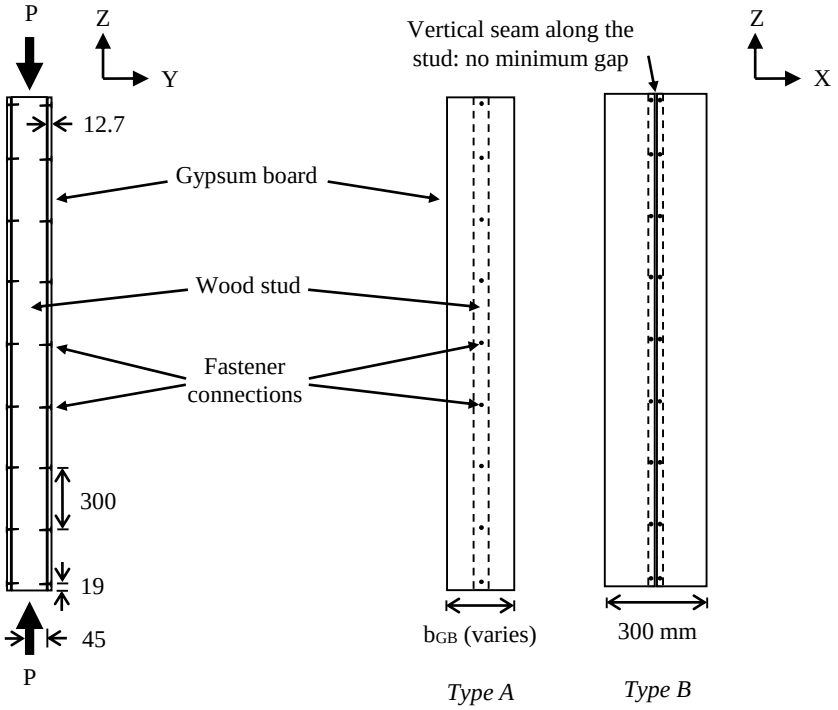

Figure 2.12: Specimen Design for Sheathed Stud (All Dimensions in mm)

Table 2.5 shows the matrix for buckling tests program. A stud from each of the five stiffness categories shown in Figure 2.9, based on E_s obtained from bending tests, were tested for each specimen type. A total of 26 Type A specimens were tested with four gypsum-board widths and five stud stiffnesses. Replicate tests were conducted for the six cases where buckling about either axis was considered to be most likely, i.e., b_{GB} = 200 mm with a very flexible to average E_s, and b_{GB} = 300 mm with an average to very stiff E_s. These replicate tests were conducted to increase the likelihood of observing strong-axis buckling.

Table 2.5: Matrix for Buckling Tests of Sheathed Studs

Specimen	b_{GB} *(mm)*	Test quantity for specific stiffness category of E_s				
		Very flexible	Flexible	Average	Stiff	Very stiff
Type A	150	1	1	1	1	1
	200	2	2	2	1	1
	300	1	1	2	2	2
	400	1	1	1	1	1
Type B	300	1	1	1	1	1

The moisture content of the material was measured before each test using a Protimeter Moisture Measurement System calibrated for soft wood. It is shown in Appendix 2C that the calibration is not suitable for accurately determining the moisture content of gypsum board, thus values obtained for gypsum board are considered nominal. All studs had moisture contents below 10%. The gypsum board in Type A specimens had moisture contents ranging from 8.7 to 12.2%, whereas the gypsum board in Type B specimens had moisture content below the minimum reading provided by the instrument, i.e., 7.8%.

2.3.3.2 Test Apparatus and Procedure

Figure 2.13 shows the test apparatus used for all specimens. The loading was applied through a hydraulic jack at the top of the stud, as shown in Figure 2.13(b). Provisions in the CSA-086 standard (CSA, 2009) and in Part 9 of the NBCC (NRC, 2010) consider the effective length of wood studs to be equal to its full length. Therefore, half-round supports at both ends, as shown in Figure 2.13(c), were used to create pinned supports about the

strong-axis of the bare stud. A 110 kN load cell was used to capture the applied axial load, and six 100 mm linear variable differential transducer (LVDT) captured the lateral displacement of each stud, i.e., at the top, mid-height, and bottom of the stud in both strong- and weak-axis direction. The load was applied manually using a hand pump. The ROL was approximately 600 N/sec (0.18 MPa/sec) at the start of each test and approached zero as the applied load reached the buckling capacity of the sheathed stud.

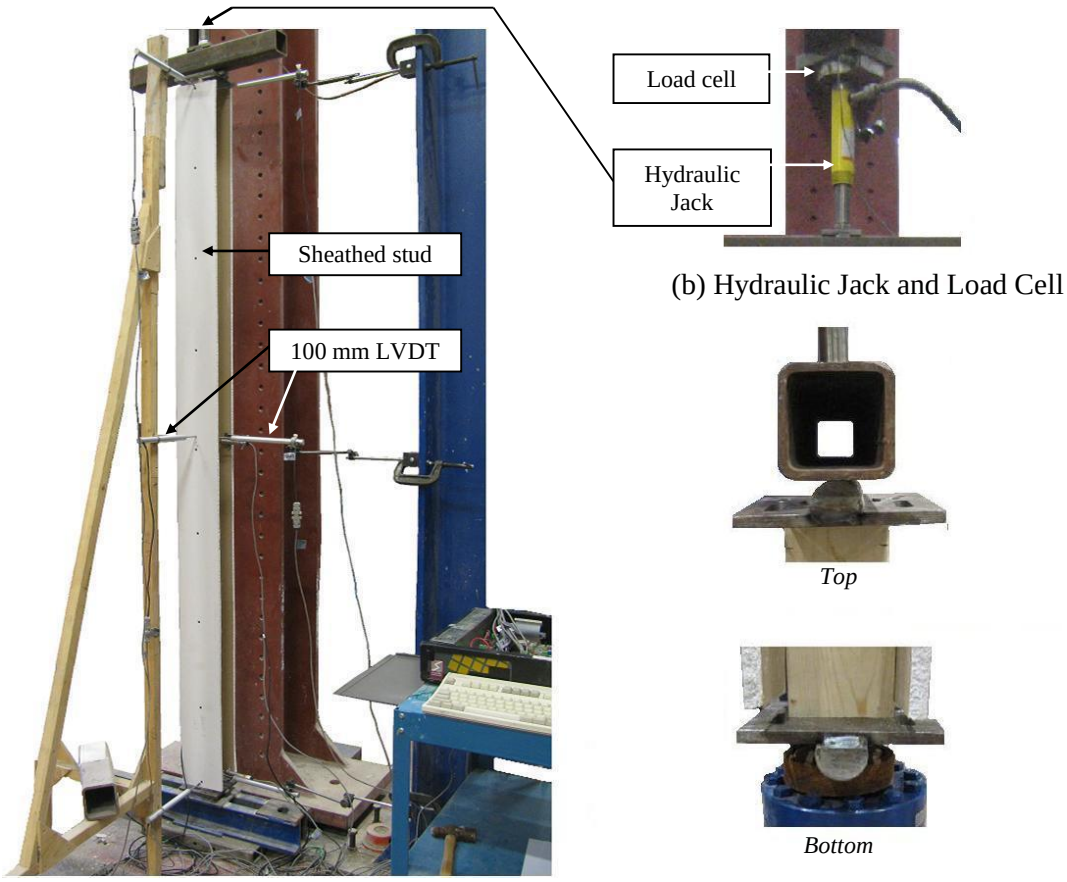

(a) Test Apparatus

(b) Hydraulic Jack and Load Cell

(c) Pinned Supports

Figure 2.13: Apparatus for Buckling Tests of Isolated Sheathed Stud

Three 25 mm LVDTs were used to capture the fastener slip caused by deformations of the stud due to strong-axis bending, as shown in Figure 2.14. Slips were measured at the fastener lines located at the bottom end and quarter-point on the concave side of the deformed stud and at the bottom end on the convex side.

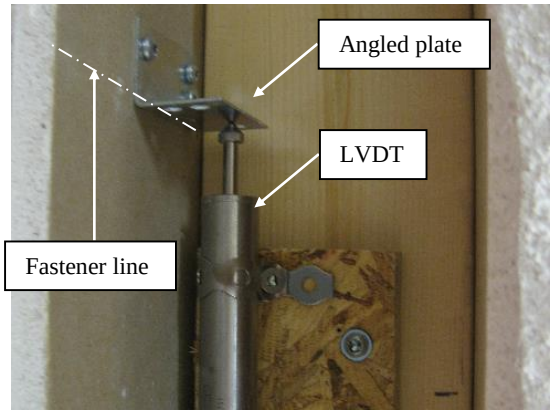

Figure 2.14: LVDT Setup to Measure Vertical Slips

2.4 Buckling Test Results

Results from buckling tests are first reviewed to validate the gypsum-board width required to ensure strong-axis buckling of the sheathed stud. Afterwards, an analysis of the P-Δ response is conducted to determine if methodologies currently available in literature are suitable to predict the axial compressive capacity of gypsum-board-sheathed wood studs.

2.4.1 Width of Gypsum Board Required to Ensure Strong-Axis Buckling

Table 2.6 gives a comparison of the lateral mid-height deflection about the strong axis and weak axis of the sheathed stud for Type A specimens at P equal to P_c. The larger of the two deflections indicates about which axis occurred the main buckling mode. Shaded in grey are all cases where strong-axis buckling was clearly observed. Fourteen of the twenty-six sheathed studs buckled about their strong-axes. Two of eight specimens with b_{GB} of 200 mm buckled about their strong-axis, whereas seven of eight specimens with b_{GB} of 300 mm buckled about their strong axes. The only stud with b_{GB} of 300 mm to buckle about its weak-axis had an extreme initial mid-height deformation about the weak axis of approximately 14 mm, thus markedly increasing its susceptibility to buckling about that axis. No specimens with b_{GB} of 150 mm and all specimens with b_{GB} of 400 mm buckled

about their strong axes. These experimental results are consistent with theoretical results presented in Section 2.3.1, which predicted that isolated sheathed studs with b_{GB} of 300 mm or greater will buckle about their strong axes.

Table 2.6: Lateral Mid-Height Deflection of Stud at Maximum Axial Load (mm)

Stud Strength Category	Δ (strong axis / weak axis)			
	b_{GB} *(mm)* 150	200	300	400
Very flexible	12.7 / 18.6	20.2 / 1.2	17.3 / 0.5	16.2 / 1.2
		4.6 / 19.2		
Flexible	17.6 / 13.6	17.0 / 22.4	12.7 / 0.1	9.3 / 0.3
		1.1 / 15.7		
Average	10.7 / 18.0	1.2 / 16.1	23.2 / 6.3	14.8 / 0.9
		19.4 / 7.3	18.6 / 0.9	
Stiff	0.9 / 19.1	0.4 / 11.5	19.6 / 0.2	16.4 / 0.7
			7.5 / 19.1	
Very stiff	5.2 / 10.5	13.2 / 10.3	19.1 / 1.0	18.1 / 0.4
			13.6 / 7.2	

2.4.2 Analysis of P-Δ Response

When analyzing the P-Δ response and axial compressive capacity of the sheathed studs, only results where strong-axis buckling was the dominant mode of failure were analyzed. Figure 2.15 shows the typical buckling response of the sheathed studs. The P-Δ curve, shown in Figure 2.15(a), is similar to Response D in Figure 2.2. It displays an initial out-of-straightness that is clearly significantly greater than 0, and an axial compressive capacity occurs at a finite mid-height deflection. Figure 2.15(b) shows the corresponding Southwell Plot, which can be examined to provide a preliminary quantification of the influences of a nonlinear stress-strain relationship in the wood stud and a nonlinear load-slip response in the fastener connections. That is, the inverse of the tangent slope of the Southwell Plot, P_1, is proportional to the tangent flexural stiffness of the sheathed stud (e.g., Southwell, 1931, and Spencer and Walker, 1975).

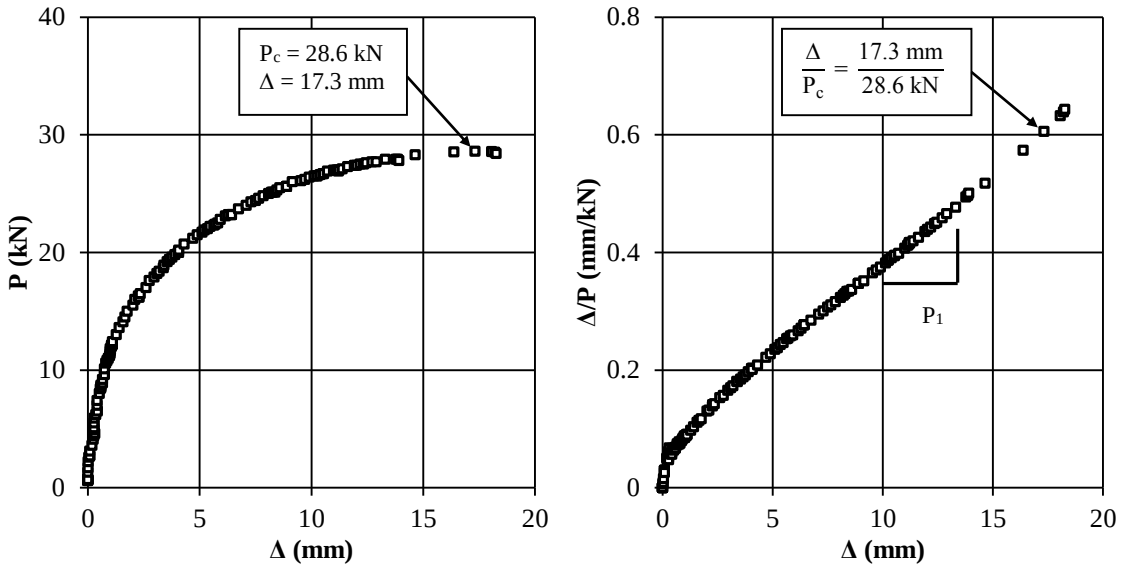

(a) Axial Load vs. Lateral Mid-Height Deflection (b) Southwell Plot

Figure 2.15: Typical Buckling Response of Type A Sheathed Stud Specimen

Figure 2.16 shows P_1 as a function of Δ. The curve has an upper bound equal to P_e for a linear-elastic response (Southwell, 1931) obtained using Equation [2.1], with EI_c computed using Equations [2.3] through [2.14]. The mean value for E_{GB}, 1780 MPa, was assumed, and k_f was taken as the mean value of the data in Appendix 3A, i.e., 940 N/mm for Type A specimens or 2100 N/mm for Type B specimens. For this specimen, E_s was determined from bending tests to be 7490 MPa, b_{GB} = 300 mm, and k_f = 940 N/mm, thus P_e was predicted to be 37.6 kN. The value for P_1 was always below P_e, indicating an immediate decrease in flexural stiffness. The early stage of the wood stress-strain relationships in compression has been idealized to be nearly perfectly linear-elastic (e.g., Ylinen, 1956; O'Halloran, 1973; Glos, 1978; and Song and Lam, 2009), whereas the early stages of the load-slip response of gypsum-board fastener connections has been shown experimentally to be nonlinear (e.g., Liew et al., 2006). Therefore, it can be presumed that the immediate decrease in flexural stiffness is due to nonlinearity in the response of the fastener connections.

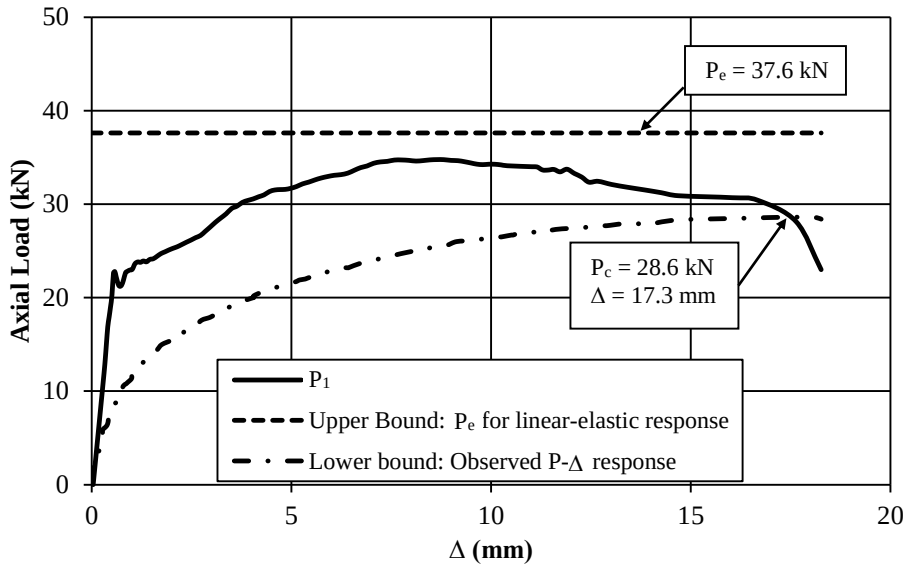

Figure 2.16: Inverse Slope of Southwell Plot, P_1, for Type A Sheathed Stud Specimen

The relationship also has a lower bound given by the actual P-Δ response of the sheathed stud from Figure 2.15(a), which is reproduced again in Figure 2.16. The axial compressive capacity of the sheathed stud corresponds to P_1 equaling the applied axial load, i.e., P_c equal to 28.6 kN when Δ equals 17.3 mm. The gradual reduction of P_1 at Δ greater than 9 mm and the sudden reduction of P_1 as Δ approached 17.3 mm can be attributed to the nonlinear wood stress-strain relationship.

The stress and strain of the wood could not be measured during the buckling tests. Thus, attributing the reduction in P_1 to the response in the wood is explained by eliminating nonlinear fastener response as a possible cause. Figure 2.17 shows the typical slips for the end and quarter-point fasteners on the concave side and end fasteners on the convex side, which were consistent from test to test. Results from Liew et al. (2006) show the fastener load-slip response to be nearly perfectly plastic for δ_f greater than 1 mm, a limit which occurred at end and quarter-point fasteners on the concave side within a mid-height deflection of 5 and 10 mm, respectively. The end fasteners on the convex side are subjected to substantially less slip, and so have a markedly smaller role. Therefore, the influence of a nonlinear fastener response on the stiffness of the sheathed stud and thus on P_1 occurs

mostly within a mid-height deflection of 10 mm, and should not have a considerable influence for Δ greater than 10 mm.

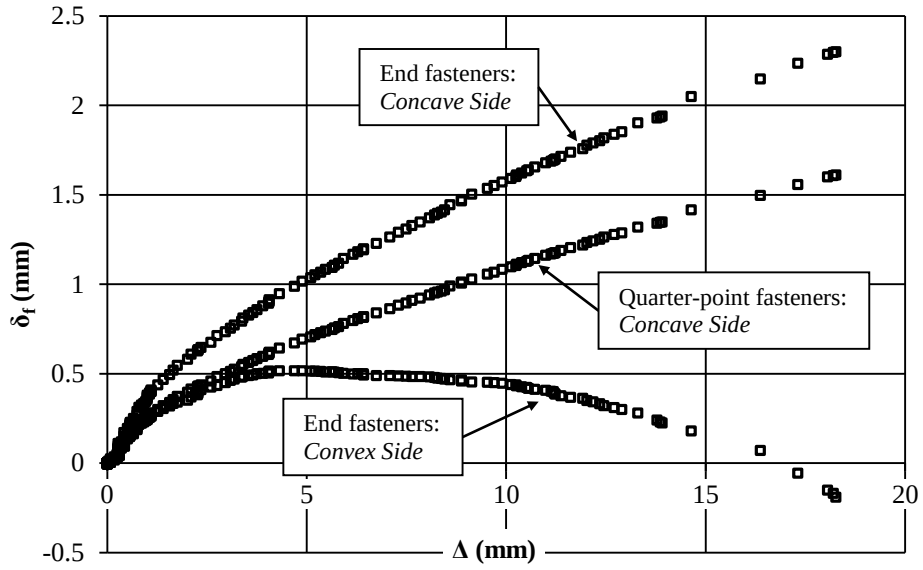

Figure 2.17: Fastener Slip on Concave and Convex Sides vs. Mid-Height Deflection

Conversely, the wood stress-strain relationship is initially linear and becomes nonlinear only once the stress is large and approaches the crushing stress (Ylinen, 1956; O'Halloran, 1973; Glos, 1978; Song and Lam, 2009). In the example shown in Figure 2.16, the stress in the extreme fiber of the stud is 18.3 MPa when Δ equals 17.3 mm, and only 8.7 MPa when Δ equals 5 mm. Assuming the crushing stress is greater than 18.3 MPa, it can be assumed that the stress-strain relationship of the wood is still linear when the stress equals 8.7 MPa. Nonlinearity in the wood stress-strain relationship should not considerably influence any difference between P_1 and P_e when Δ equals 5 mm. The observed difference can, therefore, be attributed to the nonlinearity of the fastener response.

Nonlinearity in both the wood stress-strain relationship and the fastener response reduced the capacity of the sheathed stud shown in Figure 2.16 from 37.6 kN to 28.6 kN, or by 24%. For all tests, the reduction in the sheathed stud capacity averaged approximately 20%, as shown in Table 2.7. This is a substantial reduction in axial capacity that is not properly predicted using the methodologies presented by Kamiya (1987 and 1988) and Srikanth

(1992). That is, nonlinear wood stress-strain relationship with a crushing stress and nonlinear load-slip response of fastener connections must be considered to predict the axial capacity of gypsum-board-sheathed wood studs. And so, a new analytical model is needed. To help with the subsequent validation of this new model, Table 2.7 also lists the corresponding values for E_s and b_{GB} for all sheathed studs investigated.

Table 2.7: Summary of Experimental Buckling Test Results

Stud	E_s *(MPa)*	b_{GB} *(mm)*	P_c *(kN)*	Δ at $P = P_c$ *(mm)*	P_e *(kN)*	$1 - P_c / P_e$
Type A Specimens						
1	4750	400	20.0	16.2	27.5	0.27
2	7310	200	25.9	20.2	36.0	0.28
3	7490	300	28.6	17.3	37.6	0.24
4	8140	300	33.5	12.7	40.1	0.16
5	8780	400	36.6	9.3	42.4	0.14
6	9240	300	31.9	18.6	44.3	0.28
7	9300	200	34.2	19.4	45.1	0.24
8	9890	400	35.2	14.8	47.3	0.26
9	10090	300	36.7	23.2	47.5	0.23
10	10420	300	38.1	19.6	47.7	0.20
11	11100	400	47.1	16.4	51.9	0.09
12	12170	300	46.5	19.1	55.3	0.16
13	12840	300	48.2	13.6	57.8	0.17
14	13350	400	49.1	18.1	60.3	0.19
Type B Specimens						
15	5950	300	25.7	26.2	37.9	0.32
16	8310	300	42.8	19.2	47.3	0.10
17	10000	300	45.2	20.4	53.9	0.16
18	11110	300	45.3	20.8	58.1	0.22
19	12400	300	52.3	23.2	63.1	0.17
					Average	0.20
					St. Dev	0.06

2.5 Contribution of Gypsum-board Sheathing

To compare the axial compressive resistance of the bare and sheathed studs, the same stud must be tested twice, i.e., with and without gypsum-board sheathing. Therefore, the destructive testing approach used to quantify the axial compressive resistance of sheathed studs cannot be applied to bare studs. A non-destructive testing approach is needed where axial loads are applied causing a limited mid-height deflection and uses the resulting

Southwell Plot to predict the axial compressive resistance. This method, however, does not capture the effects of nonlinear material response which occurs at larger mid-height deflections. The predicted resistance of bare studs from these non-destructive tests cannot be directly compared to the resistance of sheathed studs observed from destructive buckling tests. Therefore, to quantify of the contribution of gypsum-board sheathing, the axial compressive resistance of sheathed studs was predicted using Southwell Plots from buckling tests with similar limited mid-height deflection. For these tests, a mid-height deflection limited to 5 mm was considered to be non-destructive. At these mid-height deflections, however, the fastener responses were mostly linear. Therefore, the predicted axial capacity of the sheathed stud also does not account for nonlinear fastener response.

Twelve bare studs, braced about their weak-axis as shown in Appendix 2A, were chosen at random and subjected to non-destructive buckling tests. The tests were repeated after the gypsum-board sheathing was applied. The typical P-Δ response in Figure 2.18(a) shows the sheathed stud to have markedly greater resistance for a given mid-height deflection. The P_1 values are quantified using the Southwell Plots in Figure 2.18(b): the axial compressive resistance of the bare stud is 48.3 kN and increased by 34%, to 64.5 kN, for the sheathed stud.

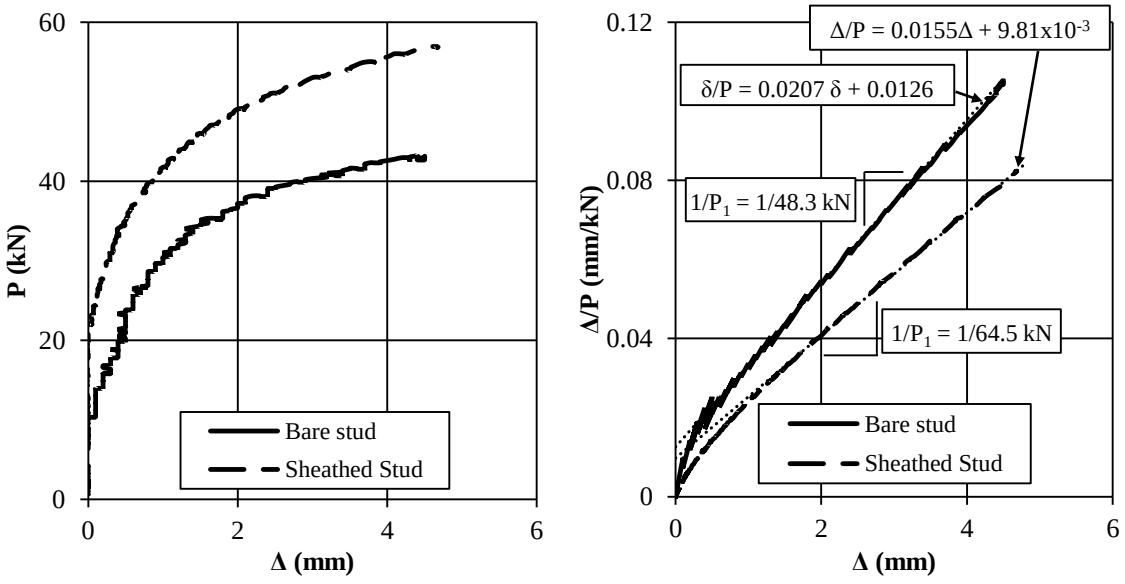

(a) Axial Load vs. Lateral Mid-Height Deflection (b) Southwell Plot

Figure 2.18: Comparison between Bare and Gypsum-board-sheathed Wood Studs

The sheathing increased the values of P_1 of the twelve wood studs by a mean of 29% with a CoV of 0.129, as shown in Table 2.8. The large CoV can be attributed to a variable wood modulus of elasticity, where the contribution of gypsum-board sheathing is expected to increase for weaker studs. Also, it can be attributed to the inconsistency in the P_1 for Δ less than 5 mm, as shown in Figure 2.16. Therefore, for more accurate estimates of the contribution of gypsum-board sheathing to the axial compressive resistance of wood studs, analytical models are needed to quantify the axial compressive resistance of bare and sheathed studs with identical wood properties.

Table 2.8: Contribution of Gypsum-board sheathing to the Inverse Slope of Southwell Plot, P_1

P_1 (kN)		$P_{1\,(SHEATHED)}$/
Bare Stud	Sheathed Stud	$P_{1\,(BARE)}$
30.4	42.2	1.39
31.2	53.7	1.72
35.0	53.5	1.53
35.3	50.3	1.42
36.8	37.0	1.01
40.8	55.3	1.36
41.2	53.3	1.29
41.8	45.2	1.08
46.3	53.9	1.16
47.2	52.1	1.10
47.4	50.1	1.06
48.3	64.5	1.34
	Mean	1.29
	CoV	0.129

2.6 Summary and Conclusions

Part 9 of the National Building Code of Canada (NRC, 2010) and the Engineering Guide for Wood-frame Construction (CWC, 2009) are mute in addressing any potential increase gypsum-board sheathing may provide to the axial compressive resistance of wood stud walls. Analytical models by Kamiya (1987 and 1988) and Srikanth (1992) were reported to predict the stiffness and axial capacity of wood studs with wood sheathing. However, the assumptions used to create these models have not been validated for use with gypsum-board-sheathed wood studs. Specifically, the effects of nonlinearity in the wood stress-

strain relationship of the stud with a crushing were consistently ignored, and only one study considered the effects of a nonlinear fastener load-slip response.

This chapter has explored the consequences of the assumptions of each model to determine the effects on the axial load vs. lateral mid-height deflection (P-Δ) response of sheathed studs. An experimental testing program was then designed to obtain realistic P-Δ responses of 19 gypsum-board-sheathed wood studs, and concentrated specifically on 2440 mm long 38 x 89 mm spruce-pine-fir (SPF) studs with 12.7 mm gypsum-board sheathing on both sides, i.e., typical dimensions in residential light-frame construction. Individual sheathed studs may fail by buckling about their weak-axis, whereas stud walls do not exhibit this failure mode. Therefore, the testing program initiated with a numerical analysis to determine the required gypsum-board width to ensure strong-axis buckling of individual sheathed studs. The resulting P-Δ responses of the testing program were analyzed and compared to predicted results from models by others. Finally, the contribution of gypsum-board sheathing was quantified using predicted capacities for bare and sheathed studs.

The conclusions of this chapter are:

1. The influences of the wood stress-strain relationship being nonlinear with a finite crushing stress, and the fastener load-slip response also being nonlinear are significant. Accounting for these features creates a distinctive P-Δ response of sheathed studs, where the maximum axial compressive resistance occurs at a finite mid-height deflection. As a result, this predicted axial capacity is smaller than that predicted assuming linear-elastic stress-strain relationships and linear fastener load-slip responses.

2. For tests of isolated sheathed studs with effective lengths of 2440 mm, a gypsum-board width of 300 mm is required to ensure strong axis buckling. This value was validated using 19 test specimens with gypsum-board widths between 150 and 400 mm. The methodology used to derive Figure 2.6 could be readily applied to investigate other effective lengths.

3. The experimentally observed P-Δ responses were similar to those predicted when accounting for nonlinear wood stress-strain relationship, with a finite crushing

stress, and nonlinear fastener load-slip response. That is, the maximum axial resistance occurred at an average mid-height deflection, Δ, of approximately 20 mm, and this axial capacity was on average 20% less than that predicted assuming linear-elastic material properties and linear load-slip responses. Therefore, the models currently available in literature, that adopt these assumption, are not suitable for predicting the axial compressive capacity of gypsum-board-sheathed wood studs; an improved analytical methodology is needed.

4. The gypsum-board sheathing increased the axial capacity of wood studs by a mean of 29% and a coefficient of variation of 0.129. This increase is computed using Southwell Plots for mid-height deflections up to 5 mm and so does not account for the nonlinear material response in the wood and nonlinear fastener response.

2.7 References

American Society for Testing and Materials (ASTM). 2007. C1002-07: Steel Self-Piercing Tapping Screws for the Application of Gypsum Panel Products or Metal Plaster Bases to Wood Studs or Steel Studs. Annual Book of ASTM Standards, West Conshohocken, PA., USA.

American Society for Testing and Materials (ASTM). 2011. C1396-11: Standard Specification for Gypsum Board. Annual Book of ASTM Standards, West Conshohocken, PA., USA.

Bleau, R., 1984. Comportement des Poutre-Colonnes en Bois. M.Sc.A. Thesis, Department of Civil Engineering, University of Sherbrooke, QC.

Buchanan, A. H., 1984. Strength Member and Design Methods for Bending and Axial Load Interaction in Timber Members. Ph.D. Thesis, Department of Civil Engineering, University of British Columbia, BC. 298 p.

Canadian Standards Association (CSA), 2009. CAN/CSA-086-09: Engineering Design in Wood. Canadian Wood Council, Ottawa, ON.

CISC, 2004. Handbook of Steel Construction: Eighth Edition, Second Printing. Canadian Institute for Steel Construction, Willowdale, ON.

CWC, 2009. Engineering Guide for Wood Frame Construction. Canadian Wood Council, Ottawa, ON.

Gad, E. F., 1997. Performance of Brick-Veneer Steel-Framed Domestic Structures under Earthquake Loading. Ph.D. Thesis, Department of Civil and Environmental Engineering, University of Melbourne, Melbourne, AUS. 360 p.

Glos, P. 1978. Berichte zur Zuverlassigkeitsheorie der Bauwerke: Zur Bestimmung des Festigkeitsverhaltens von Brettschichtholz bei Druckbeanspruchung aus Werkstoff- und Einwirkungskenngrossen. (Reliability Theory for Timber Structures: Determination of Compression Strength Behaviour of Glulam Components from Interaction of Material Properties). Heft 34/1978, Laboratorium fur den Konstrucktiven Ingenierubau, Technische Universitat Munchen, Munich, Germany. 335 p.

Gromala, D. S., 1985. Lateral Nail Resistance for Ten Common Sheathing Materials. Forest Products Journal, Vol. 35, No. 9, pp. 61-68.

Groom, K. M., 1992. Nonlinear Finite-Element Modeling of Intercomponent Connections in Light-Frame Wood Structures. M.Sc. Thesis, Department of Civil Engineering, Oregon State University, Corvallis, OR, USA. 167 p.

Kamiya, F., 1987. Buckling Theory of Sheathed Walls: Linear Analysis. Journal of Structural Engineering, Vol. 114, No. 9, pp. 625-641.

Kamiya, F., 1988. Buckling of Sheathed Walls: Nonlinear Analysis. Journal of Structural Engineering, Vol. 113, No. 3, pp. 2009-2022.

Lau, W. W., 2000. Strength Model and Finite Element Analysis of Wood Beam-Column in Truss Applications. Ph.D. Thesis, Department of Wood Science, University of British Columbia, Vancouver, BC, 188 p.

Lee, Y., 1999. Behavior of Gypsum-Sheathed Cold-Formed Steel Wall Stud Panels. Ph.D. Thesis, Department of Civil, Construction, and Environmental Engineering, Oregon State University, Corvallis, OR, USA. 327 p.

Liew, Y. L., Gad, E. F., and Duffield, C. F., 2006. Experimental and Analytical Validation of a Fastener Bearing Test as a Means of Evaluating the Bracing Characteristics of Plasterboard. Advances in Structural Engineering, Vol. 9, No. 3, pp. 421-432.

Marxhausen, P. D. and Stalnaker, J. J., 2006. Buckling of Conventionally Sheathed Stud Walls. Journal of Structural Engineering, Vol. 132, No. 5, pp. 745-750.

NRC. 2010. National Building Code of Canada - Part 9: Housing and Small Buildings. Institute for Research in Construction, National Research Council of Canada, Ottawa, ON.

O'Halloran, M. R., 1973. Curvilinear Stress-Strain Relationship for Wood in Compression. Ph.D. Thesis, Department of Civil and Environmental Engineering, Colorado State University, Fort Collins, CO. USA. 129 p.

Song, X. and Lam, F., 2009. Laterally Braced Wood Beam-Columns Subjected to Biaxial Eccentric Loading. Computers and Structures, Vol. 87, pp. 1058-1066.

Southwell, R.V. 1931. On the Analysis of Experimental Observations in Problems of Elastic Stability. Proceedings of the Royal Society of London. Series A, Containing Papers of a Mathematical and Physical Character, Vol. 135, No. 828, pp. 601-616.

Spencer, H.H., and Walker, A.C. 1975. Critique of Southwell Plots with Proposals for Alternative Methods. Experimental Mechanics, Vol. 15, No. 8, pp. 303-310.

Srikanth, T. S. 1992. Structural Reliability of Light-Frame Wood Systems with Composite Action and Load Sharing. Ph.D. Thesis, Department of Forest Products, Oregon State University, Corvallis, OR, USA. 218 p.

Ylinen, A., 1956. A Method of Determining the Buckling Stress and the Required Cross-Sectional Area for Centrally Loaded Straight Columns in Elastic and Inelastic Range. IABSA Publications, Vol. 16, pp. 529-549

Chapter 3 Experimental Investigation of Shear Load-Slip Response of Gypsum-Board-to-Wood-Stud Fastener Connections

3.1 Introduction

The increased axial compressive resistance of wood studs with gypsum-board sheathing is not addressed in Part 9 of the National Building Code of Canada (NBCC) (NRC, 2010) or the Engineering Guide for Wood-Frame Construction (CWC, 2009). The testing program reported in Chapter 2 concluded that a new analytical model is needed to predict the axial compressive capacity of sheathed studs, which is sensitive to the inherent nonlinear load-slip response of fastener connections (e.g., Gromala, 1985, and Liew et al., 2006). However, no clear idealization of the load-slip response for gypsum-board-to-wood-stud fasteners was presented in or can be inferred from the literature. Also lacking is an investigation of the effect of various fastener locations, gypsum-board edge types, gypsum-board orientation, rate-of-displacement (ROD), and moisture content (MC) appropriate to common gypsum board used in Canada. Therefore, before a new analytical model for sheathed studs can be validated, this chapter presents an experimental investigation to quantify the load-slip response of fastener connections subjected to shear.

3.1.1 Typical Slip Values

Laboratory tests (discussed in Chapter 2) captured the range of slip, δ_f, for fastener connections at the onset of buckling of a gypsum-board-sheathed wood stud, with maximum values occurring at the fasteners located at the ends of the stud, as shown in Figure 3.1. The maximum applied load generally corresponded to a lateral mid-height deflection, Δ, of 20 mm for a 2440 mm wall, i.e., $\Delta \approx L/120$. Fasteners on the concave side of the buckled shape compressed the gypsum board, and so were subjected to positive δ_f that reached up to 2.7 mm at the maximum applied load. The response of fasteners on the convex side was more complex because, as Δ increases, the direction of shear transfer on

the convex side of the buckled shape reverses (e.g., Kamiya, 1987). This response can be separated into the following three phases:

Phase 1 - A compression load is initially transferred into the gypsum board, creating positive δ_f that gradually increases to 0.5 mm when Δ is between 3 and 5 mm.

Phase 2 - The value of δ_f decreases from its maximum positive value, approaching zero when Δ is approximately 17 mm.

Phase 3 - A load reversal occurs as the δ_f becomes negative, causing tension in the gypsum board on the convex side. The value of δ_f did not exceed -0.4 mm when the axial capacity of the sheathed stud is reached.

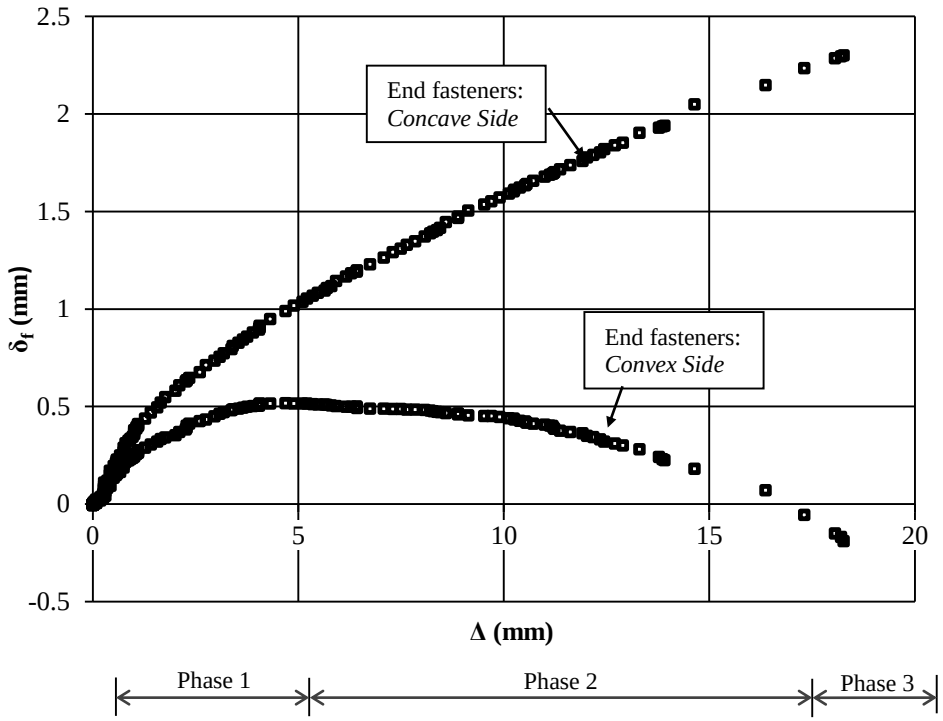

Figure 3.1: Typical Slip Values of Fastener Connections at End of Stud

In this chapter, the maximum lateral mid-height deflection, Δ, was assumed to be equal to L/100, i.e., roughly 25 mm for stud lengths of 2440 mm, to cover the full range of δ_f that

could occur. The response of the connections on the concave side and in Phase 1 on the convex side was, therefore, investigated to a maximum positive δ_f of 3 mm. The response of connections in Phase 3 on the convex side was investigated to a maximum negative δ_f of -1 mm.

3.1.2 Fastener Connection Classification

Fastener connections can be defined by their location, edge type, and paper orientation of the gypsum board, as shown in Figure 3.2. Each fastener location is defined by its side distance perpendicular to the direction of the applied load, e_s, and end distance parallel to the direction of the applied load, e_n, as shown in Figure 3.2(a). Fasteners can be located: along the side of the gypsum board with small e_s and large e_n; along the end with large e_s and small e_n; at a corner with small e_s and e_n; or, in the interior with large e_s and e_n. Each edge can be further classified as cut or tapered, as shown in Figure 3.2(b). Cut edges are created in the field using a utility knife, whereas tapered edges are formed in the factory and are thinner and denser with paper wrapped around the edge. The orientation of the gypsum board can cause paper to be loaded in the machine or cross-machine direction. Figure 3.2(c) presents the symbols used to define the location, edge type, and paper orientation of each test specimen.

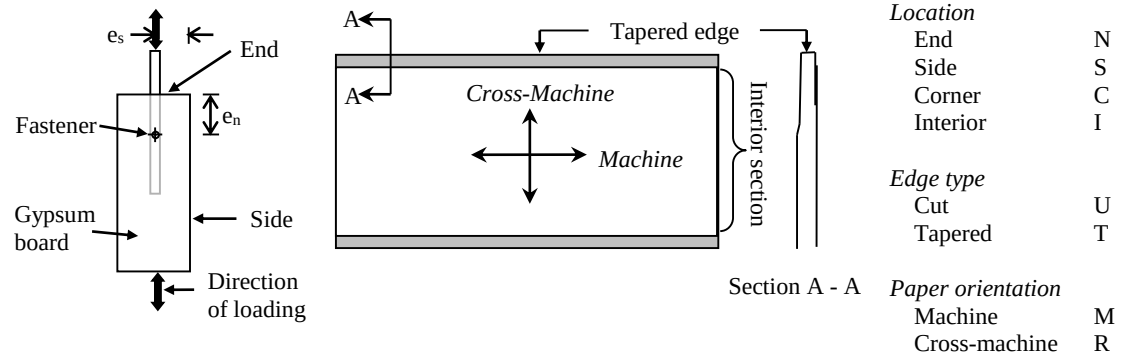

(a) End and side distance (b) Typical gypsum board (c) Symbols

Figure 3.2: Parameters Defining Gypsum-board Fastener Connections

Figure 3.3 shows the possible fastener locations on a gypsum-board-sheathed stud wall in accordance with Part 9 of the NBCC (NRC, 2010) accounting for typical construction techniques (Rousseau, 2011). End Stud 1 is typically braced by a perpendicular wall. Single Studs 4 and 6 are placed at each side of the wall opening with the headers that frame the opening connected using metal hangers, in accordance with "Advanced Framing" techniques (e.g., Lstiburek, 2005). This arrangement has a smaller buckling capacity than bulkier conventional designs with double studs on each side of the opening. Gypsum board to the left of the opening is shown with the machine direction of the paper in vertical direction. Conversely, the gypsum board to the right of the opening is shown with the machine direction of the paper in the horizontal direction. Both orientations are common in practice (Rousseau, 2011), although both would not typically be used in a single wall. Six different types of connections, labeled I to VI, define all possible gypsum-board-sheathing-to-wood-stud connections on the convex side. On the concave side of the buckled shape, Connection Types I, III, and VI do not differ from Types II, IV, and V, respectively.

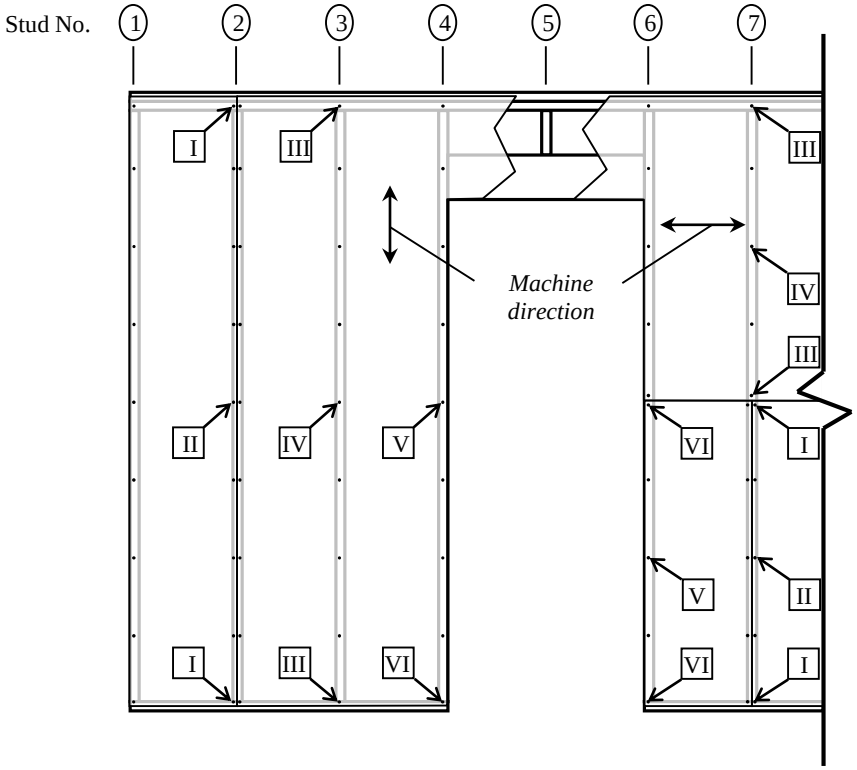

Figure 3.3: Typical Fastener Location on Sheathed Wood-Stud Wall

A detailed summary of fastener location with side and end distances, edge type, and paper orientation is presented in Table 3.1. Part 9 of the NBCC (NRC, 2010) permits fasteners to be located a minimum of 10 mm from the perimeter of the gypsum board. Installation methods for fasteners along the top and bottom plates, i.e., Connection Types I, III, and VI at the top and bottom plate in Figure 3.3, generally limit the minimum end distance to 19 mm (Rousseau, 2011). A minimum side distance of 19 mm is used for fasteners along Studs 4 and 6 near openings and can be reduced to a minimum of 10 mm for fasteners at joints along interior Studs 2 and 7.

Table 3.1: Details of Fastener Connection Types

Connection Type	Stud #	Fastener location	e_n *(mm)*	e_s *(mm)*	Edge type		Paper orientation
					Side	End	
I	2	Corner	19	10 to 19	Tapered	Cut	Machine
	7	Corner			Cut	Both[a]	Cross-Mach.
II	2	Side	∞	10 to 19	Tapered	-	Machine
	7	Side			Cut	-	Cross-Mach
III	3	End	19	∞	-	Cut	Machine
	7	End			-	Both[a]	Cross-Mach
IV	3	Interior	∞	∞	-	-	Machine
	7	Interior			-	-	Cross-Mach
V	4	Side	∞	19	Cut	-	Machine
	6	Side			Cut	-	Cross-Mach
VI	4	Corner	19	19	Cut	Cut	Machine
	6	Corner			Cut	Both[a]	Cross-Mach

[a] End of gypsum board can be either cut or tapered.

3.1.3 Literature Review of Shear Load-Slip Response

The shear load-slip response, defined by the shear load, V, at specified values of δ_f, of interior and side fastener connections located on the concave or convex sides is influenced only by the bearing strength of the gypsum board. If, however, the side distance is very small, the response of side connections may be influenced by both the bearing and block shear strengths of the gypsum board. Furthermore, the load-slip response of end and corner connections causing tension in the gypsum board on the convex side during Phase 3 of the response may also be influenced by both the bearing and block shear strengths of the

gypsum board (Liew et al., 2006). Therefore, the responses of side, end, and corner connections may be different from those of interior connections.

The strength of fastener connections in gypsum-board-sheathed wood studs subjected to monotonically increasing loads was investigated by Gromala (1985) and Liew et al. (2006). Figure 3.4 superimposes the average shear load-slip response reported by Gromala (1985) on typical results from Liew et al. (2006). Gromala (1985) tested nine specimens constructed using three different sheets of 12.7 mm gypsum board. The orientation of the paper was not controlled. Tests were conducted to ASTM D1761-74 (ASTM, 1974): only end distances of e_n of 19 mm were investigated; the gypsum board was conditioned in an environment with a relative humidity (RH) of 65%; and specimens were tested with a rate-of-displacement (ROD) of the cross-head of 2.5 mm/min (these criteria remain in ASTM D1761-06 (ASTM, 2006)). The relationship shown in Figure 3.4 was quantified using the average load at various magnitudes of δ_f. Liew et al. (2006) present typical results based on a previous experimental investigation (Liew et al., 2004) of 144 shear specimens with fasteners located at unreported small end distances and in the interior section of the gypsum board. The machine direction of the paper was always parallel to the applied load. The average MC of the gypsum boards was 10.1% with a coefficient of variation (CoV) of 0.03. Specimens were tested with a ROD of the cross-head of 25 mm/min. As shown, the end specimens tested by Gromala (1985) showed increased resistance at δ_f greater than 1 mm whereas those tested by Liew et al. (2006) showed decreased resistance at similar values of δ_f. It is not clear if this discrepancy is due to different gypsum board, ROD, or MC investigated in these studies.

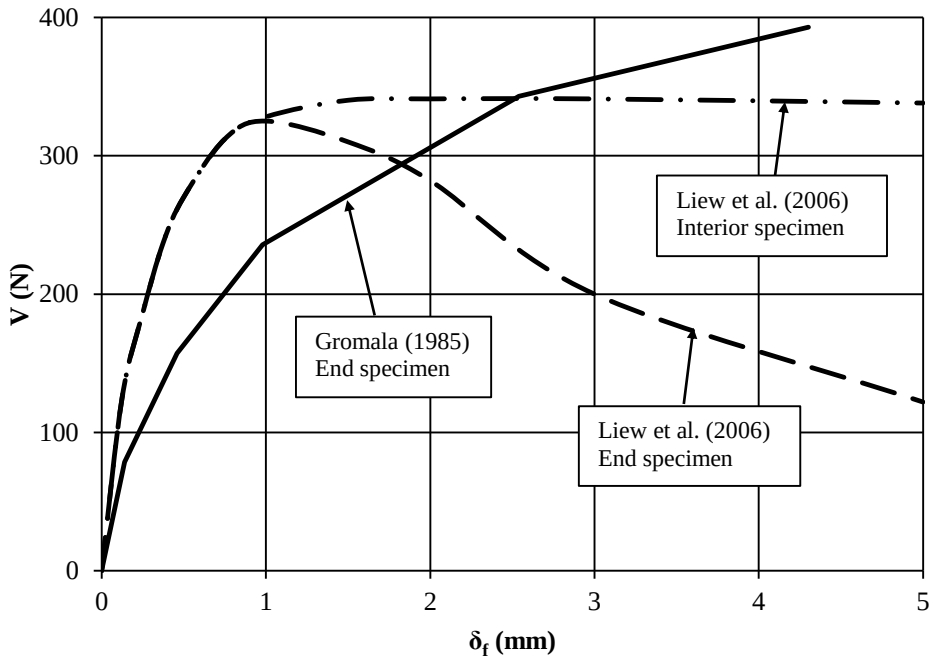

Figure 3.4: Shear Load-slip Response Reported by Gromala (1985) and Liew et al. (2006)

Gad (1997) studied the shear strength of fastener connections in steel studs, yet no data or illustrations of the shear load-slip responses were provided. Both Gad (1997) and Liew et al. (2006) derived but do not report a nonlinear idealization of the load-slip response for maximum δ_f beyond 10 mm that corresponds to shear wall failure modes. Regardless, such idealizations might not be accurate at the lower maximum δ_f that correspond to buckling of sheathed wood studs.

No studies address the impact of load reversals when fastening gypsum board to wood studs. Gromala (1985) conducted cyclic tests, although no clear conclusion can be taken from these results. Gad's (1997) work with steel studs and a study by Li et al. (2012) on nailed wood connections both identify a pinching effect, as shown in Figure 3.5, which occurs after a load reversal as the fastener slips through a previously enlarged hole, and so no longer bears against the sheathing.

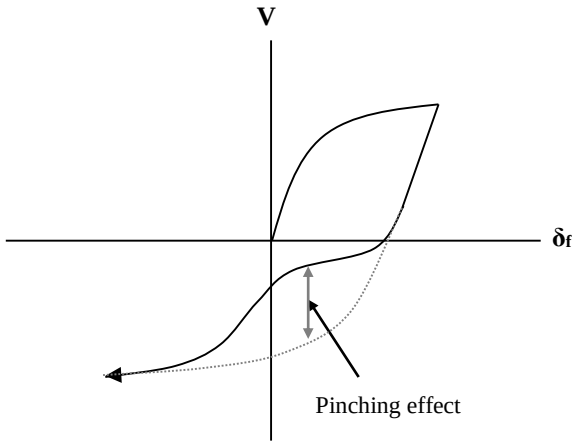

Figure 3.5: Pinching Effect in Load-Slip Response due to Load-reversal

Others have investigated the material properties of the gypsum board. Liew et al. (2004) conducted simple bearing tests on gypsum board at a temperature of 20°C and a RH of 46%. For RODs of the cross-head of 25 mm/min and 12.5 mm/min, no significant strength differences were observed. For a ROD of 25 mm/min, ultimate loads decreased by 60% when the temperature and the RH were increased to 32°C and 100%, respectively. Wolfe (1983) observed that the tensile strength of the paper, isolated from the gypsum core, was four times stronger when loaded in the machine direction compared to the cross-machine direction.

No clear conclusions can be made from these studies about the influence of the fastener location, ROD, MC, or paper orientation on the load-slip response of this connection in shear. The information is at best incomplete or obtained from poorly controlled experiments. Not all possible fastener locations are reported, e.g., side and corner connections were not tested. The influence of ROD was investigated for rates of 12.5 to 25 mm/min and does not consider slower rates. The humidity levels investigated simulated extreme conditions, given recommended interior RH levels are between 20 to 60% (e.g., CenterPoint Energy, 2006), so the gypsum-board MC may be unrealistically high. The orientation of the paper was not evaluated for shear connection tests.

3.1.4 Objectives and Methodology

The objectives of the research reported in this chapter are as follows:

1. Identify significant parameters that influence the shear load-slip response of the screw fastener connections. The parameters considered are: fastener location, edge type, orientation of gypsum board, MC of gypsum board, thickness of gypsum board, and ROD.

2. Idealize the shear load-slip response under monotonically increasing loads considering all significant parameters. This idealization would be implemented for all fasteners on the concave side as well as Phases 1 and 3 of the response for fastener connections on the convex side.

3. Investigate the effect of a single and multiple load reversals on the shear load-slip response. This will determine the behaviour during the unloading phase (Phase 2) and calibrate Phase 3 of the response for fastener connections on the convex side of the buckling shape.

These objectives are achieved through a testing program of shear connections consisting of 12.7 mm gypsum board fastened to 2x4 SPF wood studs with 32 mm coarse gypsum-board screws. Data obtained by Van Bruinessen (2012) for 15.9 mm gypsum board and 41 mm coarse gypsum-board screws are also included in the analysis. All gypsum board tested were in accordance with ASTM C1396-11 (ASTM, 2007), and all screws tested were in accordance with ASTM C1002-07 (ASTM, 2007).

Subsequent sections in this chapter present: a method for testing the shear load-slip response; an analysis of the influence of various parameters on the shear load-slip responses; and, a numerical idealization of the shear load-slip response.

3.2 Experimental Study

A total of 241 specimens with 12.7 mm thick gypsum board were tested under monotonically increasing loads. Van Bruinessen (2012) tested 42 additional specimens

with 15.9 mm thick gypsum board using the same specimen design and test setup as described herein. Another 15 specimens with 12.7 mm thick gypsum board were subjected to single load reversals.

3.2.1 Properties of Gypsum Board

Test specimens were constructed using Sheetrock® brand regular and low-density 12.7 mm gypsum board with the typical cross-sections shown in Figure 3.6. The physical and chemical properties of each gypsum board were obtained from their respective Material Safety Data Sheet (MSDS) (CGC Inc., 2012a and 2012b). The strengths of the boards are not reported by the manufacturer, yet are specified to be in accordance with ASTM C1396 (ASTM, 2011). The regular gypsum board, with a bulk density of approximately 890 kg/m^2, has been commonly used in residential structures in Canada over the last few decades. The low-density gypsum board, with a bulk density of approximately 480 kg/m^2, has recently been introduced and is now replacing regular gypsum board in the residential construction market. The chemical properties reported on the MSDS sheets for both regular and low-density gypsum boards are essentially identical. Therefore, as is clearly visible in Figure 3.6, the low-density gypsum board has larger air voids that decrease its density and may impact its compressive strength and stiffness.

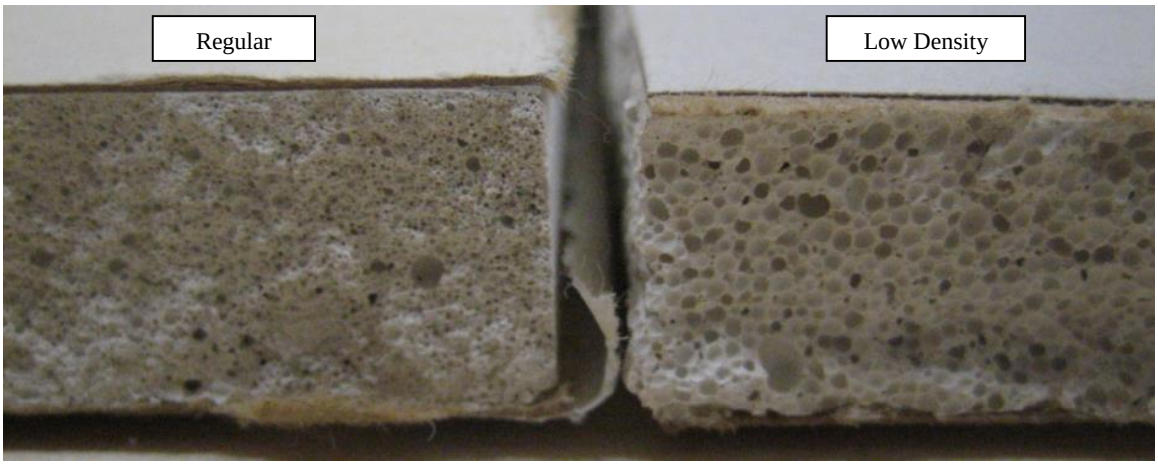

Figure 3.6: Regular and Low-density Gypsum Board

3.2.2 Monotonic Loaded Tests

Interior and side connections can transfer either compression or tensile loads to the gypsum board. These connections were tested under monotonically increasing loads to simulate the response of fastener connections on the concave side and in Phases 1 and 3 on the convex side. End and corner connections mimic side connections when transferring compression loads to the gypsum board, yet are susceptible to tear out when transferring tensile loads. Therefore, these connections were tested under monotonically increasing loads to simulate the response of fastener connections in Phase 3 on the convex side.

Table 3.2 lists the 24 test series investigated, each comprising up to 12 replicate tests, covering all connection types shown in Figure 3.3. Specimens are defined using the notation shown in Figure 3.2 by fastener location: N, S, C, or I. Subscripted symbols define the edge type (cut, U, or tapered, T) and paper orientation (machine, M, or cross-machine, R) and include a number defining the side distance (10 or 19 mm). For example, side specimen $S_{UM\text{-}19}$ has a cut edge, the machine direction of the paper parallel to the direction of loading, and a side distance of 19 mm. No side distance is specified for end or interior specimens as it is always much larger than 19 mm. Subscripted numbers in parentheses indicate the test series where specific connection settings were subjected to changes in RH, ROD, or type of gypsum board.

Table 3.2: Test Matrix – 12.7 mm Gypsum Board

Specimen / Test series	Connection Type	e_s *(mm)*	e_n *(mm)*	n	Conditioned RH *(%)*	ROD *(mm/min.)*
Regular gypsum board						
Machine direction						
C_{TM-10}[a]	I	10	19	9	25 - 50	2.5
C_{TM-19}[a]	I	19	19	11	25 - 50	2.5
S_{TM-10}	II	10	∞	10	25 - 50	2.5
$S_{TM-19\ (1)}$	II	19	∞	12	25 - 50	2.5
$S_{TM-19\ (2)}$	II	19	∞	11	65	2.5
$N_{UM\ (1)}$	III	∞	19	12	25 - 50	2.5
$N_{UM\ (2)}$	III	∞	19	4	65	2.5
$I_{UM\ (1)}$	IV	∞	∞	12	25 - 50	2.5
$I_{UM\ (2)}$	IV	∞	∞	12	65	2.5
$I_{UM\ (3)}$	IV	∞	∞	11	25 - 50	0.5
S_{UM-19}	V	19	∞	11	25 - 50	2.5
C_{UM-19}	VI	19	19	9	25 - 50	2.5
Cross-machine direction						
C_{TR-10}[b]	I	10	19	8	25 - 50	2.5
C_{TR-19}[b]	I	19	19	7	25 - 50	2.5
C_{UR-10}	I	10	19	12	25 - 50	2.5
C_{UR-19}	I	19	19	12	25 - 50	2.5
S_{UR-10}	II	10	∞	8	25 - 50	2.5
S_{UR-19}	II	19	∞	12	25 - 50	2.5
N_{TR}	III	∞	19	12	25 - 50	2.5
$N_{UR\ (1)}$	III	∞	19	12	25 - 50	2.5
$N_{UR\ (2)}$	III	∞	19	4	65	2.5
I_{UR}	IV	∞	∞	12	25 - 50	2.5
Low density gypsum board						
Machine direction						
$N_{UM\ (3)}$	III	∞	19	6	25 - 50	2.5
$I_{UM\ (4)}$	IV	∞	∞	12	25 - 50	2.5

[a] Corner specimens C_{TM-10} and C_{TM-19} have cut ends and tapered sides.
[b] Corner specimens C_{TR-10} and C_{TR-19} have tapered ends and cut sides.

A total of 193 regular gypsum-board specimens and 18 low-density gypsum-board specimens were tested under laboratory conditions where the environmental RH fluctuated between 25 and 50%. Thirty-two additional regular gypsum-board specimens were conditioned in an environment with a RH of 65%. The resulting MC in the gypsum board of all specimens was measured using a Protimeter Moisture Measurement System calibrated for soft wood, thus the values obtained for the gypsum board are considered nominal (Appendix 2C discusses the bias associated with this measuring technique). The lowest possible reading on this measurement tool is 7.8%. To consider within- and

between-sheet strength variations, gypsum board used to fabricate the specimens in each test series was from at least three different sheets and randomly located within each sheet. The rate of δ_f observed in buckling tests of sheathed studs reported in Chapter 2 ranged from approximately 0.5 mm/min at the start of each test to more than 2.5 mm/min at maximum load. Therefore, a target ROD of the cross-head of 2.5 mm/min was selected for the majority of tests, with the exception of test series $I_{UM\,(2)}$ that was tested at a target ROD of the cross-head of 0.5 mm/min to investigate the effect of varying ROD. Each specimen was tested to a maximum δ_f of 10 mm or until connection fracture occurred.

The test matrix adopted by Van Bruinessen (2012) for 15.9 mm regular gypsum board is reproduced in Table 3.3. Most specimens were tested under dry conditions in a laboratory environment with RH between 25% and 30%, with the exception of one test series where specimens were conditioned in an environment with RH of 40%.

Table 3.3: Test Matrix – 15.9 mm Gypsum Board (Van Bruinessen, 2012)

Specimen / Test series	Connection Type	e_s *(mm)*	e_n *(mm)*	n	Conditioned RH *(%)*	ROD *(mm/min.)*
Regular gypsum board						
Machine direction						
S_{TM-10}	II	10	∞	6	25 - 30	0.8
S_{TM-19}	II	19	∞	6	25 - 30	0.8
N_{UM}	III	∞	19	6	25 - 30	0.8
$I_{UM\,(1)}$	IV	∞	∞	12	25 - 30	0.8
$I_{UM\,(2)}$	IV	∞	∞	6	40	0.8
C_{UM-19}	VI	19	19	6	25 - 30	0.8

Figure 3.7 shows the unique test specimens corresponding to each fastener location. All specimens were tested in compression, so voids were placed in the gypsum board above the connections in end and corner specimens to simulate small end distances. This avoids the need to grip the specimens to conduct tension tests. The wood struts supporting the gypsum board were designed to ensure the load was applied at the gypsum-board-to-stud interface, and so minimized the out-of-plane bending moments. Screws were installed using a typical bit to ensure that the top of the conical screw head did not penetrate the gypsum-board paper. Figure 3.7(a) shows specimens with cut ends, where the load was transferred to the top of the gypsum board through three bolts. Figure 3.7(b) shows

specimens with tapered ends that could not be secured with bolts, so loads were applied at equal eccentricities on each side of the connection to simulate a concentric connection load.

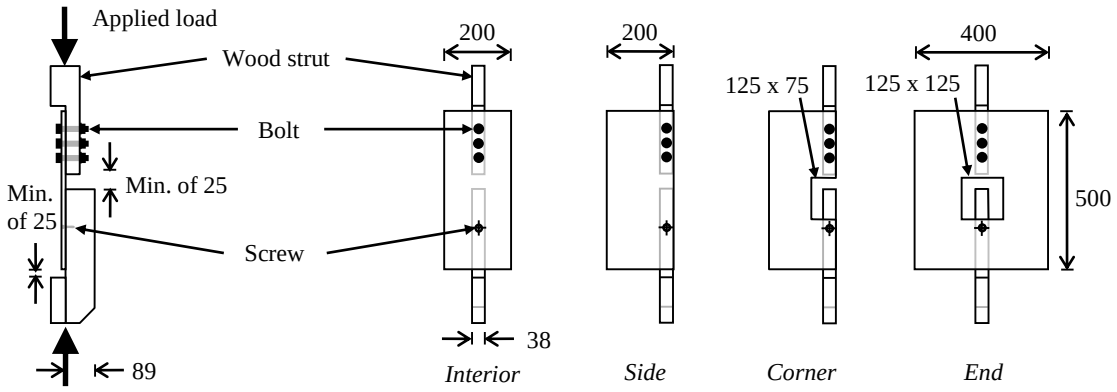

(a) Load transfer mechanism using bolts

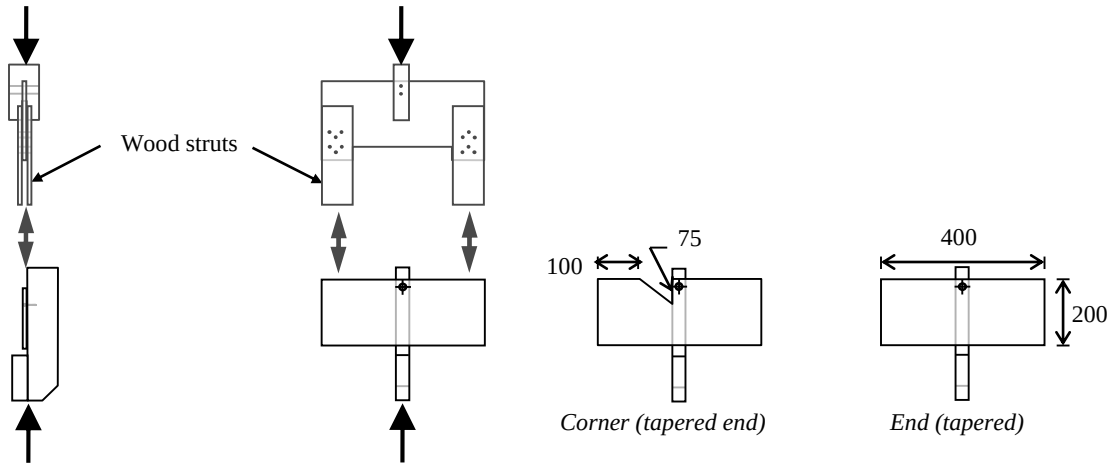

(b) Load transfer mechanism using wood arms for specimens with tapered ends

Figure 3.7: Specimen and Load Apparatus for Different Fastener Location (All Units in mm)

Test specimens were mounted on a load cell, and two 25 mm linear voltage displacement transducers (LVDT) were mounted to measure δ_f and correct for small rotations, as shown in Figure 3.8. Figure 3.8(a) and (b) show typical interior specimens (end specimens are similar). Figure 3.8(c) and (d) show typical side specimens (corner specimens are similar). Figure 3.8(e) and (f) show specimens with tapered ends.

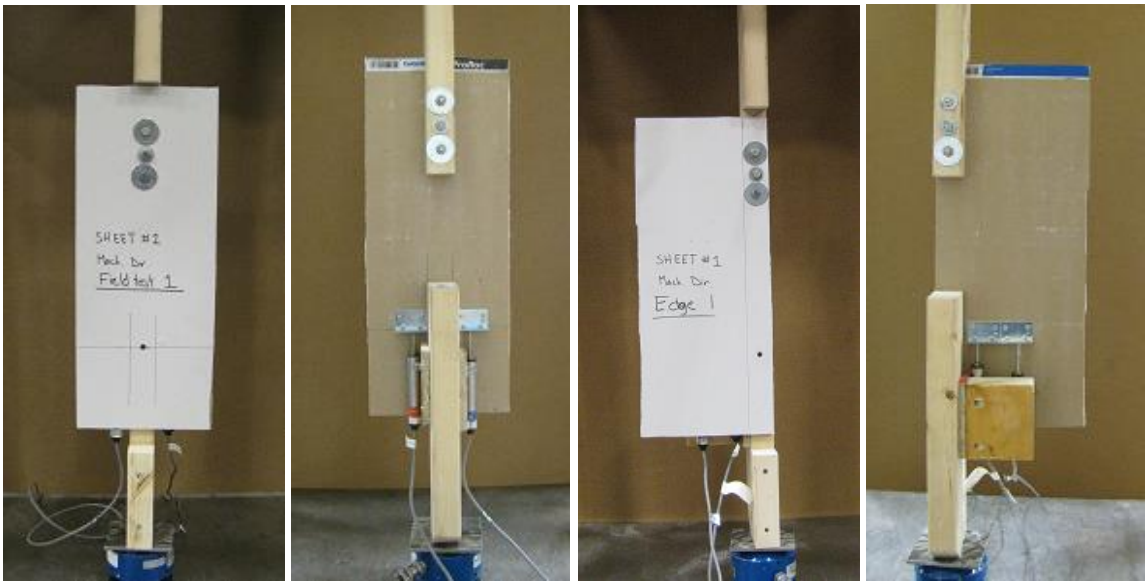

(a) (b) (c) (d)

(e) (f)

Figure 3.8: Specimens in Tinius-Olsen Testing Machine

Compressive loads were applied by opening the valve of the Tinius-Olsen machine to a constant setting to obtain a near constant ROD of the cross-head throughout the test. The

rate of δ_f at the fastener connection varied depending on the fastener stiffness and the connection stiffness between the specimen and cross-heads of the Tinius-Olsen machine. For a ROD of the cross-head of 2.5 mm/min, the rate of δ_f ranged between 0.9 and 2.3 mm/min. For a ROD of 0.5 mm/min, the rate of δ_f ranged between 0.22 and 0.44 mm/min. All specimens were tested within a temperature range of 22°C to 25°C.

3.2.3 Load Reversal Tests

Single load reversal tests were conducted to examine any pinching effect in Phase 2 of the shear load-slip response and the possible impact on the Phase 3 response. Interior and end specimens were tested to simulate connections with very large and small end distances, respectively. Side and corner specimens were not tested as it will be shown in Section 3.3.1.1 that the fastener location does not significantly influence the shear load-slip responses. The test matrix, shown in Table 3.4, includes 15 single-load-reversal tests with specimens defined using the notation adopted for monotonically increasing loads, shown in Table 3.2 and Table 3.3, and the addition of the suffix "SR" to define a single load-reversal.

Table 3.4: Load-Reversal Test Matrix

Specimen/ Test Series	Connection Type	e_s *(mm)*	e_n *(mm)*	n	δ_f *(mm)*	
					Max	Min
$I_{UM\text{-}SR\ (1)}$	IV	∞	∞	2	0.25	-2.00
$I_{UM\text{-}SR\ (2)}$	IV	∞	∞	2	0.50	-2.00
$I_{UM\text{-}SR\ (3)}$	IV	∞	∞	2	0.75	-2.00
$I_{UM\text{-}SR\ (4)}$	IV	∞	∞	2	1.00	-2.00
$I_{UM\text{-}SR\ (5)}$	IV	∞	∞	2	1.50	-2.00
$N_{UM\text{-}SR}$	III	∞	19	5	1.50	Fail.

The specimen and load apparatus designs were similar to those shown in Figure 3.7, although grips were necessary to apply tensile loads to the specimens. Wood studs and gypsum boards were conditioned together in an environment with temperature ranging from 22°C to 25°C and RH ranging from 25 to 50%. The rate of δ_f observed in fasteners subjected to a load-reversal in buckling tests reported in Chapter 2 ranged from 0.3 to 0.5

mm/min. Therefore, the target ROD of the cross-head of 0.5 mm/min was selected for load-reversal tests.

3.3 Influence of Parameters on the Load-Slip Response

3.3.1 Monotonic Load Tests

The typical connection-failure mechanism in the monotonic load tests is shown in Figure 3.9, where the gypsum board to the right of the connections was compressed. As δ_f progressed, as shown progressively in Figure 3.9(a) to (b), the fasteners gradually rotated and enlarged the hole in gypsum board, as described in detail by Van Bruinessen (2012). Figure 3.9(c) shows a typical plastic hinge of the screw (e.g. Smith and Whale, 1987) that occurred at the gypsum-board-to-stud interface, resulting in negligible damage to the wood stud during the test. The strength or stiffness of the wood stud does not, therefore, influence the capacity of the fastener connection.

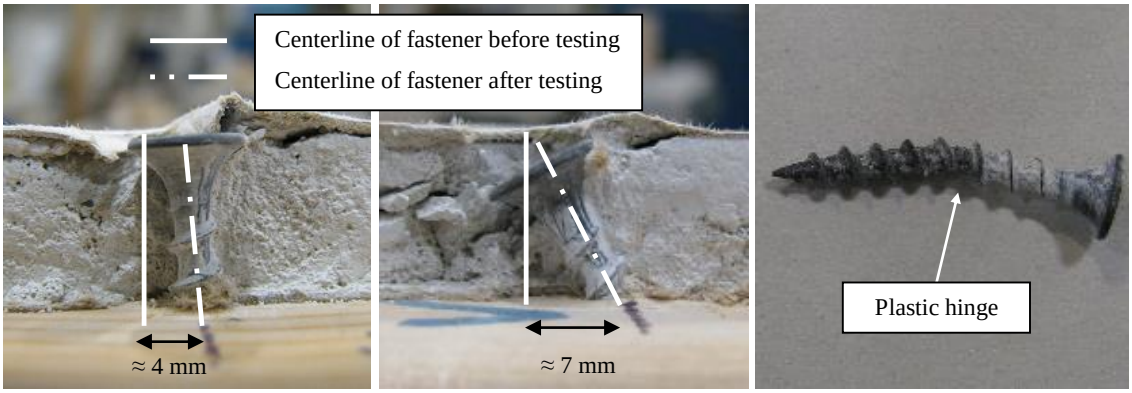

(a) δ_f = 4 mm (b) δ_f = 7 mm (c) Fastener Damage

Figure 3.9: Failure Mechanism of Fastener Connection

Figure 3.10 shows the load-slip responses of interior, side, end, and corner connections with loads applied in the machine direction, cut edges, $e_s \geq 19$ mm, RH between 25% and 50%, and ROD = 2.5 mm/min. The responses shown are the most representative of the average response. The load-slip responses are similar up to δ_f of approximately 3 mm, with nonlinear responses up to δ_f of approximately 2 mm and a near perfectly plastic response

afterwards. Corner connections (e.g., C_{UM-19}) have the least ductility, end connections (e.g., $N_{UM\ (1)}$ have slightly greater ductility, and interior and side connections (e.g., $I_{UM\ (1)}$ and $S_{UM\ (1)}$, respectively) have the greatest ductility.

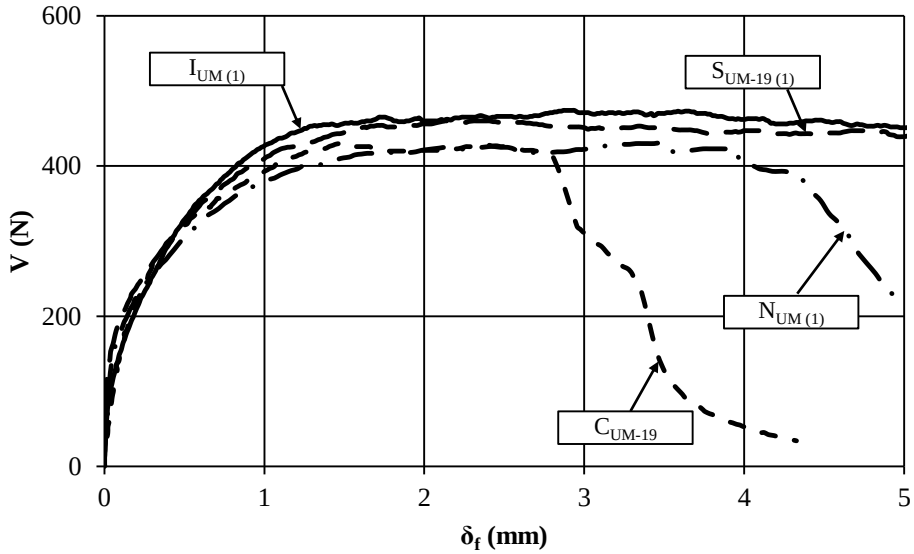

Figure 3.10: Typical Load-slip-Response of Fastener Connections

The load-slip response of fastener connections varies depending on the fastener location, edge type, side distance, ROD, paper orientation, density of gypsum board, MC, and gypsum-board thickness. The statistical significance of these parameters was estimated using regression analysis. The statistical difference of the average shear resistance at δ_f = 0.5 mm, i.e., early in the load-slip response, and at 3.0 mm, i.e., the maximum δ_f investigated (see Section 3.1.1), between test series was quantified with P-values, where a value less than 0.05 indicates the differences between the average strengths of the two test series are statistically significant.

3.3.1.1 Influence of Fastener Location

A comparison of the average strength of side specimens, S_{UM-19}, end specimens, $N_{UM\ (1)}$, and corner specimens, C_{UM-19}, to that of interior specimens, $I_{UM\ (1)}$, is shown in Table 3.5. Six of the nine corner specimens failed before δ_f reached 3.0 mm, thus were not included

in the analysis for δ_f = 3.0 mm. This will be discussed in greater detail in Section 3.3.3. The difference between the average strength of side and interior specimens was marginally significant (P-value = 0.10) at δ_f = 0.5 mm yet not statistically significant at δ_f = 3.0 mm. The average strengths of end and corner specimens are not significantly different from that of interior specimens.

Table 3.5: Strength of Specified Slips for Different Fastener Location

	δ_f = 0.5 mm				δ_f = 3.0 mm			
	$I_{UM\ (1)}$	S_{UM-19}	$N_{UM\ (1)}$	C_{UM-19}	$I_{UM\ (1)}$	S_{UM-19}	$N_{UM\ (1)}$	C_{UM-19}
n	12	11	12	9	12	11	12	3
Average (N)	284	331	294	312	429	443	416	438
St. Dev (N)	57	81	37	55	60	78	55	40
P-value	-	0.10	0.70	0.50	-	0.62	0.58	0.81

Figure 3.11(a) and (b) show the typical failure mode of interior and side specimens, respectively. The side of the gypsum board did not affect connections with e_s = 19 mm, thus side specimens behaved similar to interior specimens. This supports the observation from the regression analysis summarized in Table 3.5 that interior and side specimens have similar resistance at specified values of δ_f. Figure 3.11(c) and (d) show the typical failure modes of end and corner specimens, respectively, that are markedly different from those of interior and side specimens. It was observed in the laboratory that the crack formation and fracture occurred simultaneously in end and corner specimens. That is, the failure mode influenced the ductility of the specimens, but did not necessarily influence the load-slip response.

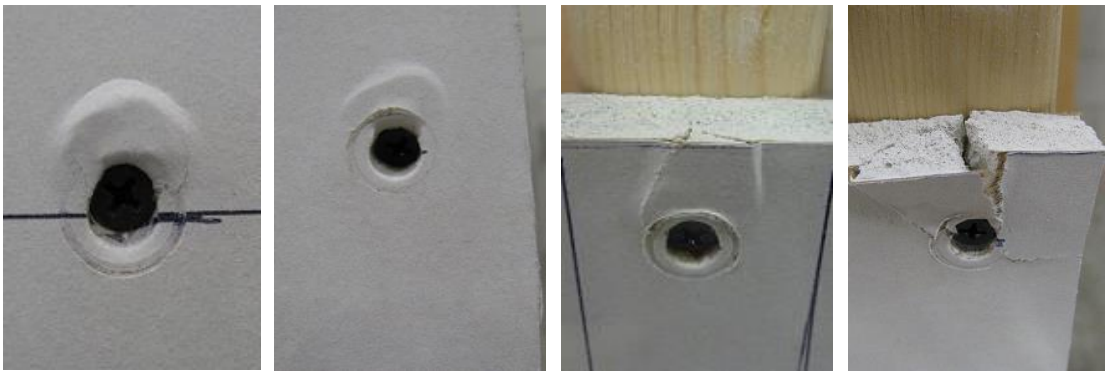

(a) $I_{UM\ (1)}$ (b) S_{UM-19} (c) $N_{UM\ (1)}$ (d) C_{UM-19}

Figure 3.11: Failure Modes of Fasteners at Various Locations

3.3.1.2 Influence of Edge Type

Table 3.6 presents a comparison of the average strength of specimens with cut edges to specimens with tapered edges. In nearly all cases, the strength of specimens with tapered edges significantly exceeds that of similar specimens with cut edges. The only exception is for corner specimens $C_{TM\text{-}19}$ and $C_{UM\text{-}19}$ for δ_f = 3.0 mm where a P-value of 0.32 is obtained, although the test has limited power due to the small number of specimens in each category. The results are attributable to the increased density of the gypsum in tapered edges having a greater impact on the strength of the connection than the decrease in thickness. This conflicts with the experimental findings of Liew et al. (2004), who observed that interior connections had on average 5% more capacity than connections along a tapered edge.

Table 3.6: Strength of Specified Slips for Different Edge Type

	δ_f = 0.5 mm				δ_f = 3.0 mm			
	n	Average *(N)*	St. Dev *(N)*	P-value	n	Average *(N)*	St. Dev *(N)*	P-value
$S_{TM\text{-}19\ (1)}$	12	409	75	0.028	12	613	113	$4.3x10^{-4}$
$S_{UM\text{-}19}$	11	331	81		11	443	78	
N_{TR}	12	403	96	0.008	12	552	70	0.001
$N_{UR\ (1)}$	12	308	49		12	452	47	
$C_{TM\text{-}19}$	11	398	112	0.041	3	488	63	0.321
$C_{UM\text{-}19}$	9	312	55		3	438	40	
$C_{TR\text{-}19}$	7	414	47	$1.9x10^{-4}$	0	-	-	-
$C_{UR\text{-}19}$	12	300	43		1	423	-	
$C_{TR\text{-}10}$	8	311	42	0.001	0	-	-	-
$C_{TR\text{-}10}$	12	234	36		0	-	-	

3.3.1.3 Influence of Side Distance

Table 3.7 summarizes the influence of reducing e_s from 19 to 10 mm. A statistically significant reduction in average strength is observed in most cases. The first exception is a marginally significant reduction for side specimens $S_{TM\text{-}19\ (1)}$ and $S_{TM\text{-}10}$ at δ_f = 0.5 mm with a P-value of 0.11, although the reduction is statistically significant at δ_f = 3.0 mm. The second exception is no statistically significant difference is observed between the average strength of corner specimens $C_{TM\text{-}19}$ and $C_{TM\text{-}10}$ at δ_f = 0.5 mm with a P-value of 0.39.

Table 3.7: Strength of Specified Slips for Different Edge Type

	δ_f = 0.5 mm				δ_f = 3.0 mm			
	n	Average *(N)*	St. Dev *(N)*	P-value	n	Average *(N)*	St. Dev *(N)*	P-value
$S_{TM-19\ (1)}$	12	409	75	0.109	12	613	113	0.046
S_{TM-10}	10	356	72		10	524	80	
S_{UR-19}	12	321	61	0.003	12	444	69	0.029
S_{UR-10}	8	245	40		5	363	55	
C_{TM-19}	11	398	112	0.394	3	488	63	-
C_{TM-10}	9	364	61		0	-	-	
C_{TR-19}	7	414	47	0.001	0	-	-	-
C_{TR-10}	8	311	42		0	-	-	
C_{UR-19}	12	300	43	0.000	1	423	-	-
C_{UR-10}	12	234	36		0	-	-	

These exceptions occur when fasteners are located along a tapered side. A side specimen with a tapered edge and e_s = 19 mm typically failed from bearing of the gypsum, as shown in Figure 3.12(a). When e_s is decreased to 10 mm, bulging occurred perpendicular to the load, as shown in Figure 3.12(b). However, this bulging typically occurred at δ_f greater than 3 mm, and so there was no statistically significant difference between the response of these two connections for $\delta_f \leq 3$ mm. There is no clear evidence, however, that a 10 mm side distance has any effect on the strength of the corner specimens with tapered sides, as shown in Figure 3.12(c) and (d). These observations for side and corner specimens are attributable to the paper wrapped around the tapered side markedly increasing the strength of the edge of the gypsum board.

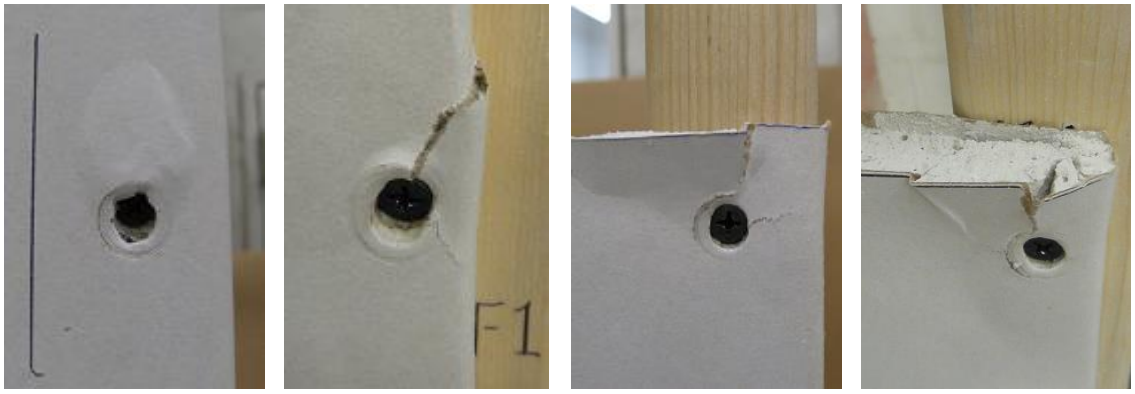

(a) $S_{TM-19\ (1)}$ (b) S_{TM-10} (c) C_{TM-19} (d) C_{TM-10}

Figure 3.12: Failure Mode of Corner Specimens with Tapered Sides

3.3.1.4 Influence of Rate-of-Displacement

The influence of ROD on the shear load-slip response was determined by comparing the average strength of test series $I_{UM\ (1)}$, with an ROD of the cross-head of 2.5 mm/min, and $I_{UM\ (3)}$, with an ROD of the cross-head of 0.5 mm/min. The average strength difference between both test series is not statistically significant, with P-values of 0.58 at δ_f = 0.5 mm and 0.85 at δ_f = 3.0 mm. This reinforces a similar conclusion by Liew et al. (2004) who used much more rapid RODs of 12.5 and 25 mm/min.

3.3.1.5 Influence of Orientation of Gypsum Board

Table 3.8 presents a comparison of the average strength of similar specimens with the applied load in the machine and cross-machine direction of the gypsum-board paper. In all cases, the difference in average strength of specimens is not statistically significant. However, with a P-value of 0.053 at δ_f = 0.5 mm, the difference between the average strengths of corner specimens $C_{TM\text{-}10}$ and $C_{TR\text{-}10}$ is almost statistically significant.

Table 3.8: Strength of Specified Slips for Machine and Cross-Machine Direction

	δ_f = 0.5 mm				δ_f = 3.0 mm			
	n	Average *(N)*	St. Dev *(N)*	P-value	n	Average *(N)*	St. Dev *(N)*	P-value
$I_{UM\ (1)}$	12	284	57	0.578	12	429	60	0.392
I_{UR}	12	269	72		12	452	72	
$S_{UM\text{-}19}$	11	331	81	0.724	11	443	78	0.975
$S_{UR\text{-}19}$	12	321	61		12	444	69	
$N_{UM\ (1)}$	12	294	37	0.434	12	416	55	0.099
$N_{UR\ (1)}$	12	388	48		12	452	47	
$C_{UM\text{-}19}$	9	312	55	0.589	0	-	-	-
$C_{UR\text{-}19}$	12	300	43		1	423	-	
$C_{TM\text{-}19}$	10	393	117	0.609	0	-	-	-
$C_{TR\text{-}19}$	7	415	47		0	-	-	
$C_{TM\text{-}10}$	9	364	61	0.053	0	-	-	-
$C_{TR\text{-}10}$	8	311	41		0	-	-	

Figure 3.13(a) shows the pre-loading condition of corner specimens $C_{TR\text{-}10}$, with cracks in the gypsum board due to installation of the screw that caused an immediate reduction in the bearing resistance of the gypsum. Such cracking was observed in all specimens in the

entire test series and is attributable to the small side distance along the cut edge. Conversely, such cracking was not observed in any corner specimen C_{TM-10}, as shown for example in Figure 3.13(b), because the gypsum is confined by the paper wrapped along the edge.

(a) C_{TR-10} (b) C_{TM-10}

Figure 3.13: Pre-loading Condition of Tapered Corner Specimens

3.3.1.6 Influence of Density of Gypsum Board

The reduction in average strength due to a reduced gypsum-board density was determined by comparing interior specimen series $I_{UM\,(1)}$ and $I_{UM\,(4)}$. There is no statistically significant difference between the average strengths at δ_f = 0.5 mm, with a P-value of 0.70, yet a marginally significant difference is observed at δ_f = 3.0 mm, with a P-value of 0.056. Therefore, the connection to the low-density gypsum board is typically weaker than the regular gypsum board, although the difference is only marginally significant.

3.3.1.7 Influence of Moisture Content

The influence of MC was initially analyzed by comparing the average strength of specimens conditioned in an environment having a RH ranging from 25 to 50%, i.e., with a nominal MC ranging from 7.8 to 11.9%, to specimens conditioned in an environment with the RH of 65%, i.e., with a nominal MC ranging from 13.9 to 14.9%, as shown in

Table 3.9. A statistically significant difference of average strengths is present only for side specimens S_{TM-19} at δ_f = 3.0 mm and N_{UM-19} at δ_f = 0.5 mm. There is no clear reason for the influence of the MC to be statistically significant in some test series and not others. Therefore, the influence of MC will be revisited in Section 3.4 using multivariate linear regression analysis.

Table 3.9: Strength of Specified Slips for Various MC Levels

	δ_f = 0.5 mm				δ_f = 3.0 mm			
	n	Average *(N)*	St. Dev *(N)*	P-value	n	Average *(N)*	St. Dev *(N)*	P-value
$I_{UM\ (1)}$	12	284	57	0.197	12	429	60	0.664
$I_{UM\ (3)}$	12	311	37		12	439	50	
$S_{TM-19\ (1)}$	12	408	75	0.572	12	613	113	0.045
$S_{TM-19\ (2)}$	11	391	67		11	533	55	
$N_{UM\ (1)}$	12	294	37	0.046	12	416	55	0.195
$N_{UM\ (2)}$	4	241	35		4	365	60	
$N_{UR\ (1)}$	12	308	49	0.285	12	452	47	0.251
$N_{UR\ (2)}$	4	291	17		4	434	23	

3.3.1.8 Influence of Gypsum-Board Thickness

The increase in average connection strength with increase of gypsum-board thickness from 12.7 mm to 15.9 mm is presented in Table 3.10. The increase is statistically significant for interior and end specimens, but no so for tapered side specimens. The increase in average strength between interior and tapered side specimens in 15.9 mm gypsum board is only marginally significant at δ_f = 0.5 mm, with a P-value of 0.098, and clearly not significant at δ_f = 3.0 mm, with a P-value of 0.64. Therefore, the increase in average connection strength for fasteners along tapered sides predominantly occurs in 12.7 mm thick boards.

Table 3.10: Strength of Specified Slips for 12.7 and 15.9 mm Thick Gypsum Board

	Thickness *(mm)*	δ_f = 0.5 mm				δ_f = 3.0 mm			
		n	Average *(N)*	St. Dev *(N)*	P-value	n	Average *(N)*	St. Dev *(N)*	P-value
I_{UM}	12.7	12	284	57	0.044	12	429	60	0.000
	15.9	12	382	143		12	651	73	
S_{TM-19}	12.7	12	408	75	0.131	12	613	113	0.280
	15.9	5	482	93		5	673	104	
N_{UM}	12.7	12	294	37	0.000	12	416	55	0.000
	15.9	6	418	41		4	636	24	

3.3.1.9 Summary

An investigation into the strength and failure modes of fastener connections revealed that connections with tapered edges are statistically stronger than connections with cut edges, connections with a 10 mm side distance are statistically weaker than connections with a 19 mm side distance, and connections in 15.9 mm thick boards are statistically stronger than those in 12.7 mm thick boards. Conversely, the parameters affecting the location, ROD, orientation of the gypsum board, and density of the gypsum board were determined to have negligible influence on the strength of fastener connections. Further analysis is needed to assess the influence of gypsum-board MC on the connection strength.

3.3.2 Load-Reversal Tests

Figure 3.14(a) and (b) show the shear load-slip responses of typical interior and end specimens subjected to a single load reversal with a maximum positive δ_f of 0.75 mm and 1.5 mm, respectively. A typical monotonic response of interior specimens I_{UM} is included for comparison of Phase 1 in both figures. For both maximum magnitudes of δ_f, the Phase 1 response resembles that typically observed in the monotonic tests. Upon load reversal, a pinching effect is observed as the fastener slips through the previously created elongated hole. When the δ_f reached zero, the fastener recommences transmitting load through bearing at the end of the elongated hole. A typical monotonic response of interior specimen I_{UM} is also included for comparison of Phase 3 of Figure 3.14(a). Conversely, the hole in the end specimen shown in Figure 3.14(b) elongated in Phase 3 towards the end of the

gypsum board, so a typical monotonic response of end specimens N_{UM} is included in the figure for comparison. For both maximum magnitudes of δ_f, Phase 3 of the loading response also resembles the typical response observed from monotonic tests.

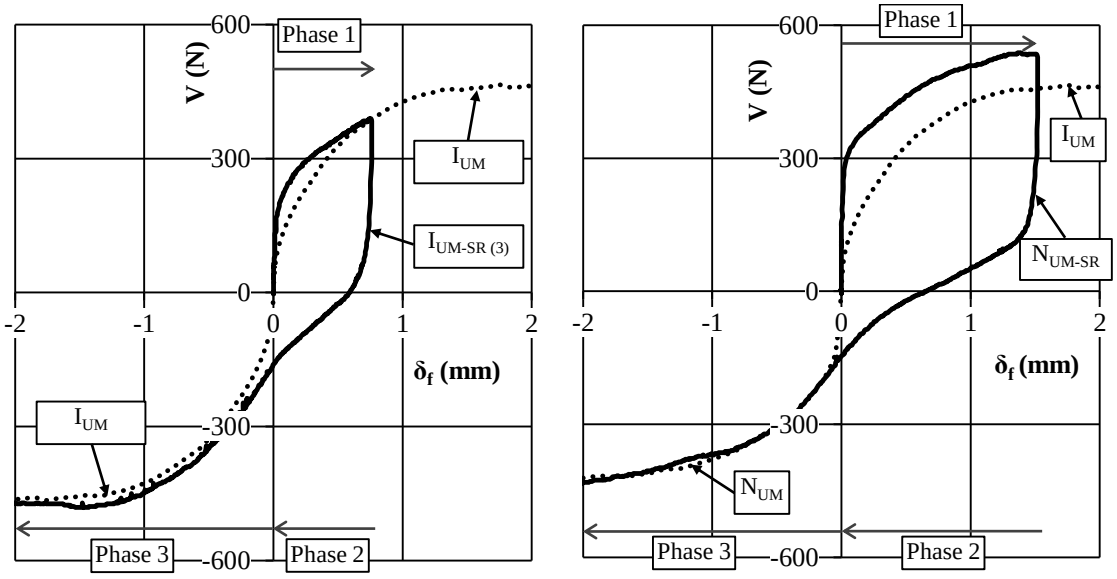

(a) Interior specimen to δ_f = 0.75 mm

(b) End specimen to δ_f = 1.5 mm

Figure 3.14: Typical Shear Load-slip Response with Single Load Reversal

Gad (1997) and Li et al. (2012) reported similar responses for fastener connections subjected to single load reversals. Both, however, reported different idealizations of the response in Phase 2, as shown in Figure 3.15. Gad (1997) modeled each connection assuming no resistance in Phase 2, whereas Li et al. (2012) presented the reduced-stiffness response shown. Neither is perfect compared to the test results shown in Figure 3.14. Li et al.'s (2012) idealization for Phase 2 captures the slope of the response from test results, but assumes only negative load, which is consistent with the response shown in Figure 3.14(a) but not that shown in Figure 3.14(b). Therefore, the present study will adopt a shear load-slip response for the single-load-reversal case that is similar to that reported by Gad (1997) because it is slightly conservative and has the simplest computational form.

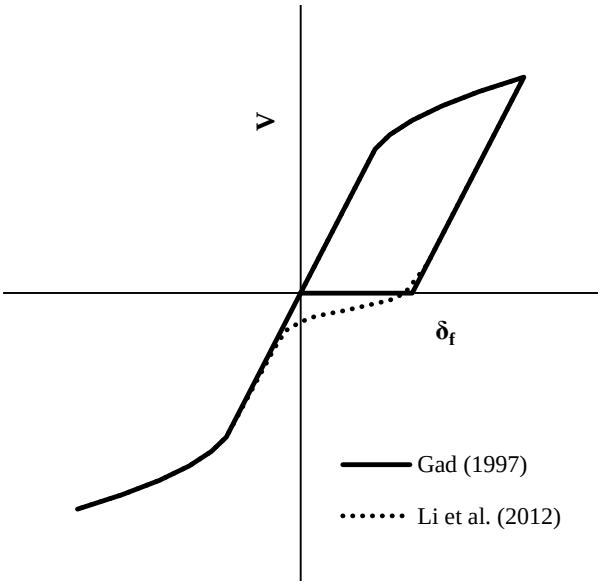

Figure 3.15: Idealization for Phase 2 of the Shear Load-slip Response by Others

A comparison of the average load at δ_f = 0.5 and 1.0 mm for end specimens in Phase 3 of load-reversal tests and from monotonic tests is presented in Table 3.11. As the P-values both greatly exceed 0.05, it is concluded that the strength of the connection in Phase 3 was not affected by a single load reversal. Therefore, the monotonic response can be used to simulate the response in Phase 1 and 3 of connections subjected to a single load reversal.

Table 3.11: Strength at Specified Slips for End Specimens

	δ_f = 0.5 mm		δ_f = 1.0 mm	
	Monotonic	Load reversal	Monotonic	Load reversal
n	12	5	12	5
Average *(N)*	294	304	358	375
St. Dev *(N)*	37	56	39	54
P-value	0.72		0.54	

3.3.3 Slip at Failure

Table 3.12 lists the summary statistics for the slip at failure, defined as the slip where the applied load decreases to 85% of its maximum value, for the test series involving monotonic loading. A lower bound slip at failure is presented and assumed equal to the mean minus two standard deviations. The slip at failure is considered satisfactory when the

lower-bound value is larger than 3 mm for connections on the concave side or smaller than -1 mm for connections on the convex side, as reported in Section 3.1.1. Otherwise, the connection may fail before the maximum capacity of a gypsum-board-sheathed-wood stud is attained. The slip at failure of some specimens tested exceeds 10 mm, thus it is not accurately known and is shown as greater than 10 mm.

Table 3.12: Slip at Failure of Fastener Connections

Specimen / Test series	Min. required slip at failure *(mm)*	Mean *(mm)*	St. dev. *(mm)*	Lower bound *(mm)*
$I_{UM\ (1\ to\ 4)}$	3	> 10	-	-
I_{UR}	3	> 10	-	-
S_{UM-19}	3	> 10	-	-
S_{UR-19}	3	> 10	-	-
S_{UR-10}	3	4.24	1.67	0.90
$S_{TM-19\ (1\ \&\ 2)}$	3	> 10	-	-
S_{TM-10}	3	> 10	-	-
$N_{UM\ (1)}$	-1	-4.57	1.23	-2.11
$N_{UM\ (2-}$	-1	-5.57	0.46	-4.65
$N_{UM\ (3)}$	-1	-4.80	1.85	-1.10
$N_{UR\ (1)}$	-1	-4.19	0.66	-2.87
$N_{UR\ (2)}$	-1	-4.82	0.51	-3.80
N_{TR}	-1	-5.22	1.64	-1.94
C_{UM-19}	-1	-2.84	0.57	-1.70
C_{UR-10}	-1	-1.05	0.18	-0.69
C_{UR-19}	-1	-1.70	0.28	-1.14
C_{TM-19}	-1	-2.56	0.60	-1.36
C_{TM-10}	-1	-1.99	0.19	-1.71
C_{TR-10}	-1	-1.40	0.16	-1.08
C_{TR-19}	-1	-1.39	0.15	-1.09

The lower-bound slip at failure for side specimens S_{UR-10} at 0.90 mm is markedly less than the minimum 3 mm required, so may impact the axial compressive capacity of sheathed studs. These connections occur at the sides of each sheet of gypsum board when the machine direction of the paper is installed in the horizontal direction, and must be reinforced before the contribution of gypsum board can be considered. The ductility of all other test series exceeds the minimum required.

3.4 Idealization of Load-Slip Response by Multivariate Linear Regression Analysis

A total of 283 test results were used to quantify the influence of various parameters on the strength of gypsum-board-to-stud fastener connections. Linear regression analyses were performed to predict the shear load at specified values of δ_f and to idealize a load-slip response. The data analyzed are provided in Appendix 3A, including those obtained by Van Bruinessen (2012).

3.4.1 Indicator Variables

The control group assumed for the multivariate linear regression analysis consisted of interior in regular 12.7 mm gypsum board with loads applied parallel to the machine direction at a ROD of 2.5 mm/min. Table 3.13 lists the ten parameters considered in this study as possible influences of the connection strength. A preliminary study using multivariate linear regression analysis determined that connections with a gypsum-board MC below 8% were statistically stronger than those above 8%. Therefore, the gypsum-board MC was divided into two categories: the control group with very dry specimens having MC below 8%, and the remaining specimens with MC equal or above 8%. Indicator variables were assigned to each parameter, and are set equal to 1 when a particular parameter is present or 0 otherwise. For example, Z_5 is equal to 1 for a connection along a tapered edge or otherwise equal to 0. The control group is the case where none of the factors are present.

Table 3.13: Indicator Variables for Regression Analysis

Parameter	Factor	Indicator variable
Fastener location	Side	Z_1
	End	Z_2
	Corner	Z_3
Side distance	e_s = 10 mm	Z_4
Edge type	Tapered edge	Z_5
Density of gypsum board	Low	Z_6
Thickness of gypsum board	Thickness = 15.9 mm	Z_7
Orientation of gypsum board	Cross-machine	Z_8
Rate of displacement	ROD = 0.5 mm/min.	Z_9
Elevated moisture content	MC $\geq$ 8.0 %	Z_{10}

A factor can be significant by itself or can also be significant only if other factors are present. For example, a MC equal or above 8% ($Z_{10} = 1$) alone may significantly decrease the strength of a connection, and may only significantly increase the strength of connections along a tapered edge ($Z_5 = 1$). To limit the total number of variables investigated, only indicator variables representing the presence of one or two factors (e.g., $Z_{11} = Z_5 \cdot Z_{10}$) were considered. Simultaneous presence of some pairs of factors is not possible, and so was not investigated: for example, a connection cannot be located along a side and at a corner simultaneously. Also, some pairs were not tested: for example, low-density gypsum-board connections along tapered edges.

3.4.2 Statistically Significant Parameters

The multivariate linear regression analysis was based on the following linear model:

[3.1] $$V_{\delta_f} = \beta_0 + \sum \beta_i Z_i + \varepsilon_r$$

where V_{δ_f} is the shear resistance at specified slips δ_f, β_0 is the average shear resistance of the control group, β_i are parameters determined by regression analysis for indicator variables Z_i, and ε_r is the inherent error, assumed independent and identically distributed for all samples.

Table 3.14 presents the statistically significant factors (i.e., with a P-value less than 0.05) that influence the strength of the connections at δ_f = 0.5, 1.0, and 2.0 mm. All parameters shown are significant for all three specified values of δ_f, and include side distance, Z_4, edge type, Z_5, thickness of gypsum board, Z_7, and MC, Z_{10}. Fastener location, ROD, orientation of gypsum board, and density of gypsum board are not statistically significant. This is consistent with previous findings reported in Section 3.3.1.

Table 3.14: Significant Parameters for Connection Resistance at Specified Slip

Parameters	δ_f = 0.5 mm			δ_f = 1.0 mm			δ_f = 2.0 mm		
	Mean *(N)*	SE[a] *(N)*	P-value[b]	Mean *(N)*	SE *(N)*	P-value[b]	Mean *(N)*	SE *(N)*	P-value[b]
β_o	310	8.5	0.00	384	7.9	0.00	440	8.2	0.00
β_4	-47.0	13.4	0.00055	-52.3	12.4	$3.6x10^{-05}$	-55.8	13.5	$5.3x10^{-05}$
β_5	80.4	13.2	$3.9x10^{-9}$	64.1	12.2	$3.3x10^{-07}$	68.9	13.0	$2.8x10^{-07}$
β_7	68.1	12.5	$1.2x10^{-7}$	97.8	11.7	0.00	132	12.0	0.00
β_{10}	-28.0	11.0	0.012	-30.0	10.2	0.0035	-41.6	10.3	$8.1x10^{-05}$
β_5 β_{10}	58.5	19.5	0.0029	78.1	18.1	$2.2x10^{-05}$	98.8	19.0	$4.6x10^{-07}$

[a] Standard Error

[b] Values less than 10^{-10} are marked with 0.00.

The analysis resulted in a poor prediction of the average strength of corner specimens C_{UR-10}, i.e., the only test series with e_s = 10 mm (Z_4 = 1) as the only significant factor. These specimens are potentially influenced by three factors: they are corner connections, with side distances of 10 mm, and orientation of the gypsum board in the cross-machine direction. Any combination of two of these three factors is not statistically significant, and the analysis did not consider a combination of three factors, as discussed previously in Section 3.4.1. Therefore, this test series was excluded from the analysis presented in Table 3.14 and analyzed separately to yield the results presented in Table 3.15. All twelve C_{UR-10} specimens exhibited a slip at failure of less than 2 mm, and so a regression analysis was conducted only for δ_f = 0.5 and 1.0 mm. The mean value for β_4 increased in magnitude from -47.0 N in Table 3.14 to -76.4 N in Table 3.15.

Table 3.15: Significance of 10 mm Side Distance for Connection Resistance at Specified Slip

Parameter	δ_f = 0.5 mm		δ_f = 1.0 mm	
	Mean *(N)*	P-value	Mean *(N)*	P-value
β_o	310		384	
β_3 β_4 β_8	-76.4	1.3E-06	-105	5.2E-07

Hereon, the twelve C_{UR-10} specimens are defined as Group 2 and the remaining 271 specimens are defined as Group 1. Table 3.16 lists the 17 possible connections involving the five statistically significant parameters defined in Table 3.14 and Table 3.15. The resulting shear load at a slip of 1.0 mm, $V_{1.0}$, is then calculated using Equation [3.1] with the mean values for β_i from Table 3.14 for Group 1 and from Table 3.15 for Group 2.

Table 3.16: Possible Connections and Resulting $V_{1.0}$

Connections	Value of indicator variable							$V_{1.0}$
	Z_3	Z_4	Z_5	Z_7	Z_8	Z_{10}	Z_5 Z_{10}	*(N)*
Group 1								
1	0	0	0	0	0	0	0	384
2	0	1	0	0	0	0	0	279
3	0	0	1	0	0	0	0	449
4	0	0	0	1	0	0	0	482
5	0	0	0	0	0	1	0	354
6	0	1	1	0	0	0	0	396
7	0	1	0	1	0	0	0	430
8	0	1	0	0	0	1	0	302
9	0	0	1	1	0	0	0	546
10	0	0	1	0	0	1	1	497
11	0	0	0	1	0	1	0	452
12	0	1	1	1	0	0	0	494
13	0	1	1	0	0	1	1	444
14	0	1	0	1	0	1	0	400
15	0	0	1	1	0	1	1	594
16	0	1	1	1	0	1	1	542
Group 2								
17	1	1	0	0	1	0	0	332

3.4.3 Idealization of the Shear Load-Slip Response

Linear regression analysis was also used to determine an equation to idealize the shear load-slip response of a gypsum-board-to-stud fastener connection given the predicted resistance at a specified value of δ_f. Because the same parameters are statistically significant for all values of δ_f examined, the load at various values of δ_f were normalized to the load at δ_f = 1.0 mm, as presented in Table 3.17. An analysis of the residuals in Group 1, presented in Appendix 3B, confirmed no statistically significant parameter was overlooked in the normalizing process. The slip at failure of all twelve $C_{UR\text{-}10}$ specimens was less than 2 mm, thus normalized loads at a slip of 2 and 3 mm are not available.

Table 3.17: Load at Specified Slips Normalized to Load at Slip of 1.0 mm

	0 mm	0.25 mm	0.5 mm	1.0 mm	2.0 mm	3.0 mm
Group 1						
Mean	0	0.666	0.826	1.000	1.13	1.18
SE	0	0.00612	0.00519	0	0.00459	0.00735
Group 2						
Mean	0	0.656	0.856	1.000	-	-
SE	0	0.0295	0.0184	0	-	-

For simplicity, the subsequent development is shown for Connection 1 in Group 1, i.e., all indicator variables in Equation [3.1] are zero, and Connection 2 in Group 2 where Z_3, Z_4, and Z_8 = 1.0. The remaining connections follow the same development, yielding the idealized curves shown in Appendix 3C.

Multiplying the normalized loads in Table 3.17 by $V_{1.0}$ defines up to five points on the shear load-slip curve for any given connection. Figure 3.16 shows these points with the natural logarithm of δ_f along the horizontal axis. Best-fit second-order polynomials through an intercept equal to $V_{1.0}$ were derived, yielding an idealization of the shear-load slip response for each connection.

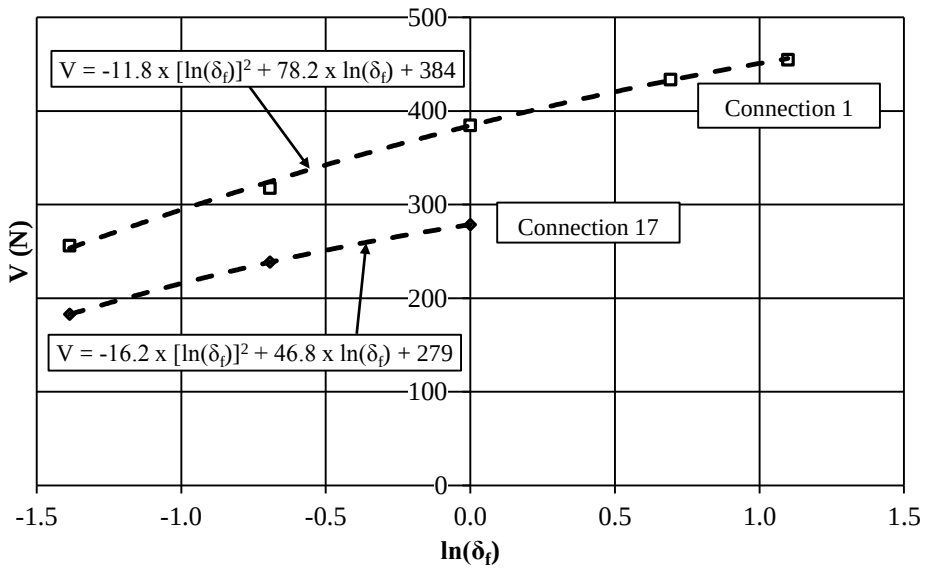

Figure 3.16: Derivation of an Idealized Shear Load-slip Response

These equations shown in Figure 3.16 are undefined at a slip of zero. It is, thus, assumed that the response is linear from the origin to the shear resistance at δ_f = 0.25 mm. Furthermore, the equation coefficients were normalized to $V_{1.0}$ so that one set of equations can represent the idealized shear load-slip response for all connections. The resulting set of equations takes the form of:

[3.2] Group 1 (all specimens except Group 2):

$$V = V_{1.0} \times 2.66 \times \delta_f \qquad 0 < \delta_f < 0.25 \text{ mm}$$

$$V = V_{1.0} [-0.0307 \times \ln(\delta_f)^2 + 0.203 \times \ln(\delta_f) + 1] \qquad \delta_f \geq 0.25 \text{ mm}$$

Group 2 (Corner specimens with 10 mm side distance loaded in the cross-machine direction):

$$V = V_{1.0} \times 2.62 \times \delta_f \qquad 0 < \delta_f < 0.25 \text{ mm}$$

$$V = V_{1.0} [-0.0580 \times \ln(\delta_f)^2 + 0.168 \times \ln(\delta_f) + 1] \qquad 0.25 < \delta_f \geq 1.00 \text{ mm}$$

Figure 3.17 shows these idealizations with the points obtained by regression analysis. It is shown Equations [3.2] provides a good model of the average monotonic load-slip response of the fastener connections for both Connections 1 and 17 in Table 3.16. The results for the remaining connections are similar and are shown in Appendix 3C.

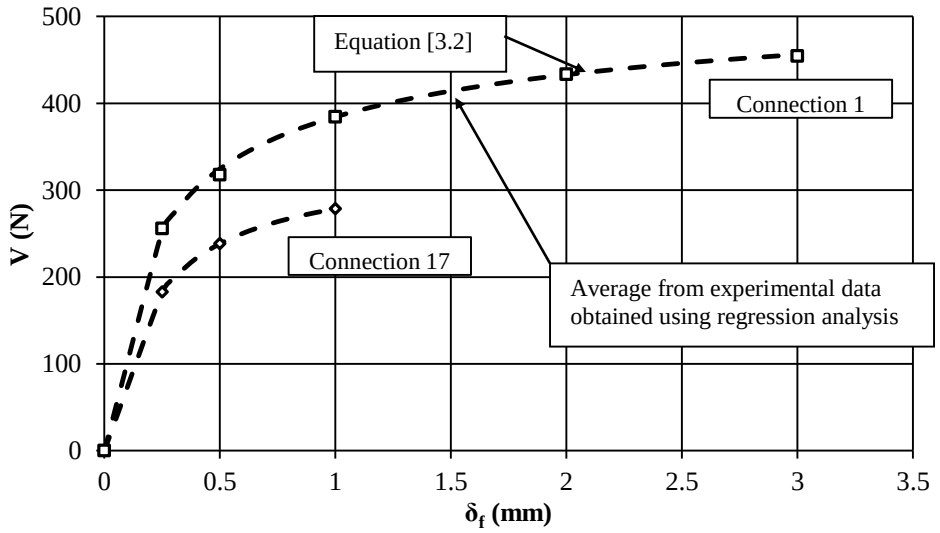

Figure 3.17: Idealized Shear Load-slip Response

3.4.4 Model Error

Table 3.18 presents the average and standard deviation of the test-to-predicted ratios at δ_f = 0.25, 0.5, 1.0, 2.0, and 3.0 mm for Connections 1 through 17. The predicted values were determined using Equation [3.2] with values for $V_{1.0}$ taken from Table 3.16. No data are available for five connections, namely 2, 7, 14, 15, and 16, because no tests were conducted for these conditions. Ratios below 1.00 indicate that the predicted load at specified δ_f is greater than the average observed load.

Table 3.18: Test-to-Predicted Ratio for Specified Slips

Connection	n	0.25 mm		0.5 mm		1.0 mm		2.0 mm		3.0 mm	
		Avg.	SD	Avg.	SD	Avg.	SD	Avg.	SD	Avg.	SD
Group 1											
1	59	0.97	0.22	0.97	0.16	1.00	0.14	1.01	0.11	1.00	0.12
2	0	-	-	-	-	-	-	-	-	-	-
3	30	1.11	0.29	1.03	0.22	1.01	0.17	1.02	0.15	1.02	0.13
4	24	0.89	0.35	0.87	0.34	1.00	0.20	1.03	0.19	1.10	0.15
5	82	0.89	0.24	0.93	0.18	1.00	0.15	1.00	0.13	0.98	0.13
6	21	1.07	0.20	1.00	0.17	0.99	0.17	1.02	0.20	0.99	0.17
7	0	-	-	-	-	-	-	-	-	-	-
8	8	0.91	0.23	0.96	0.16	1.04	0.15	1.02	0.16	1.01	0.15
9	6	1.15	0.25	1.04	0.20	1.02	0.16	1.04	0.15	1.04	0.16
10	23	1.06	0.22	1.00	0.19	0.99	0.17	1.00	0.17	0.99	0.18
11	6	1.03	0.23	0.99	0.17	1.01	0.12	1.04	0.12	1.03	0.08
12	6	1.14	0.25	1.01	0.17	0.97	0.14	0.99	0.14	0.99	0.14
13	6	1.04	0.26	1.02	0.19	1.04	0.16	1.07	0.12	1.07	0.10
14	0	-	-	-	-	-	-	-	-	-	-
15	0	-	-	-	-	-	-	-	-	-	-
16	0	-	-	-	-	-	-	-	-	-	-
Group 2											
17	12	1.01	0.22	0.98	0.15	1.00	0.12	-	-	-	-

The accuracy of the model is best at a slip of 1.0 mm where the average test-to-predicted ratios range from 0.97 to 1.04. The accuracy of the predicted load decreases slightly as the slip becomes more extreme, although the average of most test-to-predicted ratios ranges from 0.95 to 1.05. Only six cases have a test-to-predicted ratio less than 0.90 or greater than 1.10, with five of these occurring at slips of 0.25 mm where the load is mostly dependent on the elastic stiffness of the connection. A small change in stiffness causes a

large change in load at a slip of 0.25 mm. Therefore, the loads at slips of 0.25 mm are expected to be more volatile than the loads at larger specified slips.

3.4.5 Statistical Distribution of $V_{1.0}$

Figure 3.18(a) and (b) show the experimental values for $V_{1.0}$ plotted using a normal probability scale for Connections 1 and 17, respectively. The vertical axis represents the number of standard distributions between a particular value of $V_{1.0}$ and the mean value. The goodness-of-fit of the distribution was determined by calculating the standard error along the vertical axis, where a value approaching zero indicates a good fit. Assuming $V_{1.0}$ is normally distributed for all connections resulted in a standard error range from 0.10 to 0.36. Therefore, although these data sets do not fit a normal distribution perfectly, it is reasonable to assume $V_{1.0}$ is normally distributed.

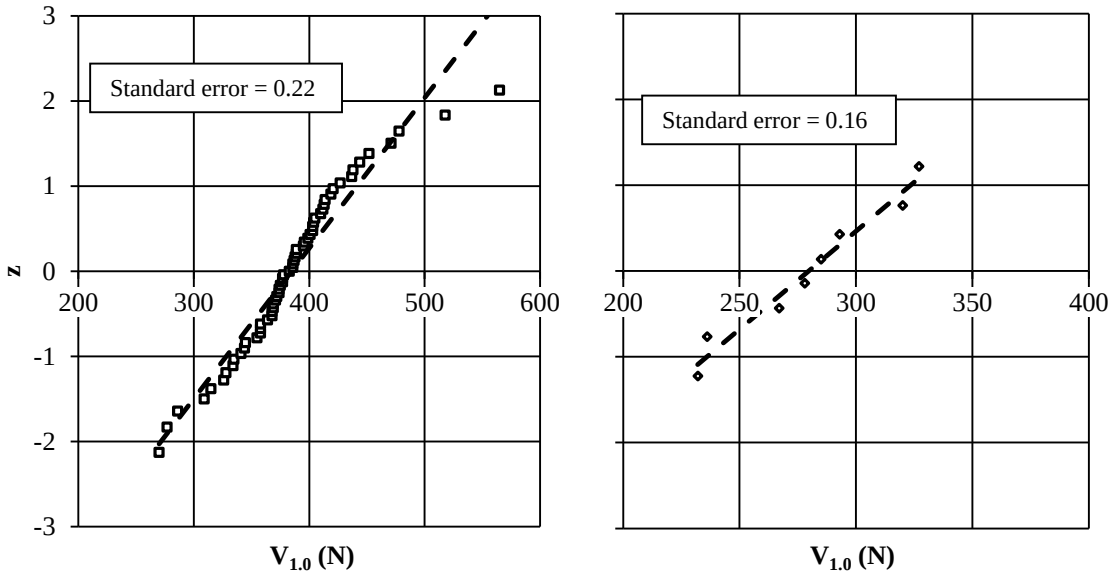

(a) Connection 1 (b) Connection 17

Figure 3.18: $V_{1.0}$ Plotted Using a Normal Probability Scale

3.5 Summary and Conclusions

This chapter has assessed the statistically significant parameters and established an idealization for the shear load-slip response of gypsum-board-to-wood-stud connections. Its findings are important because no clear idealization has been presented in or can be produced from the existing literature. A total of 283 monotonic and 25 load-reversal tests were conducted on specimens with gypsum board fastened to a nominal 2x4 SPF stud with coarse gypsum-board screws. The influence of fastener location, edge type, side distance, rate-of-displacement, paper orientation, density of gypsum board, moisture content of gypsum board, and gypsum-board thickness was investigated. The conclusions of this study are as follows:

1. The connection strength increased when located along a manufactured tapered edge and with an increase in the gypsum board thickness, yet decreased when decreasing the side distance or increasing the moisture content of the gypsum board. The influence of all other parameters on the average strength of the connections at various slips was found to be negligible.

2. The idealization of the monotonic shear load-slip response of the connections is given as:

   Group 1 (all specimens except in Group 2):

   $V = V_{1.0} \times 2.66 \times \delta_f$ $\quad 0 < \delta_f < 0.25$ mm

   $V = V_{1.0} [-0.0307 \times \ln(\delta_f)^2 + 0.203 \times \ln(\delta_f) + 1]$ $\quad \delta_f \geq 0.25$ mm

   Group 2 (Corner specimens with 10 mm side distance loaded in the cross-machine direction):

   $V = V_{1.0} \times 2.62 \times \delta_f$ $\quad 0 < \delta_f < 0.25$ mm

   $V = V_{1.0} [-0.0580 \times \ln(\delta_f)^2 + 0.168 \times \ln(\delta_f) + 1]$ $\quad \delta_f \geq 0.25$ mm

   where V is the predicted shear load in N at a specified slip, δ_f, in mm, and $V_{1.0}$ is the shear load at $\delta_f = 1.0$ determined empirically from experimental data. The idealization was separated into two groups: Group 2 consists of only corner

connections with a side distance of 10 mm with the load applied in the cross-machine direction of the paper. This idealization predicts with good accuracy the average load at $\delta_f \leq 1.0$ mm, i.e., the maximum value observed on the convex side in buckling tests. Group 1 consists of all other connections. This idealization predicts with good accuracy the average load at $\delta_f \leq 3.0$ mm, i.e., the maximum value observed in buckling tests.

3. The load-slip response of fasteners subjected to a single load reversal mimicked the monotonic load-slip responses during the initial phase (i.e., increasing positive δ_f), typically displayed a pinching effect during the unloading phase (i.e., δ_f decreasing to 0), and mimicked the monotonic load-slip responses during the final phase (i.e., increasing negative δ_f). Therefore, the suggested model assumes a monotonic response for the initial and final phases and a complete loss in capacity in the unloading phase.

3.6 References

American Society for Testing and Materials (ASTM). 1974. D1761-74: Standard Test Methods for Mechanical Fasteners in Wood. Annual Book of ASTM Standards, West Conshohocken, PA., USA.

American Society for Testing and Materials (ASTM). 2006. D1761-06: Standard Test Methods for Mechanical Fasteners in Wood. Annual Book of ASTM Standards, West Conshohocken, PA., USA.

American Society for Testing and Materials (ASTM). 2007. C1002-07: Steel Self-Piercing Tapping Screws for the Application of Gypsum Panel Products or Metal Plaster Bases to Wood Studs or Steel Studs. Annual Book of ASTM Standards, West Conshohocken, PA., USA.

American Society for Testing and Materials (ASTM). 2011. C1396-11: Standard Specification for Gypsum Board. Annual Book of ASTM Standards, West Conshohocken, PA., USA.

CenterPoint Energy, 2006. Humidity and the Indoor Environment. Retrieved August 28, 2013, from CenterPoint Energy Web site: http://www.centerpointenergy.com /staticfiles/CNP/Common/SiteAssets/doc/Humidity_indoor_environ%5B1%5D.pdf. 4 p.

CGC Inc. 2012a. Material Safety Data Sheet for Sheetrock® Regular Gypsum Panels. Retrieved September 12, 2012 from CGC Web site: http://www.cgcinc.com /media/173977/sheetrock%20gypsum%20panels54000001v7.pdf

CGC Inc. 2012b. Material Safety Data Sheet for Sheetrock® UltraLight Gypsum Panels. Retrieved September 12, 2012, from CGC Web site: http://www.cgcinc.com /media/217494/sheetrock%20brand%20ultralight%20panels54100002v2.pdf

CWC, 2009. Engineering Guide for Wood Frame Construction. Canadian Wood Council, Ottawa, ON.

Gad, E. F. 1997. Performance of Brick-Veneer Cold-Formed Steel-Framed Domestic Structures when Subjected to Earthquake Loading", Ph.D. Thesis, Department of Civil and Environmental Engineering, The University of Melbourne, Australia. 360 p.

Gromala, D.S. 1985. Lateral Nail Resistance for Ten Common Sheathing Materials. Forest Products Journal, 35(9): 61-68.

Li, M., Foschi, R. O., and Lam, F. 2012. Modeling Hysteretic Behavior of Wood Shear Walls with a Protocol-Independent Nail Connection Algorithm. Journal of Structural Engineering, 138(1): 99-108.

Liew, Y. L., Gad, E. F., and Duffield, C. F. 2004. Development of Test Method for Determining Plasterboard Bracing Performance. Journal of Structural Engineering, 130(7): 1108-1116

Liew, Y. L., Gad, E. F., and Duffield, C. F. 2006. Experimental and Analytical Validation of a Fastener Bearing Test as a Means of Evaluating the Bracing Characteristics of Plasterboard. Advances in Structural Engineering, 9(3): 421-432.

Lstiburek, J. 2005. The Future of Framing is Here. Fine Homebuilding, 174: 50-55.

National Research Council of Canada (NRC). 2010. National Building Code of Canada. Institute for Research in Construction, NRC, Ottawa, Ont.

Rousseau, J. 2011. Personal conversation with professional contractor on Sep. 8, 2011.

Smith, I. and Whale, L. R. J. 1987. Characteristic Properties of Nailed and Bolted Joints, Part 1 - Research Philosophy and Test Programme. Journal of the Institute of Wood Science, 62: 53-59.

Van Bruinessen, A. 2012. Analysis of 16 mm Gypsum Board to 38 mm Stud Framing Connections. Civil Engineering Thesis, Department of Civil and Environmental Engineering, University of Western Ontario, Canada.

Wolfe, R. W. 1983. Contribution of Gypsum Wallboard to Racking Resistance of Light-Frame Walls. USDA Forest Service Research Paper FPL 439. Forest Products Laboratory, Madison, Wis. 23 p.

Chapter 4 Analytical Modeling of Bare and Gypsum-Board-Sheathed Wood Stud

4.1 Introduction

This chapter presents finite-element analyses to quantify the contribution of 12.7 mm thick gypsum-board sheathing to the axial compressive capacity of 2440 mm long 38 x 89 mm Spruce-Pine-Fir (SPF) wood studs, i.e., typical construction in light-frame residential structures. It reviews analytical tools presented by others and develops new tools necessary to predict accurately the axial compressive capacity of bare and sheathed studs. These tools will be used in Chapter 5 to determine statistical distributions for the axial compressive capacities of bare and sheathed studs using Monte-Carlo simulation, thus quantifying the contribution of gypsum board sheathing.

4.1.1 Bare Wood Stud

Analytical models are available to predict the axial capacity of bare wood studs. Robertson (1925) considers a linear-elastic stress-strain relationship with a finite crushing stress and an initial mid-height out-of-straightness. Maholtra and Mazur (1970) consider a perfectly straight stud with a nonlinear wood stress-strain relationship, again with a finite crushing stress. Buchanan (1984) presents an empirical equation developed to predict the capacity of a general population of studs, and so does not consistently provide accurate predictions of the axial capacities of individual studs. These assumptions by others have not been validated specifically for 2440 mm long 38 x 89 mm SPF wood studs. Using experimental data from Buchanan (1984), it will be shown that nonlinear wood stress-strain relationships, with finite crushing stresses, and initial mid-height out-of-straightness must be considered to accurately predict the axial compressive capacity of bare wood studs.

4.1.2 Gypsum-Board-Sheathed Wood Stud

Chapter 2 concluded that current models available in literature (i.e., Kamiya, 1987 and 1988, and Srikanth, 1992) are not suitable for predicting the strength or stiffness of 2440 mm long 38 x 89 mm SPF wood studs with 12.7 mm gypsum-board sheathing on both sides. These models assume a linear-elastic wood stress-strain relationship, and only Kamiya (1998) considers the effects of nonlinear fastener load-slip response. Experimental testing presented in Chapter 2 determined that nonlinear wood material properties and nonlinear fastener load-slip responses markedly reduce the axial compressive capacity of gypsum-board-sheathed wood studs. Therefore, a new analytical methodology is needed. The data from the experimental tests presented in Chapter 2 will be used in this chapter to validate a new methodology.

4.1.3 Objectives and Methodology

The specific objectives of this chapter are:

1. Quantify the accuracy of current analytical models in literature for predicting the axial compressive capacity of 2440 mm long 38 x 89 mm bare SPF wood studs.

2. Develop and validate a finite element model to predict the axial compressive capacity of bare studs considering a nonlinear wood stress-strain relationship, with a finite crushing stress, and an initial mid-height out-of-straightness.

3. Develop and validate a finite element model to predict the axial compressive capacity of sheathed studs considering a nonlinear wood stress-strain relationship, with a finite crushing stress, an initial mid-height out-of-straightness, and a nonlinear fastener load-slip response.

This chapter first compares the axial compressive capacities of bare wood studs predicted using analytical models by others to those experimentally observed by Buchanan (1984). It will be shown that a more accurate analytical model for bare wood studs is desirable. This is followed by the creation of a finite element model for bare wood studs that will be validated using test data reported by Buchanan (1984). Then, the development of a finite

element model for gypsum-board-sheathed wood studs is presented as an extension of that for bare wood studs, with the addition of gypsum board and fastener connections. Finally, the sheathed stud model will be validated using experimental data from Chapter 2.

4.2 Existing Analytical Models for the Compressive Resistance of Bare Studs

In this section, three existing models for the axial compressive capacity of bare studs are critically evaluated and their accuracy will be assessed by comparison with experimental data. The Perry-Robertson Equation (Robertson, 1925) calculates the capacity assuming the stress-strain relationship is linear-elastic, with a finite crushing stress, f_c, and also accounts for an initial mid-height out-of-straightness, v:

$$[4.1] \quad P_s = \left[f_c A_s + P_e\left(1 + v y_s / r^2\right) - \sqrt{\left[f_c A_s + P_e\left(1 + v y_s / r^2\right)\right]^2 - 4 f_c A_s P_e} \right] / 2$$

where P_s is the axial compressive capacity of the stud, A_s is its cross-sectional area, P_e is the Euler buckling load obtained from Equation [2.1], y_s is the distance from the elastic neutral axis to the extreme fibre, and r is the radius of gyration.

Maholtra and Mazur (1970) reported a variation of the Perry-Robertson equation that neglects initial out-of-straightness but accounts for a nonlinear stress-strain relationship:

$$[4.2] \quad P_s = \left[P_e + f_c A_s - \sqrt{\left(P_e + f_c A_s\right)^2 - 4 P_e f_c A_s c} \right] / 2c$$

where c is a parameter depending on the shape of the stress-strain relationship proposed by Ylinen (1956). Buchanan (1984) investigated the axial compressive capacity of SPF wood stud specimens with ratios of length to depth, L/d, ranging from 0 to 48. He deemed Equation [4.2] with c taken as 0.9 to accurately predict the average capacity of a large sample of studs with L/d ranging from 0 to 48, but did not assess its accuracy to predict the capacity of individual studs with a particular L/d.

Buchanan also reported the following empirically modified cubic Rankin formula:

[4.3] $P_s = f_c A_s \left[1 + f_c (L/d)^3 / 40E_s\right]^{-1}$

where the dimensionless constant, 40, is empirically chosen to account for both initial mid-height out-of-straightness and the nonlinear wood stress-strain relationship. Equation [4.3] is the basis for the design equation used in CAN/CSA 086-09 (CSA, 2009) to predict the axial compressive capacity of bare studs. However, the empirical constant of 40 was selected to approximate the capacity for a general population of studs with L/d ranging from 0 to 48. Therefore, it is not specific to individual studs with a particular L/d ratio.

Table 4.1 summarizes the assumptions used to derive each of the three equations listed above. Robertson (1925) accounts for a finite crushing stress and an initial mid-height out-of-straightness, but does not account for a nonlinear stress-strain relationship. Maholtra and Mazur (1970) account for a nonlinear stress-strain relationship with a finite crushing stress, but do not consider any initial mid-height out-of-straightness. Finally, Buchanan (1984) accounts for a finite crushing stress and uses an empirical constant to indirectly account for nonlinear stress-strain relationships and initial mid-height out-of-straightness. These assumptions have not been validated for predicting the axial capacity of 2440 mm long 38 x 89 mm studs, i.e., L/d of 27.4.

Table 4.1: Properties Considered in Equations for Isolated Studs Reported by Others

Author	Nonlinear stress-strain relationship of wood	Crushing of wood	Initial mid-height out-of-straightness
Robertson, 1925	No	Yes	Yes
Maholtra and Mazur, 1970	Yes	Yes	No
Buchanan, 1984	Indirectly[a]	Yes	Indirectly[a]

[a] Accounted for using an empirically chosen dimensionless constant.

4.2.1 Validation of Existing Models

Buchanan (1984) reported the axial capacity of one hundred 2300 mm long 38 x 89 mm SPF wood studs, Grade No. 2 or better. These studs were a part of the same population that was used to quantify the statistical distribution of E_s reported by Bleau (1984) and f_c reported by Buchanan (1984). The length of 2300 mm used in the experimental program is very similar to the 2440 mm studied in this chapter, and so the nonlinear wood and fastener

properties reported are appropriate for use in the current study. To validate Equations [4.1] to [4.3]. Instead of measuring an initial out-of-straightness for each stud, Buchanan (1984) applied the compressive forces at 2 mm end eccentricities causing single curvature of each stud. He did not report values of E_s or f_c for individual studs. Therefore, the cumulative probability distributions of the observed and predicted values will be compared.

Monte Carlo simulation techniques were used to obtain ten thousand randomly generated values of P_s using Equations [4.1] to [4.3]. The parameters E_s and f_c were deemed to be random, each following a Weibull distribution with the parameters shown in Table 4.2:

[4.4] $$F(x) = 1 - e^{-[(x - x_o)/\alpha_w]^{k_w}}$$

where F(x) is the cumulative probability of obtaining a strength less or equal to x, x_o is the location parameter that reflects the lower strength limit, α_w is the scale parameter with the same units as x that reflects the spread of the distribution, and k_w is a dimensionless shape parameter that reflects the skewness of the distribution. The parameters for f_c in Table 4.2 are reported by Buchanan (1984) for 2000 mm long studs, whereas the length of the stud subjected to buckling tests was 2300 mm. Buchanan corrected the value of f_c to account for this length difference using the following equation:

[4.5] $$f_{c_2} = f_{c_1} / (L_2/L_1)^{1/k_L}$$

where f_{c_1} is the crushing stress for stud length L_1, f_{c_2} is the crushing stress for stud length L_2, and k_L is the length effect parameter, assumed to be 13. For L_2 of 2300 mm and L_1 of 2000 mm, the correction to the crushing stress, i.e., $f_{c_2} = 0.989\ f_{c_1}$, results in a mean of 31.5 MPa and a standard deviation of 4.75 MPa, with k equal to 7.86, α equal to 33.5 MPa, and x_o equal to 0 MPa.

Table 4.2: Random Variables in a Bare Wood Stud

Variable	Type	Mean *(MPa)*	St. Dev. *(MPa)*	k_w	α_w *(MPa)*	x_o *(MPa)*	Source
Wood stud with d = 89 mm							
E_s	Weibull	9780	1730	3.97	6740	3510	Bleau (1984)
f_c	Weibull	31.8	4.81	7.86	33.8	0	Buchanan (1984)

Foschi et al. (1989) reported a correlation coefficient, r_c, between E_s and f_c of 0.6. Buchanan (1984) reported that assuming the same percentiles for E_s and f_c values produces better predictions of P_s than no correlation. Thus, the same percentiles for E_s and f_c values was assumed for the simulations reported in this chapter that.

Equation [4.1] predicts P_s assuming an initial mid-height out-of-straightness, v, whereas Buchanan (1984) applied end eccentricities, e, to his test specimens. The secant formula derived for straight columns subjected to end eccentricities (e.g., Timoshenko and Gere, 1961) applies for this case and is given by:

$$[4.6] \quad P_s = f_c A_s \,/\, \left[1 + \left(e y_s / r^2\right)\, \sec\left(0.5\, L/r \sqrt{P_s / E_s A_s}\right)\right]$$

However, as P_s appears on both sides of the equation, an iterative solution is required. Thus, the secant formula is not very suitable for Monte Carlo techniques involving large number of simulations. Timoshenko and Gere (1961) compared Equations [4.1] and [4.6] for $P_s = P_e$ and derived the following relationship:

$$[4.7] \quad v = 4e/\pi$$

This relationship can be substituted into Equation [4.1] to approximate P_s for a straight stud subjected to axial compressive loads with end eccentricities, i.e.:

$$[4.8] \quad P_s = \left[f_c A_s + P_e\left(1 + 4e y_s \,/\, \pi r^2\right) - \sqrt{\left[f_c A_s + P_e\left(1 + 4e y_s \,/\, \pi r^2\right)\right]^2 - 4 f_c A_s P_e}\right] \,/\, 2$$

The derivation of Equations [4.1] and [4.6] requires $P_s < P_e$ and a finite value of f_c. As a result, the theoretical ratio v:e would be slightly less than $1:4/\pi$, and so the theoretical value of P_s would be slightly larger than that predicted using Equation [4.8].

Figure 4.1 shows the cumulative distribution curves for the predicted and observed values of P_s. The Euler buckling load, Equation [2.1], is included to represent the upper bound compressive capacity of a stud with linear wood properties and no crushing stress limit. This equation yields a test-to-predicted ratio of 0.88 at the 50th percentile values. The Perry-Robertson approach, Equation [4.8], is the upper bound capacity of a stud with linear-elastic wood properties, a finite crushing stress, and an initial mid-height out-of-straightness. This results in a predicted capacity that is less than the Euler buckling load, as shown. The observed values are smaller than those predicted using the Perry-Robertson approach for a cumulative probability of 0.75 or less, with a test-to-predicted ratio of 0.958 at the 50th percentile values. This indicates the finite crushing stress and the initial mid-height out-of-straightness are important parameters, but suggests the assumed linear wood properties results in an overestimation of P_s. Equation [4.2] by Maholtra and Mazur (1970), which accounts for nonlinear wood properties with a finite crushing stress but neglects an initial out-of-straightness, predicts P_s to be greater than that predicted using the Perry-Robertson approach but less than the Euler buckling load, with a test-to-predicted ratio of 0.93 at the 50th percentile values. This indicates that the nonlinear material response is important but has less influence than the initial mid-height out-of-straightness. Therefore, Equation [4.2] overestimates P_s having a cumulative probability of 0.75 or less for 2440 mm long 38x89 mm studs. Conversely, the top 20th percentile observed values are underestimated using the Perry-Robertson approach and are well predicted using the Equation [4.2], likely due to a lack of importance of initial out-of-straightness for these studs. However, the upper 20th percentile of the distribution has little influence on the reliability of the studs, and so is not of interest in this study. Equation [4.3] by Buchanan (1984) predicts P_s to be greater than the Euler buckling load, with a test-to-predicted ratio of 0.79 at the 50th percentile values. It is derived empirically for a general population with L/d ranging from 0 to 48, but poorly predicts P_s for 2300 mm long 38 x 89 mm SPF studs, i.e., with L/d = 25.8. The strength equation specified in CAN/CSA 086-09 (CSA, 2009) is identical to Equation [4.3] except that the dimensionless constant in the denominator, i.e.,

40 in Equation [4.3] is reduced to 35. The CSA-086 equation gives results that are similar to Equation [2.1]. The overestimation from all five equations suggests that the nonlinearity in the wood stress-strain relationship, wood crushing stress, and the initial mid-height out-of-straightness all have a significant influence on P_s. Therefore, a new analytical methodology is needed for more accurate predictions of P_s.

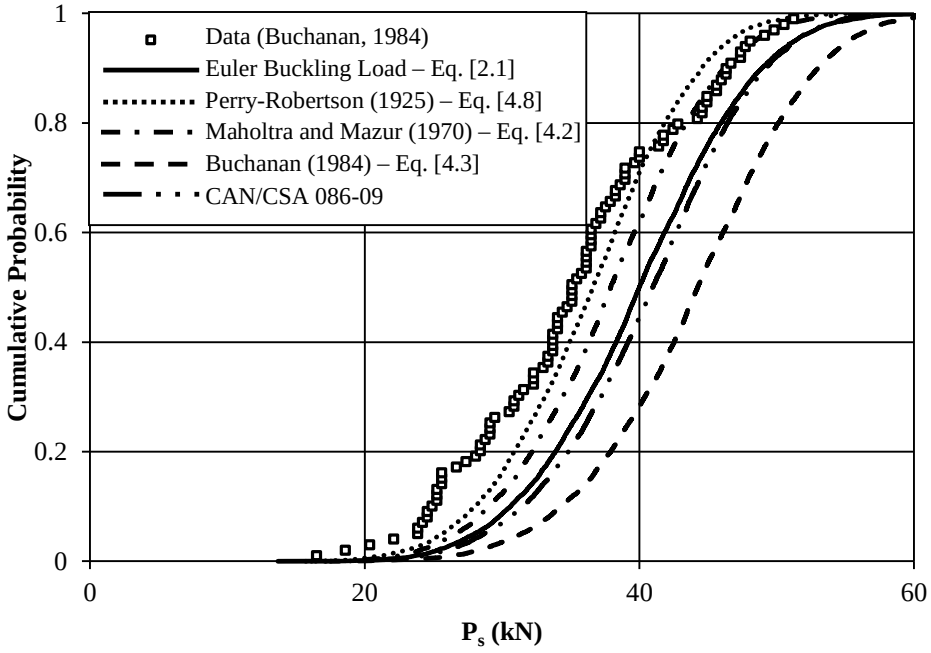

Figure 4.1: Cumulative Probability Distribution of P_s as Predicted by Others

4.3 Finite Element Modeling of Bare Stud

In this section, a finite element model is presented that accounts for a nonlinear wood stress-strain relationship, with a finite crushing stress, and an initial out-of-straightness of the stud. The model will be validated using the test data reported by Buchanan (1984).

4.3.1 Design of Model

Figure 4.2 shows a two-dimensional idealization of a bare stud modeled using ANSYS (ANSYS, 2012), with a length of 1220 mm and a depth of 89 mm. The buckled shape is symmetric about the stud mid-height, so only the top half of the stud is idealized, as shown,

with a free end at the top and a fixed end at mid-height, achieving an effective length of 2440 mm. The wood stud comprises four-node plane-stress elements with uniform thicknesses of 38 mm. Elements were sized such that changing the mesh size by a factor of 0.5 or 2.0 had negligible effect on the accuracy of the results or the speed of the solution. The 89 mm depth of the stud was divided into four 22.25 mm wide elements, and the 1220 mm height of the stud was divided into sixty-one 20 mm long elements.

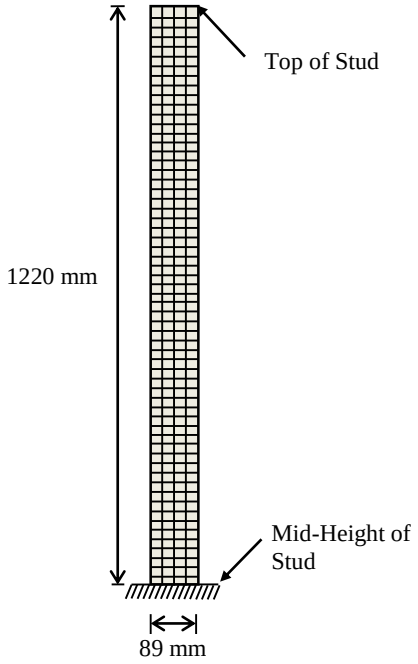

Figure 4.2: Finite Element Model for Isolated Stud

Four equations proposed for the wood stress-strain relationship for compressive stress parallel to the grain (Ylinen, 1956; O'Halloran, 1973; Glos, 1978; and Song and Lam, 2009) were reviewed. Buchanan (1984) and Bleau (1984) both used O'Halloran's equation to model bare studs subjected to axial compression, whereas Lau (2000) used Glos' equation to model beam-column interactions of bare studs. As shown in Figure 4.3, these relationships are very similar, thus, the present study adopted the most current relationship reported by Song and Lam:

[4.9] $$\sigma = (r_n - 2)f_c(\varepsilon / \varepsilon_1)^3 + (3r_n - 2)f_c(\varepsilon / \varepsilon_1)^2 + E_s\varepsilon$$

where σ is the stress, ε is the strain, ε_1 is the strain at $\sigma = f_c$, and r_n is an index of nonlinearity given by:

[4.10] $r_n = \varepsilon_1 E_s / f_c$

This index was originally proposed by Ylinen (1956) and is consistently used in all four proposed material relationships. It has therefore been studied extensively: O'Halloran (1973) found that r_n of 1.25 best fits data for clear wood specimens; Glos (1978) found that r_n of 1.35 best fits data for German spruce timber with defects; and Song and Lam (2009) estimated r to be between 1.06 and 1.67 for SPF studs. Buchanan (1984) and Bleau (1984) selected r_n of 1.35 to simulate bare SPF wood studs subjected to axial compression loads, and so this value has also been adopted for the present study.

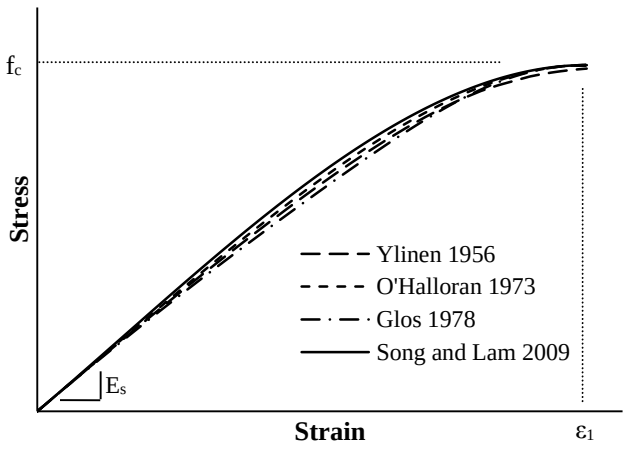

Figure 4.3: Stress-Strain Relationship of Wood as Reported by Others

The wood stress-strain relationship in tension is assumed to be linear-elastic (e.g., Buchanan, 1984) with a constant slope equal to E_s in compression. No tensile failures were observed experimentally in bare wood studs subjected to axial compressive loads with small eccentricities of 2 mm (Buchanan, 1984). Thus, no limiting tensile stress was considered.

The initial out-of-straightness was created using a horizontal linear temperature gradient to induce a curvature in the stud with negligible residual stresses (e.g., Krisciunas, 2011). The

applied temperatures ranged from -50°C at the extreme fibre of the concave side linearly to +50°C at the extreme fibre of the convex side. The resulting initial mid-height out-of-straightness was controlled by varying the coefficient of thermal expansion. For example, a coefficient of thermal expansion of 1.12×10^{-6}/°C introduced a lateral displacement of 1 mm: other out-of-straightness magnitudes could be achieved by proportional scaling.

Subsequently, an axial compressive load was applied concentrically at the top of the stud using the displacement control feature in ANSYS, which allowed for better definition of the axial load versus lateral mid-height deflection response of the stud as the maximum resistance was approached. This method ensured the effects of a nonlinear wood stress-strain relationship and geometric nonlinearities due to large deformations would be accurately captured. The accuracy of the solution was assessed using displacement increments of 0.125 and 0.0125 mm, which resulted in a negligible effect on P_s. Therefore, a displacement increment of 0.125 mm was selected as it substantially reduced the time required to run a full analysis.

4.3.2 Validation of Model

The finite element model was modified to compare the predicted results to those observed by Buchanan (1984). Specifically, the length of the stud was shortened to 2300 mm ($L/2$ = 1150 mm), with $v = 0$, and end eccentricities of 2 mm were introduced by shifting the point of load application. The stud depth, number of elements, end connections, and material properties were otherwise unchanged.

A Monte Carlo simulation was conducted using the Latin Hypercube sampling method (e.g., Iman and Conover, 1980) to sample the input random variables E_s and f_c as it markedly reduces the number of simulation needed to obtain an accurate cumulative probability distribution of the output P_s (e.g., Iman and Helton, 1988). The purpose of these simulations was to compare the predicted P_s distribution to that obtained from the 100 test values of P_s reported by Buchanan (1984). A total of 1000 simulations was performed using the ANSYS software.

Input values for E_s and f_c were taken from Table 4.2. The ANSYS software can simulate partially correlated variables by adjusting input values for each random variable such that the desired r value is approached as the sample size is increased. Figure 4.4 shows the 1000 input E_s and f_c pairs: The resulting r_c of 0.587 is very close to the target value of 0.6.

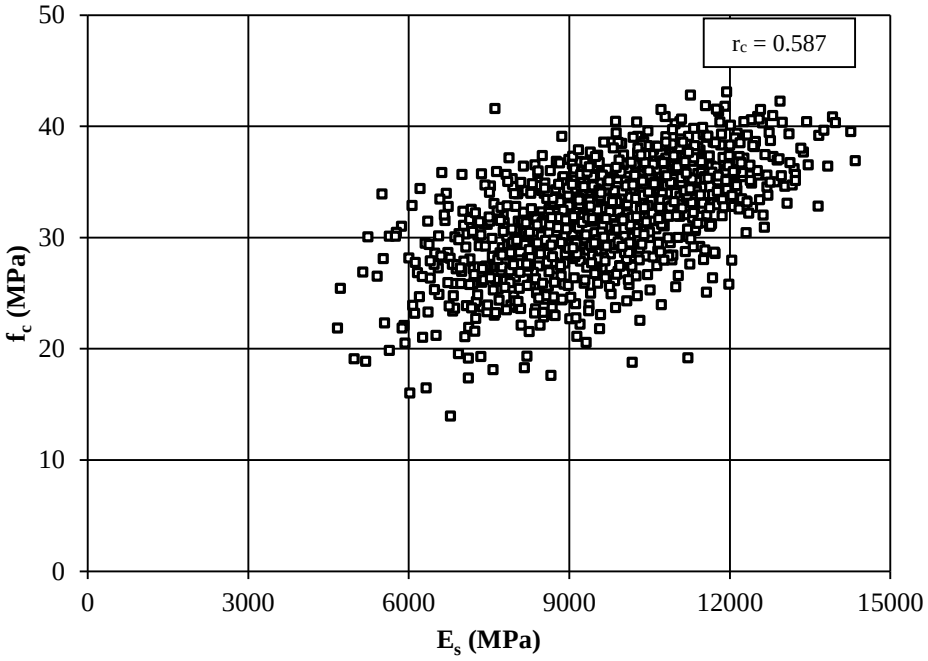

Figure 4.4: Correlation between E_s and F_c for Monte Carlo Simulations

Figure 4.5 is an adaption of Figure 4.1, with the cumulative probability distribution of the ANSYS model added. The proposed model predictions are in very good agreement with most of the observed data by Buchanan (1984), with a test-to-predicted ratio of 1.00 at the 50^{th} percentile values. The upper tails of the predicted and observed distributions are not in good agreement. However, as discussed with Figure 4.1, these values have little influence on the reliability of the studs, and so are not of particular interest. There is a very good agreement between the predicted and observed distribution below the 10^{th} percentile and above the 30^{th} percentile values. The predicted distribution is slightly unconservative between the 10^{th} and 30^{th} percentile values, perhaps due to the small sample size. Therefore, this model will be used in the present study to predict the axial compressive capacity of bare 2440 mm long 38 x 89 mm long SPF wood studs.

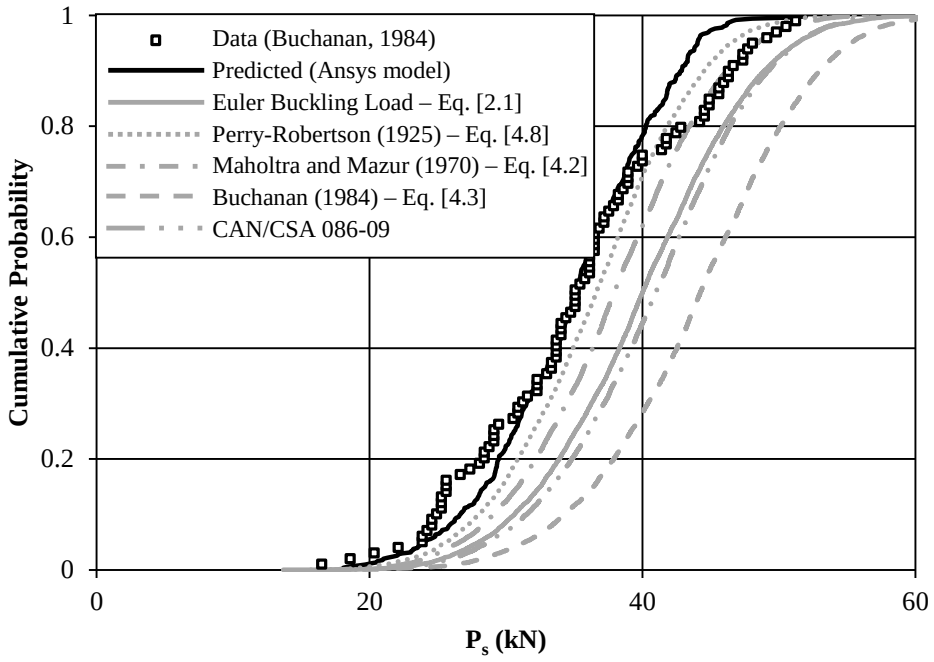

Figure 4.5: Cumulative Probability Distribution of P_s as Predicted using the Proposed Model

4.4 Finite Element Modeling of Sheathed Stud

In this section, a finite element model is presented for the sheathed stud that includes a nonlinear wood stress-strain relationship, with a finite crushing stress, initial out-of-straightness of the stud, and nonlinear fastener load-slip response. The validity of the model will be investigated using the test data reported in Chapter 2.

4.4.1 Design of Model

The finite element model of the gypsum-board-sheathed stud, shown in Figure 4.6, is an extension of that of the bare stud presented in Section 4.3, with the addition of gypsum-board sheathing and fastener connections. As was the case for the bare stud, only the top half of the sheathed stud is modeled with a free end at the top and a fixed end at mid-height. Figure 4.6(a) shows the gypsum board centroid at a distance of half its thickness, i.e., t/2, from each edge of the stud exterior plate-elements, and fasteners located at uniform

spacing, s, that is a function of the number of fasteners. A fastener end-distance of 20 mm was used at the top to simulate typical installation practice (Rousseau, 2011).

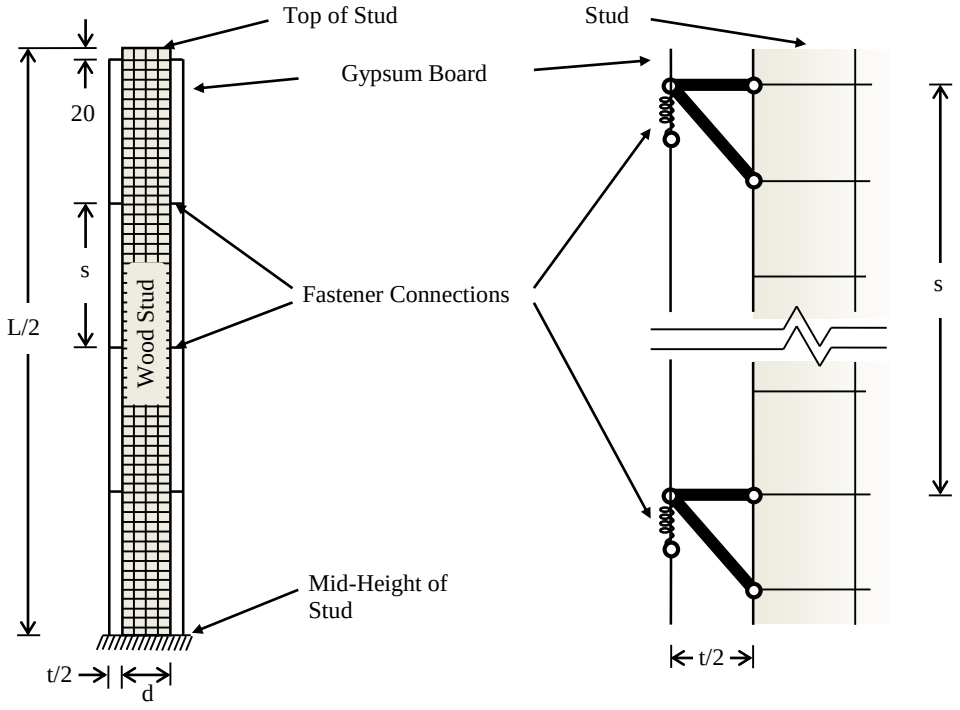

(a) Full Model (b) Details of Fastener Connections

Figure 4.6: Design of Gypsum-board Sheathed Wood-stud Model (N.T.S.)

Two methods for modeling the gypsum board were considered. One uses shell elements to capture the effect of shear lag and account for moment resistance across the gypsum-board thickness. Shear lag reduces the effective area of the gypsum-board width, b_{GB}, and so reduces the stiffness of the sheathed stud. Conversely, accounting for moment resistance across the gypsum-board thickness, t, very slightly increases the stiffness of the sheathed stud. The other method neglected both of these effects: link elements extended from one fastener to the next with cross-sectional areas equal to that of the gypsum board neglecting shear lag. Both methods obtained nearly identical results. The analysis time using link elements was roughly $1/30^{th}$ of that using shell elements, so link elements were selected to simulate the response of the gypsum board.

Figure 4.6(b) shows the idealization of the fastener connections, with vertical springs modeled using link elements at a distance of t/2 from the edge of the wood that connect to the gypsum board. The spring elements were given cross-sectional areas of 1 mm^2 for simplicity. Rigid axial truss elements connect the vertical springs to the wood stud in lieu of rigid horizontal beams: the latter required fixed ends at the edge of the stud that are difficult to model correctly. Conversely, the axial truss elements were simple to model and did not affect the response.

The size of each wood-stud element was the same as that used for the bare stud: 38 mm thick by 22.5 mm wide by 20 mm tall. The gypsum-board links are simple axial members, thus were idealized using single elements of length s. The vertical spring elements are simple axial members idealized using single elements of 10 mm in length, i.e., a length capable of accommodating deflections greater than the maximum slip of 3 mm considered in the idealization of the fastener load-slip response in Chapter 3.

The gypsum-board stress-strain relationship is not well defined in literature. A linear-elastic stress-strain relationship with a stress limit of 2 MPa, identical in tension and compression was assumed based on flexural tests data reported by Groom (1992) (Section 2.2). The consequence of assuming this stress-strain relationship will be determined from a sensitivity analysis presented in Section 5.3.

Equation [3.2] is an idealization of the nonlinear load-slip response of gypsum-board-to-wood stud fastener connections derived from experimental results. The axial load-deflection relationship of the spring elements representing each fastener was defined to be consistent with the idealized load-slip response. Thus, for a cross-sectional area of 1 mm^2 and a length of 10 mm, the stress-strain relationship assigned to the spring elements was:

[4.11] Group 1 (all specimens except in Group 2):

$$\sigma = V_{1.0} \times 26.6 \times \varepsilon \qquad 0 < \varepsilon < 0.025$$

$$\sigma = V_{1.0} [-0.0307 \times \ln(10\varepsilon)^2 + 0.203 \times \ln(10\varepsilon) + 1] \qquad \varepsilon \geq 0.025$$

Group 2 (Corner specimens with 10 mm side distance loaded in the cross-machine direction):

$$\sigma = V_{1.0} \times 26.2 \times \varepsilon \qquad 0 < \varepsilon < 0.025$$

$$\sigma = V_{1.0} [-0.0580 \times \ln(10\varepsilon)^2 + 0.168 \times \ln(10\varepsilon) + 1] \qquad \varepsilon \geq 0.025$$

where σ is the axial stress, ε is the axial strain, and $V_{1.0}$ is the load at a slip of 1.0 mm and is a function of the distance of fastener from side of gypsum board, type of gypsum-board edge (cut or tapered), gypsum-board thickness, and moisture content in the gypsum board. The equations for Group 2 are for conditions where fasteners are located at a corner 10 mm from a cut side of 12.7 mm gypsum board oriented with the load applied in the cross-machine direction of the paper. The equations for Group 1 are for all other conditions.

Fasteners on the convex side of the buckled shape are subjected to a single load-reversal with a hysteretic load-slip response previously idealized by Gad (1997), shown in Figure 3.15. To simulate this response, fastener connections on the convex side of the buckled shape were modeled with one spring element capable of resisting compression only and, superimposed at the same location, another capable of resisting tension only.

An initial mid-height out-of-straightness, v, was created following the method used for bare studs. A linear thermal gradient was applied across all horizontal cross-sections to induce a lateral displacement at the top of the stud, which is equivalent to a mid-height displacement for a full-length stud. Subsequently, loads were applied in displacement control again in increments of 0.125 mm to capture accurately effects of nonlinear wood stress-strain relationship, the nonlinear fastener load-slip response, and geometric nonlinearities due to large deformations.

4.4.2 Validation of Model

In this section, predicted buckling responses of gypsum-board sheathed wood studs are compared to those observed from tests reported in Chapter 2. Before the comparison can be made, however, the input parameters adopted to simulate the test results are presented.

4.4.2.1 Test Data

Table 4.3 presents the input parameters used to simulate the 19 experimental tests reported in Chapter 2. The modulus of elasticity of the stud, E_s, and gypsum-board width, b_{GB}, were obtained directly from Table 2.7. The crushing stress f_c is unknown, and so it was assumed to be perfectly correlated with E_s, as reported in Section 4.2.1. That is, the i^{th} percentile of f_c corresponds exactly to the i^{th} percentile of E_s. The grade of the wood studs was assumed to be No. 2 or better, thus the statistical distributions for E_s and f_c were taken from Table 4.2. Values for f_c were corrected using Equation [4.5] to account for stud lengths of 2440 mm. Thus, f_c is assumed to follow a Weibull distribution having a mean of 31.4 MPa and a standard deviation of 4.73 MPa, with k of 7.86, α of 33.3 MPa, and x_o equal to 0 MPa.

Table 4.3: Input Data for Simulating Sheathed Stud Test Results

Specimen	E_s *(MPa)*	Percentile of E_s	f_c *(MPa)*	v *(mm)*	$V_{1.0}$ *(N)*	b_{GB} *(mm)*
Type A Specimens						
1	4750	0.001	14.1	2.4	354	400
2	7310	0.097	25.0	3.2	354	200
3	7490	0.116	25.5	2.0	354	300
4	8140	0.201	27.6	1.4	354	300
5	8780	0.313	29.4	0.5	354	300
6	9240	0.408	30.7	3.2	354	300
7	9300	0.421	30.9	2.6	354	400
8	9890	0.552	32.4	1.3	354	400
9	10090	0.597	32.9	2.8	354	300
10	10420	0.668	33.7	1.5	354	200
11	11100	0.798	35.4	0.8	354	400
12	12170	0.933	37.8	0.8	354	300
13	12840	0.974	39.3	0.1	354	300
14	13350	0.989	40.3	1.0	354	400
Type B Specimens						
15	5950	0.017	19.9	6.5	792	300
16	8310	0.227	28.0	1.4	792	300
17	10000	0.577	32.7	3.0	792	300
18	11110	0.798	35.4	1.5	792	300
19	12400	0.950	38.3	1.5	792	300

Values for v were obtained from the Southwell Plot derived using experimental data for the sheathed stud. An example of this procedure is shown in Figure 4.7. Figure 4.7(a) shows the observed Southwell Plot and predicted linear-elastic Southwell Plots using Equation

[2.15], derived assuming a linear-elastic buckling response (Southwell, 1931), with P_e from Table [2.7]. Thus, only the initial section of the observed Southwell Plot, corresponding to the linear-elastic regions of the wood stress-strain relationship and the fastener load-slip response, is of interest. The initial few points of the observed response corresponding to mid-height deflections, Δ, approximately between 0 and 0.2 mm, indicate initial flexibility of the testing apparatus, and so are an artifact due to the testing procedure that should be ignored. The following few points, for Δ between 0.2 and 0.7 mm, have a similar slope as that of the predicted Southwell Plots, thus are assumed to represent the linear-elastic response. The predicted Southwell Plots were then adjusted by varying v until the predicted linear plot approximated the linear-elastic region of the Southwell Plot for the observed. For this specimen: P_e equals 37.6 kN; the predicted Southwell Plots are graphed for v values of 1.0, 1.5, 2.0, 2.5, and 3.0 mm; and the curve derived using v of 2.0 mm best fits the observed response. This is confirmed by superimposing the predicted axial load versus lateral mid-height deflection (P-Δ) responses on the observed P-Δ response, as shown in Figure 4.7(b). The response of the sheathed stud for Δ between 0.2 and 0.7 mm corresponds most closely to that defined by v equal to 2.0 mm. Smaller and larger assumed values for v lead to initial predicted responses that are clearly below and above, respectively, the response observed in this mid-height deflection range. Therefore, for this specimen, v is taken as 2.0 mm.

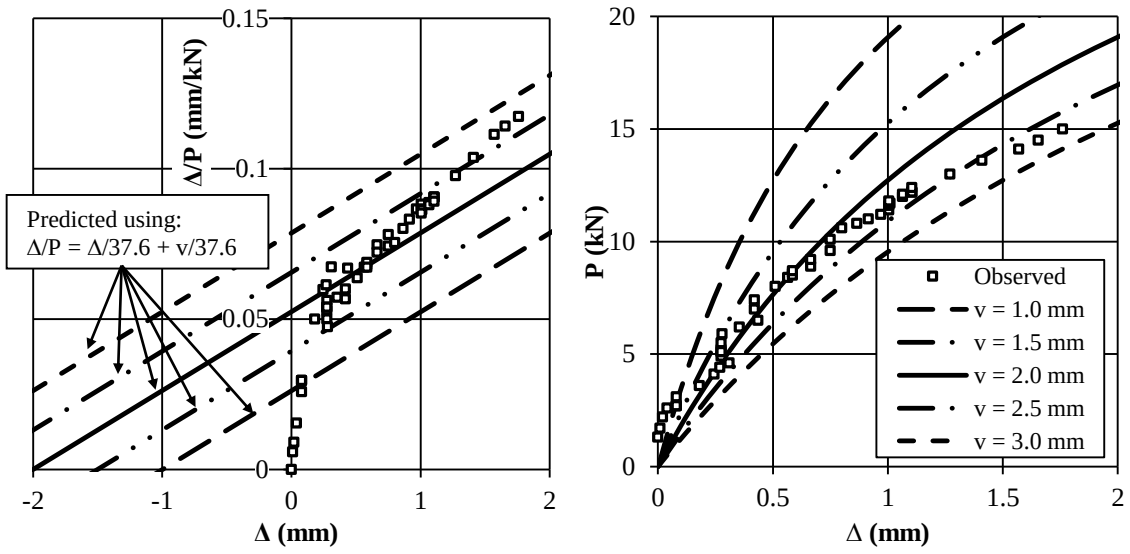

(a) Southwell Plot (b) Load-Deflection Response

Figure 4.7: Estimate of Initial Mid-height Out-of-straightness of Sheathed Stud

Two fastener arrangements were investigated in the sheathed stud tests. Type A specimens had fasteners inserted away from all edges of gypsum board with nominal moisture content greater than 8.0%. Type B specimens had fasteners with a 10 mm side distance along the tapered edge of gypsum board with nominal moisture content less than 8.0%. All gypsum board tested was 12.7 mm thick. The mean values of $V_{1.0}$ obtained from the regression analyses reported in Chapter 3 for Type A and Type B specimens were 354 N and 396 N, respectively. Type B specimens were constructed with two fasteners at each fastener line on both sides of the stud, whereas the numerical model idealizes only one fastener at each fastener line on both sides of the stud. Therefore, the input value for $V_{1.0}$ to simulate Type B specimens was increased to (2 x 396 N =) 792 N. The mean value for E_{GB} of 1780 MPa, as reported in Section 2.2, was assumed for all gypsum board.

4.4.3 Comparison between Test and Predicted Results

The accuracy of the model predictions was quantified using the experimentally observed P-Δ response, fastener slip as a function of mid-height deflection (δ_f-Δ response), and maximum axial compressive resistance, P_c. Similar P-Δ responses indicates that the model

accurately predicts the general buckling response of gypsum-board-sheathed wood studs, whereas similar δ_f-Δ responses indicates that the model also accurately predicts the influence of the gypsum board and fastener connections. If the predicted and observed buckling responses are similar, then so should be the resulting P_c. Agreement is considered good if the predicted and observed data have similar P-Δ and δ_f-Δ responses, thus a test-to-predicted ratio of P_c should be approximately 1.00. The results are presented as two distinct groups: one where fourteen test results and model predictions are in good agreement, and the other where five test results are not in as good agreement with the model predictions.

4.4.3.1 Good Agreement between Test and Predicted Results

Figure 4.8 shows a typical predicted response that is in good agreement with test results. Graphs showing similar agreement between the predicted and observe responses for the other thirteen specimens are provided in Appendix 4A. Figure 4.8(a) shows the predicted P-Δ response to be nearly identical to that observed experimentally. The predicted maximum axial compressive resistance of the gypsum-board-sheathed wood stud, 29.3 kN, is close to the observed P_c of 28.6 kN, i.e., a test-to-predicted ratio of 0.98. Figure 4.8(b) shows typical predicted and observed δ_f-Δ response of end and quarter-point fasteners on the concave side and end fasteners on the convex side. The predicted responses at all three fastener locations are in good agreement with the observed responses, indicating that the model correctly captures the influence of the fastener connections throughout the buckling behaviour.

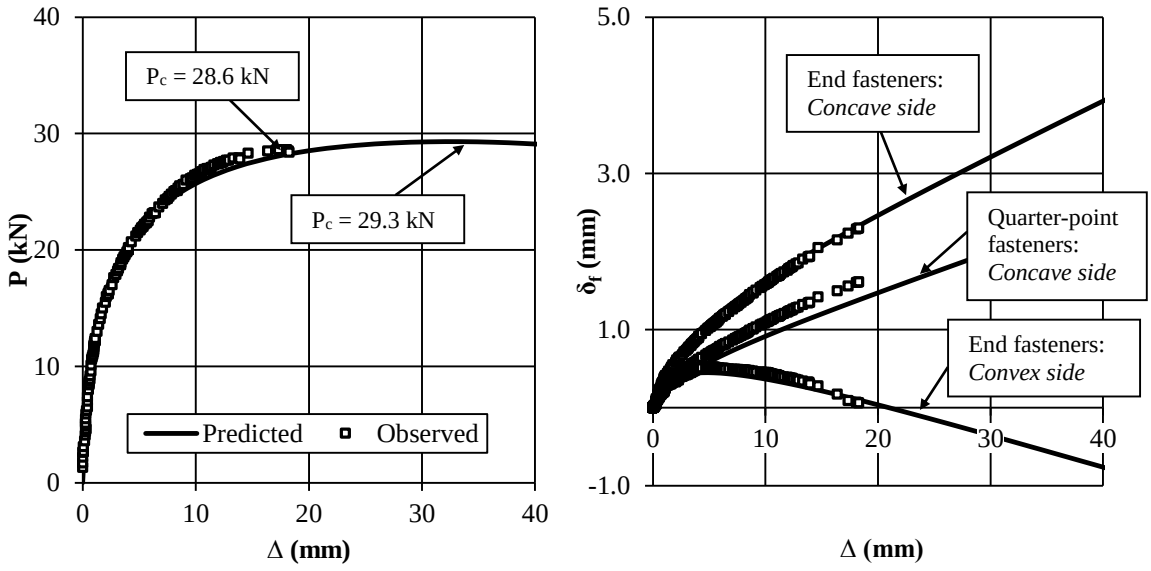

(a) Axial Load vs. Mid-height Deflection (b) Fastener Slip vs. Mid-height Deflection

Figure 4.8: Predicted vs. Observed Response

Table 4.4 summarizes the test and predicted values of P_c and the test-to-predicted ratios for the fourteen specimens in this group. The predicted values slightly overestimate the observed values, with a mean test-to-predicted ratio of 0.98 with a coefficient of variation (CoV) of 0.035. This error is small, and can be attributable to the following errors in input values: (1) the same percentile E_s and f_c values were assumed although a correlation coefficient 0.6 is believed to be more accurate (Foschi et al., 1989), (2) the mean values of $V_{1.0}$ were assumed for all fasteners, and (3) $r_n = 1.35$ was assumed for all studs. Even so, the mean and coefficient of variation of the test-to-predicted values indicate good agreement between predicted and observed values.

Table 4.4: Test-to-Predicted Ratio of P_c

Specimen	P_c (kN)		Test / Predicted
	Tests	Predicted	
1	20.0	19.5	1.03
2	25.9	27.7	0.94
3	28.6	29.3	0.98
6	31.9	34.1	0.94
7	34.2	34.9	0.98
8	35.2	37.8	0.93
9	36.7	37.0	0.99
10	38.1	39.1	0.97
12	46.5	45.9	1.01
13	48.2	49.3	0.98
14	49.1	49.5	0.99
15	25.7	25.4	1.01
18	45.2	45.7	0.99
19	52.4	49.8	1.04
		Mean	0.98
		CoV	0.035

4.4.3.2 Not-as-good Agreement between Test and Predicted Results

There are five specimens where the observed and predicted P-Δ response are markedly different, as is shown for the case of Specimen 4 in Figure 4.9(a). Here, the predicted response is similar to the observed response up to a Δ of 1 mm, indicating that the input value of v is appropriate. However, the predicted response markedly underestimates the observed loads at greater mid-height deflections, indicating the flexural stiffness of the sheathed stud is underestimated. Similar discrepancies occurred for the other four specimens as reported in Appendix 4A. Predictions with the 95th percentile input values of f_c, $E_{GB,}$ and $V_{1.0}$ did not fare much better, indicating the discrepancies cannot be attributable to the input parameter values adopted. To obtain predicted responses that are similar to those observe, it is necessary to increase the value of E_s unrealistically, e.g., by 35% for Specimen 4. Therefore, the discrepancies are due to substantial increases in the flexural stiffness of the stud that were not accounted for in the model.

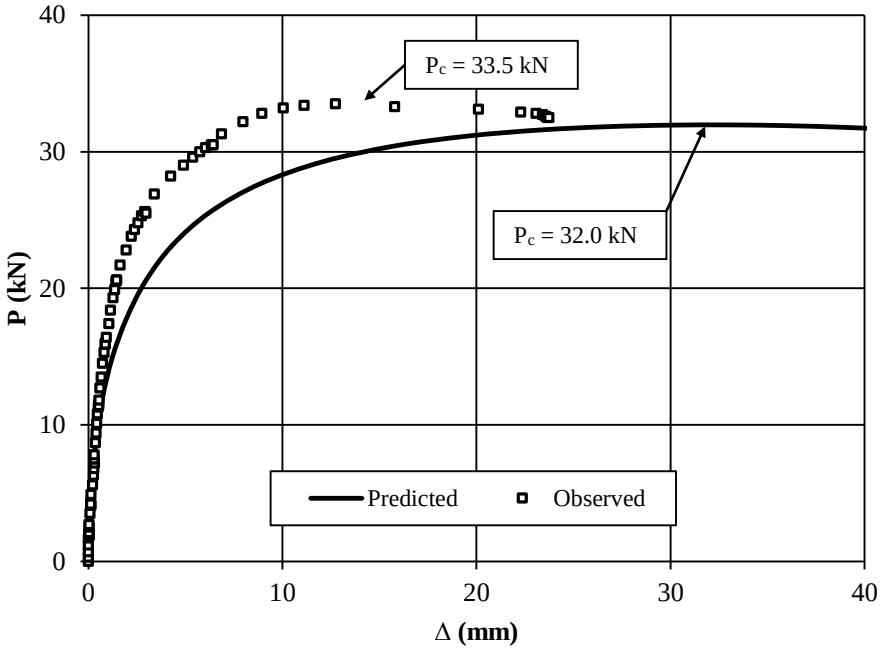

Figure 4.9: Inaccurate Prediction of Axial Load vs. Mid-height Deflection

Figure 4.10 illustrates that double curvature in the original out-of-straightness of the stud (e.g., Johansson et al., 2003, and Yagana et al., 2003) is a possible explanation for the observed increase the flexural stiffness. An inflexion point occurs at a distance L_1 from the top of the stud and L_2 from the bottom of the stud. The greater of the two distances is the effective length of the stud. In its original state, the inflexion point is above mid-height, thus L_2 is the effective length of the stud. Because $L_2 < L$, the flexural stiffness of the stud, i.e., EI/L_2, is markedly larger than predicted, i.e., EI/L^2. When the mid-height deflection, Δ, increases, L_2 increases, thus the flexural stiffness of the stud decreases. Only at large values of deflection does the buckled shape resemble a sinusoidal curve, where L_2 is approximately equal to L and the flexural stiffness of the stud is accurately predicted. The resulting P-Δ response of the stud is initially steeper than predicted and so is expected to yield a larger axial compressive capacity, which is similar to the discrepancy shown in Figure 4.9. Once the axial compressive capacity is reached, L_2 continues to increase as Δ increases, and so the flexural stiffness continues to decrease. This results in a more sudden reduction of axial load after the peak load is reached, also shown in Figure 4.9.

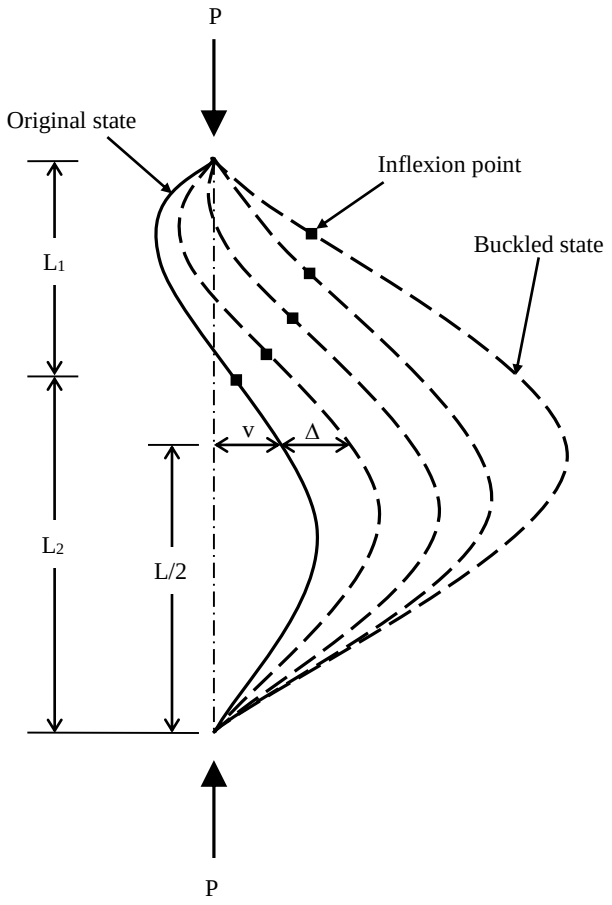

Figure 4.10: Buckled Shape of Stud with Inflexion Point

The initial out-of-straightness of eighteen randomly chosen from the 2440 mm long 38 x 89 mm SPF wood studs tested in Chapter 2 was measured at their mid- and quarter-points. The results are shown in Figure 4.11. The lighter curves correspond to 14 studs that exhibited single curvature. Conversely, the darker curves correspond to 4 studs with double curvature - clear inflexion points are visible near the quarter-points for three studs and near mid-height for one stud. This confirms the possibility of the explanation presented with Figure 4.10.

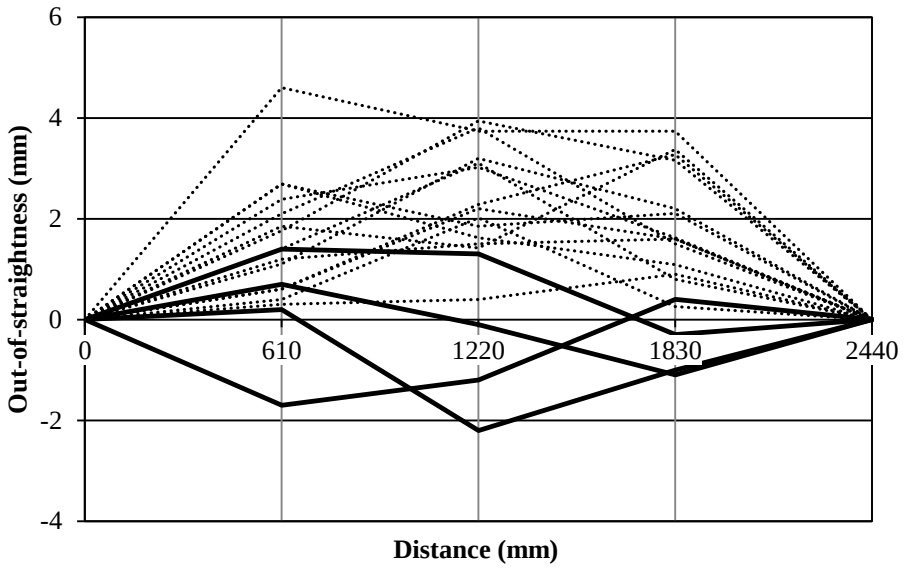

Figure 4.11: Measured Initial Out-of-straightness of Wood Studs

Table 4.5 presents the test-to-predicted P_c ratios for the five studs with not-as-good agreement between observed and predicted results. The observed values for all specimens are greater than that predicted, with a mean of 1.10 and a CoV of 0.054. Thus, although the model cannot accurately predict the compressive capacity of sheathed studs with an initial double curvature profile, at least it predicts a capacity that is less than the actual capacity.

Table 4.5: Test-to-Predicted Ratio of P_c

Stud	P_c (kN)		Test / Predicted
	Tests	Predicted	
4	33.5	32.0	1.05
5	36.6	34.9	1.05
11	47.1	42.5	1.11
16	42.8	36.4	1.18
17	45.2	40.5	1.12
		Mean	1.10
		CoV	0.054

When considering all 19 specimens, the test-to-predicted P_c ratios have a mean of 1.01 and a CoV of 0.060. Therefore, the finite element model for the sheathed stud presented in this chapter is suitable for predicting the capacity of gypsum-board sheathed wood studs subjected to concentric axial compressive loads.

4.5 Contribution of Gypsum-board Sheathing

Table 4.6 compares the axial compressive resistance and associated mid-height deformation of Studs 1 through 19 as computed using the finite-element models presented in this chapter. The gypsum-board sheathing increased the axial compressive resistance of these studs by an average of 18%. This value accounts for the effects of nonlinear material properties and nonlinear fastener response, and so is smaller than the average increase of 29% reported in Chapter 2, which accounts for linear-elastic material properties and linear-elastic fastener response. The predicted 18% increase presented in Table 4.6, therefore, appears to coincide with experimental observations. The gypsum-board sheathing also increased the mid-height deformation associated with the axial compressive resistance by an average of 19%, which is beneficial when addressing the reliability of wood studs subjected to axial compressive loads.

Table 4.6: Contribution of Gypsum-board Sheathing to the Axial Compressive Resistance and Associated Mid-height Deflection of Wood Studs

Stud	Axial compressive resistance			Associated mid-height deflection		
	P_s *(kN)*	P_c *(kN)*	P_c/P_s	Bare stud *(mm)*	Sheathed stud *(mm)*	Sheathed/ Bare
1	15.4	19.5	1.27	32.4	28.9	0.89
2	23.3	27.7	1.19	34.0	35.6	1.05
3	24.6	29.3	1.19	27.9	33.5	1.20
4	26.4	32.0	1.21	27.6	33.1	1.20
5	30.5	34.9	1.14	21.2	30.2	1.42
6	29.3	34.1	1.16	33.9	36.2	1.07
7	30.7	34.9	1.14	31.1	32.0	1.03
8	33.2	37.8	1.14	27.4	30.8	1.12
9	32.6	37.0	1.13	29.7	32.6	1.10
10	37.1	39.1	1.05	23.1	28.6	1.24
11	42.2	42.5	1.01	21.0	28.0	1.33
12	41.6	45.9	1.10	24.2	24.8	1.02
13	45.7	49.3	1.08	9.9	23.9	2.41
14	45.3	49.5	1.09	20.2	25.5	1.26
15	17.5	25.4	1.45	40.9	33.9	0.83
16	26.9	36.4	1.35	27.6	32.6	1.18
17	31.0	40.5	1.31	26.3	31.8	1.21
18	37.0	45.7	1.24	27.4	28.5	1.04
19	41.3	49.8	1.21	27.3	29.2	1.07
Average	32.2	37.4	1.18	27.0	30.5	1.19
St. Dev	8.77	8.50	0.11	6.6	3.5	0.33

Figure 4.12 compares the predicted P-Δ responses of the bare and sheathed studs. Figure 4.12(a) shows typical responses, which correspond to Stud 3. The sheathed stud is stiffer than the bare stud and so has a smaller mid-height deflection for a given load. However, it has a larger mid-height deflection at the maximum load than that of the bare stud. Figure 4.12(b) corresponds to Stud 13, where the ratio of mid-height deflections at the maximum load for the sheathed and bare stud of 2.41 is markedly larger than the mean. Stud 13 has the smallest initial mid-height out-of-straightness of 0.1 mm. Thus the bare stud appears to be almost infinitely stiff because the initial out-of-straightness approaches zero, and so nearly follows the Euler buckling response (see Curve A in Figure 2.2). The associated mid-height deflection at maximum load is very small. The load-deformation response of the sheathed stud is more conventional. The associate mid-height deflection at maximum load is relatively large because the fasteners on the concave side at the ends of the stud have reached their linear load-slip limit.

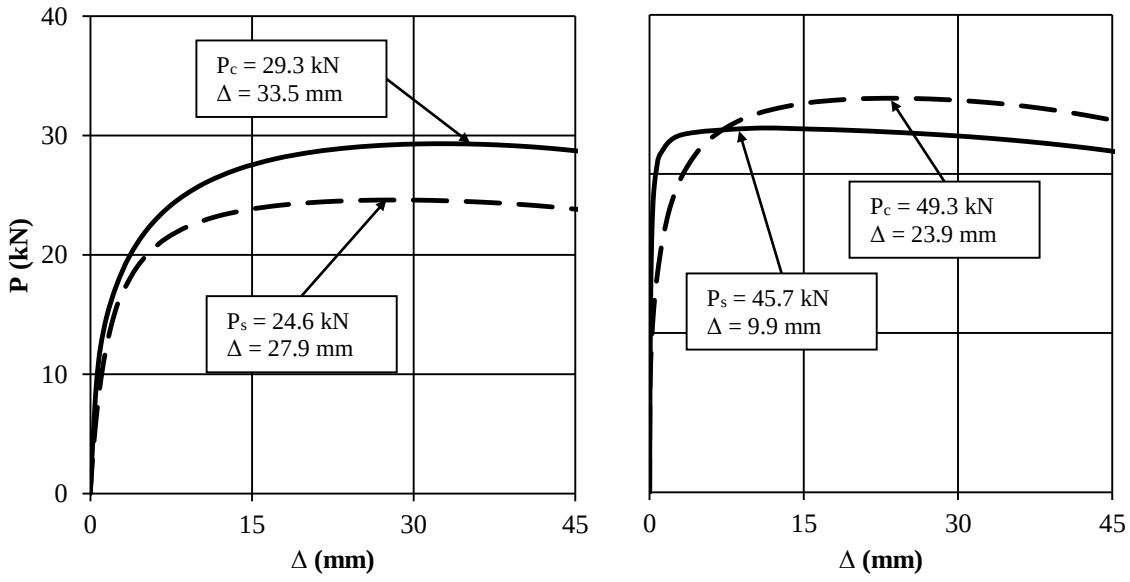

(a) Stud 3 (b) Stud 13

Figure 4.12: Comparison of Predicted Buckling Response of Bare and Sheathed Stud

4.6 Summary and Conclusions

Analytical models available in the literature to predict the axial capacity of bare wood studs (i.e., Robertson, 1925; Maholtra and Mazur, 1970; and Buchanan, 1984) are derived from assumptions that have not been validated for 2440 mm long 38 x 89 mm Spruce-Pine-Fir (SPF) wood studs. That is, no existing models account for both a nonlinear wood stress-strain relationship, with finite crushing stresses, and an initial mid-height out-of-straightness. The accuracy of these models was assessed by comparison with experimental data reported by Buchanan (1984). A new finite element model for bare wood studs was developed in this chapter to address these shortcomings and its accuracy was also checked using Buchanan's experimental data.

The experimental results reported in Chapter 2 clearly indicate that available models in the literature do not accurately predict the axial compressive capacity SPF wood studs sheathed with gypsum-board on both sides. Specifically, they do not account for a nonlinear wood stress-strain relationship with a finite crushing stress, an initial mid-height out-of-straightness, or a nonlinear fastener load-slip response. Therefore, a new analytical model for sheathed studs has been developed in this chapter by extending the bare stud model to include gypsum board and fastener connections and so to account for all these factors. The accuracy of this new model was assessed using experimental data in Chapter 2.

The specific conclusions of this chapter are:

1. Assumptions used to derive all three models reported by others in the literature yield overestimated, thus unsafe, predictions of the axial compressive capacity of 2440 mm long 38 x 89 mm SPF studs.

2. The new finite element model for the bare stud was found to be in good agreement with Buchanan's experimental data, thus is suitable for accurate predictions of the axial compressive capacity of the bare studs. The influence of both nonlinear wood stress-strain relationships with finite crushing stresses and the initial mid-height out-of-straightness must be considered to predict accurately the axial capacity of bare studs.

3. In some cases, the predicted responses of the gypsum-board sheathed wood studs markedly underestimated the observed strength and stiffness. These discrepancies are consistent with the initial deformed shape exhibiting double curvature instead of single curvature which increases the flexural stiffness and compressive strength of the stud. The predictions by the finite element model were always conservative.

4. The model accurately predicted the observed responses of all 19 gypsum-board-sheathed wood studs reported in Chapter 2. The mean test-to-predicted ratio is 1.01 having a coefficient of variation (CoV) of 0.060. Thus, the finite element model for the gypsum-board-sheathed wood studs is suitable to predict axial compressive capacities.

5. The model predicted the gypsum-board sheathing to have increased the axial compressive resistance of the 19 gypsum-board-sheathed wood studs by an average 18%. Similarly, the ductility of these studs was predicted to have increased of 19%.

4.7 References

ANSYS Inc., 2012. ANSYS Academic Research, Release 14.5. Canonsburg, Pennsylvania, U.S.A

Bleau, R., 1984. Comportement des Poutre-Colonnes en Bois. M.Sc.A. Thesis, Department of Civil Engineering, University of Sherbrooke, QC.

Buchanan, A. H., 1984. Strength Member and Design Methods for Bending and Axial Load Interaction in Timber Members. Ph.D. Thesis, Department of Civil Engineering, University of British Columbia, BC. 298 p.

Canadian Standards Association (CSA), 2009. CAN/CSA-086-09: Engineering Design in Wood. Canadian Wood Council, Ottawa, ON.

Foschi, R.O., Folz, B., Yao, F.Z., 1989. Reliability-Based Design of Wood Structures. Structural Research Series, Report No. 34, Department of Civil Engineering, University of British Columbia. 282 p.

Gad, E. F. 1997. Performance of Brick-Veneer Cold-Formed Steel-Framed Domestic Structures when Subjected to Earthquake Loading", Ph.D. Thesis, Department of Civil and Environmental Engineering, The University of Melbourne, Australia. 360 p.

Gerhard, C.C. 1983. Characterization of Physical and Mechanical Properties of 2 by 4 Truss Lumber. USDA Forest Serv. Res. Pap. FPL-431, Forest Products Laboratory, Madison, WI, 24 p.

Glos, P. 1978. Berichte zur Zuverlassigkeitsheorie der Bauwerke: Zur Bestimmung des Festigkeitsverhaltens von Brettschichtholz bei Druckbeanspruchung aus Werkstoff- und Einwirkungskenngrossen. (Reliability Theory for Timber Structures: Determination of Compression Strength Behaviour of Glulam Components from Interaction of Material Properties). Heft 34/1978, Laboratorium fur den Konstrucktiven Ingenierubau, Technische Universitat Munchen, Munich, Germany. 335 p.

Iman R. and Conover W., 1980. Small Sample Sensitivity Analysis Techniques for Computer Models, with an Application to Risk Assessment. Communications in Statistics, Theory and Methods, Vol. A9, No. 17, pp. 1749–1842.

Iman, R. and Helton, J., 1988. An Investigation of Uncertainty and Sensitivity Analysis Techniques for Computer Models. Risk Analysis, Vol. 8, No. 1, pp. 71-90.

Johansson, M., Nystrom, J., and Ohman, M., 2003. Prediction of Longitudinal Shrinkage and Bow in Norway Spruce Studs using Scanning Techniques. Journal of Wood Science, Vol. 49, pp. 291-297.

Kamiya, F., 1987. Buckling Theory of Sheathed Walls: Linear Analysis. Journal of Structural Engineering, Vol. 114, No. 9, pp. 625-641.

Kamiya, F., 1988. Buckling of Sheathed Walls: Nonlinear Analysis. Journal of Structural Engineering, Vol. 113, No. 3, pp. 2009-2022.

Krisciunas, A., 2011. Local Buckling in Corroded Steel Bridge Compression Members. M.E.Sc. Thesis, Department of Civil and Environmental Engineering, Western University, London, ON. 162 p.

Lau, W. W., 2000. Strength Model and Finite Element Analysis of Wood Beam-Column in Truss Applications. Ph.D. Thesis, Department of Wood Science, University of British Columbia, Vancouver, BC, 188 p.

Maholtra, S. K. and Mazur, S. J., 1970. Buckling Strength of Solid Timber Columns. Transactions of the Engineering Institute of Canada, Vol. 13, No. A-4, pp. I-VII.

Nocent, J. A., 2005. Instrumentation to Determine Load Paths in Full-Scale Wood House. M.E.Sc. Thesis, Department of Civil and Environmental Engineering, University of Western Ontario, London, ON.

O'Halloran, M. R., 1973. Curvilinear Stress-Strain Relationship for Wood in Compression. Ph.D. Thesis, Department of Civil and Environmental Engineering, Colorado State University, Fort Collins, CO. USA. 129 p.

Robertson, A., 1925. The Strength of Struts. Institution for Civil Engineers, No. 28. 55 p.

Rousseau, J., 2011. Personal conversation with professional contractor on Sep. 8, 2011.

Song, X. and Lam, F., 2009. Laterally Braced Wood Beam-Columns Subjected to Biaxial Eccentric Loading. Computers and Structures, Vol. 87, pp. 1058-1066.

Southwell, R.V. 1931. On the Analysis of Experimental Observations in Problems of Elastic Stability. Proceedings of the Royal Society of London. Series A, Containing Papers of a Mathematical and Physical Character, Vol. 135, No. 828, pp. 601-616.

Srikanth, T. S. 1992. Structural Reliability of Light-Frame Wood Systems with Composite Action and Load Sharing. Ph.D. Thesis, Department of Forest Products, Oregon State University, Corvallis, OR, USA. 218 p.

Timoshenko, S. P. and Gere, J. M. 1961. Theory of Elastic Stability. 2nd edition, McGraw-Hill, New York, NY, USA. 541 p.

Yanaga, K., Mochida, T., Sasaki, Y., and Hirai, T., 2003. Reduction of effective resistance of nailed shear walls caused by misnailing III. Reduction of effective resistance caused by bows of frame members. Journal of the Japan Wood Research Society, Vol. 49, No. 3, pp. 220-226.

Ylinen, A., 1956. A Method of Determining the Buckling Stress and the Required Cross-Sectional Area for Centrally Loaded Straight Columns in Elastic and Inelastic Range. IABSE Publications, Vol. 16, pp. 529-549

Chapter 5 Quantifying the Contribution of Gypsum Board to the Axial Compressive Capacity of Wood Studs

5.1 Introduction

The contribution of gypsum-board sheathing to the axial compressive resistance of wood studs can vary depending on the physical dimensions and material properties of the wood and gypsum board, and the mechanical properties of fastener connections. It is desirable to quantify the sensitivity of the resistance of bare and sheathed studs to these factors to identify instances where the strength enhancement attributable to the gypsum board is sufficiently large that it should be accounted for in design.

Wood designs conventionally specify the 5^{th} percentile strength (CWC, 1994). The strength contribution of gypsum-board sheathing can thus be quantified by comparing the 5^{th} percentile axial capacity of the bare and sheathed stud. Statistical distributions for the axial capacity of bare and sheathed studs, therefore, need to be quantified for each instance identified to be significant.

5.1.1 Objectives and Methodology

The specific objectives of this chapter are:

1. Identify variables that cause the contribution of gypsum-board sheathing to the axial compressive capacity of a wood stud to be significant. The specific deterministic variables to be considered are: stud depth, stud length, gypsum-board orientation, gypsum-board thickness, gypsum-board width, and fastener spacing. The random variables considered include the modulus of elasticity and crushing stress of the wood, the initial mid-height out-of-straightness of the stud, the modulus of elasticity of the gypsum board, and the strength of fastener connections.
2. Use Monte Carlo simulation to determine statistical distributions of the axial capacities of bare and sheathed studs.

3. Quantify the contribution of the gypsum board to the 5th percentile axial compressive resistance of sheathed studs.

The research presented in this chapter uses the validated finite element models presented in Chapter 4 to analyze the axial compressive resistance of bare Spruce-Pine-Fir (SPF) wood studs and studs with gypsum-board sheathing on both sides to simulate interior walls in light-frame wood construction. Before presenting the sensitivity analysis and Monte Carlo simulation results, the ranges of the deterministic variables and statistical parameters for the random variables will be quantified. Then the sensitivity analysis results will be presented and the deterministic and random variables that significantly impact the strength contribution of gypsum-board sheathing will be identified. Next, Monte Carlo simulation will be used to generate data sets and define statistical distributions of the axial compressive capacities of the bare and sheathed studs. The contribution of gypsum-board will then be quantified by comparing the strength distributions of the bare and sheathed studs.

5.2 Quantification of Variables

This section presents the ranges of all deterministic variables investigated and the statistical parameters for all random variables considered.

5.2.1 Deterministic Variables

Table 5.1 lists the deterministic variables investigated. Gypsum board is installed with the machine direction of the paper either vertical or horizontal (CMHC, 2013). Vertical installation typically requires no horizontal seams near the middle of the wall, whereas horizontal installation requires horizontal seams because the typical gypsum-board panel width is only 1220 mm. Part 9 of the NBCC (NRC, 2010) lists stud depths of 89 and 140 mm to be most commonly used in light-frame wood-stud-wall construction. The variability of these stud depths is negligible (e.g., Gerhards, 1983) and so is ignored. Typical residential construction features stud walls cut at lengths of 2440 mm, although 3660 and 4280 mm studs are also specified in Part 9. Construction tolerances typically limits

variation in stud lengths due to human error to a few mm at most, which is negligible and so is ignored. Gypsum-board sheets are commonly available in lengths up to 3660 mm, which is the length limit considered in this study for sheathed studs with gypsum board installed vertically. A gypsum-board thickness of 12.7 mm is most commonly used in residential and commercial applications, whereas a larger thickness of 15.9 mm is generally used to increase fire ratings (CMHC, 2013, and Rousseau, 2013). It will be shown that the strength and stiffness of the gypsum board is not significant, and so any variability in the thickness can be ignored. Fastener spacings of 300 mm, i.e., the maximum permitted by Part 9 of the NBCC (NRC, 2010), and 100 mm were investigated. Values for b_{GB} varied from 600 mm, corresponding to the maximum stud spacing permitted by Part 9 of the NBCC, to reduced values of 400 mm, i.e., the typical spacing used in construction, and 300 mm, i.e., the smallest spacing prescribed in Part 9. The effect of varying spacings due to human error was not investigated.

Table 5.1: Deterministic Variables Investigated

Parameter	Dimensions *(mm)*	Criteria
Gypsum-board orientation	-	Vertical and horizontal installation
d	89 and 140	
L	2440, 3660, and 4280[a]	
t	12.7 and 15.9	
s	100 and 300	
b_{GB}	300, 400, and 600	

[a] Only for sheathed studs with gypsum board installed horizontally.

5.2.2 Random Variables

Table 4.2 lists the five random variables considered in the present study. The distribution type, representative statistical parameters, and the associated source are shown for each variable. The wood modulus of elasticity, E_s, and crushing stress, f_c, are assumed to have a correlation coefficient, r_c, of 0.6 (Foschi et al., 1989) and follow Weibull cumulative distributions given by Equation [4.4]. The statistical parameters presented for f_c are representative of 2000 mm long 38 x 89 mm studs and 3000 mm long 38 x 140 mm studs (Buchanan, 1984). Thus, before any analysis was conducted, the values of f_c were adjusted using Equation [4.5] to pertain to stud lengths of 2440, 3660, or 4280 mm. The modulus

of elasticity of the gypsum-board, E_{GB}, is assumed to be normally distributed based an analysis of the data reported by Lee (1999), with the same properties in the machine and cross-machine directions. The fastener capacity at a slip of 1 mm, $V_{1.0}$, is assumed to be normally distributed, as described in Chapter 3, and is a function of the fastener location along the gypsum board, the side distance, moisture content, and gypsum-board thickness. Chapter 4 demonstrated that studs with two fasteners at each connection location, due to a gypsum-board seam along the length of the stud, can be idealized as one fastener with a strength and stiffness that is twice that of a single fastener. The governing fastener condition is therefore the interior fastener case because fasteners along a seam, even for an edge distance of 10 mm, are doubled up and so are stronger and stiffer. The values for $V_{1.0}$ pertain to gypsum-board moisture contents above 8.0% because these correspond to recommended interior relative humidity levels of up to 60% (e.g., CenterPoint Energy, 2006).

Table 5.2: Statistical Parameters of Random Variables Investigated

Variable	Type	Mean	St. Dev.	k	α *(MPa)*	x_o *(MPa)*	Source
Wood stud							
E_s	Weibull	9780 MPa	1730 MPa	3.97	6740	3510	Bleau (1984)
f_c *(d=89 mm)*	Weibull	31.8 MPa	4.80 MPa	7.86	33.8	0	Buchanan (1984)[a]
f_c *(d=140 mm)*	Weibull	26.8 MPa	3.78 MPa	8.45	28.4	0	Buchanan (1984)[b]
v	Half-normal	$7.6x10^{-6}Ld$	$5.8x10^{-6}Ld$	-	-	-	Proposed
Gypsum board							
E_{GB}	Normal	1780 MPa	132 MPa	-	-	-	Lee (1999)
Fasteners in 12.7 mm gypsum board							
$V_{1.0}$	Normal	354 N	52.4 N	-	-	-	Chapter 3
Fasteners in 15.9 mm gypsum board							
$V_{1.0}$	Normal	459 N	55.7 N	-	-	-	Chapter 3

[a] Derived from a stud length of 2000 mm
[b] Derived from a stud length of 3000 mm

The statistical distribution of the initial stud out-of-straightness, v, has not previously been quantified. Yanaga et al. (2003) reported that the angle of rotation at the ends of 3000 mm long Grade 1 and 2 dry 38 x 89 mm SPF wood studs due to shrinkage have a mean of 0 radians with a standard deviation of 0.0048 radians. The initial wood stud profile often feature double curvature, with an inflexion point along the length of the stud, as shown in

Figure 4.10 (e.g., Johansson et al., 2003, and Yanaga et al., 2003). For stud lengths that are compatible with common wall heights, it can be assumed that the rotation at the ends of studs is not strongly correlated with the length of the stud. It was thus assumed that the mean and standard deviation reported can be applied to stud lengths of 2440, 3660, and 4280 mm. To estimate the corresponding v, it can be assumed that the rotation at the left and right ends, θ_1 and θ_2, respectively, are the result of applied end moments M_1 and M_2, as shown in Figure 5.1, given by (e.g., Beer and Johnston, 1992):

[5.1] $M_1 = 2\theta_1 EI_s / L + 4\theta_2 EI_s / L$

[5.2] $M_2 = 4\theta_1 EI_s / L + 2\theta_2 EI_s / L$

where EI_s is the flexural rigidity of the bare stud. The deflection at the mid-height of the stud can be calculated as a function of the end moments: (e.g., Beer and Johnston, 1992)

[5.3] $v = (M_1 - M_2)L^2 / 16EI_s$

Equations [5.1] to [5.3] are used to derive v as a function of θ_1 and θ_2, given by:

[5.4] $v = -(\theta_1 + \theta_2)L / 8$

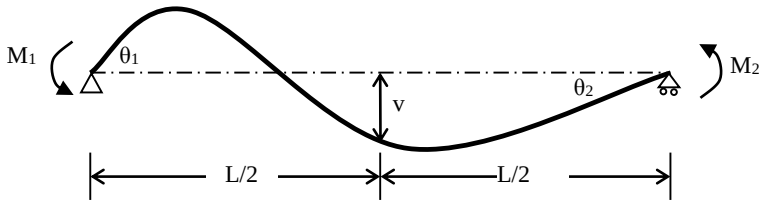

Figure 5.1: Initial Mid-height Out-of-straightness due to End Rotation of Stud

From Equation [5.4], v has a mean value of 0 mm and a standard deviation of $((0.0048L/8)\sqrt{2}=)$ $8.5\text{x}10^{-4}L$. However, the behaviour of a stud subjected to concentric axial compression is independent of the sense of initial mid-height out-of-straightness. Thus, the magnitude of v follows a half-normal distribution (e.g., Elandt, 1961) with a

mean of ($8.5x10^{-4}L\sqrt{2/\pi}$=) $6.8x10^{-4}L$ and a standard deviation of ($8.5x10^{-4}L\sqrt{1-2/\pi}$=) $5.1x10^{-4}L$.

Figure 5.2 shows the cumulative distribution of v for L = 2440 mm predicted using Equation [5.4] with values observed experimentally for 12 bare studs reported in Appendix 2A and 19 sheathed studs reported in Chapter 2. The observed results are in good agreement with the assumed half-normal distribution. Therefore, this distribution, with the parameters shown in Table 4.2, is appropriate to represent the initial mid-height out-of-straightness of the sheathed stud.

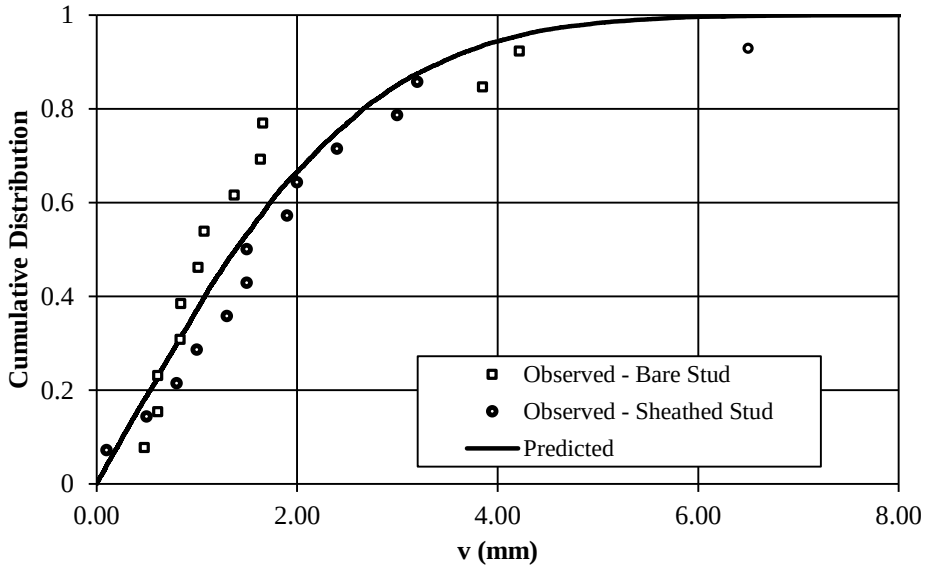

Figure 5.2: Initial Mid-height Out-of-straightness of 38 x 89 mm SPF Stud for L of 2440 mm

Foschi et al. (1989) conducted the landmark reliability analyses of bare studs subjected to concentric axial compression loads. In these analyses, each stud was idealized to have loads applied at small eccentricities to each end, and no initial out-of-straightness. The end eccentricities were assumed to be proportional to the stud depth. Adopting this assumption in the present investigation v can be quantified as having a mean of $7.6x10^{-6}Ld$ and a standard deviation of $5.8x10^{-6}Ld$ because Yanaga et al. (2003) data are for studs with d of 89 mm.

5.3 Sensitivity Analysis

This section presents an analysis to quantify the sensitivity of the axial compressive resistance of the bare and sheathed stud to the variables listed in Table 5.1 and Table 5.2. It is conventional in wood design to specify the 5^{th} percentile strength (CWC, 1994). Therefore, the influence of deterministic variables was assessed by setting the value of most random variables to the 5^{th} percentile values. The initial mid-height out-of-straightness, v, was set at the 95^{th} percentile value because an increase in v decreases the capacity of the stud (Southwell, 1931). Similarly, the influence of each random variable was assessed by varying it within a range that extends beyond the 5^{th} and 95^{th} percentile values.

5.3.1 Influence of Deterministic Variables

Deterministic variables were investigated to delineate conditions where the contribution of gypsum-board sheathing is significant or negligible. Thus, the influence of each deterministic variable was assessed by considering its impact on the ratio of the axial compressive capacity of the sheathed stud, P_c, to that of the bare stud, P_s. A deterministic variable was considered significant when the strength increase attributable to gypsum-board sheathing is sufficient to be included in design practice.

5.3.1.1 Stud Depth and Length, and Gypsum-Board Thickness and Orientation

The influences of the stud depth, stud length, and gypsum-board thickness were investigated concurrently for gypsum board oriented either vertically or horizontally. Figure 5.3 shows the results for gypsum board oriented vertically, i.e., with no horizontal seams. Figure 5.3(a) and (b) show the ratio of P_c/P_s as a function of stud length for d of 89 and 140 mm, respectively, with results presented for t of 12.7 and 15.9 mm. Results were obtained for lengths ranging from 1830 mm to 4280 mm, with markers shown at L of 2440 and 3660 mm. Clearly, an increase in the stud length increases the gypsum-board contribution. For example, for d of 89 mm and t of 12.7 mm, P_c/P_s increases from 1.18 to 1.37 as L increases from 2440 mm to 3660 mm. This increase in gypsum-board

contribution can be attributed to two factors: 1) an increase in the quantity of fasteners needed to fasten longer sheets of gypsum-board to longer studs, and 2) a reduction of the flexural stiffness of the longer stud that makes the stiffening provided by the gypsum board more effective. This can be explained by considering the stud and sheathing as two springs in parallel:

[5.5] $k_c = k_s + k_o$

where k_c is the stiffness of the sheathed stud, k_s is the stiffness of the bare stud, and k_o is the combined stiffness of the gypsum board and fastener. If k_o increases, e.g., more fasteners are provided, and/or k_s decreases, e.g., the stud length increases, then k_c/k_s increases. Figure 5.3 also clearly shows that an increase in stud depth decreases the gypsum-board contribution. For example, for L of 2440 mm and t of 12.7 mm, P_c/P_s decreases from 1.18 to 1.05 as d increases from 89 to 140 mm. This can also be explained using Equation [5.5]: if k_s increases and k_o remains constant, then k_c/k_s decreases. Finally, an increase in gypsum-board thickness increases the gypsum-board contribution, as would be expected. For example, for L of 2440 mm and d of 89 mm, P_c/P_s increases from 1.18 to 1.25 as t increases from 12.7 to 15.9 mm. An increase in gypsum-board thickness is accompanied by an increase in fastener strength, as shown in Table 5.2. Section 5.3.2.5 will show that the strength enhancement due to the increased gypsum-board thickness is mostly due to the increased fastener strength and not the increased flexural stiffness provided by the thicker gypsum board.

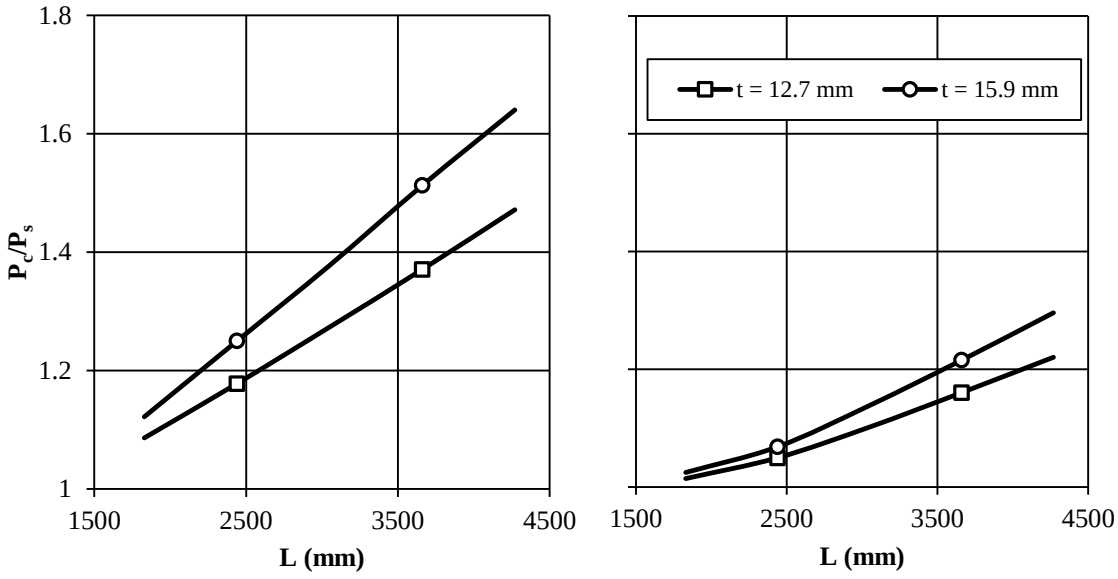

(a) d = 89 mm (b) d = 140 mm

Figure 5.3: Sensitivity of Axial Capacity to Stud Depth, Stud Length, and Gypsum-board Thickness for Gypsum Board Oriented Vertically

These three deterministic variables yield eight different combinations and thus eight different values of P_c/P_s. Six of the eight combinations, i.e., all combinations with d of 89 mm and combinations with d of 140 mm and L of 3660 mm, yield P_c/P_s values ranging between 1.16 and 1.51, which are substantial increases of axial capacity. Conversely, the other two combinations, i.e., with L of 2440 mm and d of 140 mm, yield P_c/P_s values ranging between 1.05 and 1.07, which are only marginal increases. It is, however, difficult to determine whether any of these increases are negligible in practice. Therefore, all eight combinations were investigated further.

Figure 5.4 shows the results for gypsum board oriented horizontally on both sides of the 1830 to 4280 mm long studs, with markers shown at L of 2440, 3660, and 4280 mm. Gypsum boards typically have widths of 1220 mm, thus stud lengths of 2440 mm have only one seam at mid-height. However, stud lengths of 3660 mm must have a minimum of two seams at third-points, and stud length of 4280 mm must have a minimum of three seams with locations depending on the whether a full board is used at the top or bottom of the stud wall. Therefore, the analysis presented in this figure is best-case scenario. Sheathed

studs with horizontally oriented gypsum board are markedly weaker than sheathed studs with gypsum board oriented vertically, as shown from comparison between Figure 5.3, with a vertical axis up to $P_c/P_s = 1.8$, and Figure 5.4, with a vertical axis up to $P_c/P_s = 1.3$. For example, a sheathed stud with L of 2440 mm, d of 89 mm, t of 12.7 mm, and vertically oriented gypsum board yields a P_c/P_s value of 1.18. An otherwise identical sheathed stud with horizontally oriented gypsum board yields a P_c/P_s value of only 1.07. Marginal increases are observed for the axial compressive capacity of 2440 and 3660 mm studs with d of 89 mm, while more substantial increases are observed with L of 4280 mm. Sheathed studs with d of 140 mm yield negligible increases for 2440 mm, and marginal increases for L of 3660 and 4280 mm.

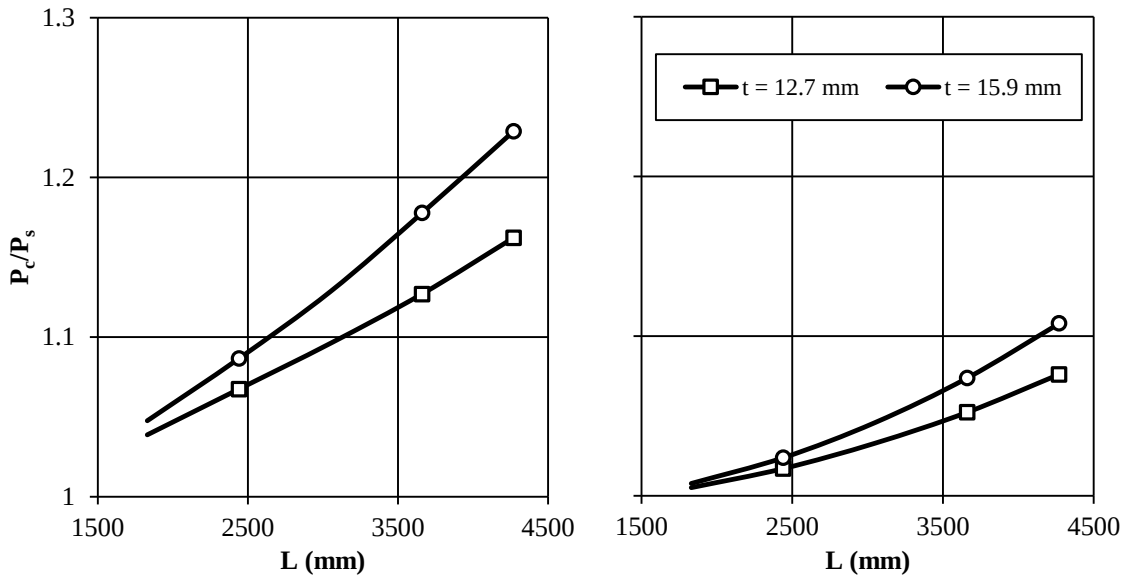

(a) d = 89 mm (b) d = 140 mm

Figure 5.4: Sensitivity of Axial Capacity to Stud Depth, Stud Length, and Gypsum-board Thickness for Gypsum Board Oriented Horizontally

The influence of additional seams for L of 3660 and 4280 mm will further decrease the ratio of P_c/P_s with respect to those shown in Figure 5.4. Seams in gypsum board are generally taped and filled with compound (CMHC, 2013), thus may transfer some axial loads. However, this has not been quantified in the literature and is outside in the scope of

the present research. Therefore, studs with gypsum board oriented horizontally will not be further investigated in this chapter.

5.3.1.2 Fastener Spacing

The sensitivity of the axial compressive strength to the fastener spacing is similar for all eight combinations with gypsum board oriented in the vertical direction. Therefore, results of the analyses on studs with L of 2440 mm, d of 89 mm, and t of 12.7 and 15.9 mm are presented herein with results for the other combinations presented in Appendix 5A.

Figure 5.5 shows the variation of P_c/P_s with fastener spacing, s. Results were obtained for s ranging from 40 mm to 600 mm with markers shown for s equal to 100 and 300 mm. Reducing s from 300 mm to 100 mm markedly increases P_c/P_s from 1.18 to 1.38 for t of 12.7 mm and from 1.25 to 1.50 for t of 15.9 mm. Thus, this reduction in spacing increases P_c by 17% or 20% for t of 12.7 or 15.9 mm, respectively. For new construction, a reduction in fastener spacing from 300 to 100 mm is associated with additional labour costs that may not be economical in practice. Conversely, if an existing sheathed wall requires additional axial capacity, adding fasteners can be a cost-effective alternative. Therefore, the impact of a reduction in fastener spacing was investigated further.

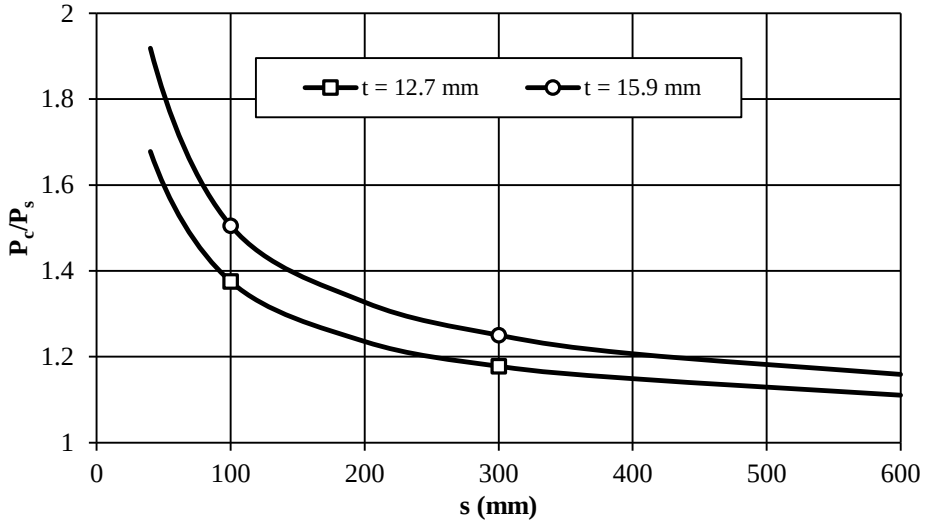

Figure 5.5: Sensitivity of Axial Capacity to Fastener Spacing for L of 2440 mm and d of 89 mm

The data in Figure 5.5 include results for s up to 600 mm (i.e., five fasteners along the 2440 mm length of the stud) to assess the impact on P_c/P_s of spacings that, due to human error, exceed the maximum of 300 mm permitted in Part 9 of the NBCC (NRC, 2010). The ratio of P_c/P_s is reduced for s of 600 mm to 1.11 or 1.16 for t of 12.7 or 15.9 mm, respectively. That is a reduction of 6% for t of 12.7 and 7% for t of 15.9 mm. Therefore, caution is needed to ensure Part 9 provisions are met.

5.3.1.3 Gypsum-Board Width

The finite element model for the sheathed stud was derived in Chapter 4 ignoring shear lag in the gypsum board, i.e., assuming its entire cross-sectional area is effective. The axial capacity increases caused by the gypsum board are very insensitive to the effective gypsum-board width, with P_c/P_s increasing by only 1% when b_{GB} increases from 300 mm to 600 mm. This can be explained by considering the gypsum board and fasteners to behave as two springs in series, with:

[5.6] $$1 / k_o = 1 / k_{GB} + 1 / k_f$$

where k_{GB} is the gypsum-board axial stiffness and k_f is the fastener stiffness. For k_{GB} values that are significantly larger than k_f, k_o approaches the smaller value, k_f. Values for k_{GB}, k_f, and thus k_o can be approximated numerically to demonstrate this. The fastener response may be assumed to be nonlinear with k_f initially between 350 and 2000 N/mm (Appendix 3A) and reducing to less than 100 N/mm when fastener slip increases beyond 1 mm. The smallest value of k_{GB} occurs considering the gypsum-board length from mid-height of the stud to the end fasteners, i.e., 1200 mm for a 2440 mm long stud. Thus, assuming E_{GB} of 1560 MPa and t of 12.7 mm, k_{GB} equals 4950 or 9900 N/mm respectively for b_{GB} of 300 or 600 mm. Thus when end-fastener slips exceed 1 mm (i.e., $k_f < 100$ N/mm), k_o is estimated to be 98.0 or 99.0 N/mm for b_{GB} of 300 or 600 mm, respectively.

Figure 5.6 shows the influence of decreasing the effective width of the gypsum board from 300 mm to zero on P_c/P_s. The results are specific to sheathed studs with d of 89 mm, L of 2440 mm, and t of 12.7 mm, although are similar for sheathed studs with d of 140 mm, L

of 3660 mm, and/or t of 15.9 mm. A decrease of b_{GB} from 300 to 100 mm decreases P_c/P_s from 1.18 to 1.15 (i.e., 2.5% decrease in capacity). When b_{GB} equals 30 mm, which is smaller than the width of the stud, P_c/P_s is still 1.11. Clearly, even for narrow gypsum-board widths, k_{GB} has negligible influence on P_c/P_s. Therefore, the influence of b_{GB} will not be further investigated.

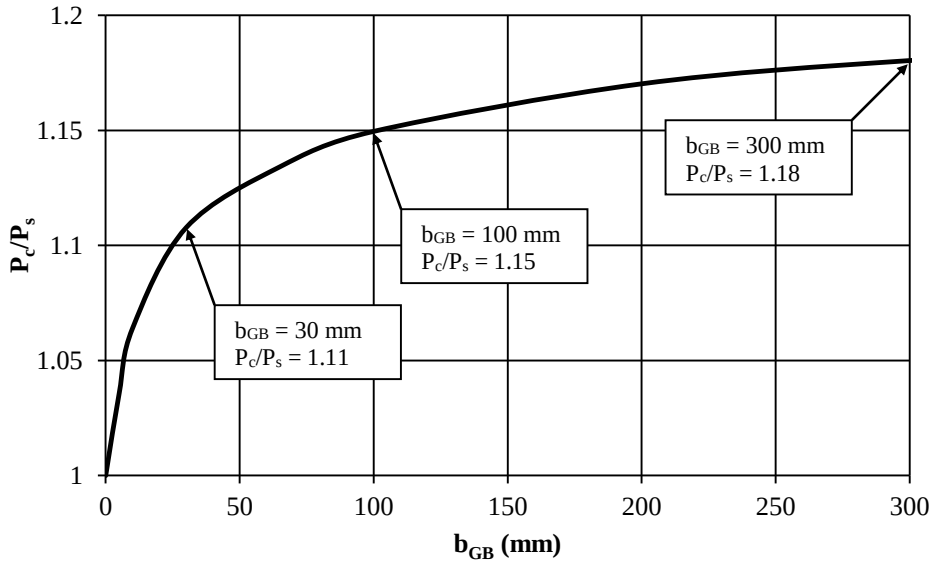

Figure 5.6: Sensitivity of Axial Capacity to Gypsum-board Width

5.3.2 Influence of Random Variables

A sensitivity analysis involving the random variables shown in Table 5.2 was conducted to determine their influence on the axial compressive capacity of bare and sheathed studs. The gypsum-board width, b_{GB}, was held constant at 400 mm for all analyses. For brevity, results presented herein are for sheathed studs with L of 2440 mm and d of 89 mm. The results for L of 3660 mm and d of 140 mm are similar and presented in Appendix 5A.

5.3.2.1 Modulus of Elasticity of Wood

Figure 5.7 shows the influence of the modulus of elasticity of the wood, E_s, over the range from 5000 to 15000 MPa, with markers indicating its 5^{th} and 95^{th} percentile values. This

figure was created assuming E_s and the wood crushing stress, f_c, are not correlated: f_c was held constant at its 5th percentile value. Figure 5.7(a) shows the axial capacity of the bare and sheathed studs with t of either 12.7 or 15.9 mm markedly increases when increasing E_s. The slopes of all three relationships gradually decrease from the 5th percentile values to the 95th percentile value, due to the gradual transition from instability failure influenced by the flexural stiffness of the stud, towards cross-sectional failure influenced by the crushing of the wood. Figure 5.7(b) shows that P_c/P_s decreases substantially with increasing values of E_s. This implies the sensitivity of the axial capacity of the stud to E_s is reduced if the contribution of the gypsum-board sheathing is accounted for. This can again be explained using Equation [5.5] where an increase in E_s increases k_s without increasing k_o, thus k_c/k_s reduces.

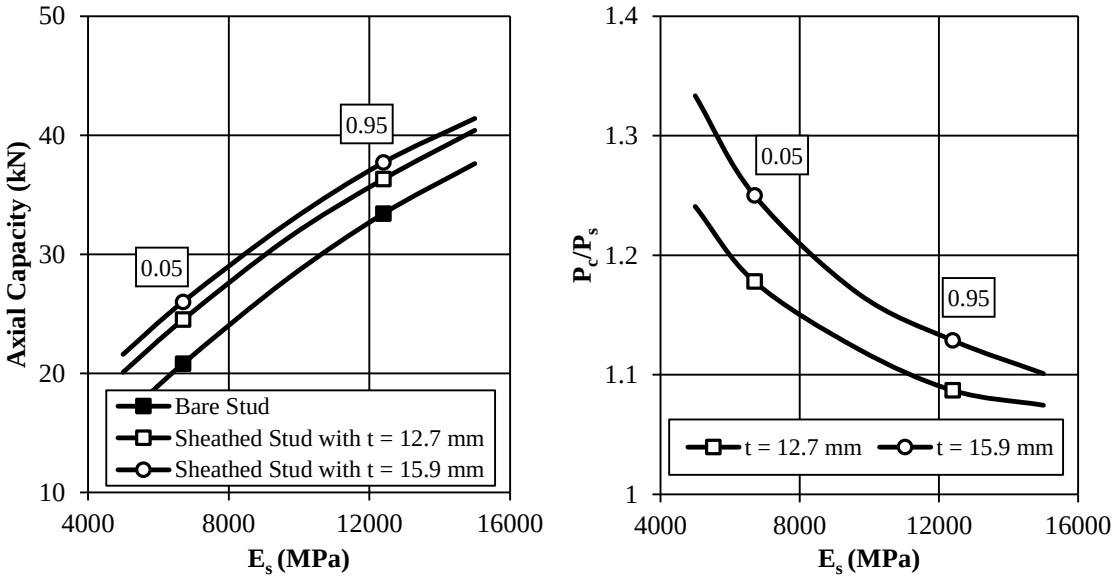

(a) Axial Capacity (b) Gypsum-board Contribution

Figure 5.7: Sensitivity of Axial Capacity to Modulus of Elasticity of Wood for L of 2440 mm and d of 89 mm

5.3.2.2 Crushing Stress of Wood

Figure 5.8 shows the influence of the crushing stress, f_c, over the range from 25 to 45 MPa, with markers indicating its 5th and 95th percentile values. This figure was also created

assuming E_s and f_c are uncorrelated, with E_s held constant at its 5th percentile value. Figure 5.8(a) shows the axial capacities of the bare and sheathed studs are not particularly sensitive to f_c with axial capacities increasing only marginally as f_c is increased from its 5th to 95th percentile values. The slopes of all three relationships also gradually decrease as f_c is increased from its 5th to 95th percentile values, which is due to a gradual transition from a cross-sectional failure to an instability failure. When f_c and E_s are assumed uncorrelated, larger values of f_c corresponds to larger strains and thus greater curvature in the wood before cross-sectional failures occur. An increase in the curvature corresponds to a greater likelihood of instability failure. As a result, as f_c increases, its influence on the axial capacity reduces. Figure 5.8(b) shows that P_c/P_s increases marginally with increasing values of f_c, because the flexural stiffness of sheathed studs is greater than that of bare studs, thus the axial capacity of the sheathed stud is more sensitive to f_c.

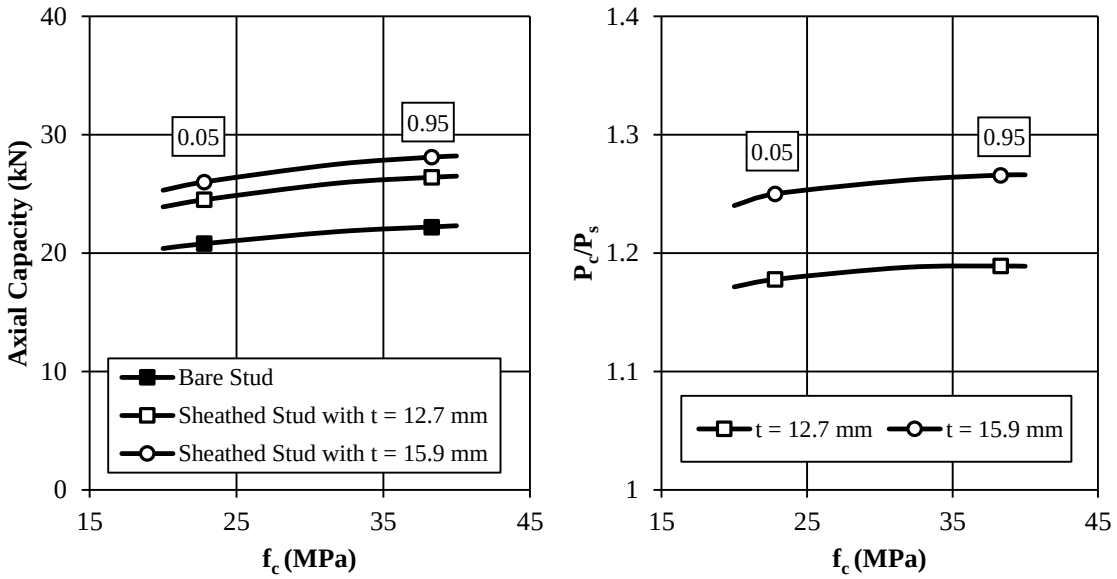

(a) Axial Capacity (b) Gypsum-board Contribution

Figure 5.8: Sensitivity of Axial Capacity to Crushing Stress of Wood

Figure 5.9 shows the influence of the wood modulus of elasticity, E_s, when assumed the percentile of E_s and f_c values are the same. Figure 5.9(a) shows the axial capacities of the bare and sheathed studs markedly increases when increasing E_s, with axial capacities at the 5th and 95th percentile values that are similar to that shown in Figure 5.7(a), but markedly

different from that shown in Figure 5.8(a). Therefore, the axial compressive capacity of bare and sheathed studs is markedly more sensitive to E_s than that to f_c. Figure 5.9(b) shows P_c/P_s to decrease markedly with increasing values of E_s. This is again similar to the results shown in Figure 5.7(a), but markedly different from those shown in Figure 5.8(b). This confirms that the axial capacity is more sensitive to E_s than it is to f_c.

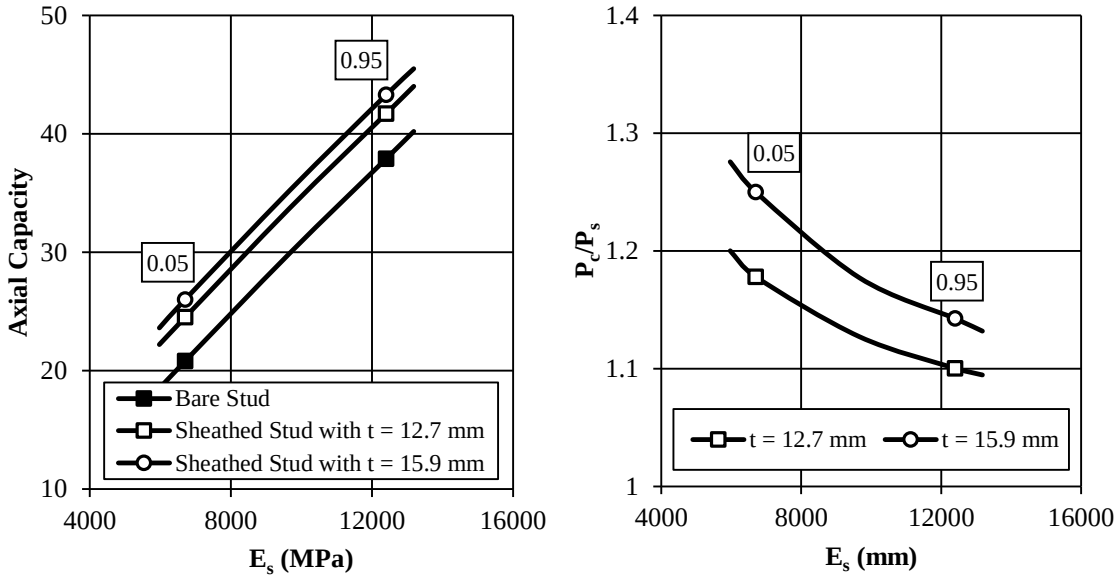

(a) Axial Capacity (b) Gypsum-board Contribution

Figure 5.9: Sensitivity of Axial Capacity to Fully Correlated Young's Modulus and Crushing Stress of Wood

5.3.2.3 Initial Mid-height Out-of-straightness of Stud

Figure 5.10 shows the influence of the initial mid-height out-of-straightness, v, over the range from (0.001d =) 0.09 mm to (0.06d =) 5.34 mm with markers indicating the 5th and 95th percentile values. Figure 5.10(a) shows nearly straight lines having a slight negative slope, indicating that an increase of v marginally decreases P_s and $P_{c,}$ Figure 5.10(b) shows P_c/P_s increasing with increasing v. A larger out-of-straightness yields a larger mid-height deflection at maximum axial load (e.g., Southwell, 1931, and Buchanan, 1984), which corresponds an increase in the contribution of gypsum board due to two factors. First, it increases the slip of fastener connections, thus increases the load resisted by the gypsum

board. Second, it increases stress and strain in the wood, which increases the curvature in the stud for a given load, and thus decreases its flexural stiffness. It was shown in Section 5.3.1.1 that the contribution of gypsum-board sheathing increases when the flexural stiffness of the wood decreases. As a result, larger values of v yield larger relative contributions of the gypsum board.

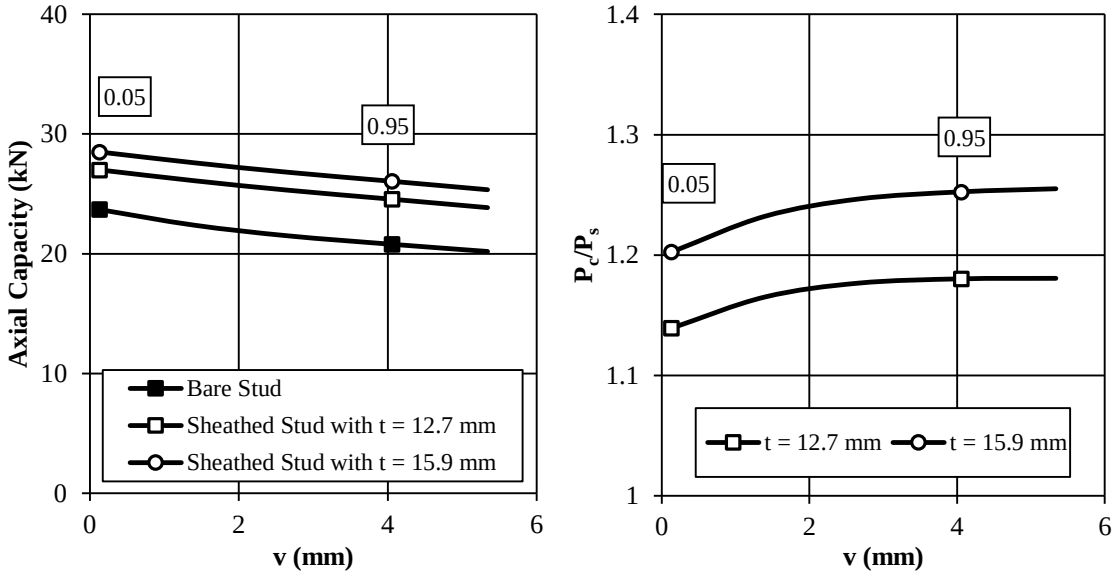

(a) Axial Capacity (b) Gypsum-board Contribution

Figure 5.10: Sensitivity of Axial Capacity to Initial Mid-height Out-of-straightness of Stud

5.3.2.4 Modulus of Elasticity of Gypsum Board

In addition to ignoring shear lag in the gypsum board, the finite element model for sheathed studs presented in Chapter 4 also ignored moment resistance through the gypsum-board thickness. This assumption simplified the model because only the axial stiffness of the gypsum board is idealized. Therefore, the sensitivity of the axial capacity to the modulus of elasticity of the gypsum-board, E_{GB}, is equivalent to that of the gypsum-board width, b_{GB}. In this case, increasing E_{GB} from its 5^{th} percentile value to its 95^{th} percentile value yielded an increase in the axial capacities of the sheathed studs of up to 0.4%. The influence of E_{GB} can thus be considered negligible over the realistic range of this variable.

5.3.2.5 Fastener Strength

Figure 5.11 shows the influence of $V_{1.0}$ over the range 200 to 600 N on the axial compressive capacity of sheathed studs with t of 12.7 or 15.9 mm. The markers for both thicknesses, indicating the 5th and 95th percentile values, are horizontally staggered because $V_{1.0}$ was found in Chapter 3 to be a function of the gypsum-board thickness. This is the primary explanation for the sheathed studs having greater capacities for the thicker gypsum board, as shown in Figure 5.5 through Figure 5.10. This distinction is eliminated in Figure 5.11: the slight difference is attributable solely to an increase in the distance between the gypsum-board force resultants, from 101.7 mm for t of 12.7 mm to 104.9 mm for t of 15.9 mm. The larger difference observed in Figure 5.5 through Figure 5.10 is attributable to an increase in P_c associated with the 5th percentile values of $V_{1.0}$ for t of 12.7 mm to that for t of 15.9 mm. The axial capacity of sheathed studs, thus the contribution of gypsum board, marginally increases with an increase in $V_{1.0}$. Both relationships are nearly linear, indicating that the sensitivity of P_c is relatively constant for the range of $V_{1.0}$ values investigated.

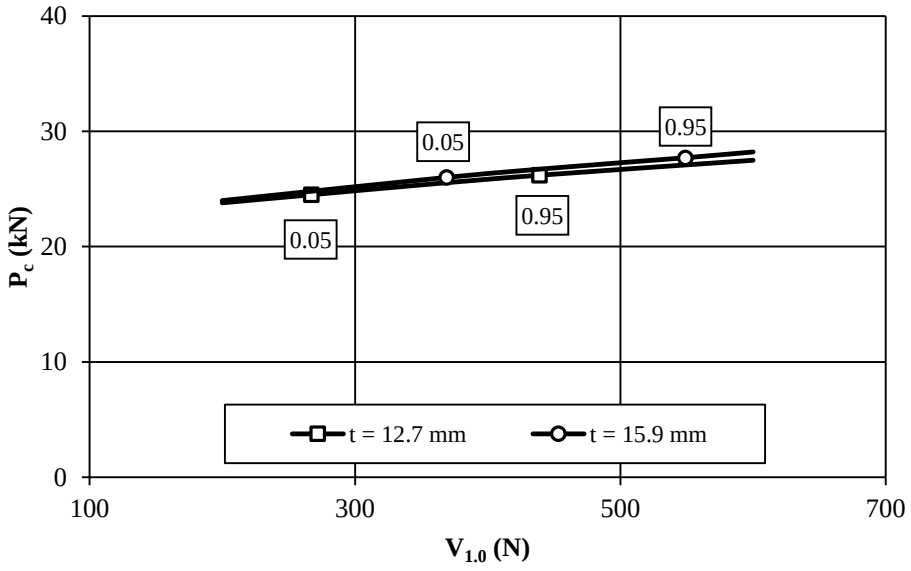

Figure 5.11: Sensitivity of Axial Capacity to Fastener Strength

5.3.2.6 Sensitivity Index

The sensitivity of P_s and P_c to each the random variable presented in Figure 5.7 to Figure 5.11 can be quantified using a dimensionless sensitivity index, d', given by:

[5.7] $$d' = \frac{dP_{max}}{dX}\left(\sigma_x / P_{s\,(x_{.05})}\right)$$

The first term on the right-hand side of this equation, dP_{max}/dx, is the slope of the various relationships shown in Figure 5.7(a) to Figure 5.11(a), and defines the sensitivity of the axial capacity, P_{max}, to variation of random variable x. However, a more useful index must also account for the variability of x. For example, if P_{max} for the 5^{th} and 95^{th} percentile values of random variables x_1 and x_2 are equal, then the influence of x_1 and x_2 on the axial capacity can be considered equal. However, if the standard deviation of x_1 is greater than that of x_2, then P_{max} is more sensitive to x_2 than x_1. Therefore, to account for the variability of x in Equation [5.7], dx is normalized by dividing it by the standard deviation of x, σ_x. To make the sensitivity index dimensionless, the change in axial capacity, dP_{max}, is normalized by $P_{s\,(x_{.05})}$, i.e., the axial capacity of the bare stud associated with the 5^{th} (or in the case of v, the 95^{th}) percentile values of random variables x. Thus larger d' values indicate variables with greater influence on the axial capacity. Conversely, d' values that approaches zero indicate variables with negligible influence on the axial capacity.

Table 5.3 presents the sensitivity index for bare and sheathed studs with L of 2440 mm, d of 89 mm, and s of 300 mm. The relationships shown in Figure 5.7(a) to Figure 5.11(a) are typically nonlinear, thus dP_{max}/dx is not constant across the range of x. To capture this, the sensitivity index was also computed for dP_{max}/dx at the 50^{th} percentile value of x as shown. It is clear that:

1. E_s has a substantially greater influence than any other variable. For example, for t of 12.7 mm, the magnitude of d' for E_s is approximately 5 times that for f_c, v, and $V_{1.0}$ and up to 180 times that for E_{GB}.

2. The magnitude of d' for f_c, v, and $V_{1.0}$ are between 0.02 and 0.05, indicating these random variables can be considered to have a marginal influence on the statistical distribution of the axial compressive capacity of bare and/or sheathed studs.

3. The influence of E_{GB} is negligible.

Thus, the random nature of E_s, f_c, v, and $V_{1.0}$ will be considered when quantifying the statistical distribution of P_s and/or P_c. E_{GB}, however, can be treated as deterministic.

Table 5.3: Sensitivity Index for L of 2440 mm and d of 89 mm

Random variable	Percentile of random variable	d'		
		Bare Stud	Sheathed Stud *t = 12.7 mm*	Sheathed Stud *t = 15.9 mm*
E_s *(r_c = 0)*	5^{th}	0.217	0.205	0.205
	50^{th}	0.182	0.172	0.169
f_c *(r_c = 0)*	5^{th}	0.030	0.041	0.045
	50^{th}	0.020	0.029	0.032
E_s & f_c *(same percentile)*	5^{th}	0.261	0.263	0.267
	50^{th}	0.250	0.251	0.253
v	95^{th}	-0.029	-0.032	-0.032
	50^{th}	-0.049	-0.039	-0.039
$V_{1.0}$	5^{th}	-	0.039	0.029
	50^{th}	-	0.041	0.026
E_{GB}	5^{th}	-	1.2×10^{-3}	1.9×10^{-3}
	50^{th}	-	1.2×10^{-3}	1.6×10^{-3}

If the magnitude of d' for a sheathed stud is less than the associated value for a bare stud, the sheathing decreases the sensitivity of the axial compressive capacity to that particular variable x. The standard deviation of the axial compressive capacity over the range of that particular variable is also reduced. The gypsum-board sheathing has little impact on the magnitudes of d' shown Table 5.3, with similar values for the bare and sheathed studs. For example, the largest difference between the bare and sheathed stud with t of 12.7 mm occurs for the 5^{th} percentile of E_s when r_c equals 0, where a slight reduction in d' from 0.217 to 0.205 is observed from a bare stud to a sheathed stud. Therefore, gypsum-board sheathing has negligible impact on the sensitivity of the increase in axial compressive capacity to the variation of the random variables. As a result, the standard deviations of the distribution of the axial compressive capacity of the bare and sheathed studs are expected to be similar.

5.4 Monte Carlo Simulation

Table 5.4 lists the combination of deterministic variables considered in the Monte Carlo simulations. Values for d varied between 89 and 140 mm; L varied between 2440 and 3660 mm; t varied between 12.7 and 15.9 mm; and s varied between 100 and 300 mm. The simulations with s of 100 mm were limited to one combination with d of 89 mm, L of 2440 mm, and t of 12.7 mm as these are typical dimensions of sheathed studs in existing residential structures. The statistical distribution of P_c and associated P_s were obtained for the nine combinations shown. Random variables E_s, f_c, and v were generated using Monte Carlo techniques available in ANSYS and inputted into the finite element model of the bare stud to determine P_s values. The values for E_s and f_c were assumed to have a correlation coefficient equal to 0.6 (Foschi et al., 1989). The capacity of the sheathed stud was determined using the finite element model for the same variables plus a randomly generated $V_{1.0}$ value. For all combinations, the gypsum board was oriented in the vertical direction, and variables b_{GB} and E_{GB} were kept constant at 400 mm and 1560 MPa, respectively.

Table 5.4: Deterministic Variable Combinations for Monte Carlo Simulations

Combination	d *(mm)*	L *(mm)*	t *(mm)*	s *(mm)*
1	89	2440	12.7	100
2	89	2440	12.7	300
3	89	2440	15.9	300
4	89	3660	12.7	300
5	89	3660	15.9	300
6	140	2440	12.7	300
7	140	2440	15.9	300
8	140	3660	12.7	300
9	140	3660	15.9	300

Figure 5.12 shows the coefficient of variation (CoV) of the 5^{th} percentile value of P_c for Combination 1 in Table 5.4 as a function of the sample size. Monte Carlo simulations were repeated for a total of 20000 samples that were separated into 80 groups of 250 samples, 40 groups of 500 samples, 20 groups of 1000 samples, 10 groups of 2000 samples, and 4 groups of 5000 samples. The 5^{th} percentile value of P_c was obtained from each groups. The tolerable uncertainty was set as CoV $\leq$ 0.01. A sample size of 1000 yielded a CoV of

0.0101, whereas a sample size of 2000 yielded a CoV of 0.00820. Therefore, a sample size of 2000 was used in this study.

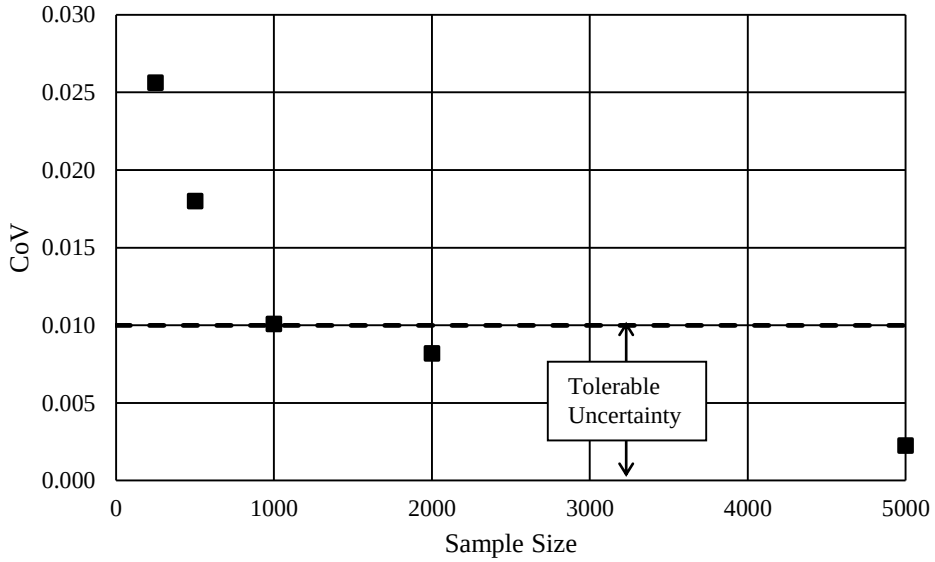

Figure 5.12: Relationship between Uncertainty of 5th Percentile Capacity and Sample Size

5.4.1 Results

Figure 5.13 shows the Monte Carlo simulation results for the bare and sheathed studs with L of 2440 mm, d of 89 mm, s of 300 mm, and t of 12.7 and 15.9 mm. Similar figures for all other combinations of deterministic variables are presented in Appendix 5A. Figure 5.13(a) shows the cumulative probability distribution with markers identifying the 5^{th}, 50^{th}, and 95^{th} percentile values. The increases in axial compressive capacity from the bare stud to the sheathed stud are relatively constant at all percentile values for both sheathing thicknesses. The standard deviations for the bare stud, the stud with 12.7 mm sheathing, and the stud with 15.9 mm sheathing are 5.56, 5.57, and 5.54 kN, respectively, and the corresponding CoVs are 0.174, 0.151, and 0.145, respectively. This is consistent with the discussion of the sensitivity index presented earlier with Table 5.3. Figure 5.13(b) shows the simulation results graphed on normal probability paper, with linear trends observed approximately between z = 2.2 and -2.2, i.e., the 1^{st} and 99^{th} percentile values. The axial compressive capacity of bare and sheathed studs are most sensitive to E_s. Although E_s

follows a Weibull distribution, Figure 5.14 shows it does not deviate far from a straight line, shown as a dashed line between the 1st and 99th percentile of E_s, when graphed on normal probability paper. Therefore, it is appropriate that the simulation results appear to be normally distributed.

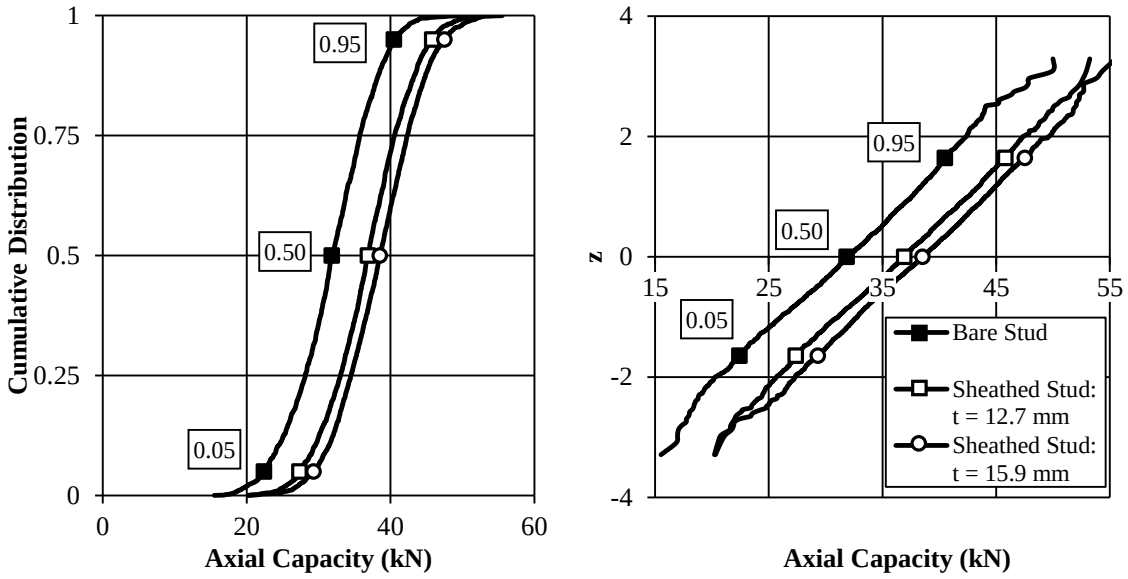

(a) Untransformed Axes (b) Normal Probability Paper

Figure 5.13: Cumulative Distribution of Axial Capacity of a 2x4 Wood Stud

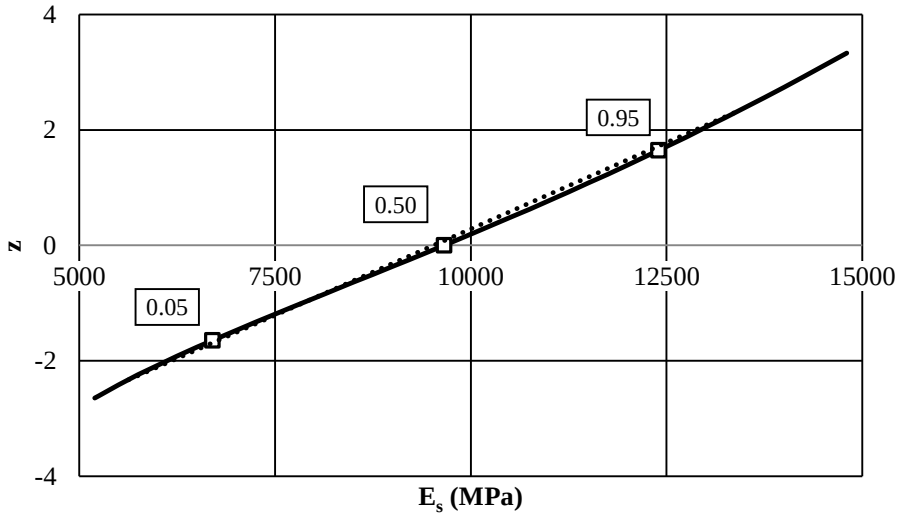

Figure 5.14: Modulus of Elasticity of Wood Graphed on a Normal Probability Paper

Table 5.5 presents the mean, CoV, and 5th percentile values of the axial compressive capacities of bare and sheathed studs for a normal distribution fitted to simulation results, and the 5th percentile values obtained from the Monte Carlo simulation results. Similar values of the standard deviations are observed for the bare and sheathed studs with the same values for d and L, resulting in a smaller CoV for sheathed studs. The effects of a decreased CoV on the reliability of wood studs will be discussed in detail in Chapter 6. The 5th percentile values from the fitted normal distribution match well with the 5th percentile values corresponding to simulation results, indicating the quality of the fit is good. Tolerance limits on the 5th percentile values corresponding to simulation results are provided in Appendix 5B.

Table 5.5: Axial Compressive Capacity of Bare and Sheathed Studs

d *(mm)*	L *(mm)*	t *(mm)*	s *(mm)*	Fitted Normal Distribution			5th percentile of simulation results *(kN)*
				Mean *(kN)*	CoV	5th percentile *(kN)*	
Bare Stud							
89	2440	-	-	31.9	0.182	22.7	22.4
89	3660	-	-	14.8	0.178	10.5	10.5
140	2440	-	-	93.4	0.168	67.6	67.2
140	3660	-	-	51.7	0.175	36.8	37.1
Sheathed Stud							
89	2440	12.7	100	41.7	0.139	32.2	31.9
89	2440	12.7	300	36.6	0.151	27.6	27.4
89	2440	15.9	300	38.1	0.140	29.3	29.3
89	3660	12.7	300	19.6	0.142	15.1	15.0
89	3660	15.9	300	21.1	0.135	16.4	16.2
140	2440	12.7	300	94.9	0.154	70.8	70.3
140	2440	15.9	300	95.8	0.151	72.0	71.5
140	3660	12.7	300	57.9	0.156	43.0	43.0
140	3660	15.9	300	60.3	0.146	45.8	45.3

5.4.2 Contribution of Gypsum-Board Sheathing

Table 5.6 presents the contribution of gypsum-board sheathing, quantified as the ratio of the 5th percentile axial compressive resistance of the sheathed stud, $P_{c.05}$, to that of the bare stud, $P_{s.05}$, obtained from the fitted normal distribution values in Table 5.5. The sheathing provides substantial strength increases for shallow (d = 89 mm) or longer (L = 3660 mm) studs. For these cases, it may be practical in design to account for the gypsum-board

contribution. Conversely, the sheathing provides small strength increases for deeper (d = 140 mm, shorter (L = 2440 mm) studs. For these cases, the small strength increase provided by the gypsum board may not warrant its consideration in practical design applications.

Table 5.6: Contribution of Gypsum-Board Sheathing to Axial Compressive Capacity

d *(mm)*	L *(mm)*	t *(mm)*	s *(mm)*	$P_{c.05}/P_{s.05}$
89	2440	12.7	100	1.42
89	2440	12.7	300	1.22
89	2440	15.9	300	1.29
89	3660	12.7	300	1.44
89	3660	15.9	300	1.56
140	2440	12.7	300	1.05
140	2440	15.9	300	1.06
140	3660	12.7	300	1.17
140	3660	15.9	300	1.24

5.5 Summary and Conclusions

This chapter presented an analytical study of the axial compressive capacity of bare Spruce-Pine-Fir wood studs and with gypsum-board sheathing on both sides of the stud to simulate interior walls in light-frame wood construction. A sensitivity analysis, conducted using finite element models developed and validated in Chapter 4, identified instances where the strength enhancement attributable to the gypsum board is sufficiently large that it should be accounted for in design. The sensitivity analysis also quantified the influence of random variables on the axial strength distribution of the sheathed stud. Monte Carlo simulations were conducted to quantify the probability distributions of the axial compressive capacity of various bare and sheathed stud combinations accurately. The contribution of gypsum-board sheathing was quantified by comparing the 5^{th} percentile capacities of the bare and sheathed studs.

The conclusions of the sensitivity analysis are as follows:

1. The strength increase attributable to gypsum-board sheathing is sufficient to be considered in design practice for the following deterministic variables: gypsum board oriented vertically; stud depths, d, of 89 and 140 mm; stud lengths, L, of 2440 and 3660 mm; gypsum-board thicknesses, t, of 12.7 and 15.9 mm; and, fastener

spacing, s, of 100 and 300 mm. These variables were investigated further using Monte Carlo simulation.

2. The strength increase attributable to gypsum-board sheathing is not sufficient to be considered in design practice for gypsum board oriented horizontally and for varying gypsum-board widths. Therefore, the gypsum board oriented horizontally was not included in Monte Carlo simulation, and the gypsum-board width was treated as deterministic.

3. The sensitivity of the axial compressive resistance of gypsum-board sheathed studs to the wood modulus of elasticity is approximately five times greater than the sensitivity to the wood crushing stress, the initial mid-height out-of-straightness, or the fastener strength. These four random variables were included in Monte Carlo simulations. The sensitivity to the wood modulus of elasticity is up to 180 times greater than that to the gypsum-board modulus of elasticity, which was thus treated as deterministic in subsequent Monte Carlo simulations.

The conclusions of the Monte Carlo simulations are as follows:

4. The axial compressive capacities of the bare and gypsum-board-sheathed wood studs follow a normal distribution, even though E_s follows a Weibull distribution. This is because when graphed on normal probability paper the E_s distribution does not deviate far from a straight line between the 1^{st} and 99^{th} percentile of E_s,

5. For d of 140 mm, L of 2440 mm, and s of 300 mm, the gypsum board increases the 5^{th} percentile axial capacity by a factor of only 1.05 or 1.06 for t of 12.7 or 15.9 mm, respectively. Thus, the strength contribution of gypsum-board sheathing for this combination of deterministic variable is considered practically negligible.

6. For d of 89 mm or L of 3660 mm, with s of 300 mm, the gypsum board increases the 5^{th} percentile axial capacity by a factor of 1.17 to 1.56, depending on the gypsum-board thickness. Thus, the strength contribution of gypsum-board sheathing for these deterministic variables is significant and should be accounted for in design practices.

7. For d of 89 mm, L of 2440 mm, and t of 12.7 mm a decrease of s from 300 to 100 mm increases the strength contribution of gypsum-board sheathing from a factor of 1.22 to 1.42. This increase is significant and should also be considered in design practices. However, for new construction, a reduction in fastener spacing is associated with additional labour costs that may not be cost-effective in practice. Conversely, if an existing sheathed wall requires additional capacity, adding fasteners can be a cost-effective alternative.

5.6 References

Beer, F.P., Johnston, E.R., 1992. Mechanics of Materials. McGraw-Hill, New York, USA.

Bleau, R., 1984. Comportement des Poutre-Colonnes en Bois. M.Sc.A. Thesis, Department of Civil Engineering, University of Sherbrooke, QC.

Buchanan, A.H., 1984. Strength Member and Design Methods for Bending and Axial Load Interaction in Timber Members. Ph.D. Thesis, Department of Civil Engineering, University of British Columbia, BC. 298 p.

Canadian Wood Council (CWC), 1994. Canadian Lumber Properties. Canadian Wood Council, Ottawa, ON.

CenterPoint Energy, 2006. Humidity and the Indoor Environment. Retrieved August 28, 2013, from CenterPoint Energy Web site: http://www.centerpointenergy.com/staticfiles/CNP/Common/SiteAssets/doc/Humidity_indoor_environ%5B1%5D.pdf. 4 p.

CMHC, 2013. Canadian Wood-Frame House Construction. Canadian Mortgage and Housing Corporation, Ottawa, ON, 315 p.

Elandt, R. C. 1961. The Folded Normal Distribution: Two Methods of Estimating Parameters from Moments, Technometrics, Vol. 3, No. 4, pp. 551-562.

Foschi, R.O., Folz, B., Yao, F.Z., 1989. Reliability-Based Design of Wood Structures. Structural Research Series, Report No. 34, Department of Civil Engineering, University of British Columbia. 282 p.

Gerhards, C. C., 1983. Characterization of Physical and Mechanical Properties of 2 by 4 Truss Lumber. USDA Forest Service Research Paper FPL 431. Forest Products Laboratory, Madison, Wis. 24 p.

Johansson, M., Nystrom, J., and Ohman, M., 2003. Prediction of Longitudinal Shrinkage and Bow in Norway Spruce Studs using Scanning Techniques. Journal of Wood Science, Vol. 49, pp. 291-297.

Lee, Y., 1999. Behavior of Gypsum-Sheathed Cold-Formed Steel Wall Stud Panels. Ph.D. Thesis, Department of Civil, Construction, and Environmental Engineering, Oregon State University, Corvallis, OR, USA. 327 p.

National Research Council of Canada (NRC). 2010. National Building Code of Canada - Part 9. Institute for Research in Construction, National Research Council of Canada, Ottawa, Ont.

Natrella, M. G., 1963. Experimental Statistics. NBS Handbook 91, National Bureau of Standards, Washington, DC. 600 p.

Rousseau, J. 2013. Personal conversation with professional contractor, Oct 28, 2013.

Southwell, R.V. 1931. On the Analysis of Experimental Observations in Problems of Elastic Stability. Proceedings of the Royal Society of London. Series A, Containing Papers of a Mathematical and Physical Character, Vol. 135, No. 828, pp. 601-616.

Yagana, K., Mochida, T., Sasaki, Y., and Hirai, T., 2003. Reduction of Effective Resistance of Nailed Shear Walls caused by Misnailing III. Reduction of Effective Resistance caused by Bows of Frame Members. Journal of the Japan Wood Research Society, Vol. 49, No. 3, pp. 220-226.

Chapter 6 Design Implications

6.1 Introduction

Table 6.1 presents the stud size, spacing, and length requirements for interior walls in light-frame wood residential construction in Table 9.23.10.1 of the National Building Code of Canada, NBCC, (NRC, 2010), which are solely dependent on the quantity of supported floors, accessibility to the attic, and whether or not the wall must support a roof. Although these provisions markedly simplify the design procedure, they are "based mainly on performance history" (CWC, 2009), and so the demand for each load case and the stud resistance are not well documented.

Table 6.1: Size and Spacing of Studs for Interior Walls in NBCC Table 9.23.10.1

Supported load case	Min. stud size *(mm)*	Max. stud spacing *(mm)*	Max. unsupported height *(mm)*
Attic not accessible by stairway	38x89	600	3600
Attic accessible by stairway & 1 floor	38x89	400	3600
Roof load plus one floor	38x89	400	3600
Attic not accessible by stairway & 2 floors	38x89	400	3600
Roof load	38x64	400	2400
Attic accessible by stairway	38x64	400	2400
Attic not accessible by stairway & 1 floor	38x89	600	3600
Attic accessible by stairway & 2 floors	38x89	300	3600
	38x140	400	4200
Attic accessible by stairway & 3 floors	38x140	300	4200

Alternatively, the axial compressive resistance of wood studs can be computed from provisions in CAN/CSA-O86-09 (CSA, 2009), depending on the wood species and grade, the stud size, the type and duration of load, the wood moisture content, and the presence of chemical preservative treatment. In either case, the contribution of gypsum-board sheathing to the axial compressive capacity of wood studs is not considered.

Chapter 5 quantified the contribution of gypsum-board oriented vertically on both sides of a stud to simulate a typical interior load-bearing wall. It was shown that the gypsum-board sheathing can markedly increase the axial compressive capacity of wood studs. For

example, the 5th percentile resistance of a 38 x 89 mm stud (i.e., typical dimensions in a residential structure) buckling about its strong axis when sheathed with 12.7 mm thick gypsum board increases by 22% and 44% for stud lengths of 2440 mm and 3660 mm, respectively. These substantial increases in axial compressive resistance can increase the design loads that the interior walls of light-frame wood structures can resist. Therefore, it is beneficial to define methodologies for predicting the axial compressive capacity of sheathed studs, and to implement them as revisions to NBCC Table 9.23.10.1 and in CAN/CSA O86-09.

This chapter presents revisions recommended for NBCC Table 9.23.10.1 to account for the contribution of gypsum-board sheathing to the axial compressive resistance of interior load-bearing walls. The demand is quantified for the various usages provided in the NBCC, and then compared to the resistance for both the bare and sheathed stud. The equation presented in CAN/CSA 086-09 was derived for all slenderness ratios (Johns, 1991). It can be considered complex for slender studs, with a computational form that is not intuitive. A new empirical equation is therefore presented to simplify the process of calculating the axial compressive resistance of wood studs. Both the equation presented in CAN/CSA 086-09 and the new empirical equation will be used to quantify the resistance of bare and sheathed studs. It will be shown that the current stud size, spacing, and length requirements in the current NBCC Table 9.23.10.1 are typically unsafe. Therefore, the recommended revisions will prohibit certain designs that are currently acceptable. It will also be shown that this can be somewhat mitigated by providing a greater selection of stud sizes, spacings, and lengths that are currently not considered, and by accounting for the contribution of gypsum-board sheathing to the wall compressive strength.

6.1.1 Objectives and Methodology

The specific objectives of this chapter are:

1. Create a new empirical equation to quantify the axial compressive resistance of bare and gypsum-board sheathed wood studs.

2. Quantify a modification factor to apply to the axial resistance equation currently in CAN/CSA-O86-09 to account for the contribution gypsum-board sheathing.

3. Investigate rationally the suitability of the acceptable stud size, spacing, and length provisions given in NBCC Table 9.23.10.1, and recommend revisions to eliminate deficient values in the table and account for the contribution of gypsum-board sheathing, if present.

This chapter first quantifies the axial compressive resistance of bare and sheathed wood studs. Experimental and analytical results are obtained assuming only short-term loading is applied, and so creep is ignored. This assumption is also taken in this chapter. An empirical equation is derived from regression analysis of results of the Monte Carlo simulations presented in Chapter 5. A modification factor is also derived to account for the increase in axial compressive resistance, due to the presence of gypsum-board sheathing in the CAN/CSA-086-09 equation. The reliability associated with the use of both the new empirical equation and the modified CAN/CSA-086-09 equation has not been established, and so a review of the appropriate associated resistance factors will be presented. NBCC Table 9.23.10.1 is then investigated by comparing the factored axial loads to the associated factored resistances obtained using the empirical equation and CAN/CSA 086-09. Finally, changes to NBCC Table 9.23.10.1 are recommended to ensure that the factored resistance is always greater than the applied factored load effects that account for the increased resistance due to the contribution of gypsum-board sheathing.

6.2 Contribution of Gypsum-Board Sheathing to the Axial Resistance

Table 6.2 presents the deterministic variables considered in Chapter 5 that cause the contribution of gypsum-board sheathing oriented vertically to the axial compressive capacity of wood studs to be marked. Wood studs with gypsum-board sheathing oriented horizontally, with a seam at mid-height, are markedly weaker and so are not considered. When the stud depth, d, is 89 mm and the fastener spacing, s, is 300 mm, gypsum-board sheathing with thicknesses of 12.7 or 15.9 mm markedly increase the axial compressive resistance of studs that are equal to or longer than 2440 mm. However, for d of 140 mm

and s of 300 mm, the compressive strength increase due to the gypsum-board sheathing was negligible for a stud length, L, of 2440 mm. A reduction in fastener spacing from 300 to 100 mm was also found to markedly enhance the contribution of gypsum-board sheathing for the case with L of 2440 mm, d of 89 mm, and t of 12.7 mm.

Table 6.2: Deterministic Variables that Influence the Contribution of Gypsum Board

Parameter	Definition	Value
L	Stud length	2440 and 3660 mm
d	Stud depth	89 and 140 mm
t	Gypsum-board thickness	12.7 and 15.9 mm
s	Fastener spacing	100 and 300 mm

This section presents two methods to account for the contribution of gypsum-board sheathing for the range of deterministic variables shown in Table 6.2.

6.2.1 Empirical Equation

The sensitivity analysis in Chapter 5 showed the axial compressive capacity of bare studs, P_s, and sheathed studs, P_c, to be approximately five times more sensitive to the wood modulus of elasticity, E_s, than any other random variable investigated. Therefore, relationships between the axial compressive capacity of the bare and sheathed stud and the wood modulus of elasticity were obtained by generating graphs similar to that shown in Figure 6.1. This figure shows 500 data points from the Monte Carlo simulations reported in Chapter 5 for L of 2440 mm, d of 89 mm, t of 12.7 mm, and s of 300 mm. A linear relationship between P_s (or P_c) and E_s was observed for all combinations of stud length and depth, gypsum-board thickness, and fastener spacing investigated. This is intuitive when considering the Euler buckling load (Equation [2.1]) has the same linear relationship. Therefore, linear regression analysis was used to quantify the relationship.

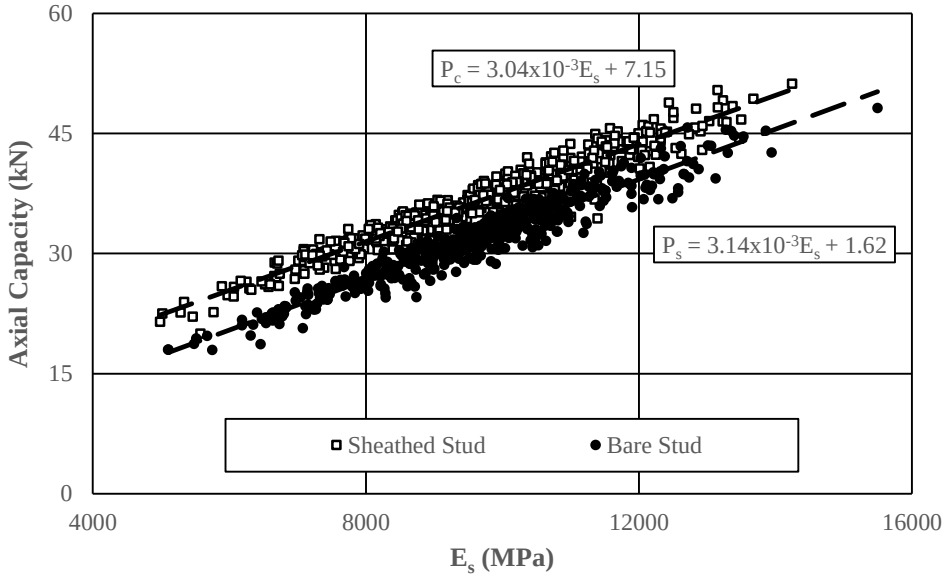

Figure 6.1: Axial Capacity vs. Wood Modulus of Elasticity for
L of 2440 mm, d of 89 mm, and t of 12.7 mm

The regression analyses are based on the following multiple linear model:

[6.1] $$P = (\beta_1 + \beta_2 Z_S + \beta_3 Z_t)E_s + \beta_4 + \beta_5 Z_S + \beta_6 Z_t + \varepsilon_r$$

where: the values β_1 through β_6 are obtained by regression analysis; Z_S is an indicator variable for sheathing, equal to 1 when the stud is sheathed and 0 otherwise; Z_t is an indicator variable for gypsum-board thickness, equal to 1 when t = 15.9 mm and 0 otherwise; and ε_r is the inherent error, assumed independent and identically distributed for all samples.

A multivariate linear regression analysis was conducted to quantify the values β_1 through β_6 and determine their statistical significance. P-values are computed for these parameter estimates: a P-value less than 0.05 indicates the associated parameter is statistically different from zero, and so is statistically significant. P-values for slopes β_2 and β_3 range from 0.053 to 0.81 and 0.094 to 0.89, respectively, as presents in detail in Appendix 6A, and so are not statistically significant. This indicates that the contribution of the gypsum-board can be quantified by the change in the intercept for this relationship. Therefore, the regression analysis was repeated neglecting β_2 and β_3 yielding the parameter estimates and

associated P-values (in brackets) shown in Table 6.3. The value for β_4 for studs having L of 3660 mm and d of 89 mm is no longer statistically significant, with a P-value of 0.76. This β_4 value of 0.0251 kN is also practically insignificant. All other parameter estimates are statistically significant. Thus, Equation [6.1] can be simplified as:

[6.2] $$\hat{P}_c = \hat{\beta}_1 E_s + \hat{\beta}_4 + \hat{\beta}_5 Z_S + \hat{\beta}_6 Z_t$$

where $\hat{P}_c$ is the predicted compressive strength and $\hat{\beta}_1$, $\hat{\beta}_4$, $\hat{\beta}_5$, and $\hat{\beta}_6$ are the parameter estimates shown in Table 6.3. For studs with d of 89 mm, s of 300 mm, and L of 3660 mm, it is assumed $\hat{\beta}_4 = 0$.

Table 6.3: Quantification of Slope and Vertical Intercept from Regression Analysis (P-Value)

L *(mm)*	d *(mm)*	s *(mm)*	β_1 *(kN/MPa)*	β_4 *(kN)*	β_5 *(kN)*	β_6 *(kN)*	Standard error *(kN)*
2440	89	100	0.00317 (0.00)	1.28 ($8.0\text{x}10^{-5}$)	9.92 (0.00)	-	1.73
2440	89	300	0.00308 (0.00)	2.13 (0.00)	4.61 (0.00)	1.56 (0.00)	1.50
3660	89	300	0.00154 (0.00)	0.0251 (0.76)	4.77 (0.00)	1.53 (0.00)	0.64
3660	140	300	0.00490 (0.00)	4.79 (0.00)	6.18 (0.00)	1.92 (0.00)	3.59

[a] P-values smaller than 10^{-10} are indicated as 0.00.

Table 6.4 compares predicted values of P_c, obtained using Equation [6.2] with the 5th percentile values of E_s of 6700 MPa used in Chapter 5, to the 5th percentile values obtained from the fitted normal distribution reported in Chapter 5. The fitted-distribution-to-predicted ratio ranges from 0.982 to 1.012, with an average of 0.997 and a standard deviation of 0.011. This indicates that Equation [6.2], with the parameters estimates shown in Table 6.3, is an effective and accurate method for calculating the axial compressive capacity of gypsum-board-sheathed wood studs. Results are also shown with E_s equal to 6500 MPa, i.e., design value in CAN/CSA 086-09 for No. 2 or better SPF lumber, so that a direct comparison can be made with predictions obtained using the current equation in CAN/CSA 086-09. In this case, the fitted-distribution-to-predicted ratio ranges from 1.005 to 1.034, with an average of 1.019 and a standard deviation of 0.012.

Table 6.4: Accuracy of 5th Percentile of P_c Values from Empirical Equation

L *(mm)*	d *(mm)*	s *(mm)*	t *(mm)*	5th percentile P_c *(kN)*			Fitted Distribution/ Predicted	
				Predicted E_s = *6700 MPa*	E_s = *6500 MPa*	Fitted distribution	E_s = *6700 MPa*	E_s = *6500 MPa*
2440	89	100	12.7	32.5	31.9	31.9	0.991	1.010
2440	89	300	12.7	27.4	26.8	27.4	1.007	1.030
2440	89	300	15.9	29.0	28.3	29.3	1.012	1.034
3660	89	300	12.7	15.1	14.8	15.0	1.000	1.021
3660	89	300	15.9	16.6	16.3	16.2	0.987	1.005
3660	140	300	12.7	43.8	42.8	43.0	0.982	1.005
3660	140	300	15.7	45.7	44.7	45.3	1.002	1.024
						Avg.	0.997	1.019
						Std. Dev.	0.011	0.012

6.2.2 Gypsum-Board Factor for CAN/CSA 086-09 Equations

This section presents a modification factor to account for the presence of gypsum-board sheathing in the CAN/CSA-O86-09 equations that define the compressive resistance of wood studs parallel to the grain. The equations in the current standard will first be summarized.

6.2.2.1 Compressive Resistance Parallel to Grain

The factored compressive resistance of light-frame wood studs, P_r, is computed in accordance with Article 5.5.6.2 using:

[6.3] $$P_r = \varphi_s F_c A_s K_{Zc} K_c$$

where φ_s is the resistance factor for a bare stud equal to 0.8, A_s is the cross-sectional area of the stud, F_c is the compressive strength parallel to the grain, K_{Zc} is the size factor for compression parallel to the grain, and K_c is the slenderness factor. Values for F_c, K_{Zc}, and K_c are determined using following equations:

[6.4] $$F_c = f_c(K_D K_H K_{Sc} K_T)$$

where f_c is the specified strength in compression parallel to the grain, K_D is the load-duration factor, K_H is the system factor, K_{Sc} is the service condition factor for compression parallel to the grain, and K_T is the treatment factor;

[6.5] $K_{Zc} = 6.3(dL)^{-0.13} \leq 1.3$

where d is the dimension in the direction of buckling (i.e., stud depth) and L is the effective length (i.e., stud length); and,

[6.6] $K_c = \left[1.0 + \left(F_c K_{Zc} C_c^3\right) / \left(35 E_{05} K_{SE} K_T\right)\right]^{-1}$

where C_c is the slenderness ratio (equal to L/d), E_{05} is the wood modulus of elasticity for design in compression (i.e., the 5th percentile modulus of elasticity of the wood (Foschi et al., 1989)), and K_{SE} is the service condition factor for the modulus of elasticity.

Table 6.5 presents values of each modification factor adopted in the present study. A standard load duration was assumed because light-frame wood studs typically resist a combination of dead, live, and snow loads. System behaviour is, perhaps conservatively, ignored. Interior wall studs typically have moisture contents of 6 to 14%, whereas a dry condition is defined to occur when the "average moisture is 15% or less over a year and does not exceed 19% at any time" (CWC, 2010). Therefore, a dry service condition was assumed to quantify the modification factors for modulus of elasticity and compression strength. Finally, interior studs do not typically require preservatives, thus have been assumed untreated.

Table 6.5: Modification Factors in CAN/CSA O86-09 for Compression Parallel to Grain

Factor	Value	Criteria
K_D	1.0	Standard duration
K_H	1.0	No system behaviour
K_{Sc}	1.0	Dry service conditions
K_{SE}	1.0	Dry service conditions
K_T	1.0	Untreated lumber

6.2.2.2 Modification Factor for Gypsum Board Sheathing, K_{SH}

A proposed new modification factor to account for the effects of gypsum-board sheathing is given by:

[6.7] $$K_{SH} = P_c/P_s = 1 + \left(\hat{\beta}_5 Z_S + \hat{\beta}_6 Z_t\right)/\left(\hat{\beta}_1 E_s + \hat{\beta}_4\right)$$

where K_{SH} is the modification factor for gypsum-board sheathing, P_c is the sheathed stud capacity obtained using Equation [6.2] with values for $\hat{\beta}_1$ through $\hat{\beta}_6$ from Table 6.3, and P_s is the bare stud capacity obtained using Equation [6.2] with Z_S and Z_t equal to 0. Consequently, K_{SH} is a function of the wood modulus of elasticity.

Figure 6.2 shows the variation of K_{SH} with E_{05} for all deterministic variable combinations presented in Table 6.2. Various grades of wood studs are defined in the codes, with design values for the wood modulus of elasticity ranging from 5500 MPa for No. 3 grade SPF studs to 16500 MPa for machine-stress-rated grade 3000F_b-2.4E SPF studs. The resulting range of values for K_{SH} at E_{05} of 5500 MPa is between 1.20 and 1.60, and decreases to a range from 1.07 to 1.27 at E_{05} of 16500 MPa, depending on the applicable combination of s, L, d, and t. For No. 2 or better SPF studs, i.e., E_{05} is equal to 6500 MPa, the value of K_{SH} ranges from 1.17 to 1.51. Values of K_{SH} are very sensitive to the slenderness of the stud, with the largest values obtained for L of 3660 mm and d of 89 mm, and to the fastener spacing, with larger values obtained for s of 100 mm. Values for K_{SH} are relatively less sensitive to the gypsum-board thickness, with larger values obtained when t is equal to 15.9 mm.

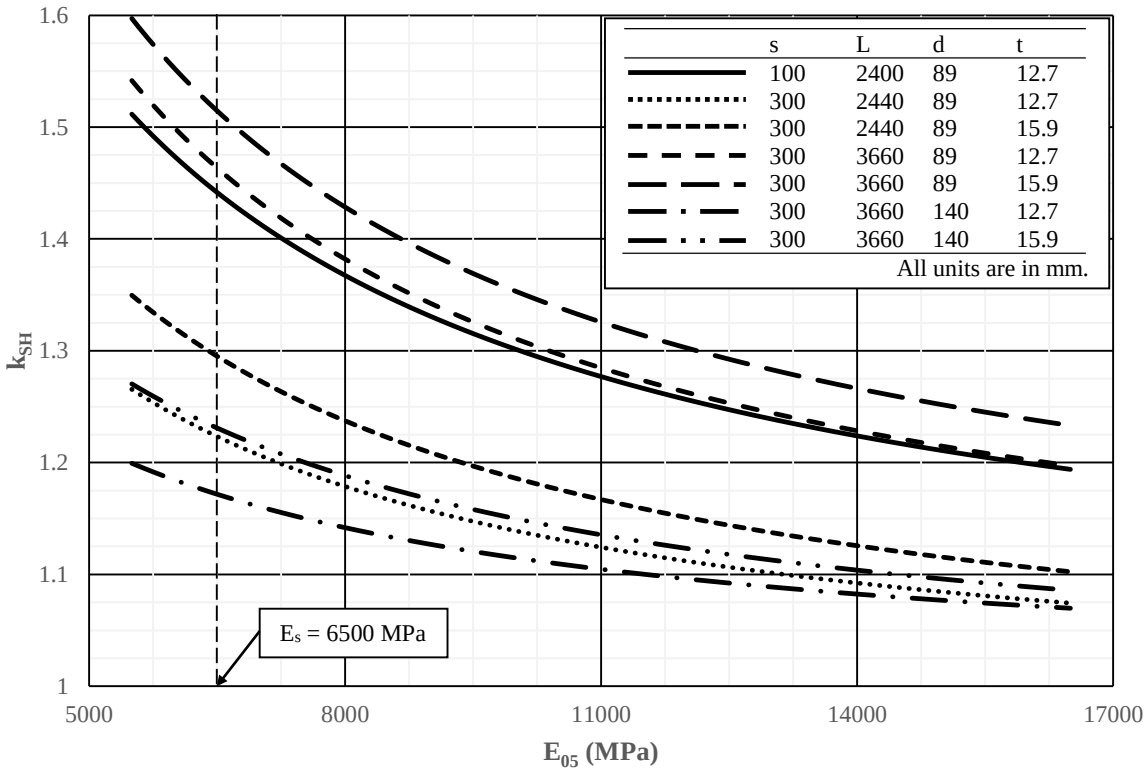

Figure 6.2: Influence of E_s on the Modification Factor for Gypsum Board, K_{SH}

6.2.2.3 Implementation of the Modification Factor for Gypsum Board Sheathing

The modification factor K_{SH} is proposed to be implemented in the CAN/CSA O86-09 equations by applying it directly to Equation [5.5] as follows:

[6.8] $$P_r = \varphi_s F_c A_s K_{Zc} K_c K_{SH}$$

Table 6.6 compares the specified resistance of bare and sheathed studs using Equation [6.8], with f_c of 11.5 MPa and E_{05} of 6500 MPa for No. 2 grade or better SPF lumber and φ_s = 1.0, to the 5th percentile resistance from the fitted normal distributions reported in Chapter 5. Values for K_{SH} are equal to 1.0 for the bare stud and are obtained from Figure 6.2 for the sheathed stud. The predicted capacities for the bare and sheathed studs are slightly conservative, with identical average fitted-distribution-to-predicted ratios of 1.097. Therefore, Equation [6.8] is a suitable revision to Equation [5.5] to account for the contribution of gypsum-board sheathing. However, Equation [6.8] is less accurate than

Equation [6.2], which has an average fitted-distribution-to-predicted ratio of 1.019 when using E_s of 6500 MPa.

Table 6.6: Specified Resistance of Bare and Sheathed Wood Studs

L *(mm)*	d *(mm)*	s *(mm)*	t *(mm)*	Equation [6.8] *(kN)*		5th perc. values from fitted distribution *(kN)*		Fitted distribution/ Predicted	
				Bare Stud	Sheathed Stud	Bare Stud	Sheathed Stud	Bare Stud	Sheathed Stud
2440	89	100	12.7	21.3	30.7	22.7	32.2	1.066	1.049
2440	89	300	12.7	21.3	26.1	22.7	27.6	1.066	1.057
2440	89	300	15.9	21.3	27.6	22.7	29.3	1.066	1.062
3660	89	300	12.7	8.96	13.1	10.5	15.1	1.172	1.153
3660	89	300	15.9	8.96	13.6	10.5	16.4	1.172	1.206
3660	140	300	12.7	34.4	40.3	36.8	43.0	1.070	1.067
3660	140	300	15.9	34.4	42.3	36.8	45.8	1.070	1.083
							Avg.	1.097	1.097
							Std. dev.	0.051	0.059

6.2.3 Resistance Factor, φ

The reliability associated with the use of Equations [6.2] and [6.8] for design has not been evaluated, and so appropriate resistance factors have not yet been defined. CSA-S408-11 (CSA, 2011) reports the resistance factor can be calculated using:

$$[6.9] \qquad \varphi_s = \delta_{R_S}(\sum \alpha_i S_i \ / \ \bar{S}) \exp\left(-\beta' \sqrt{V_{R_S}{}^2 + V_S{}^2}\right)$$

where δ_{R_S} is the bias coefficient of the resistance for the bare stud, i.e., the ratio of the mean to nominal resistance, α_i is the load factor for load effect type i, S_i is the specified load effect, $\bar{S}$ is the mean load effect, β' is the reliability index, and V_{R_S} and V_S are the coefficient of variations of the resistance and load effect, respectively. The values for α, S, and $\bar{S}$ are assumed to be the same for bare and sheathed studs. Gypsum-board sheathing marginally increases the ductility of studs failing in axial compression, as shown in Chapter 4, thus it is appropriate, perhaps conservative, to assume the same value for β' for bare and

sheathed studs. Therefore, the resistance factor for the sheathed studs, φ_c, can be determined from the ratio φ_c/φ_s which eliminates α, S, and $\bar{S}$, yielding:

$$[6.10] \quad \varphi_c = \varphi_s \, \delta_{R_c} / \delta_{R_s} \exp\left[\beta' \left(\sqrt{V_{R_s}^2 + V_S^2} - \sqrt{V_{R_c}^2 + V_S^2}\right)\right]$$

where φ_s, δ_{R_s}, and V_{R_s} pertain to bare studs and φ_c, δ_{R_c}, and V_{R_c} pertain to sheathed studs.

The Commentary of CAN/CSA-O86-09 cites Foschi et al., (1989) who reported a mean β' value of 2.81 for wood columns with φ_s equal to 0.8. Therefore, the resistance factor for the sheathed studs is computed using Equation [6.10] with β' = 2.81. Values for the remaining parameters in Equation [6.10], i.e., δ_{R_s}, δ_{R_c}, V_{R_s}, and V_{R_c}, are presented in Table 6.7. Values for δ_{R_s} are equal to the ratio of mean bare stud resistance presented in Table 5.5 to the specified bare stud resistances presented in Table 6.6. Values for δ_{R_c} are equal to the ratio of mean sheathed stud resistance presented in Table 5.5 to the specified sheathed stud resistances presented in Table 6.4 for Equation [6.2] and Table 6.6 for Equation [6.8]. Therefore, there are two values of δ_{R_c} shown in Table 6.6 for each combination of L, d, s, and t. Values for V_{R_s} and V_{R_c} are equal to the bare and sheathed stud coefficient of variations, respectively, presented in Table 5.5. Although two values of δ_{R_c} are obtained for each combination, the sheathed stud has one mean value and standard deviation for each combination, and so there is only one associated value of V_{R_c}

Table 6.7: Bias Coefficient and Coefficient of Variation of Resistance of Bare and Sheathed Stud

L *(mm)*	d *(mm)*	s *(mm)*	t *(mm)*	δ_{R_s}	δ_{R_c}		V_{R_s}	V_{R_c}
					Eq. [6.2]	*Eq. [6.8]*		
2440	89	100	12.7	1.495	1.283	1.359	0.182	0.139
2440	89	300	12.7	1.495	1.336	1.412	0.182	0.151
2440	89	300	15.9	1.495	1.314	1.394	0.182	0.140
3660	89	300	12.7	1.655	1.298	1.496	0.178	0.142
3660	89	300	15.9	1.655	1.271	1.554	0.178	0.135
3660	140	300	12.7	1.504	1.322	1.437	0.175	0.156
3660	140	300	15.9	1.504	1.319	1.425	0.175	0.146

Foschi et al. (1989) report the coefficient of variation is equal to 0.10 for dead loads, is between 0.13 and 0.27 for live loads, and is equal to 0.50 for snow loads. Bartlett et al. (2005) adopted a coefficient of variation of 0.100 for dead loads, 0.206 for live loads, and 0.420 for snow loads for the calibration of load factors in the 2005 NBCC. As such, the value for V_S depends on the loading combination. However, roof loads are typically directed to exterior walls, and so are not supported by interior load-bearing walls. Therefore, V_S for an interior wall typically ranges between 0.1 and 0.2.

Figure 6.3 shows the relationship between the φ_c values corresponding to the resistance computed using Equation [6.2] and V_S. Values for φ_c for sheathed studs with L of 3660 mm and d of 89 mm, range from 0.66 to 0.68 for V_S between 0.1 and 0.2. Therefore, the resistance factor for these sheathed studs is recommended to be 0.65 when the resistance is calculated using Equation [6.2]. Conversely, values for φ_c for all other sheathed studs ranges from 0.73 to 0.78 for V_S between 0.1 and 0.2. Therefore, the resistance factor for these sheathed studs is recommended to be 0.75 when the resistance is calculated using Equation [6.2].

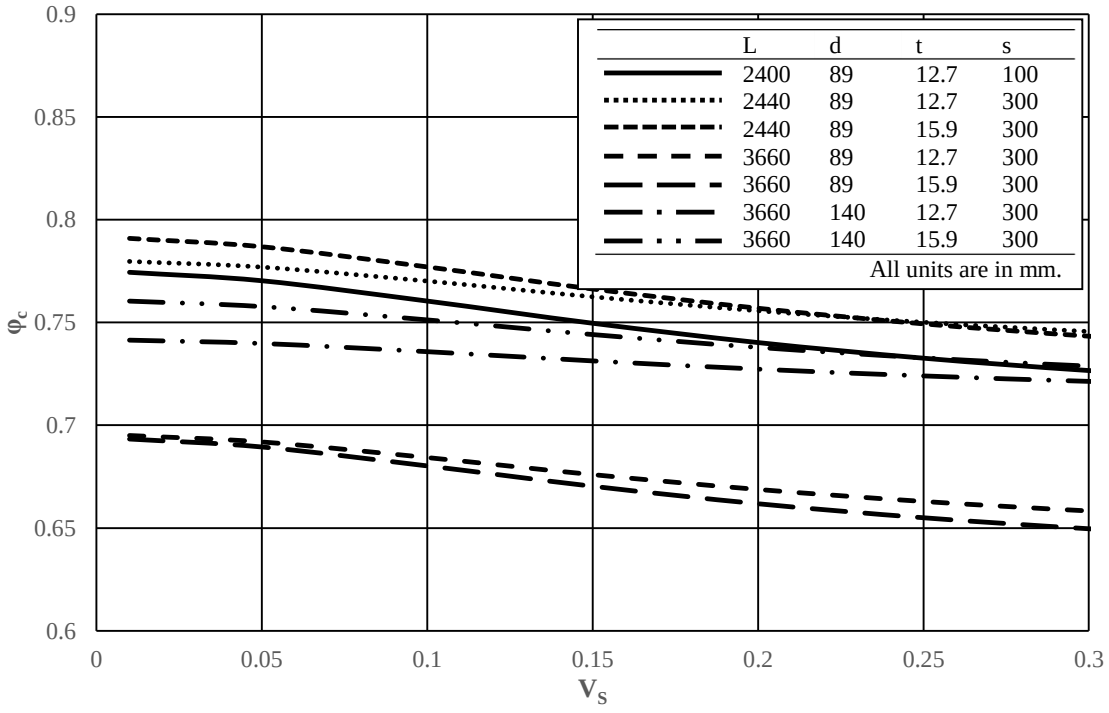

Figure 6.3: Resistance Factor for Gypsum-Board Sheathed Stud using Equation [6.2]

Figure 6.4 shows the relationship between φ_c if the resistance is computed using Equation [6.8] and V_S. Values for φ_c range from 0.77 and 0.83 for V_S between 0.1 and 0.2. Therefore, the resistance factor for sheathed studs is recommended to remain at 0.8 if the resistance is computed using K_{SH} in the equations in CAN/CSA 086-09.

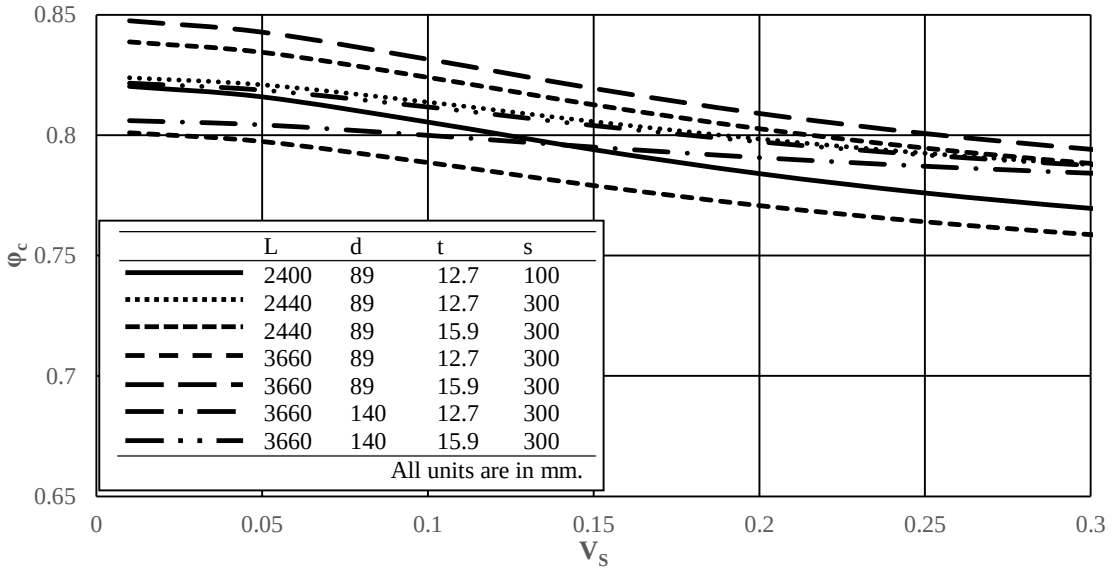

Figure 6.4: Resistance Factor for Gypsum Board Sheathed Stud using Equation [6.8]

Figure 6.3 and 6.4 were also regenerated assuming a lognormal distribution fit to the lower 25th percentile of the resistance distribution of bare and sheathed studs. This is appropriate because Equation [6.9] is based on lognormally distributed demands due to applied loads and resistances. The results, shown in Appendix 6C, yield resistance factors that are identical to those recommended above assuming a normal distribution.

Table 6.8 compares the factored axial resistance for sheathed studs computed using Equations [6.2] and [6.8]. The value for E_s used to calculate P_r is 6500 MPa, which corresponds to No. 2 or better SPF in CAN/CSA 086-09. The values for P_r obtained using Equation [6.2] are consistently conservative, ranging from 91 to 98% of the values obtained using Equation [6.8]. Therefore, although Equation [6.2] more accurately predicts the specified compressive resistance of sheathed studs, the recommended resistance factors cause it to be slightly more conservative.

Table 6.8: Comparison of Factored Resistances of Sheathed Studs

L *(mm)*	d *(mm)*	s *(mm)*	t *(mm)*	P_r *(kN) Eq. [6.2]*	P_r *(kN) Eq. [6.8]*	$P_{r(Eq.\ [6.2])} / P_{r(Eq.\ [6.8])}$
2440	89	100	12.7	24.4	25.8	0.95
2440	89	300	12.7	20.6	21.4	0.96
2440	89	300	15.9	21.7	22.7	0.96
3660	89	300	12.7	9.82	10.8	0.91
3660	89	300	15.9	10.8	11.9	0.91
3660	140	300	12.7	32.9	33.6	0.98
3660	140	300	15.9	34.3	35.1	0.98

6.3 Influence of Gypsum-Board Sheathing on Stud Size and Spacing Values in NBCC Table 9.23.10.1

This section presents the analysis of the stud size and spacing values specified for interior walls in NBCC Table 9.23.10.1 (NRC, 2010) and recommends revisions to the table that account for the contribution of gypsum-board sheathing oriented vertically.

6.3.1 Accuracy of Existing NBCC Table 9.23.10.1

Table 6.9 compares the factored demands and factored resistances for the supported load categories in the NBCC Table 9.23.10.1. The factored demand in kN applied to an individual stud, P_f, is the product of the factored demand per meter width of wall in kN/m and the stud spacing in meters. The factored demand per meter width of wall was computed assuming the interior load-bearing walls are spaced at the maximum floor joist spans (6 m) and ceiling joist spans (10 m) permitted in Part 9 of the NBCC for No. 2 grade SPF lumber. The support loads included factored dead, live, and snow loads applied to the roof, attic, and floors as defined in the NBCC. The details of these calculations are presented in Appendix 6B. The specified snow loads, SL, vary between 1.0 and 3.0 kPa across Canada, thus the demands for cases with roof loads are shown for SL of 1.0, 2.0, and 3.0 kPa. The factored resistances shown for the bare stud are computed using Equation [5.5] assuming No. 2 or better SPF lumber, i.e., f_c of 11.5 MPa and E_{05} of 6500 MPa. Interior walls typically consist of more than three adjacent studs, so a beneficial system behaviour occurs corresponding to K_H of 1.1. Also presented are the predicted factored resistances of studs

sheathed using Equation [6.8], with 12.7 and 15.9 mm thick gypsum-board on both sides and fastener spacing of 300 mm. Because the current NBCC Table 9.23.10.1 does not specify a stud size of 38x89 mm and a maximum unsupported height of 2400 mm, the contribution of gypsum-board sheathing with s of 100 mm could not be compared. For the bare stud, P_r exceeds P_f in only five of the fourteen cases shown. The worst case occurs for an interior wall when supporting an attic not accessible by stairway plus two floors. The factored load, P_f, is 17.4 kN, but the stud resistance is only 7.6 kN. Accounting for the effects of gypsum board markedly increases P_r, but P_r exceeds P_f in only six of the fourteen cases shown. It is clear that the minimum stud sizes, maximum stud spacings, and/or maximum unsupported heights currently listed in the NBCC Table 9.23.10.1 need to be reconsidered.

Table 6.9: Accuracy of Stud Size and Spacing in NBCC Table 9.23.10.1

Supported load case	SL *(kPa)*	Min. stud size *(mm)*	Max. stud spacing *(mm)*	Max. unsupported height *(mm)*	P_f *(kN)*	P_r *(kN)*			P_r / P_f		
						Bare Stud	Sheathed Stud *t = 12.7 mm* [b]	Sheathed Stud *t = 15.9 mm* [b]	Bare Stud	Sheathed Stud *t = 12.7 mm*	Sheathed Stud *t = 15.9 mm*
Attic not accessible by stairway	-	38x89	600	3600	5.4	7.6	11.2	12.3	1.41	2.07	2.28
Attic accessible by stairway & 1 floor	-	38x89	400	3600	14.9	7.6	11.2	12.3	0.51	0.75	0.83
Roof load plus one floor	1.0	38x89	400	3600	11.0	7.6	11.2	12.3	0.69	1.02	1.12
	2.0				12.5	7.6	11.2	12.3	0.61	0.90	0.98
	3.0				16.1	7.6	11.2	12.3	0.47	0.70	0.76
Attic not accessible by stairway & 2 floors	-	38x89	400	3600	17.4	7.6	11.2	12.3	0.44	0.64	0.71
Roof load	1.0	38x64[a]	400	2400	5.1	6.7	-	-	1.31	-	-
	2.0				8.7	6.7	-	-	0.77	-	-
	3.0				12.3	6.7	-	-	0.54	-	-
Attic accessible by stairway	-	38x64[a]	400	2400	6.6	6.7	-	-	1.02	-	-
Attic not accessible by stairway & 1 floor	-	38x89	600	3600	16.3	7.6	11.2	12.3	0.47	0.69	0.75
Attic accessible by stairway & 2 floors	-	38x89	300	3600	16.1	7.6	11.2	12.3	0.47	0.70	0.76
		38x140	400	4200	21.4	22.5	-	-	1.05	-	-
Attic accessible by stairway & 3 floors	-	38x140	300	4200	21.0	22.5	-	-	1.07	-	-

[a] No provisions presented in the NBCC for 38x89 or 38x140 mm stud.

[b] Gypsum-board contribution is not considered for 38x64 mm studs and for 4200 mm stud lengths.

6.3.2 Recommended Revisions to NBCC Table 9.23.10.1

The purpose of NBCC Table 9.23.10.1 is to simplify the design process by providing the critical combination of stud size and spacing that has been shown, through a history of satisfactory performance, to be sufficient for the various supported load categories. This objective is clearly not achieved, however, if the maximum spans permitted by Part 9 of the NBCC are assumed. It is, therefore, necessary to increase the minimum stud size, decrease the maximum stud spacing, and/or reduce the maximum stud length to ensure that the associated factored resistance of the stud is consistently greater than the factored demand.

This requirement will prohibit certain designs that are currently acceptable. This can be somewhat mitigated by allowing the designer to choose from a greater selection of stud sizes, spacings, and lengths. The current table allows the designer to increase stud size, decrease stud spacing, or decrease stud length, but does not address the possibility of changing two or more criteria simultaneously. For example, according to the existing Table 9.23.10.1, a wall supporting an attic accessible by a stairway plus one floor must comprise a stud with a minimum d of 89 mm, a maximum L of 3660, and a maximum s of 400 mm. Increasing d to 140 mm, decreasing L to 2440 mm, or decreasing s to 300 mm are all acceptable substitutions. However, the existing table does not indicate whether decreasing L to 2440 mm while increasing s to 600 mm is acceptable if d remains at 89 mm. It would, therefore, be beneficial to expand the range of solutions permitted by NBCC Table 9.23.10.1.

Table 6.10 presents the recommended new size, spacing, and unsupported length combinations for NBCC Table 9.23.10.1. All possible alternatives for stud size, spacing and unsupported length values listed for all supported load classifications were obtained using: two stud sizes, 38x89 mm and 38x140 mm; three stud spacings, 300, 400, and 600 mm; and three stud lengths, 2400, 3600, and 4200 mm. The 38x64 mm stud is not considered because it is not typically used for load-bearing walls (CMHC, 2013). The current NBCC Table 9.23.10.1 does not list a stud length of 4200 mm for a 38x89 mm stud size, and so the maximum length in this case is limited to 3600 mm. The factored

resistances shown were obtained using Equation [6.8] assuming No. 2 or better SPF wood studs with gypsum-board sheathing applied vertically on both sides. Values are shown for bare studs, sheathed studs with t of 12.7 mm and s of 300 mm, sheathed studs with t of 15.9 mm and s of 300 mm, and sheathed studs with t of 12.7 mm and s of 100 mm. The strength contribution of gypsum-board sheathing is ignored for 89x140 mm studs with L of 2400 mm, as it is negligible, and 4200 mm, which is longer than commonly available gypsum-board lengths. New recommended size, spacing, and unsupported length values not shown in the current NBCC Table 9.23.10.1 are shaded, whereas the unshaded values are as currently shown. Clearly most of the proposed combinations are new.

Table 6.10: Recommended Design Limits for NBCC Table 9.23.10.1 for SPF Wood Studs

Supported load case	SL *(kPa)*	Min. stud size *(mm)*	Max. stud spacing *(mm)*	Max. unsupp. height *(mm)*	P_f *(kN)*	P_r *(kN)*			
						Bare Stud	Sheathed Stud		
							t = 12.7 mm s = 300 mm	*t = 15.9 mm s = 300 mm*	*t = 12.7 mm s = 100 mm*
Attic not accessible by stairway	-	38x89	600	3600	5.4	7.6	-	-	-
		38x140	600	4200	5.4	22.5	-	-	-
Attic accessible by stairway & 1 floor	-	38x89	300	2400	11.2	18.3	-	-	-
		38x89	300	3600	11.2	-	11.2	-	-
		38x89	400	2400	14.9	18.3	-	-	-
		38x89	600	2400	22.4	-	-	23.4	26.6
		38x140	600	4200	22.4	22.5	-	-	-
Roof load plus one floor	1.0	38x89	400	3600	11.0	-	11.2	-	-
		38x89	600	2400	16.5	18.3	-	-	-
		38x140	600	4200	16.5	22.5	-	-	-
	2.0	38x89	300	3600	9.4	-	11.2	-	-
		38x89	400	2400	12.5	18.3	-	-	-
		38x89	600	2400	18.8	-	22.1	-	-
		38x140	600	4200	18.8	22.5	-	-	-
	3.0	38x89	400	2400	16.1	18.3	-	-	-
		38x89	400	2400	24.2	-	-	-	26.6
		38x140	600	3600	24.2	29.6	-	-	-
Attic not accessible by stairway & 2 floors	-	38x89	400	2400	17.4	18.3	-	-	-
		38x89	600	2400	26.1	-	-	-	26.6
		38x140	600	3600	26.1	29.6	-	-	-
Roof load	1.0	38x89	400	3600	5.1	7.6	-	-	-
		38x89	600	3600	7.7	-	11.2	-	-
		38x140	600	4200	7.7	22.5	-	-	-
	2.0	38x89	300	3600	5.8	7.6	-	-	-
		38x89	400	3600	8.7	-	11.2	-	-

Supported load case	SL *(kPa)*	Min. stud size *(mm)*	Max. stud spacing *(mm)*	Max. unsupp. height *(mm)*	P_f *(kN)*	P_r *(kN)*			
						Bare Stud	Sheathed Stud		
							t = 12.7 mm s = 300 mm	*t = 15.9 mm s = 300 mm*	*t = 12.7 mm s = 100 mm*
Roof load	2.0	38x89	600	2400	13.1	18.3	-	-	-
		38x140	600	4200	13.1	22.5	-	-	-
	3.0	38x89	300	3600	9.3	-	11.2	-	-
		38x89	400	3600	12.4	-	-	12.4	-
		38x89	600	2400	18.5	-	22.1	-	-
		38x140	600	4200	18.5	22.5	-	-	-
Attic accessible by stairway	-	38x89	400	3600	6.6	7.6	-	-	-
		38x89	600	3600	9.9	-	11.2	-	-
		38x140	600	4200	9.9	22.5	-	-	-
Attic not accessible by stairway & 1 floor	-	38x89	300	3600	7.3	7.6	-	-	-
		38x89	400	3600	10.9	-	11.2	-	-
		38x89	600	2400	16.3	18.3	-	-	-
		38x140	600	4200	16.3	22.5	-	-	-
Attic accessible by stairway & 2 floors	-	38x89	300	2400	16.1	18.3	-	-	-
		38x89	400	2400	21.4	-	22.1	-	-
		38x140	400	4200	21.4	22.5	-	-	-
		38x140	600	3600	32.1	-	34.6	-	-
Attic accessible by stairway & 3 floors	-	38x140	300	4200	21.0	22.5	-	-	-
		38x140	400	3600	28.0	29.6	-	-	-
		38x140	600	2400	42.0	48.5	-	-	-

The possible stud designs are increased from 14 in Table 6.9 to 45 in Table 6.10. A total of 29 bare stud designs are adequate, with a factored resistance that exceeds the factored demand. An additional 16 stud designs are adequate when accounting for the enhanced capacity due to gypsum-board sheathing. For these designs to be acceptable, the orientation of the gypsum board must be specified in the vertical direction with no horizontal seams. A total of 41 of 45 stud designs are adequate for sheathed studs with t of 12.7 mm and s of 300 mm. A total of 43 of 45 stud designs are adequate for sheathed studs with t = 15.9 mm and s of 300 mm. Finally, all 45 stud designs are adequate for sheathed studs with t of 12.7 mm and s of 100 mm. It is emphasized that the values shown in Table 6.10 are valid only if the orientation of the gypsum board is specified in the vertical direction with no horizontal seams.

6.4 Summary and Conclusions

Table 9.23.10.1 of the National Building Code of Canada, NBCC, (NRC, 2010) markedly simplifies the design process for light-frame wood structures by providing the smallest stud size, maximum spacing, and maximum length for various supported load categories. However, this table is based on a history of satisfactory performance, and so its suitability is not rigorously documented. Also, the contribution of gypsum-board sheathing to the strength of wood studs subjected to axial compressive loads is not considered.

This chapter has analyzed the provisions specified in NBCC Table 9.23.10.1 and has presented recommended revisions to account for the contribution of gypsum-board sheathing oriented vertically to the axial compressive resistance of interior load-bearing walls. The demand was quantified for the various usages provided in the NBCC, and then compared to the resistance for both the bare and sheathed stud. The factored resistance of the bare and sheathed studs were quantified using either of two methods: 1) a new empirical equation derived from linear regression; and, 2) CAN/CSA-O86-09 equations (CSA, 2009), with a modification factor to account for the strength contribution of gypsum-board sheathing.

The specific conclusions of this chapter are as follows:

1. The empirical equation represents a simple linear relationships between the axial compressive resistance of sheathed studs and the modulus of elasticity of wood, E_s. The accuracy of the empirical equation was checked by comparing its predicted 5^{th} percentile axial compressive resistances for seven combinations of stud length, stud depth, gypsum-board thickness, and fastener spacing to the 5^{th} percentile resistance of the fitted normal distribution in Chapter 5. For the seven cases investigated, the mean fitted distribution-to-predicted ratio is 0.997 and the standard deviation is 0.011. Therefore, the empirical equation can very accurately predict the specified 5^{th} percentile resistance of gypsum-board sheathed studs.

2. The modification factor, applied to the current CAN/CSA-O86-09 equations to account for the contribution gypsum-board sheathing, is equal to the specified

sheathed-to-bare-stud capacity ratio obtained using the empirical equation. The modification factor increases as the wood modulus of elasticity decreases. The accuracy of these equations using the modification factor was checked by comparing its specified design resistances for the seven cases investigated to the 5^{th} percentile resistance of the fitted normal distribution in Chapter 5. The mean fitted distribution-to-predicted ratio is 1.097 with a standard deviation of 0.059. Therefore, the modified CAN/CSA-086-09 equations yield conservative predictions of the specified 5^{th} percentile resistance of gypsum-board sheathed studs.

3. A resistance factor of 0.65 is recommended when the axial capacity of a sheathed stud is computed using the empirical equation when the stud length is 3660 mm and stud depth is 89 mm. This value may increase to 0.75 when the stud length is 2440 mm or the stud depth is 140 mm.

4. A resistance factor of 0.80 is recommended when the axial capacity of a sheathed stud is computed using the modified CAN/CSA 086-09 equations.

5. The factored axial capacity of sheathed studs computed using the empirical equation ranges from 91 to 98% of the values computed using the modified CAN/CSA 086-09 equations. Thus, the modified CAN/CSA 086-09 equation is less conservative, so was used to define the suitability of NBCC Table 9.23.10.1.

6. Nine of the fourteen supported load cases for interior load-bearing walls permitted in the current NBCC Table 9.23.10.1 are unsafe if the maximum floor joist span (6 m) and maximum ceiling joist spans (10 m) permitted by Part 9 in the NBCC are assumed. Eight of the fourteen are unsafe even when the contribution 12.7 or 15.9 mm gypsum-board sheathing connected to both sides of the stud is considered. Therefore, revisions are necessary that will prohibit certain designs that are currently not acceptable.

7. The recommended revisions to provisions of NBCC Table 9.23.10.1 increase the quantity of possible stud designs from 14 to 45. A total of 29 stud designs are adequate when using bare studs. A total of 41 stud designs are adequate when using

sheathed studs with a gypsum-board thickness of 12.7 mm and a fastener spacing of 300 mm. A total of 43 stud designs are adequate when the gypsum-board thickness is increased to 15.9 mm. Finally, all 45 stud designs are adequate when the fastener spacing is reduced to 100 mm. It is, therefore, recommended that the contribution of gypsum-board sheathing be accounted for to maximize the quantity of acceptable designs for interior walls.

6.5 References

Bartlett, F. M., Hong, H. P., Zhou, W., 2003. Load factor calibration for the proposed 2005 edition of the National Building Code of Canada: Statistics of loads and load effects. Canadian Journal of Civil Engineering, Vol. 30, pp. 429-439.

Bleau, R., 1984. Comportement des Poutre-Colonnes en Bois. M.Sc.A. Thesis, Department of Civil Engineering, University of Sherbrooke, QC.

Canadian Standards Association (CSA), 2009. CAN/CSA-O86-09: Engineering Design in Wood. Canadian Wood Council, Ottawa, ON.

Canadian Standards Association (CSA), 2011. CSA-S408-11 Guidelines for the Development of Limit States Design Standards. Canadian Wood Council, Ottawa, ON.

CWC, 2010. Wood Design Manual. Canadian Wood Council, Ottawa, ON.

CWC, 2009. Engineering Guide for Wood Frame Construction. Canadian Wood Council, Ottawa, ON.

Foschi, R.O., Folz, B., Yao, F.Z., 1989. Reliability-Based Design of Wood Structures. Structural Research Series, Report No. 34, Department of Civil Engineering, University of British Columbia. 282 p.

National Research Council of Canada (NRC), 2010. National Building Code of Canada. Institute for Research in Construction, National Research Council of Canada, Ottawa, Ont.

Chapter 7 Summary, Conclusions, and Suggested Future Work

7.1 Summary

Gypsum board is the most commonly used sheathing material in Canadian light-frame wood construction. Part 9 “Housing and Small Buildings” of the National Building Code of Canada (NBCC) (NRC, 2010) and the Engineering Guide for Wood-Frame Construction (CWC, 2009) recognize gypsum-board provides bracing and shear resistance. However, the possible increase in axial compressive resistance of wood studs due to gypsum-board sheathing is not currently recognized in either document. The research presented in this thesis therefore investigated this possible increase for light-frame wood walls comprised of Spruce-Pine-Fir (SPF) studs and sheathed with gypsum-board on both sides of the stud.

The research can be summarized using three categories: experimental data acquisition, numerical modeling, and contribution of gypsum-board sheathing

7.1.1 Experimental Data Acquisition

Chapter 2 presented full-scale tests designed to obtain realistic axial compressive load versus mid-height deflections responses (P-Δ) of 19 individual gypsum-board-sheathed wood studs. The tests concentrated specifically on 2440 mm long 38 x 89 mm SPF studs with 12.7 mm gypsum-board sheathing on both sides, i.e., typical dimensions in residential light-frame construction. The P-Δ responses were compared to predicted responses from numerical models in the literature.

Chapter 3 presented an experimental investigation of the shear load-slip response of gypsum-board-to-wood-stud connections. A total of 283 monotonic tests and 20 single load-reversal tests were conducted using 32 and 41 mm screws fastening 12.7 and 15.9 mm thick gypsum board, respectively, to SPF wood studs. The results were analyzed to identify statistically significant parameters and idealize the load-slip response of the fastener connections in shear. The influence of fastener location, edge type, side distance, rate-of-

displacement, paper orientation, density of gypsum board, moisture content of gypsum board, and gypsum-board thickness was investigated.

7.1.2 Numerical Modeling

Chapter 4 presented new numerical models to predict the axial compressive resistance of bare and sheathed studs that were developed in the finite element software ANSYS (ANSYS, 2012). These models account for: a nonlinear wood stress-strain relationship with a finite crushing stress (e.g., Song and Lam, 2009); the load-slip response of fastener connections idealized in Chapter 3; and, initial out-of-straightness. They are readily modified to account for: various stud lengths and depths; various gypsum-board thicknesses, orientations, and widths; and fastener spacings. The bare stud model was validated using experimental data reported by Buchanan (1984). The sheathed stud model was validated using the experimental data reported in Chapter 2.

7.1.3 Contribution of Gypsum-Board Sheathing

Chapter 5 presented a sensitivity analysis, using the numerical models presented in Chapter 4, of the axial capacity of bare and gypsum-board-sheathed SPF wood studs. The deterministic variables analyzed are: stud length and depth; gypsum-board thickness, orientation, and width; and, fastener spacings. The random variables analyzed are: the modulus of elasticity, the crushing stress, and the initial mid-height out-of-straightness of the wood; the modulus of elasticity of the gypsum-board; and the resistance of fastener connections at a slip of 1.0 mm. Wood design convention is to specify the 5^{th} percentile strength (CWC, 1994). Therefore, the influence of deterministic and random variables was assessed using the 5^{th} percentile values for most random variables, and the 95^{th} percentile value of the initial mid-height out-of-straightness because an increased value decreases the capacity of the stud.

The strength distribution of the axial capacity of the bare and sheathed studs were quantified using Monte Carlo simulations to obtain a total of 2000 samples for each

significant deterministic variable combination. The contribution of gypsum-board was quantified by comparing the 5th percentile capacities of the bare and sheathed studs.

Chapter 6 addressed means to account for the contribution of gypsum-board sheathing in CAN/CSA-086-09 and NBCC Table 9.23.10.1. A modification factor, to be included in the current CAN/CSA-086-09 equations to account for the strength increment provided by the gypsum-board sheathing, was derived from linear regression using the data sets in Chapter 5. Alternatively, an empirical equation was also developed from linear regression using the data sets in Chapter 5 to compute the axial compressive resistance of bare and sheathed studs. The reliability associated with using such a modification factor or with the empirical equation has not been established. Therefore, appropriate resistance factors were computed assuming the target reliability index is equal for bare and sheathed studs. The least conservative option was used to compute the factored axial compressive resistance of gypsum-board-sheathed wood studs for the given stud size and lengths specified in NBCC Table 9.23.10.1.

The suitability of NBCC Table 9.23.10.1 was assessed by comparing the factored demand for each load categories for interior load-bearing walls to the factored axial capacity of sheathed studs for the given specified size and length. Recommended revisions were presented, prohibiting certain designs that are currently acceptable, and including acceptable alternative designs.

7.2 Conclusions

The general conclusions are:

1. Methods to compute the axial compressive resistances of gypsum-board sheathed studs must explicitly account for the nonlinear wood stress-strain relationship and nonlinear fastener load-slip response. Numerical models reported by others in the literature do not account for these factors. The true axial capacities are on average 20% less than those predicted assuming linear-elastic material properties of the wood and linear-elastic response of the fastener connections. The minimum and

maximum difference observed are 9 and 32%, respectively. Therefore, a new numerical model for gypsum-board-sheathed stud is needed.

2. The monotonic shear load-slip response of most fastener connections investigated can be idealized as:

$$V = V_{1.0} \times 2.66 \times \delta_f \qquad 0 < \delta_f < 0.25 \text{ mm}$$

$$V = V_{1.0} [-0.0307 \times \ln(\delta_f)^2 + 0.203 \times \ln(\delta_f) + 1] \qquad \delta_f \geq 0.25 \text{ mm}$$

where V is the shear load in N, δ_f is the slip in mm, and $V_{1.0}$ is the shear load in N at δ_f equal to 1.0 mm. Values for $V_{1.0}$ were determined empirically from experimental data and are quantified in Table 3.16 based on the gypsum-board edge, side distance, moisture content in the gypsum board, and gypsum-board thickness. This equation is valid for rates-of-displacement of 0.5 to 2.5 mm/min, for loads applied in the machine and cross-machine direction of the gypsum-board paper, and for both regular and low-density gypsum boards typically used in Canada. The mean test-to-predicted ratio for δ_f of 1 mm ranges from 0.97 to 1.04 with a maximum standard deviation of 0.20. The mean test-to-predicted ratio for δ_f of 3 mm ranges from 0.98 to 1.10 with a maximum standard deviation of 0.18.

3. Fastener connections located at corners of the gypsum board, with 10 mm side distances, and loaded in the cross-machine direction can be idealized as:

$$V = V_{1.0} \times 2.62 \times \delta_f \qquad 0 < \delta_f < 0.25 \text{ mm}$$

$$V = V_{1.0} [-0.0580 \times \ln(\delta_f)^2 + 0.168 \times \ln(\delta_f) + 1] \qquad 0.25 < \delta_f \geq 1.00 \text{ mm}$$

The mean test-to-predicted ratio for δ_f of 1 mm is 1.00 with a standard deviation of 0.12.

4. The shear load-slip responses of fasteners subjected to a single load reversal mimicked the monotonic load-slip responses during the loading phase. However, during unloading, when the slip decreased from its maximum value to zero, the load-slip response was pinched as the fastener slipped through the elongated hole. Similar observations were noted by Gad (1997), who investigated gypsum board connected to steel studs, and Li et al. (2012), who investigated plywood connected

to wood studs with nails. It is, therefore, recommended that fastener connections in gypsum-board-sheathed studs be idealized using the above equations for the monotonic loading for the loading phase and a complete loss of capacity for the unloading phase.

5. The predicted cumulative distributions of the axial compressive resistance of bare studs using numerical models in the literature markedly overestimate those observed from 100 tests results of 2300 mm long 38x89 mm studs reported by Buchanan (1984), with test-to-predicted ratios ranging from 0.79 to 0.96 at the 50^{th} percentile values. Therefore a new finite element model for bare studs is needed.

6. The new model developed using ANSYS (ANSYS, 2012) finite element software yielded a predicted cumulative distribution of the axial compressive resistance that is in good agreement up to the 80^{th} percentile value of the observed data by Buchanan (1984), with a test-to-predicted ratio of 1.00 at the 50^{th} percentile values. The upper 20^{th} percentile values have little influence on the reliability of the studs, and so are not of interest in this study. Therefore, this model is suitable for accurate predictions of the axial compressive capacity of bare studs.

7. The new ANSYS finite element model for sheathed studs accurately predicted the observed responses of all 19 gypsum-board-sheathed wood studs reported in Chapter 2: the mean test-to-predicted ratio was 1.01 with a coefficient of variation (CoV) of 0.060.

8. The sensitivity analysis concluded that the strengths of the sheathed and unsheathed studs are sufficiently different to recommend changes to design practice to account for the contribution of the gypsum board if: the gypsum board is oriented vertically; stud depths are 89 or 140 mm; stud lengths are 2440 or 3660 mm; gypsum-board thickness are 12.7 or 15.9 mm; and, fastener spacings are 300 mm or less. If the gypsum-board is oriented horizontally, the strengths of the sheathed and unsheathed walls are not sufficiently different to warrant changes to design practice. The additional strength provided by the gypsum board is insensitive to the gypsum-board width between studs if the stud spacing exceeds 100 mm.

9. The modulus of elasticity of wood has the greatest influence on the axial compressive resistances of bare and sheathed studs. The influence of the wood crushing stress, the initial mid-height out-of-straightness of the stud, and the fastener strength were found to be marginally significant. Therefore, the strength distributions were computed accounting for the random nature of these variables. The modulus of elasticity of the gypsum board has negligible influence on the axial compressive capacity of sheathed studs.

10. The axial compressive resistance of bare and sheathed No. 2 or better SPF studs are normally distributed with means and CoV presented in Table 5.5.

Table 7.1: Axial Compressive Capacity of Bare and Sheathed Studs

Stud depth *(mm)*	Stud length *(mm)*	Gypsum-board thickness *(mm)*	Stud spacing *(mm)*	Mean *(kN)*	CoV	5^{th} percentile *(kN)*
Bare Stud						
89	2440	-	-	31.9	0.182	22.7
89	3660	-	-	14.8	0.178	10.5
140	2440	-	-	93.4	0.168	67.6
140	3660	-	-	51.7	0.175	36.8
Sheathed Stud						
89	2440	12.7	100	41.7	0.139	32.2
89	2440	12.7	300	36.6	0.151	27.6
89	2440	15.9	300	38.1	0.140	29.3
89	3660	12.7	300	19.6	0.142	15.1
89	3660	15.9	300	21.1	0.135	16.4
140	2440	12.7	300	94.9	0.154	70.8
140	2440	15.9	300	95.8	0.151	72.0
140	3660	12.7	300	57.9	0.156	43.0
140	3660	15.9	300	60.3	0.146	45.8

11. For a stud depth of 89 mm or a stud length of 3660 mm, with a fastener spacing of 300 mm, the gypsum increases the 5^{th} percentile axial compressive resistance by a factor of 1.17 to 1.56, depending on the gypsum-board thickness. These increases are sufficient to recommend changes to the current CAN/CSA-086-09 equations and NBCC Table 9.23.10.1 for these deterministic variable combinations. Conversely, for a stud depth of 140 mm and stud length of 2440 mm, the gypsum board increases the 5^{th} percentile axial capacity by a factor of only 1.05 or 1.06 for

a gypsum-board thickness of 12.7 or 15.9 mm, respectively. These increase are not sufficient to recommend changes to design practices.

12. For d of 89 mm, L of 2440 mm, and t of 12.7 mm, a decrease of s from 300 to 100 mm increases the strength contribution of gypsum-board sheathing by a factor of 1.22 to 1.42 with respect to the capacity of the bare stud. If an existing sheathed wall structure requires additional capacity, adding fasteners can be a cost-effective alternative. Therefore, changes are recommended for to the current CAN/CSA-086-09 equations and NBCC Table 9.23.10.1 for this case.

13. The new empirical equation is given by:

[7.1] $$\hat{P}_c = \hat{\beta}_1 E_s + \hat{\beta}_4 + \hat{\beta}_5 Z_S + \hat{\beta}_6 Z_t$$

where $\hat{P}_c$ is the predicted compressive strength; E_s is the wood modulus of elasticity; $\hat{\beta}_1$, $\hat{\beta}_4$, $\hat{\beta}_5$, and $\hat{\beta}_6$ are the parameter estimates shown in Table 6.3; Z_S is the indicator variable equal to 1 when the wood stud is sheathed with gypsum board and 0 otherwise; and, Z_t is the indicator variable equal to 1 when the gypsum-board thickness is equal to 19 mm, and 0 otherwise. This equation accurately predicts the specified 5^{th} percentile axial compressive resistance of gypsum-board sheathed studs, with a mean fitted distribution-to-predicted ratio of 0.997 and a standard deviation of 0.011. An associated resistance factor of 0.75 is recommended for 2440 mm long studs with depths of 89 or 140 mm and for 3660 mm long studs with depths of 140 mm. The resistance factor should be reduced to 0.65 for 3660 mm long stud with depths of 89 mm.

14. The modification factor, K_{SH}, recommended for implementation with the current CAN/CSA-086-09 equations, accounting for the strength contribution of gypsum-board sheathing, is given by:

[7.2] $$K_{SH} = 1 + \left(\hat{\beta}_5 Z_S + \hat{\beta}_6 Z_t\right) / \left(\hat{\beta}_1 E_s + \hat{\beta}_4\right)$$

An associated resistance factor of 0.80 is recommended. The factored axial capacity of sheathed studs computed using the empirical equation ranges from 91 to 98% of

the values computed using the modified CAN/CSA 086-09 equations. This is because smaller resistance factors are recommended for the empirical equation. Thus, the modified CAN/CSA 086-09 equation is less conservative, so was used to define the accuracy of the provisions in NBCC Table 9.23.10.1.

15. The factored demands for nine of the fourteen load categories for interior walls in NBCC Table 9.23.10.1 exceed the factored axial capacities of the bare stud if the maximum permitted floor and ceiling joist spans are assumed. Eight of the fourteen remain unsafe if for the strength contribution of gypsum-board sheathing is accounted for. Therefore, revisions are necessary to prohibit certain stud designs that are currently acceptable.

16. Revisions to NBCC Table 9.23.10.1 are recommended to increase the number of acceptable stud size, spacing, and length combinations from 14 to 29 for bare studs. An additional 12 designs are acceptable when the extra strength provided by 12.7 mm sheathing with a fastener spacing of 300 mm is accounted for. Two more designs are acceptable when the gypsum-board thickness is 15.9 mm, or three more designs are acceptable if the fastener spacing is reduced to 100 mm.

7.3 Suggested Future Work

The conclusions in this thesis present suggested changes to an equation in the CAN/CSA-086-09 standard (CSA, 2009) and to Table 9.23.10.1 in Part 9 of the National Building Code of Canada (NRC, 2010). The process to initial consideration of such changes requires completion of "Proposed Change Forms" that are then submitted to the technical committees responsible for these documents. However, before this is done, it may be prudent to first extend the research in this thesis and address the following suggested work.

1. Extend the research to include exterior load-bearing walls, which are fabricated with gypsum board on the inside face of the stud only (CMHC, 2013). Marxhausen and Stalnaker (2006) reported preliminary tests on gypsum-board sheathed stud walls subjected to axial compressive loads, and found the resistance of sheathed studs to be similar when sheathed with gypsum board on one or both sides.

Therefore, the strength enhancement attributable to the gypsum-board sheathing on side only may be sufficiently large that it should be accounted for in design. The authors focused on the bracing abilities of the gypsum-board, and so did not expand on the buckling behaviour of the sheathed stud. Therefore, the contribution of sheathing to the axial compressive resistance of exterior wood stud walls has not yet been quantified. The experimental and numerical approaches used in this thesis could be used for exterior walls.

Investigation of the accuracy of the provisions in NBCC Table 9.23.10.1 for the design of exterior walls remains outstanding. The approach presented in Chapter 6 could be applied to exterior walls to modify the current CAN/CSA-08-09 equations and revise NBCC Table 9.23.10.1 as necessary.

2. Investigate the impact of possible human error during the installation of gypsum-board sheathing on the strength enhancement to the axial compressive resistance of wood studs. This research briefly investigated the sensitivity of the strength enhancement to fastener spacings greater than the 300 mm maximum specified in Part 9 of the NBCC (NRC, 2010) and to decreased gypsum-board widths. However, the strength enhancement for these conditions were not quantified. Also, the reduction in fastener strength for less-than-minimum distances along the edge of the gypsum board remains outstanding. The procedure used in this study could also be used to study the impact of human errors.

3. Identify fastening designs that markedly increase the strength enhancement of gypsum-board sheathing to the axial compressive resistance of wood studs. It was concluded in this study that a decrease in fastener spacing from 300 to 100 mm markedly increased the axial compressive resistance of gypsum-board-sheathed wood studs. However, this methodology may at time also come with additional labour cost. Other methods to increase the axial compressive resistance of sheathed studs that have not been investigated in this study may include, for example, additional fasteners at both ends of the studs only. The approach used in Chapters 4 through 6 could apply to various other fastener designs.

4. Investigate the impact of loading gypsum-board-sheathed wood studs under various deterministic and variable conditions that have not been considered in this study. This includes but is not limited to stud lengths not equal to 2400, 3600, or 4200 mm; various load rates; sustained loads; moisture contents in the wood; gypsum board installed horizontally with taped joints; and tensile loads. The experimental methodology described in Chapter 2 could be applied to most compressive loading cases, but may need to be revised for tensile loading cases. Bracing design may be needed to ensure strong-axis buckling of sheathed studs with gypsum board installed horizontally. The analytical approach in Chapters 4 through 6 could be applied to these loading cases.

7.4 References

ANSYS Inc., 2012. ANSYS Academic Research, Release 14.5. Canonsburg, Pennsylvania, U.S.A

Buchanan, A.H., 1984. Strength Member and Design Methods for Bending and Axial Load Interaction in Timber Members. Ph.D. Thesis, Department of Civil Engineering, University of British Columbia, BC. 298 p.

Canadian Standards Association (CSA), 2009. CAN/CSA-086-09: Engineering Design in Wood. Canadian Wood Council, Ottawa, ON.

Canadian Wood Council (CWC), 1994. Canadian Lumber Properties. Canadian Wood Council, Ottawa, ON.

Canadian Wood Council (CWC), 2009. Engineering Guide for Wood Frame Construction. Canadian Wood Council, Ottawa, ON.

CMHC, 2013. Canadian Wood-Frame House Construction. Canadian Mortgage and Housing Company, Ottawa, ON, 315 p.

Gromala, D.S. 1985. Lateral Nail Resistance for Ten Common Sheathing Materials. Forest Products Journal, 35(9): 61-68.

Gad, E. F. 1997. Performance of Brick-Veneer Cold-Formed Steel-Framed Domestic Structures when Subjected to Earthquake Loading", Ph.D. Thesis, Department of Civil and Environmental Engineering, The University of Melbourne, Australia. 360 p.

Kamiya, F., 1987. Buckling Theory of Sheathed Walls: Linear Analysis. Journal of Structural Engineering, Vol. 114, No. 9, pp. 625-641.

Kamiya, F., 1988. Buckling of Sheathed Walls: Nonlinear Analysis. Journal of Structural Engineering, Vol. 113, No. 3, pp. 2009-2022.

Liew, Y. L., Gad, E. F., and Duffield, C. F. 2006. Experimental and Analytical Validation of a Fastener Bearing Test as a Means of Evaluating the Bracing Characteristics of Plasterboard. Advances in Structural Engineering, 9(3): 421-432.

Marxhausen, P. D. and Stalnaker, J. J., 2006. Buckling of Conventionally Sheathed Stud Walls. Journal of Structural Engineering, Vol. 132, No. 5, pp. 745-750.

Maholtra, S. K. and Mazur, S. J., 1970. Buckling Strength of Solid Timber Columns. Transactions of the Engineering Institute of Canada, Vol. 13, No. A-4, pp. I-VII.

National Research Council of Canada (NRC). 2010. National Building Code of Canada - Part 9. Institute for Research in Construction, National Research Council of Canada, Ottawa, Ont.

Robertson, A., 1925. The Strength of Struts. Institution for Civil Engineers, No. 28. 55 p.

Song, X. and Lam, F., 2009. Laterally Braced Wood Beam-Columns Subjected to Biaxial Eccentric Loading. Computers and Structures, Vol. 87, pp. 1058-1066.

Southwell, R.V. 1931. On the Analysis of Experimental Observations in Problems of Elastic Stability. Proceedings of the Royal Society of London. Series A, Containing Papers of a Mathematical and Physical Character, Vol. 135, No. 828, pp. 601-616.

Srikanth, T. S. 1992. Structural Reliability of Light-Frame Wood Systems with Composite Action and Load Sharing. Ph.D. Thesis, Department of Forest Products, Oregon State University, Corvallis, OR, USA. 218 p.

Appendix 2A Initial Mid-Height Out-of-Straightness of Bare Studs

This appendix presents the methodology used to quantify the initial mid-height out-of-straightness about the strong and weak axis of 2440 mm long bare 38x89 mm Spruce-Pine-Fir studs, and the associated results.

Twelve studs were tested about their strong axis, and twenty-five studs were tested about their weak axis. Each stud was initially subjected to flexural tests as described in Section 2.3.2 to determine the modulus of elasticity of the wood, E_s, prior to being subjected to buckling tests. To force strong-axis buckling to occur, the weak axis of two studs was braced as shown in Figure 2A.1(a), to prevent weak-axis buckling of the stud. Figure 2A.1(b) shows the test setup with pinned supports concentrically located at the end of each stud and the loading applied through a simply supported beam at the top of each stud. Two 450 kN load cells and two 100 mm linear-voltage-differential-transducers (LVDT) captured the axial load and mid-height displacement of each stud, respectively.

(a) Braced pair of studs (b) Test setup

Figure 2A.1: Strong-Axis Buckling Test of Bare Studs

Figure 2A.2(a) shows the test setup for the buckling tests about the weak axis of the studs, with pinned supports concentrically located at the end of the stud, as shown in Figure 2A.2(b). A 450 kN load cells and a 100 mm LVDT captured the axial load and mid-height displacement of each stud, respectively.

(a) Test Setup (b) Pinned Connection

Figure 2A.2: Weak-Axis Buckling Tests of Bare Studs

The load was applied in displacement control at a rate of 1 mm/min (approximately 90 kPa/min at the start of the tests), and the data were sampled at a frequency of 4 Hz. The moisture content of the stud was measured prior to testing to ensure the studs had the same moisture content for both flexural and buckling tests.

Figure 2A.3 is a typical Southwell Plot (Southwell, 1931) for one of the studs buckling about its strong axis, with the vertical intercept equal to the ratio of the initial mid-height out-of-straightness, v, to the inverse of the tangent slope, P_1. The initial few points of the observed response, indicate initial flexibility of the testing apparatus, and so are an artifact of the testing procedure that should be ignored. The Southwell Plot for all studs was linear when buckling about either axes. Southwell (1931) shows that for linear Southwell Plots, the inverse of the tangent slope is equal to the Euler Buckling load, P_e, which was computed

using Equation [2.1] with E_s from flexural tests. Linear Southwell Plots were observed for all studs, indicating that the wood response remained linear elastic.

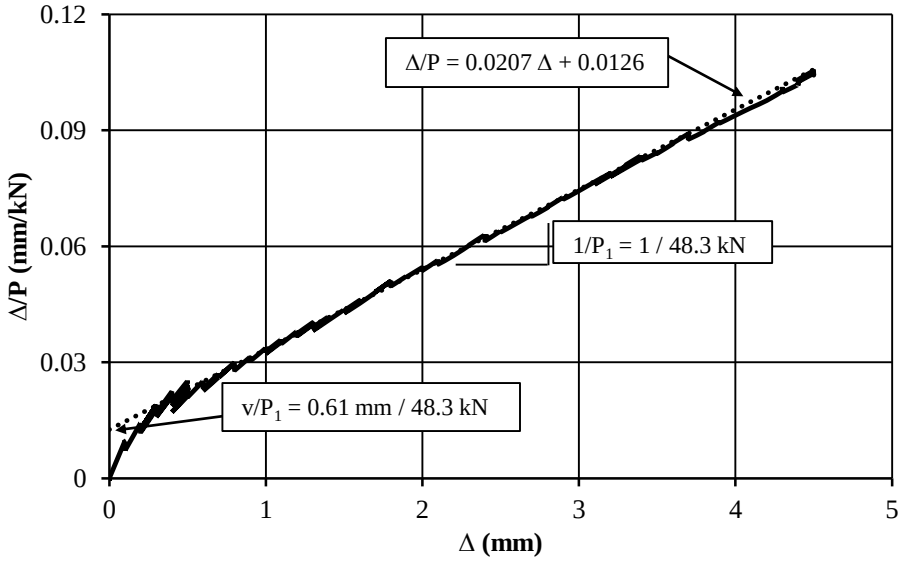

Figure 2A.3: Typical Southwell Plot from Buckling Tests of Bare Stud about Strong Axis

Table 2A.1 summarizes the initial mid-height out-of-straightness for all twelve studs tested about their strong axis and twenty five studs tested about their weak axis. The mean, standard deviation and parametric 5^{th} and 95^{th} percentiles are shown for both axes.

Table 2A.1: Initial Mid-Height Out-of-Straightness of Bare Studs

Stud	Strong axis *(mm)*	Weak axis *(mm)*
1	1.66	1.25
2	0.61	5.26
3	0.84	0.01
4	0.61	3.50
5	1.07	1.04
6	0.48	2.19
7	1.01	1.27
8	1.37	1.92
9	1.64	4.21
10	3.85	1.65
11	4.22	9.81
12	0.83	0.77
13	-	1.83
14	-	9.36
15	-	2.26
16	-	0.02
17	-	3.18
18	-	9.99
19	-	5.45
20	-	5.85
21	-	13.2
22	-	3.45
23	-	12.4
24	-	0.74
25	-	4.32
Average	1.52	4.19
SD	1.24	3.89
95^{th} Perc.	4.02	11.9
5^{th} Perc.	0.55	0.17

References

Southwell, R.V. 1931. On the Analysis of Experimental Observations in Problems of Elastic Stability. Proceedings of the Royal Society of London. Series A, Containing Papers of a Mathematical and Physical Character, Vol. 135, No. 828, pp. 601-616.

Appendix 2B Estimate of Wood Modulus of Elasticity from Flexural Testing

An investigation of the effect of variable cross-sectional strength was performed to minimize possible errors when estimating the wood modulus of elasticity from flexural tests for predicting buckling behaviour. Consider a four-point flexural test for a stud, as shown in Figure 2B.1, with varying modulus of elasticity, E, say E_1 up to a distance w_1 from the end supports and E_2 at the center:

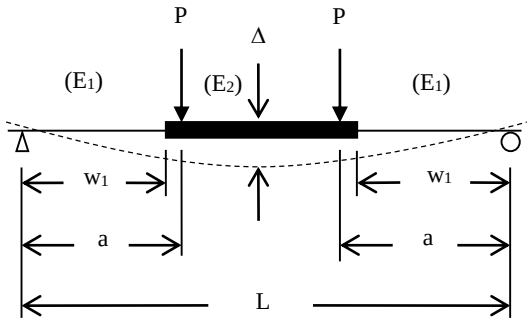

Figure 2B.1: Four-Point Bending Test for Stud with Varying Modulus of Elasticity

Equations [2B.1] and [2B.2] were derived to calculate the mid-height deflection:

[2B.1] $\Delta = Pa\left[3L^2 - 4a^2 + 8w_1^2(E_2 / E_1 - 1) / a\right] / 24E_2I;$ for $w_1 < a$

[2B.2] $\Delta = Pa\left[3L^2 - 4a^2(E_2/E_1) + 12w_1^2(E_2 / E_1 - 1)\right] / 24E_2I;$ for $w_1 > a$

When $E_1 = E_2$, Equations [2B.1] and [2B.2] are identical to Equation [2.17] in Section 2.3.2. When $a = w_1$, Equations [2B.1] is identical to [2B.2]. An equivalent modulus of elasticity for flexure, $E_{eq(f)}$, can be obtained by setting Equation [2.17] equal to Equations [2B.1] and [2B.2], to give:

[2B.3] $E_{eq(f)} = E_2\left(3L^2 - 4a^2\right) / \left[3L^2 - 4a^2 + 8w_1^3(E_2 / E_1 - 1) / a\right];$ for $w_1 < a$

[2B.4] $E_{eq(f)} = E_2\left(3L^2 - 4a^2\right) / \left[3L^2 - 4a^2(E_2 / E_1) + 12w_1^2(E_2 / E_1 - 1)\right]$; for $w_1 > a$

Timoshenko and Gere (1961) developed an equation to estimate the buckling capacity of a stud with varying modulus of elasticity shown in Figure 2B.1, given by:

[2B.5] $P_{cr} = \pi^2 E_2 I / \left\{4L^2 \left[1 + (E_2 / E_1 - 1)(2w_1 / L - \sin\pi(1 - 2w_1 / L) / \pi)\right]\right\}$

An equivalent modulus of elasticity for buckling, $E_{eq(b)}$, was derived by setting Equation [2B.5] equal to the Euler buckling load (Equation [2.1]) to give:

[2B.6] $E_{eq(b)} = E_2 / \{1 + (E_2 / E_1 - 1)[2w_1 / L - \sin\pi(1 - 2w_1 / L) / \pi]\}$

Figure 2B.2 shows a ratio of $E_{eq(f)}$ to $E_{eq(b)}$ for a varying ratio of w_1/L: Figure 2B.2(a) shows a three-point load system with a/L = 0.5; Figure 2B.2(b) shows the system employed by Bleau (1984) and Buchanan (1984) with a/L = 0.33; Figure 2B.2(c) shows the optimum system with a/L = 0.24; and, Figure 2B.2(d) shows an extreme case where a/L = 0.1. For each load system, a relationship is shown for E_2/E_1 = 0.5, 0.8, 1.25, and 2.0. Nocent (2005) states the modulus of elasticity varies around 20 to 30 % along the length of the stud. That would limit E_2/E_1 to a range of 0.77 to 1.30. The ratio of $E_{eq(f)}$ to $E_{eq(b)}$, i.e., the potential error in predicting the wood modulus of elasticity from flexural tests for the purpose of predicting buckling capacities, is substantial for a/L = 0.5, reduces to a minimum at a/L = 0.24, and increases again at a/L = 0.1.

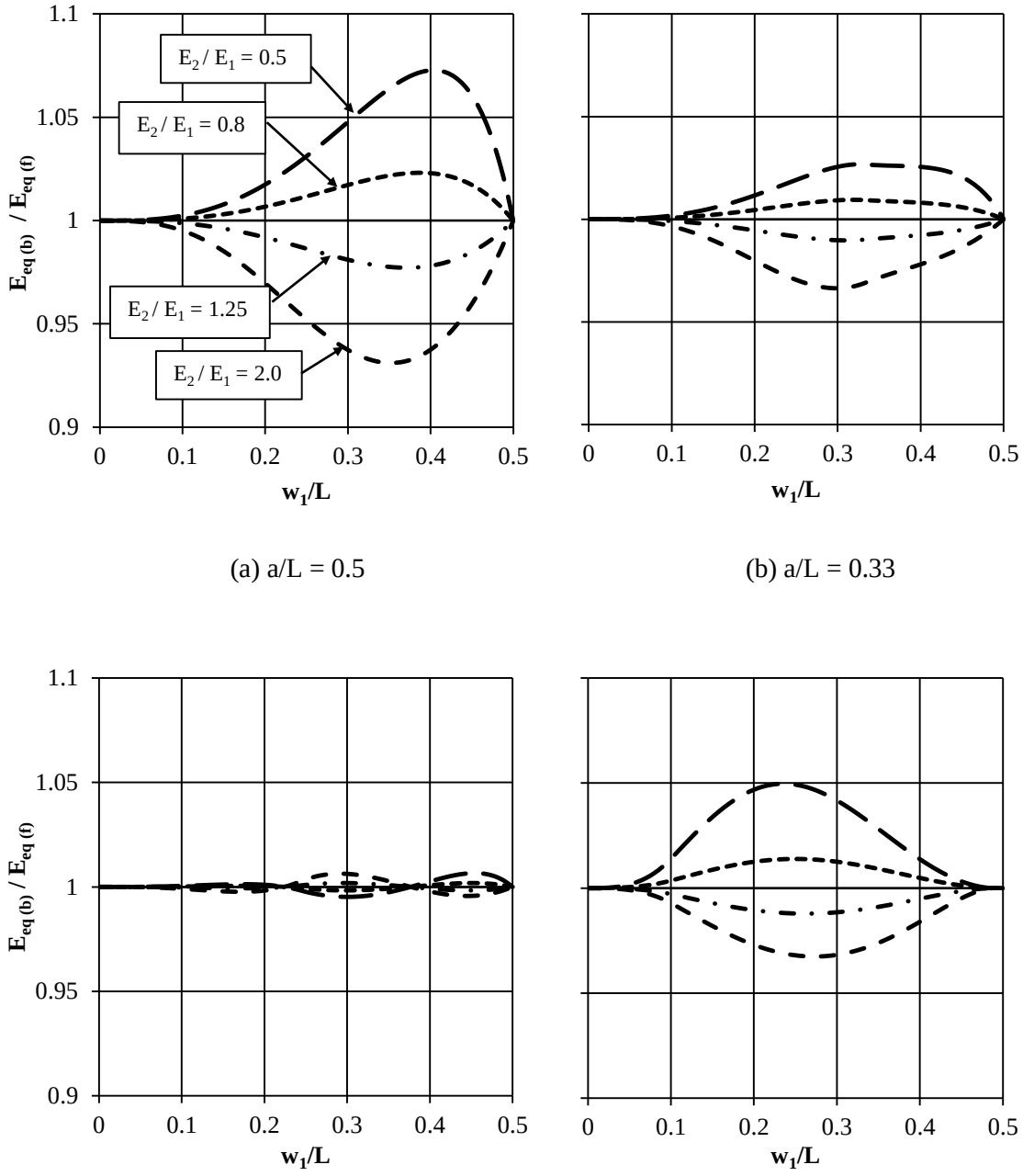

(a) a/L = 0.5

(b) a/L = 0.33

(c) a/L = 0.24

(d) a/L = 0.1

Figure 2B.2: Comparison of Modulus of Elasticity from Flexural and Buckling Tests

Table 2B.1 presents the maximum potential error for a/L = 0.33 and 0.24 for ratio of E_2/E_1. The potential error with a/L = 0.33 is less than 1% between E_2/E_1 = 0.8 to 1.25, but increases to over 2% for E_2 / E_1 = 0.5 and 2.0. The potential error for a/L = 0.24 remains well below 1% for all perceivable values of E_2 / E_1.

Table 2B.1: Maximum Potential Error for Modulus of Elasticity

E_2/E_1	$E_{eq(b)} / E_{eq(f)}$	
	a/L = 0.33	a/L = 0.24
0.50	1.027	1.007
0.80	1.009	1.002
1.25	0.990	1.002
2.00	0.966	1.006

The length of the stud for a bending test in Section 2.3.2 is intentionally decreased to 2390 mm, allowing for practical supports 25 mm from both edges of a 2440 mm length stud. Because L - $2w_1$, i.e., the length of E_2, remains constant for both flexural and buckling tests, the value for w_1, i.e., the length of E_1, becomes 25 mm smaller for flexural conditions than buckling tests. A repeat of the analysis with the new lengths was conducted, with the optimum value for a/L then reduced from 0.24 to 0.22, i.e., a = 525 mm for L = 2390 mm.

References

Bleau, R., 1984. Comportement des Poutre-Colonnes en Bois. M.Sc.A. Thesis, Department of Civil Engineering, University of Sherbrooke, QC.

Buchanan, A. H., 1984. Strength Member and Design Methods for Bending and Axial Load Interaction in Timber Members. Ph.D. Thesis, Department of Civil Engineering, University of British Columbia, BC. 298 p.

Nocent, J. A., 2005. Instrumentation to Determine Load Paths in Full-Scale Wood House. M.E.Sc. Thesis, Department of Civil and Environmental Engineering, University of Western Ontario, London, ON.

Timoshenko, S. P. and Gere, J. M. 1961. Theory of Elastic Stability. 2nd edition, McGraw-Hill, New York, NY, USA. 541 p.

Appendix 2C Accuracy of Moisture Content Measurements in Gypsum Board

The moisture content (MC) in gypsum board was measured using a Protimeter Moisture Measurement System calibrated for soft wood, thus yields a wood-equivalent MC that is not very accurate. Tests using six samples of 12.7 mm low density and regular density gypsum board (physical and chemical properties of the gypsum board are provided in Section 3.2.1) and 15.9 mm regular density gypsum board were conducted to compare the MC readings and the actual water content by weight. Samples were conditioned at a temperature of 23°C and a relative humidity (RH) of 20%, 40%, 60%, 80%, and 100% for one week. The initial weight and MC reading were taken for each sample before they were placed in an oven at 105°C. The final weight was taken once all moisture was removed. The actual water content by weight is equal to the initial-to-final weight ratio.

Figure 2C.1 shows the actual MC on the vertical axis and the MC readings on the horizontal axis. The MC readings for samples conditioned at a RH of 100% were unrealistically elevated, with readings generally above 80% when the actual MC was closer to 25%. These values are well beyond the limits of this figure. The minimum MC reading for the instrument used is 7.8%. Thus, for cases where no reading could be obtained because it was less than 7.8%, a value of 7.8 is used instead. There appears to be a good positive correlation between both the wood-equivalent and actual MC in the gypsum board and the RH of the air. However, the wood-equivalent MC readings consistently overestimated the actual MC in the gypsum board. The only two exceptions occurred for 12.7 mm low density gypsum-board samples conditioned to a RH of 80%, and all samples conditioned to a RH of 100% (not shown). The MC obtained, regardless of method, varied depending on the type and thickness of the gypsum board. For a given RH, 12.7 mm low density gypsum board consistently had the lowest actual MC and highest wood-equivalent MC; 12.7 mm regular density gypsum board consistently had the lowest wood-equivalent MC; and the 15.9 mm regular density gypsum board consistently had the highest actual MC.

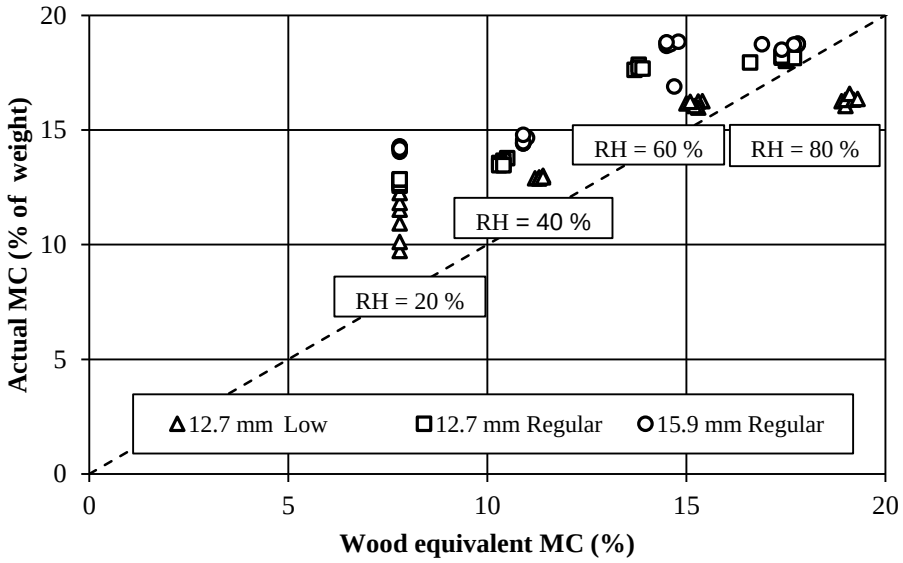

Figure 2C.1: Accuracy of Moisture Content Readings for Various Gypsum-board Densities and Thicknesses

Appendix 3A Raw Data of Load-Slip Response of Fasteners in Shear

The data presented in Table 3A.1 were obtained from the load-slip response of fasteners in shear for all 283 tests conducted in Chapter 3. The moisture content (MC) values shown were obtained using a Protimeter Moisture Measurement System calibrated for soft wood, where no value presented indicates the reading was below 7.8%.

Table 3A: Applied Shear Load at Specified Slip

Specimen	Observed Load in at specified slip *(N)*								MC
	0.25 mm	*0.5 mm*	*1.0 mm*	*1.5 mm*	*2.0 mm*	*2.5 mm*	*3.0 mm*	*5.0 mm*	*(%)*
C_{TM-10}	249	342	427	444	0	0	0	0	-
	394	458	558	601	604	0	0	0	-
	242	296	373	413	439	0	0	0	-
	275	363	398	0	0	0	0	0	-
	253	310	361	377	0	0	0	0	-
	223	288	357	0	0	0	0	0	-
	325	377	447	487	494	0	0	0	-
	354	406	469	496	491	0	0	0	-
	362	434	498	525	0	0	0	0	-
C_{TM-19}	514	600	627	0	0	0	0	0	8.4
	344	396	464	488	0	0	0	0	8.3
	380	463	545	583	580	0	0	0	8.6
	262	328	408	414	0	0	0	0	8.3
	443	519	568	578	0	0	0	0	8.6
	341	399	391	0	0	0	0	0	8.6
	149	178	245	310	368	405	426	0	-
	261	337	411	446	471	482	0	0	-
	342	396	445	440	0	0	0	0	-
	250	315	408	455	474	482	486	0	-
	394	451	500	527	537	547	551	0	-
S_{TM-10}	357	437	523	552	560	554	564	545	8.2
	235	267	313	330	340	348	361	405	7.9
	280	342	391	429	460	479	501	516	8.1
	244	299	367	400	411	423	438	477	7.9
	327	398	460	486	508	525	530	542	7.8
	220	298	392	454	492	507	532	551	7.8
	343	426	503	551	578	604	617	628	8.1

Specimen	Observed Load in at specified slip *(N)*								MC
	0.25 mm	*0.5 mm*	*1.0 mm*	*1.5 mm*	*2.0 mm*	*2.5 mm*	*3.0 mm*	*5.0 mm*	*(%)*
S_{TM-10}	321	386	464	502	527	545	566	609	8
	368	446	535	580	609	624	630	642	8.2
	165	262	361	428	469	499	503	491	8.1
$S_{TM-19\ (1)}$	371	453	547	598	650	683	716	771	10.4
	250	340	445	515	553	573	566	570	10.3
	384	478	608	707	756	785	811	864	8.9
	291	346	388	432	470	490	512	555	9.3
	432	509	591	580	600	612	621	597	8.9
	386	486	622	708	751	782	794	839	9.7
	390	453	517	552	574	601	616	643	-
	363	444	498	550	586	597	617	622	-
	265	317	377	397	414	424	426	431	-
	194	302	398	458	473	487	519	564	-
	387	443	501	523	546	561	572	624	-
	264	331	425	427	534	560	580	612	-
$S_{TM-19\ (2)}$	386	441	507	552	569	568	573	561	14.3
	376	438	501	529	552	580	604	669	14.9
	429	535	612	653	648	642	631	608	14.7
	313	390	456	475	484	495	491	509	14.7
	237	315	411	467	502	526	537	530	14.5
	266	341	439	487	510	512	511	535	14.8
	293	353	421	437	436	450	451	481	14.7
	373	446	504	516	547	545	548	557	14.7
	308	378	453	477	479	490	497	551	14.2
	263	317	385	427	444	462	473	494	14.5
	302	352	419	473	509	535	543	532	14.8
$N_{UM\ (1)}$	320	344	378	395	407	411	416	344	10
	210	316	386	442	443	452	462	0	10.4
	226	298	362	396	412	417	418	0	10.3
	220	283	360	385	405	412	424	0	10.4
	155	216	260	281	293	295	281	0	9.9
	108	265	328	343	346	360	363	0	8.9
	275	326	386	420	445	466	474	500	-
	268	324	389	418	440	448	473	533	-
	182	264	328	351	375	383	378	0	-
	180	261	341	384	406	412	409	0	-
	243	322	396	431	453	457	466	492	-
	241	309	378	412	422	425	423	0	-
$N_{UM\ (2)}$	180	228	289	306	317	318	327	335	13.9
	130	200	263	292	308	317	319	348	14.3

Specimen	Observed Load in at specified slip *(N)*								MC
	0.25 mm	*0.5 mm*	*1.0 mm*	*1.5 mm*	*2.0 mm*	*2.5 mm*	*3.0 mm*	*5.0 mm*	*(%)*
$N_{UM\ (2)}$	220	281	350	392	416	440	450	446	14.3
	225	256	304	329	337	354	362	397	14.3
$I_{UM\ (1)}$	235	329	426	457	460	466	471	451	8.9
	231	293	358	362	350	343	339	343	9.5
	210	275	357	387	399	405	403	411	9.5
	148	228	334	382	390	394	401	400	10.5
	132	195	290	361	403	423	429	442	10.2
	139	211	284	318	333	350	350	383	8.9
	287	352	410	447	466	473	473	514	-
	253	342	419	453	466	477	490	519	-
	176	242	315	347	362	377	395	403	-
	186	269	334	351	362	367	377	423	-
	309	366	444	483	500	502	504	560	-
	238	308	399	458	481	499	512	544	-
$I_{UM\ (2)}$	247	320	395	431	443	455	459	451	14.3
	274	333	407	427	446	450	455	448	14.3
	181	255	332	362	375	374	382	379	14.7
	250	330	422	471	499	508	514	508	14.6
	228	288	362	391	412	413	421	447	14.8
	233	309	385	433	457	474	474	474	14.3
	252	327	403	443	471	488	498	498	14.4
	186	259	331	363	357	350	357	367	14.2
	200	258	334	360	375	378	390	420	14.2
	294	355	398	413	419	433	433	455	14
	261	328	387	412	420	414	398	414	14.5
	289	364	439	464	484	479	482	514	14.2
$I_{UM\ (3)}$	194	278	345	367	376	380	390	417	9.9
	279	355	433	440	454	465	469	472	10
	193	262	327	352	352	352	366	360	9.9
	157	227	317	355	375	386	400	428	10.2
	248	329	404	404	388	362	362	386	9.8
	278	353	433	455	452	449	461	500	10.5
	195	269	372	421	454	464	468	510	-
	205	288	388	436	449	466	464	473	-
	215	315	403	436	453	473	478	500	-
	212	293	374	416	440	455	468	516	-
	195	282	371	399	414	427	436	462	-
$S_{UM\text{-}19}$	258	327	409	444	456	459	451	439	9.4
	228	306	398	432	436	436	437	437	9.9
	190	254	321	345	340	331	343	351	10

Specimen	Observed Load in at specified slip *(N)*								MC
	0.25 mm	*0.5 mm*	*1.0 mm*	*1.5 mm*	*2.0 mm*	*2.5 mm*	*3.0 mm*	*5.0 mm*	*(%)*
S_{UM-19}	177	228	297	335	345	354	366	390	11.2
	250	323	416	451	452	444	423	432	11.7
	202	298	386	418	427	436	451	499	-
	230	497	565	563	565	573	581	623	-
	346	386	437	460	480	487	492	524	-
	259	334	405	428	444	459	464	468	-
	196	256	309	338	350	335	328	377	-
	377	437	518	543	538	535	539	565	-
C_{UM-19}	247	298	364	399	416	416	0	0	8.4
	242	321	393	428	421	425	0	0	8.4
	192	242	294	322	315	0	0	0	8.7
	173	232	322	371	393	401	0	0	8.7
	299	366	426	391	0	0	0	0	8.1
	246	313	383	414	434	440	447	0	-
	208	281	358	382	388	392	394	0	-
	313	377	421	442	441	0	0	0	-
	321	379	438	456	469	474	473	0	-
C_{TR-10}	279	318	336	0	0	0	0	0	-
	220	258	306	327	325	0	0	0	-
	318	361	364	0	0	0	0	0	-
	267	327	383	388	0	0	0	0	-
	256	287	332	342	0	0	0	0	-
	214	257	299	0	0	0	0	0	-
	315	365	415	0	0	0	0	0	-
	276	315	356	353	0	0	0	0	-
C_{TR-19}	368	432	506	0	0	0	0	0	-
	426	468	456	0	0	0	0	0	-
	285	332	391	0	0	0	0	0	-
	366	422	437	0	0	0	0	0	-
	339	395	448	475	481	0	0	0	-
	397	461	527	0	0	0	0	0	-
	351	392	410	0	0	0	0	0	-
C_{UR-10}	225	242	0	0	0	0	0	0	-
	211	248	0	0	0	0	0	0	-
	175	222	270	0	0	0	0	0	-
	141	171	0	0	0	0	0	0	-
	248	298	320	0	0	0	0	0	-
	178	223	285	0	0	0	0	0	-
	197	248	293	0	0	0	0	0	-
	162	212	232	0	0	0	0	0	-

Specimen	Observed Load in at specified slip *(N)*								MC
	0.25 mm	*0.5 mm*	*1.0 mm*	*1.5 mm*	*2.0 mm*	*2.5 mm*	*3.0 mm*	*5.0 mm*	*(%)*
C_{UR-10}	147	223	278	300	0	0	0	0	-
	241	288	327	349	0	0	0	0	-
	122	188	236	0	0	0	0	0	-
	160	240	267	0	0	0	0	0	-
C_{UR-19}	227	285	389	406	410	419	423	0	-
	232	296	368	408	422	0	0	0	-
	284	345	412	0	0	0	0	0	-
	256	320	377	405	417	417	0	0	-
	220	272	345	395	417	437	0	0	-
	279	346	401	0	0	0	0	0	-
	282	349	404	420	0	0	0	0	-
	151	235	286	0	0	0	0	0	-
	254	311	358	386	0	0	0	0	-
	136	218	277	292	0	0	0	0	-
	258	332	403	441	0	0	0	0	-
	213	290	358	0	0	0	0	0	-
S_{UR-10}	133	219	319	331	328	327	323	0	9.2
	230	306	380	423	432	434	438	0	9.2
	207	268	327	324	308	305	300	0	9.1
	234	259	295	320	326	0	0	0	9.1
	149	213	290	332	353	360	362	360	8.9
	120	184	232	259	259	262	0	0	9
	221	281	353	380	393	394	391	399	8.7
	163	229	315	343	365	336	0	0	8.7
S_{UR-19}	226	280	347	401	444	474	486	520	11.8
	284	354	419	457	470	469	477	510	11.5
	280	346	408	441	458	466	469	457	10.6
	181	242	306	334	314	314	320	365	11.3
	217	301	398	451	467	477	489	468	10.4
	181	238	303	338	359	368	383	404	9.9
	356	403	452	479	495	501	520	536	-
	309	389	471	504	514	528	542	596	-
	217	273	335	347	349	352	375	377	-
	278	323	369	385	398	398	398	411	-
	363	413	478	499	503	497	489	523	-
	221	286	344	371	374	379	382	403	-
N_{TR}	330	385	457	489	517	525	542	0	-
	323	392	454	495	526	545	566	0	-
	366	440	510	549	568	585	584	0	-
	444	506	579	618	616	601	595	0	-

Specimen	Observed Load in at specified slip *(N)*								MC
	0.25 mm	*0.5 mm*	*1.0 mm*	*1.5 mm*	*2.0 mm*	*2.5 mm*	*3.0 mm*	*5.0 mm*	*(%)*
N_{TR}	125	175	257	315	351	375	382	442	-
	335	411	503	548	571	573	571	0	-
	278	346	433	478	507	526	529	0	-
	297	345	400	420	439	448	457	476	-
	361	432	514	564	595	612	610	553	-
	266	386	452	497	532	543	558	576	-
	536	569	593	604	612	620	628	604	-
	389	450	532	577	595	602	606	591	-
$N_{UR\ (1)}$	250	307	355	381	404	429	441	0	-
	293	339	375	370	381	392	406	457	-
	242	325	395	419	432	450	460	0	-
	319	366	427	464	491	519	536	0	-
	197	262	326	364	385	402	413	0	-
	248	309	377	404	413	421	439	0	-
	208	291	368	402	416	426	437	0	-
	226	284	374	429	459	480	489	0	-
	250	308	364	389	410	425	437	0	-
	113	191	270	314	338	358	368	406	-
	297	356	414	437	451	474	490	0	-
	304	359	413	456	482	496	505	0	-
$N_{UR\ (2)}$	265	310	353	391	419	437	454	215	14.4
	240	299	371	408	432	441	451	417	14.2
	220	270	327	362	383	395	408	363	14.2
	249	284	331	364	382	402	421	457	14
I_{UR}	119	195	285	336	358	375	377	373	10.5
	182	255	338	370	384	395	416	444	9.5
	143	222	313	368	406	419	423	425	10.3
	117	183	248	289	328	354	377	427	11.1
	144	209	280	312	335	342	349	390	9.9
	175	258	372	436	468	506	527	533	9.7
	235	294	369	408	436	449	467	491	7.8
	202	284	387	448	471	498	524	630	7.8
	266	342	423	433	451	464	480	532	8.1
	345	422	494	533	557	570	578	603	8
	155	223	301	345	364	381	402	432	8.1
	255	344	419	467	484	494	508	549	8
$N_{UM\ (3)}$	105	185	293	349	368	381	375	386	12
	130	225	300	323	340	342	346	328	11.9
	159	165	264	265	0	0	0	0	11.7
	143	240	342	373	383	378	398	397	11.6

Specimen	Observed Load in at specified slip *(N)*								MC
	0.25 mm	*0.5 mm*	*1.0 mm*	*1.5 mm*	*2.0 mm*	*2.5 mm*	*3.0 mm*	*5.0 mm*	*(%)*
$N_{UM\ (3)}$	124	264	349	384	415	415	378	0	12
	191	257	319	335	349	355	367	341	11.7
$I_{UM\ (4)}$	222	261	302	331	350	354	369	378	11.3
	270	357	434	440	422	413	410	394	11.3
	135	219	328	387	395	400	420	423	11.3
	264	341	419	445	438	428	427	440	11.6
	160	240	301	355	348	370	368	412	11.7
	186	269	362	372	345	346	351	361	11.1
	161	239	317	344	359	367	374	362	11.9
	260	328	388	413	417	425	428	478	11.8
	183	250	316	348	356	358	365	364	11.7
	95	182	286	334	348	370	378	404	11.7
	272	340	411	427	421	419	405	386	11.7
	207	275	339	362	362	377	377	393	11.9

Appendix 3B Residuals from Linear Regression of Load-Slip Response

The residuals from the linear regression in Section 3.4 are presented in Table 3B.1 For each indicator variable or combination thereof, the mean and standard deviation of the residuals associated with an indicator variable of 1 were compared to the mean and standard deviation of the residuals associated with an indicator variable of 0. A P-value of more than 0.05 indicates that the parameter was not statistically significant. Almost all indicator variables or combinations thereof presented in the table are not significant. The only exception occurs with a fastener located in the corner and is loaded in the cross-machine direction, i.e., dependent indicator variable Z_3 Z_5, which is statistically significant for a slip of 1.0 mm and is marginally statistically significant for a slip of 2.0 mm, yet is not statistically significant for a slip of 0.5 mm. This connection only occurs in Phase 3 on the convex side (see Section 3.1.1), where the range of slip is generally less than 1.0 mm. Therefore, this indicator variable combination is not considered significant.

Table 3B.1: P-value of Statistically Insignificant Parameters

	Indicator variable = 1			Indicator variable = 0			P-value
	Mean	SD	n	Mean	SD	n	
Slip = 0.5 mm							
Z_1	7.0	67	76	-2.7	66	201	0.28
Z_2	-3.9	60	56	1.0	68	221	0.62
Z_3	-1.4	61	68	0.47	68	209	0.84
Z_6	-23	55	18	1.61	66	259	0.12
Z_8	-0.12	57	99	0.069	71	178	0.98
Z_9	0.70	45	11	-0.029	67	266	0.97
Z_3 Z_5	4.1	73	35	-0.60	65	242	0.69
Z_3 Z_8	-11	43	39	1.8	69	238	0.28
Z_4 Z_7	-2.7	71	6	0.061	66	271	0.92
Slip = 1.0 mm							
Z_1	10	69	76	-3.9	60	198	0.095
Z_2	-6.9	56	56	1.8	64	218	0.36
Z_3	-9.1	61	65	2.8	63	209	0.18
Z_6	-18	49	18	1.3	63	256	0.21
Z_8	-4.1	57	96	2.2	65	178	0.43
Z_9	13	40	11	-0.53	63	263	0.49
Z_3 Z_5	-5.6	75	35	0.83	61	239	0.57
Z_3 Z_8	-23	43	36	3.49	64	238	0.018
Z_4 Z_7	-8.4	70	6	0.19	63	268	0.74
Slip = 2.0 mm							
Z_1	4.2	74	76	-2.0	55	158	0.48
Z_2	-6.3	54	55	1.9	64	179	0.39
Z_3	-12	56	26	1.5	63	208	0.30
Z_6	-21	33	17	1.6	64	217	0.16
Z_8	3.3	61	66	-1.3	63	168	0.61
Z_9	4.0	32	11	-0.20	63	223	0.83
Z_3 Z_5	-16	81	11	0.81	61	223	0.37
Z_3 Z_8	-41	47	6	1.1	62	228	0.10
Z_4 Z_7	-16	80	6	0.42	62	228	0.53

Appendix 3C Idealized Load-Slip Response of Fastener Connections

Figures 3C.1 and 3C.2 show the idealized curves provided by Equation [3.2] graphed along with markers obtained from Tables 3.16 and 3.17. Figure 3C.1 presents all cases with 12.7 mm thick gypsum board, and Figure 3C.2 presents all cases with 15.9 mm thick gypsum board.

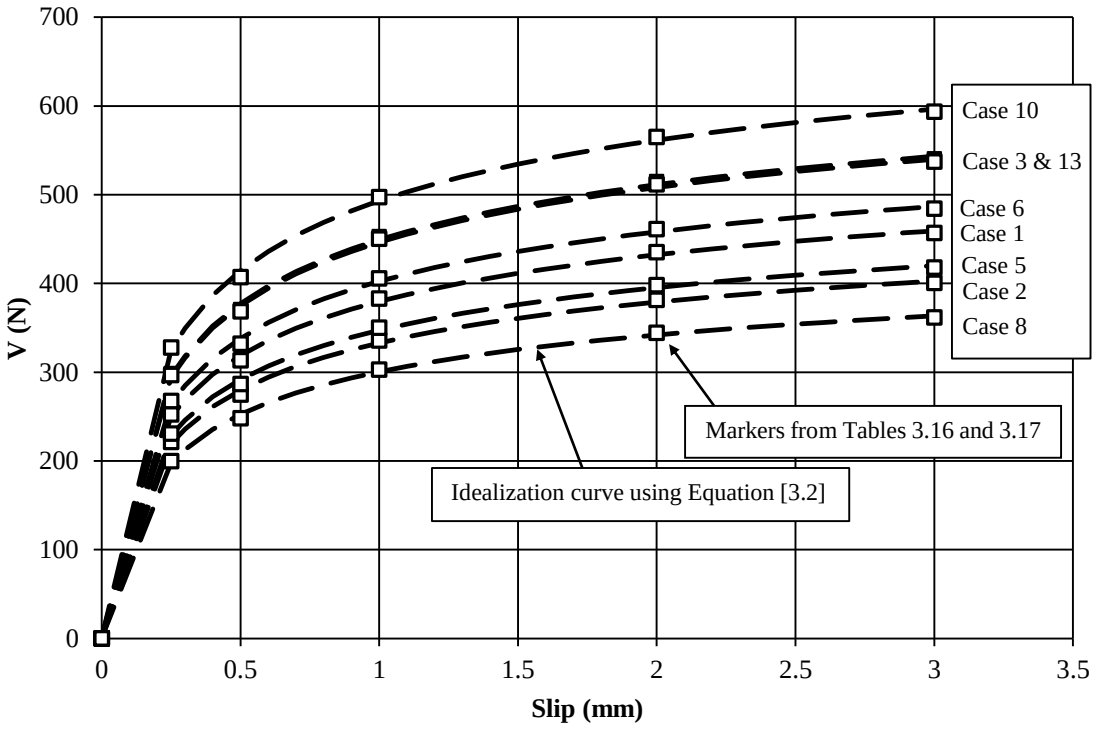

Figure 3C.1: Idealization Curves for 12.7 mm Gypsum Board

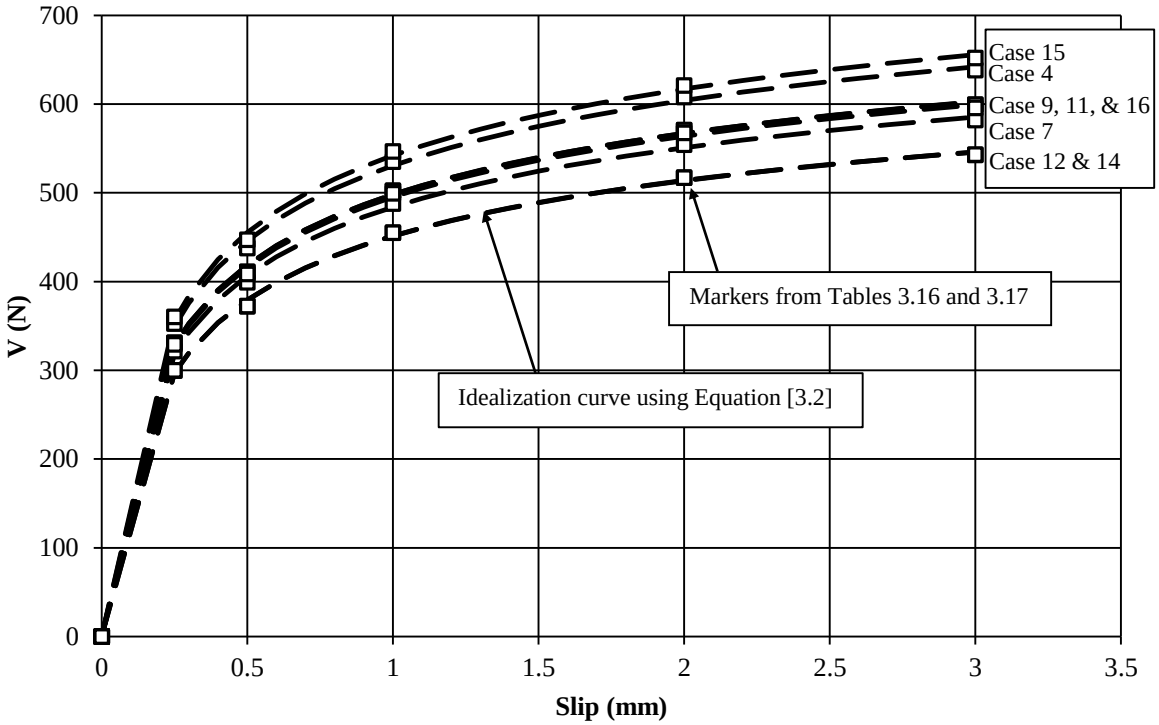

Figure 3C.2: Idealization Curves for 15.9 mm Gypsum Board

Appendix 4A Predicted versus Observed Relationship between Axial Load and Mid-Height Deflection

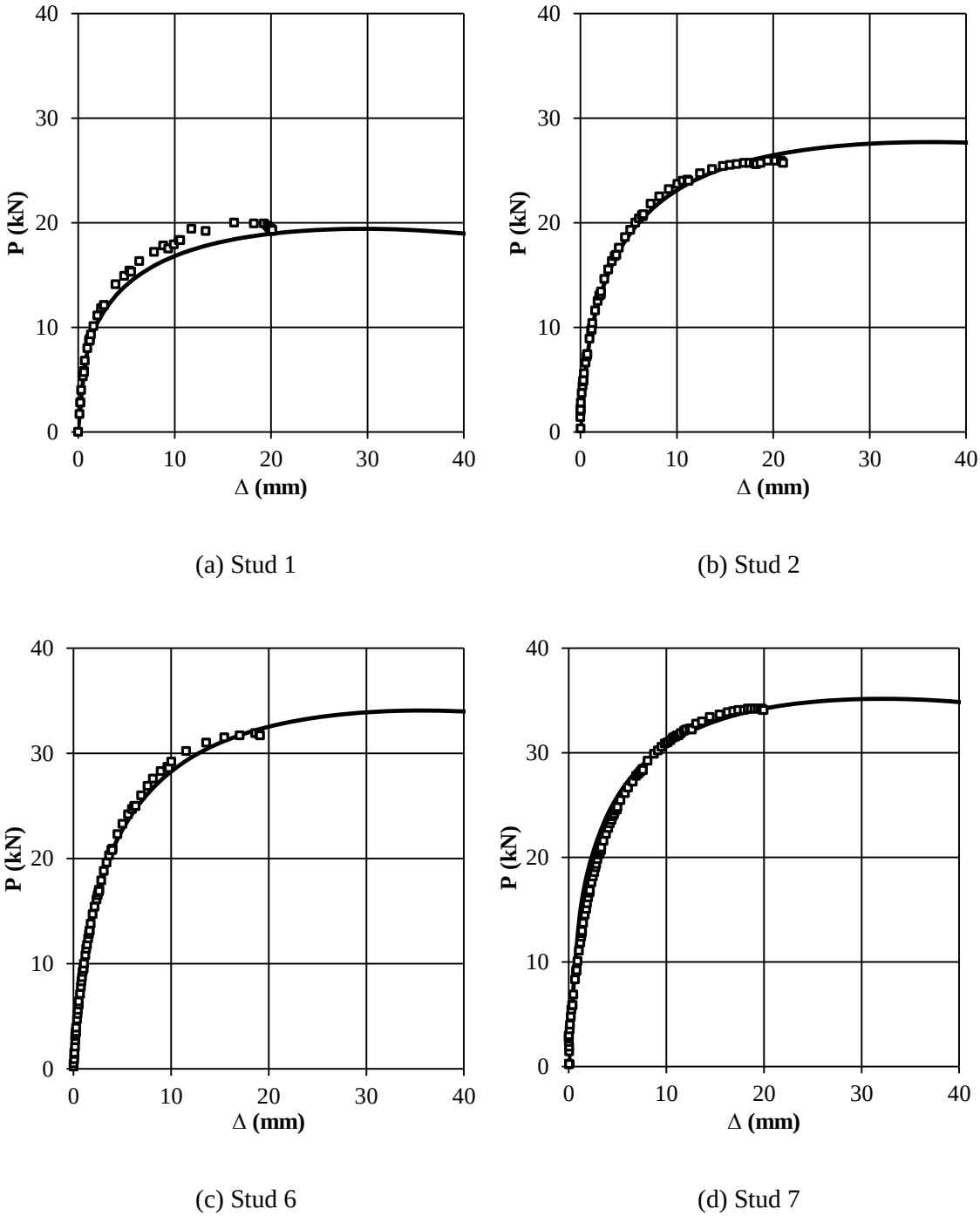

(a) Stud 1

(b) Stud 2

(c) Stud 6

(d) Stud 7

Figure 4A.1: Good Agreement between Predicted and Observed Results

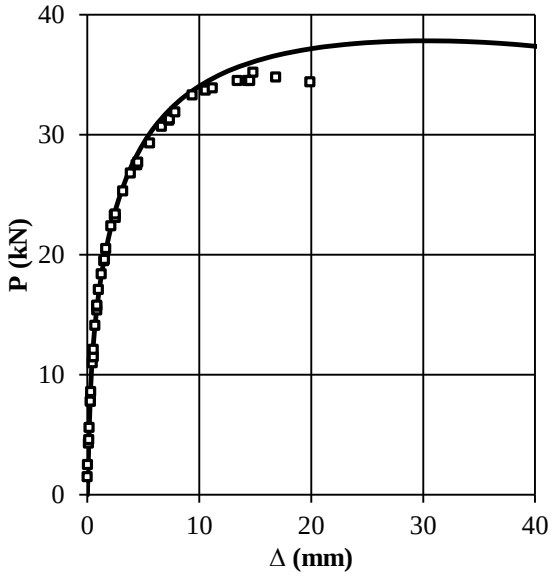

(e) Stud 8

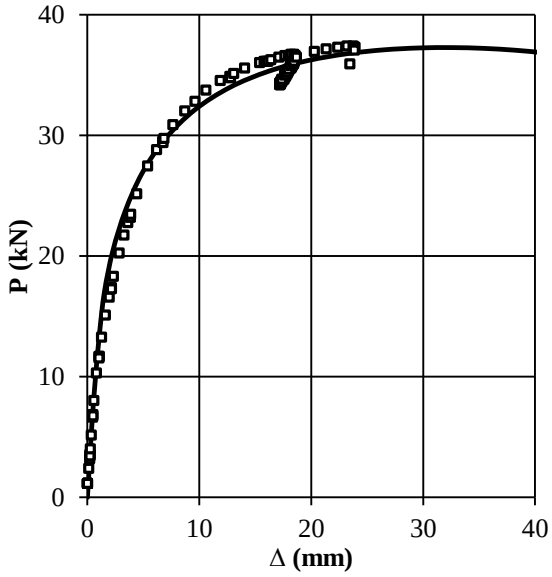

(f) Stud 9

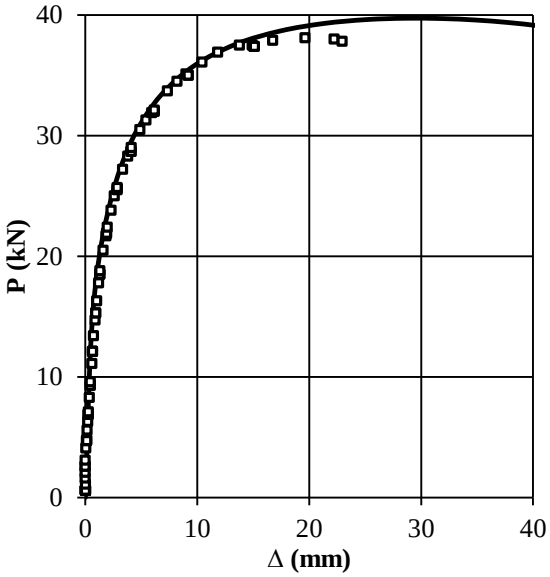

(g) Stud 10

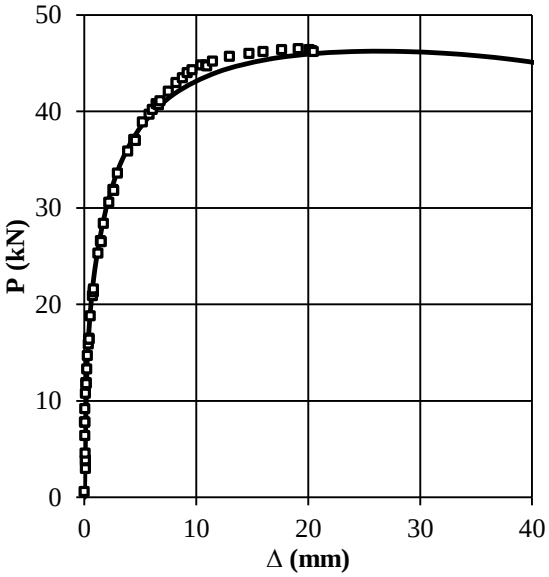

(h) Stud 12

Figure 4A.1 (con't): Good Agreement between Predicted and Observed Results

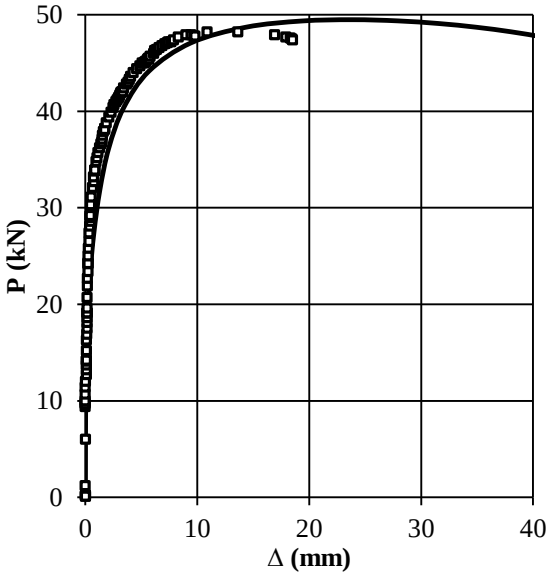

(i) Stud 13

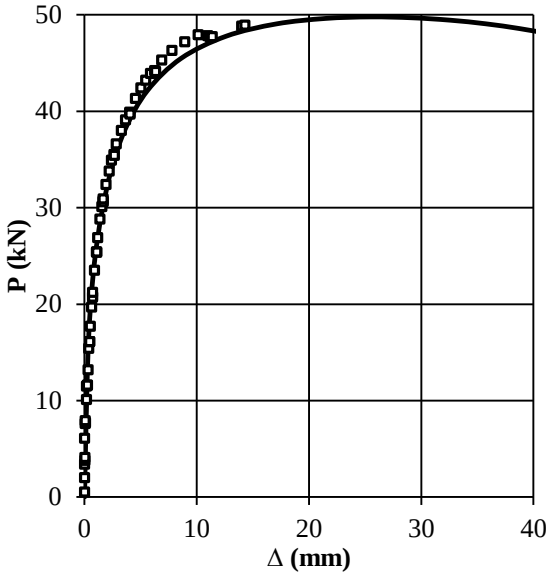

(j) Stud 14

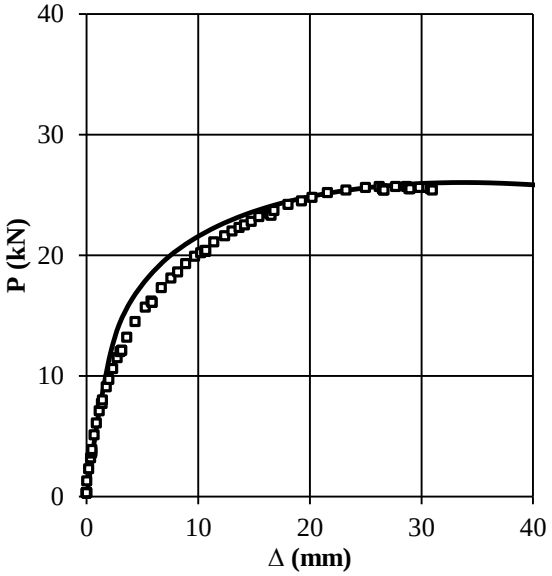

(k) Stud 15

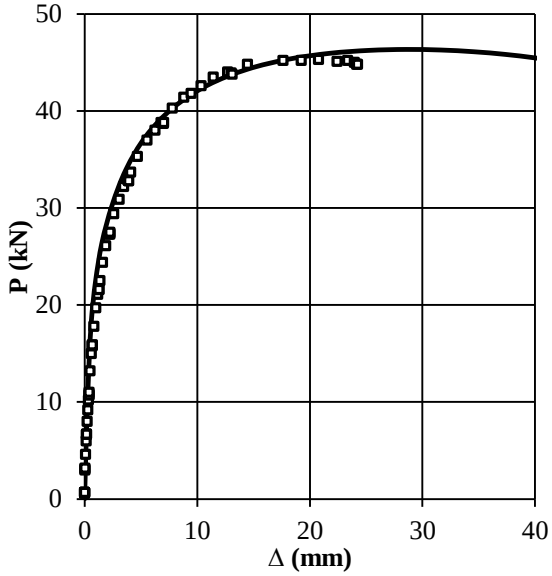

(l) Stud 18

Figure 4A.1 (con't): Good Agreement between Predicted and Observed Results

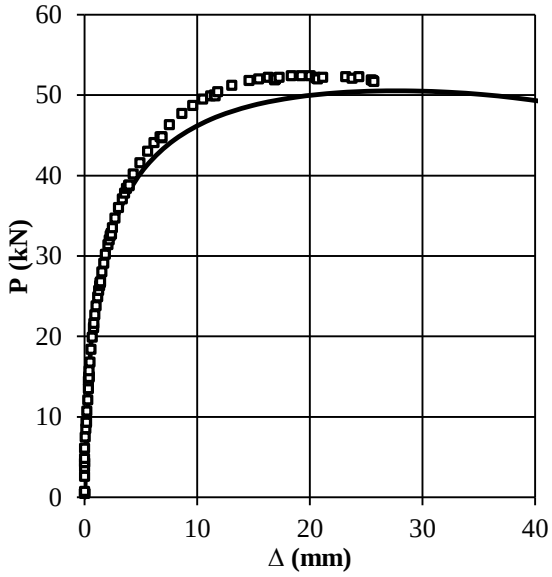

(m) Stud 19

Figure 4A.1 (con't): Good Agreement between Predicted and Observed Results

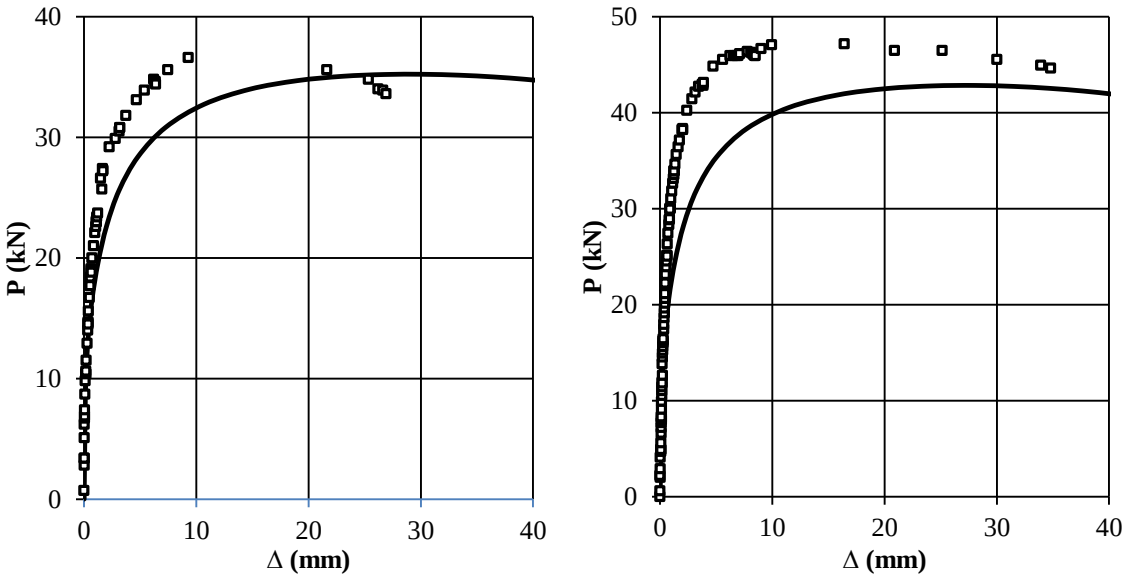

(a) Stud 5

(b) Stud 11

Figure 4B.2: Not-as-Good Agreement between Predicted and Observed Results

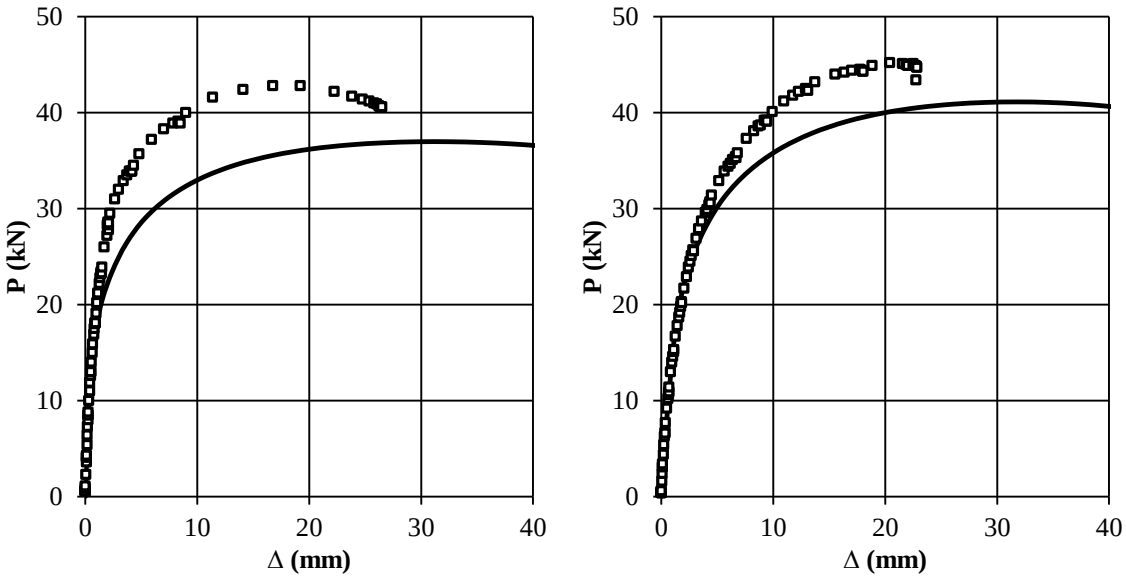

(c) Stud 16 (d) Stud 17

Figure 4A.2 (con't): Not-as-Good Agreement between Predicted and Observed Results

Appendix 5A Additional Results from Sensitivity Analysis

Figures 5A.1 to 5A.5 show additional results from the sensitivity analysis reported in Section 5.3. The legend is consistent for all figures in this appendix, thus is only shown in Figure 5A.1

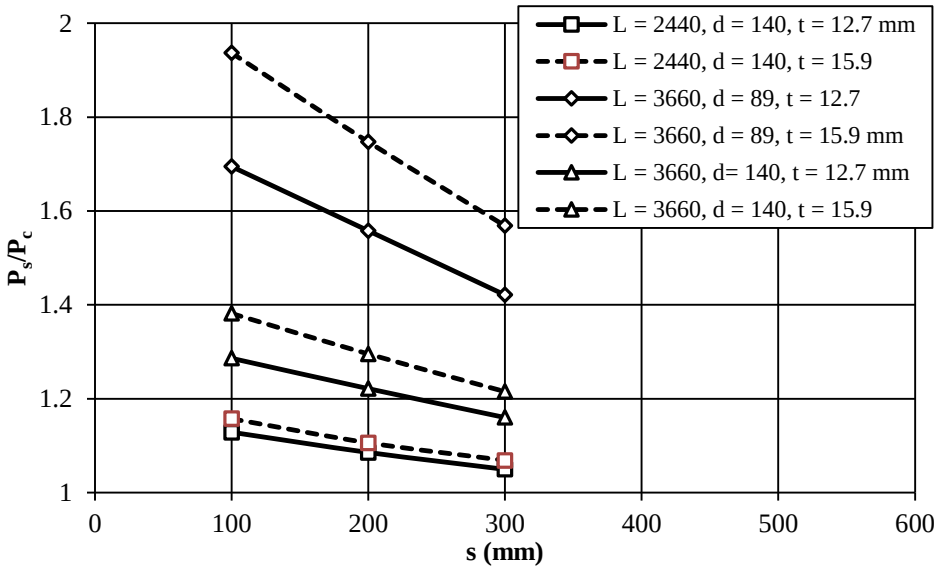

Figure 5A.1: Sensitivity of Strength Contribution of Gypsum-Board Sheathing to Fastener Spacing

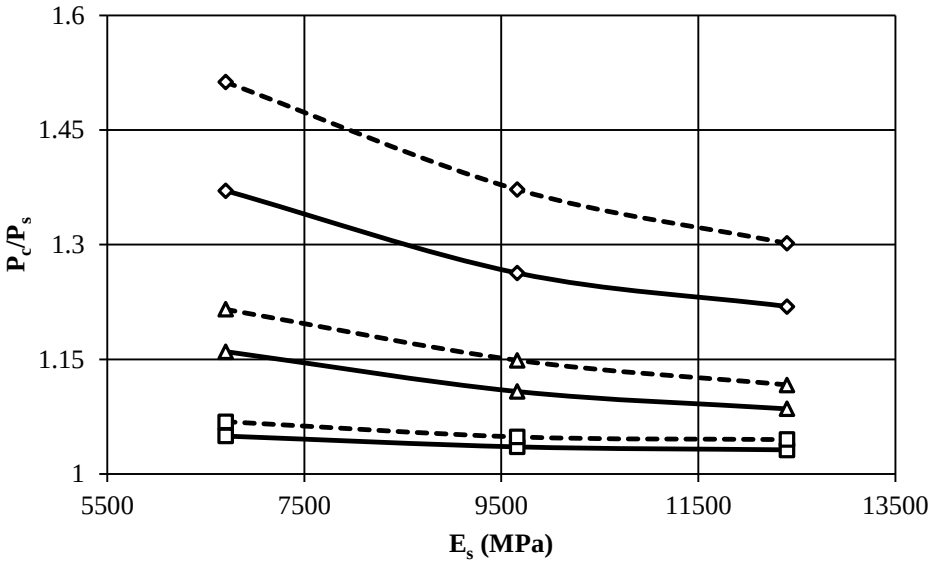

Figure 5A.2: Sensitivity of Strength Contribution of Gypsum-Board Sheathing to the Wood Modulus of Elasticity

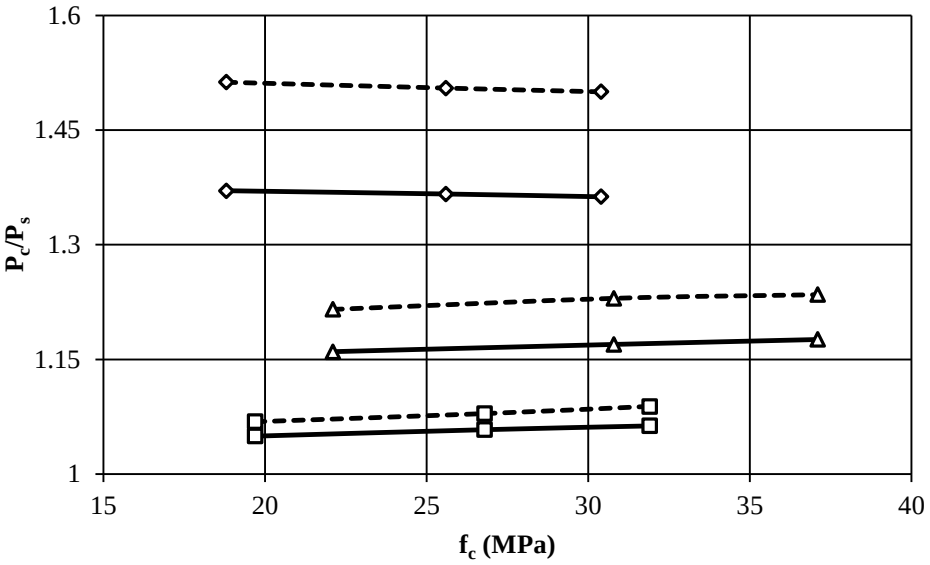

Figure 5A.3: Sensitivity of Strength Contribution of Gypsum-Board Sheathing to Wood Crushing Stress

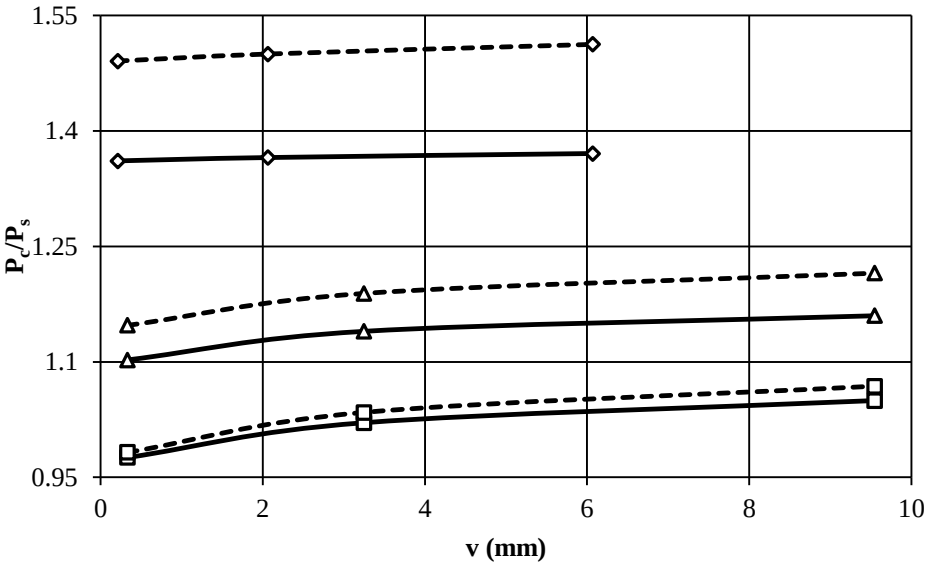

Figure 5A.4: Sensitivity of Strength Contribution of Gypsum-Board Sheathing to Initial Mid-Height Out-of-Straightness

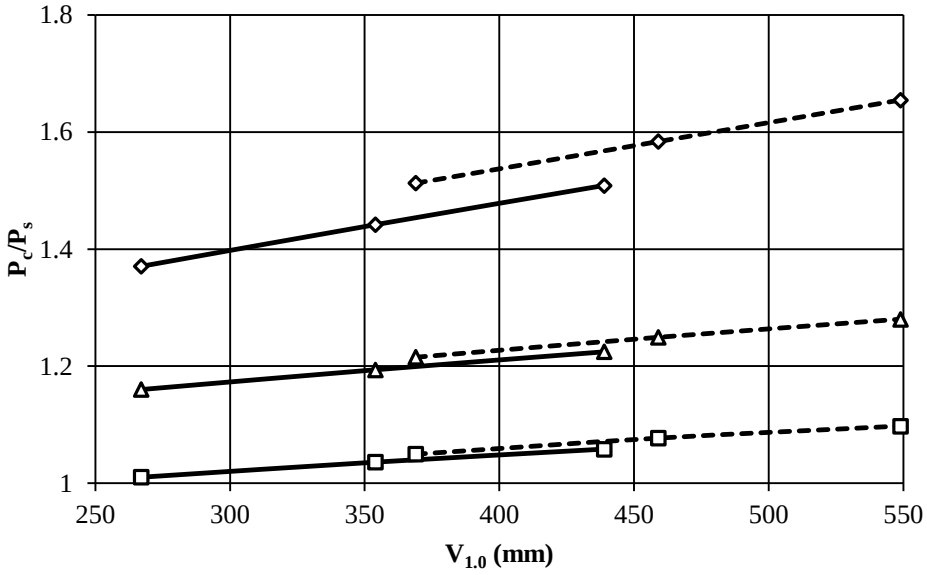

Figure 5A.5: Sensitivity of Strength Contribution of Gypsum-Board Sheathing to Fastener Strength at Slip of 1.0 mm

Appendix 5B Tolerance Limits of 5th Percentile Axial Compressive Resistance

The Monte Carlo simulation results yield mean values and standard deviations of the axial compressive capacities. These values, however, are approximations of the means and standard deviations of the underlying populations. It is, therefore, beneficial to quantify tolerance limits defining the specific value that bounds with a predefined confidence the population values (e.g., Natrella, 1963). For a given confidence level, an increase in the sample size allows the tolerance limits to be relaxed because the uncertainties of the sample mean and sample standard deviation are reduced due to the larger sample size. This methodology is used in CWC (1994) to quantify the accuracy of material properties for lumber predicted using experimental studies.

For the design of wood members, the lower-bound tolerance limit on the 5th percentile is typically of interest (e.g., CWC, 1994). For normal distributions, lower-bound tolerance limits are computed using (e.g., Natrella, 1963):

[5B.1] $$X_L = \bar{x} - K\sigma_a$$

where X_L is the lower-bound tolerance limit, $\bar{x}$ is the sample mean, σ_a is the standard deviation of the sample, and K is given by (e.g., Natrella, 1963):

[5B.2] $$K = \left(z_\rho + \sqrt{z_\rho^2 - a'b'}\right) / a'$$

where z_ρ is the ρ-percentile value of the standard normal distribution having a mean of 0 and a standard deviation of 1. Values for a' and b' are computed using:

[5B.3] $$a' = 1 - z_\gamma^2 / [2(n - 1)]$$

[5B.4] $$b' = z_\rho^2 - z_\gamma^2 / n$$

where z_γ is the standard normal distribution value for a confidence level γ and n is the sample size. For $n = \infty$, $a = 1$, $b = z_\rho^2$, $K = z_\rho$, and X_L is equal to the ρ-percentile value of the data set. However, for $n < \infty$, $K > z_\rho$, thus X_L is smaller than the ρ-percentile value of the data set. The uncertainty inherent in the data set reduces as the difference between the lower-bound tolerance limits, X_L, and the ρ-percentile value of the data set decreases.

Table 5B.1 presents values of the lower-bound tolerance limits, X_L, for the 5th percentile values of the axial compressive capacity, $\rho = 0.05$. Tolerance limits were computed for confidence levels of $\gamma = 0.75$, 0.90, 0.95, and 0.99: all are greater than 99.0, 98.1, 97.9, and 97.6%, respectively, of the 5th percentile values of the Monte Carlo simulation results presented in Table 5.5. This confirms that a sample size of 2000 is considered adequate for accurately quantifying the 5th percentile of the axial compressive capacity of the bare and sheathed studs.

Table 5B.1: Lower-Bound Tolerance Limit of the 5th Percentile Values

d	L	t	s	X_L for 0.05-percentile values *(kN)*			
(mm)	*(mm)*	*(mm)*	*(mm)*	$\gamma = 0.75$	$\gamma = 0.90$	$\gamma = 0.95$	$\gamma = 0.99$
Bare Stud							
89	2440	-	-	22.4	22.2	22.1	22.0
89	3660	-	-	10.4	10.4	10.3	10.3
140	2440	-	-	67.1	66.5	66.2	66.0
140	3660	-	-	37.0	36.8	36.6	36.4
Sheathed Stud							
89	2440	12.7	100	31.7	31.6	31.6	31.5
89	2440	12.7	300	27.3	27.2	27.1	27.0
89	2440	15.9	300	29.2	29.1	29.0	28.7
89	3660	12.7	300	14.9	14.8	14.8	14.7
89	3660	15.9	300	16.2	16.1	16.0	16.0
140	2440	12.7	300	70.1	69.5	69.2	68.9
140	2440	15.9	300	71.2	70.8	70.7	70.6
140	3660	12.7	300	42.6	42.2	42.1	42.0
140	3660	15.9	300	45.1	44.9	44.8	44.6

Appendix 6A Statistical Significance of Parameter Estimates in Equation 6.1

Table 6A.1 presents the P-values for parameters β_1 to β_6 determined from linear regression using Equation [6.1] when β_2 and β_3 are assumed statistically different from zero.

Table 6A.1: P-Values when β_2 and β_3 are assumed Statistically Different from Zero

L	d	s	P-Value[a]					
(mm)	*(mm)*	*(mm)*	β_1	β_2	β_3	β_4	β_5	β_6
2440	89	100	0	0.33	-	6.5×10^{-4}	0	-
2440	89	300	0	0.053	0.89	2.9×10^{-8}	0	0.0026
3660	89	300	0	0.15	0.94	0.020	0	2.3×10^{-7}
3660	140	300	0	0.81	0.55	0	5.6×10^{-9}	0.036

[a] Values smaller than 10^{-10} are shown as equal to 0.

Appendix 6B Quantification of Factored Demand Loads for Provisions in NBC Table 9.23.10.1

There is no specific quantification of design loads associated with the load categories in Table 9.23.10.1 of the NBCC (NRC, 2010). This appendix presents the methodology used to quantify the design loads on interior load-bearing walls based on the maximum allowable ceiling and joist spans supported. The results presented are for No.2 or better Spruce-Pine-Fir (SPF) wood stud.

Figure 6B.1 shows a free body diagram of gravitational loads applied to an interior load-bearing wall. A uniformly distributed load, w, is applied over a tributary area equal to a tributary length, L_T, by a unit width of wall, resulting in an axial compressive load per unit width of wall, Q. To determine the design loads applied to interior load-bearing walls, L_T and w must be quantified.

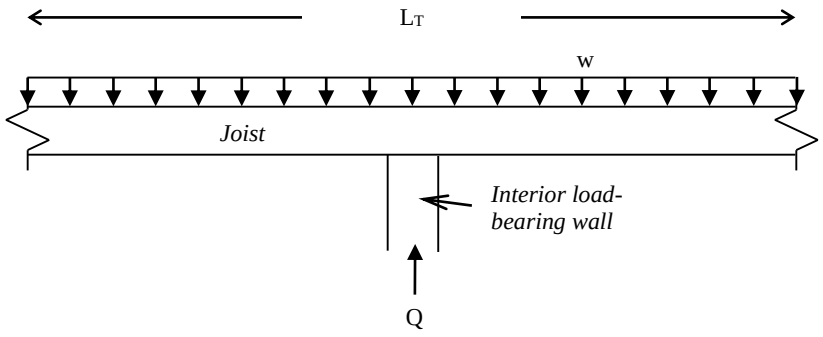

Figure 6B.1: Free Body Diagram of Gravitational Loads Applied to Interior Walls

Tributary Length, L_T

The tributary length is equal to the maximum span between load-bearing walls, i.e., assuming equal spans on both sides. Article 9.23.1.1 (1) of the NBCC (NRC, 2010) limits the span between load-bearing walls to 12.20 m. This span may occur for exterior walls when supporting roof trusses. However, the maximum span between interior load-bearing

walls is limited by the resistance of floor and ceiling joists reported in Article 9.23.4.1 of the NBCC. Table 6B.1 presents the maximum allowable span of No. 2 grade or better SPF floor and ceiling joists. Furring strips placed along the underside of the floor joists resists against the bottom kicking-out, thus allowing the span to be increased. A concrete topping is considered to add stiffness to the floor system, allowing the span to be further increased.

Table 6B.1: Maximum Span of No. 2 Grade or Better SPF Floor and Ceiling Joists in the NBCC

Criteria	Maximum Span *(m)*	Source
Floor joists without furring or concrete topping	5.17	Article 9.23.4.1 - Table A-1
Floor joists with furring and no concrete topping	5.93	Article 9.23.4.1 - Table A-2
Floor joists with furring and concrete topping	6.24	Article 9.23.4.1 - Table A-2
Ceiling joists	10.00	Article 9.23.4.1 - Table A-3

Table 6B.2 presents the tributary lengths selected for calculating the design loads for Table 9.23.10.1 in the NBCC. Floors and attics accessible by stairways are considered to be supported by floor joists with furring strips and no concrete topping, thus can span a maximum of 5.93 m between interior load-bearing walls. A marginally larger span of 6.00 m is considered in this analysis. Attics not accessible by stairways are considered to be supported by ceiling joists, thus can span a maximum of 10 m between interior load-bearing walls. Pitched roofs are generally designed with roof trusses that distribute gravitational loads to exterior walls. Therefore, this analysis assumes only flat roofs are supported by interior walls. No criteria for maximum span are provided for flat roofs, thus this case is assumed to be similar to floors, with a maximum span of 6.00 m.

Table 6B.2: Summary of Tributary Lengths Supported by Load-Bearing Walls

Supported Load	L_T *(m)*	Comments
Floor	6.00	Proposed span marginally exceeds maximum spans in Article 9.23.4.1 - Tables A-1 and A-2
Attic accessible by a stairway	6.00	Assumed equal to maximum floor span
Attic not accessible by a stairway	10.00	As per Article 9.23.4.1 - Table A-3
Flat roof	6.00	Assumed equal to maximum floor span

Axial Compressive Load per Unit Width of Wall, Q

Gravitational load types for wood stud walls include dead load, live load, and snow loads. Table 6B.3 lists the specified dead, live, and snow loads that are considered to be applied to interior walls. Most values are defined in the building code, with the exception of roof and attic dead loads. Roof dead load was assumed equal to 0.5 kPa to accounts for (e.g., CWC, 2005): gypsum board (0.18 kPa), joists (0.05 kPa), steel deck (0.07 kPa) or plywood structural decking (0.08 kPa), insulation (0.05 kPa), and asphalt without gravel (0.14 kPa). The attic dead load is assumed, perhaps conservatively, equal to the roof dead load.

Table 6B.3: Summary of Specified Loads on Roof, Attic, and Floor(s)

Load type	Load location	Value *(kPa)*	Source
Dead	Floor	0.5	NBCC: Article 9.23.4.4
	Roof	0.5	Computed
	Attic	0.5	Computed
Live	1st floor	1.9	NBCC: Article 4.1.5.3
	Additional floors	1.4	NBCC: Article 4.1.5.3
	Attic accessible by stairway	1.4	NBCC: Article 4.1.5.3
	Attic not accessible by stairway	0.0	NBCC: Article A-9.4.2.4 (1)
Snow	Roof	1.0, 2.0, and 3.0	NBCC: Article 9.4.2.2 and NBCC: Article A-9.4.2.1 (1)

The snow load, S, were calculated using the equation provided in Article 9.4.2.2 of the NBCC, given by:

[6B.1] $S = C_b S_s + S_r$

where S is the specified roof snow load, C_b is the basic snow-load roof factor equal to 0.55 for a width of roof exceeding 4.3 m, S_s is the ground snow listed in Appendix C of the NBCC, and S_r is the associated rain load listed in Appendix C of the NBCC.

Table 6B.4 presents the value for S_s, S_r, and SL for six Canadian cities. Quebec City has the largest specified snow load at 2.6 kPa, whereas Saskatoon has the smallest at 1.0 kPa. Therefore, this analysis includes snow loads of 1.0, 2.0 and 3.0 kPa.

Table 6B.4: Snow Loads for various Cities across Canada

City	S_s (kPa)	S_r (kPa)	SL (kPa)
Vancouver	1.8	0.2	1.2
Halifax	1.9	0.6	1.7
Arvida (Jonquiere)	3.1	0.4	2.1
Ottawa	2.4	0.4	1.7
Saskatoon	1.7	0.1	1.0
Quebec City	3.6	0.6	2.6

Table 6B.5 presents the specified axial compressive load per unit width of wall, Q, depending on the load supported. Uniformly distributed loads for dead loads, DL, live loads, LD, and snow loads, SL, for each supported load case are multiplied by the associated tributary length. The first floor has a live load of 1.9 kPa and the second and third floor have a reduced specified live load of 1.4 kPa each.

Table 6B.5: Specified Axial Compressive Loads per Meter Width of Wall

Supported load	w_{DL} *(kPa)*	w_{LL} *(kPa)*	w_S *(kPa)*	L_T *(m)*	Q_{DL} *(kN/m)*	Q_{LL} *(kN/m)*	Q_S *(kN/m)*
Attic not accessible by a stairway	0.5	0.0	0.0	10	5.0	0.0	0.0
Attic accessible by a stairway	0.5	1.4	0.0	6	3.0	8.4	0.0
Roof	0.5	0.0	1.0	6	3.0	0.0	6.0
			2.0				12.0
			3.0				18.0
One floor	0.5	1.9	0.0	6	3.0	11.4	0.0
Two floors	1.0	3.3	0.0	6	6.0	19.8	0.0
Three floors	1.5	4.7	0.0	6	9.0	28.2	0.0

Three Ultimate Limit State (ULS) cases from Table 4.1.3.2 in the NBCC are used to quantify the factored axial compressive loads per unit width of wall, Q_f:

1. 1.4 DL
2. 1.25 DL + 1.5 LL + 0.5 SL
3. 1.25 DL + 1.5 SL + 0.5 LL

Table 6B.6 summarizes computed values of Q_f, with respect to the supported load defined in Table 9.23.10.1 in the NBCC. The results shown for each supported load was quantified

using the ULS case that results in the largest value of Q_f. For example, a wall supporting a roof load plus one floor has 0.5 kPa of dead load, 1.9 kPa of live load, and 1.0 to 3.0 kPa of roof snow load. When only supporting 1.0 kPa of roof snow load, the live load is greater than the snow load, thus ULS case '2' governs. Conversely, when supporting 2.0 kPa or greater of roof snow load, the live load is smaller, thus ULS case '3' governs.

Table 6B.6: Factored Axial Loads per Meter Width of Wall for Supported Loads in Table 9.23.10.1 in the NBCC

Supported load	ULS case	SL *(kPa)*	Q_f *(kN/m)*
Attic not accessible by a stairway	1	-	9.0
Attic accessible by a stairway plus one floor	2	-	37.2
Roof load plus one floor	2	1.0	27.6
	3	2.0	31.2
	3	3.0	40.2
Attic not accessible by stairway plus 2 floors	2	-	43.5
Roof load	3	1.0	12.8
		2.0	21.8
		3.0	30.8
Attic accessible by stairway	2	-	16.4
Attic not accessible by stairway plus one floor	2	-	27.1
Attic accessible by a stairway plus 2 floors	2	-	53.6
Attic accessible by a stairway plus 3 floors	2	-	69.9

Reference

National Research Council of Canada (NRC), 2010. National Building Code of Canada. Institute for Research in Construction, National Research Council of Canada, Ottawa, Ont.

Appendix 6C Quantification of Resistance Factor for Sheathed Stud assuming Strength Distribution is Lognormally Distributed

Results presented in this appendix assume a lognormal fit to the lower 25th percentile capacity of the bare and sheathed stud. Table 6C.1 presents the bias coefficient and coefficient of variation of the resistance of bare and sheathed studs.

Table 6C.1: Bias Coefficient and Coefficient of Variation of Resistance of Bare and Sheathed Stud

L *(mm)*	d *(mm)*	s *(mm)*	t *(mm)*	δ_{R_S}	δ_{R_c}		V_{R_S}	V_{R_c}
					Eq. [6.2]	*Eq. [6.8]*		
2440	89	100	12.7	1.551	1.332	1.384	0.184	0.142
2440	89	300	12.7	1.551	1.403	1.443	0.184	0.157
2440	89	300	15.9	1.551	1.397	1.434	0.184	0.150
3660	89	300	12.7	1.720	1.362	1.538	0.187	0.147
3660	89	300	15.9	1.720	1.329	1.597	0.187	0.139
3660	140	300	12.7	1.554	1.409	1.497	0.182	0.162
3660	140	300	15.9	1.554	1.395	1.474	0.182	0.152

Figure 6C.1 shows the relationship between the φ_c values corresponding to the resistance computed using Equation [6.2] and V_S. Values for φ_c for sheathed studs with L of 3660 mm and d of 89 mm, range from 0.67 to 0.69 for V_S between 0.1 and 0.2. Therefore, the resistance factor for these sheathed studs is recommended to be 0.65 when the resistance is calculated using Equation [6.2]. Conversely, values for φ_c for all other sheathed studs ranges from 0.73 to 0.77 for V_S between 0.1 and 0.2. Therefore, the resistance factor for these sheathed studs is recommended to be 0.75 when the resistance is calculated using Equation [6.2]. These recommended values are identical to those recommended in Chapter 6 assuming the capacities for the bare and sheathed stud are normally distributed.

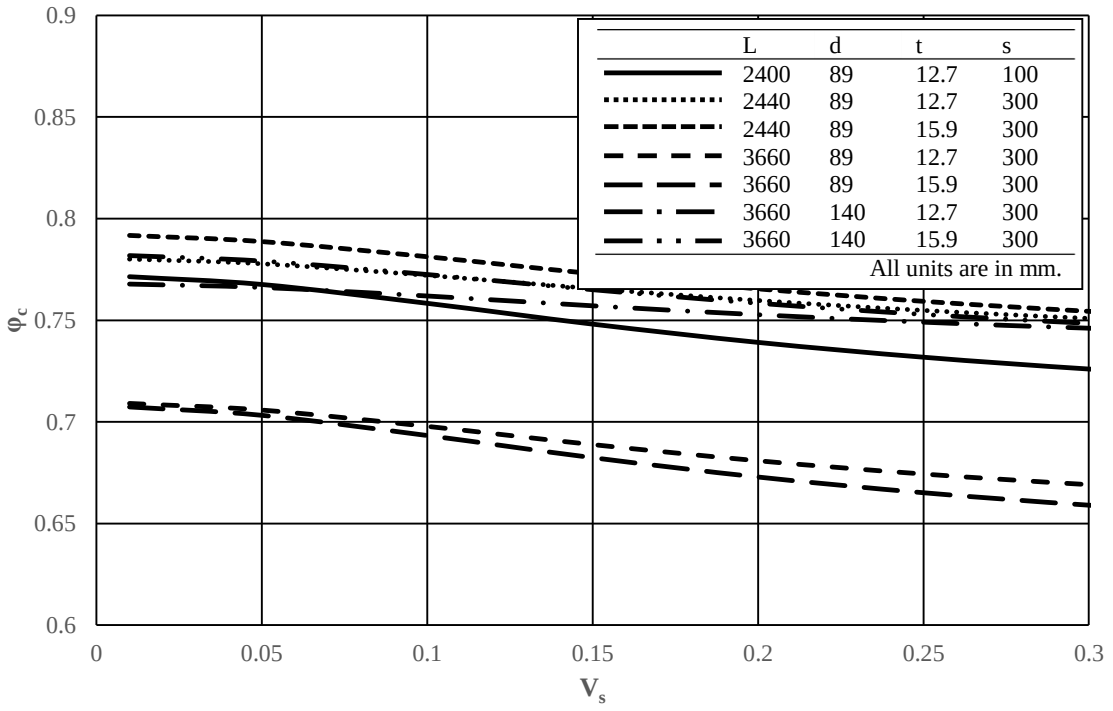

Figure 6C.1: Resistance Factor for Gypsum-Board Sheathed Stud using Equation [6.2]

Figure 6C.2 shows the relationship between φ_c if the resistance is computed using Equation [6.8] and V_S. Values for φ_c range from 0.77 and 0.83 for V_S between 0.1 and 0.2. Therefore, the resistance factor for sheathed studs is recommended to remain at 0.8 if the resistance is computed using K_{SH} in the equations in CAN/CSA 086-09. Again, these recommended values are identical to those recommended in Chapter 6 assuming the capacities for the bare and sheathed stud are normally distributed.

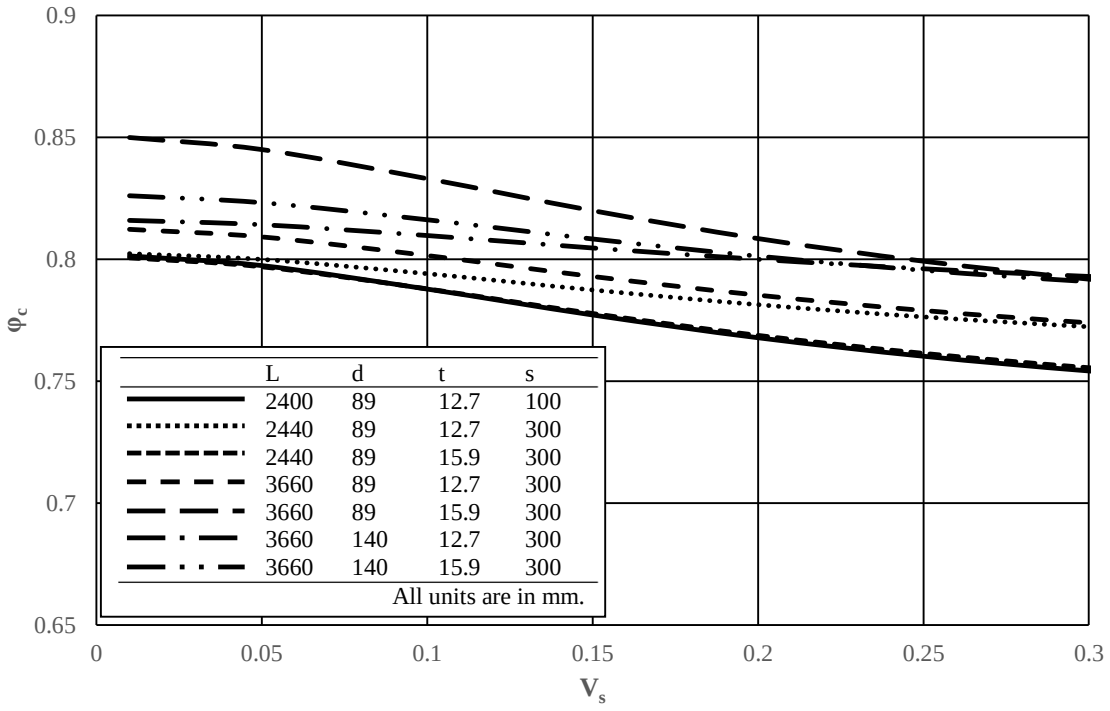

Figure 6C.2: Resistance Factor for Gypsum Board Sheathed Stud using Equation [6.8]

Curriculum Vitae

Name:	Daniel J. Grenier
Post-secondary Education and Degrees:	University of Windsor Windsor, Ontario, Canada 2002-2006 B.A.Sc. University of Windsor Windsor, Ontario, Canada 2006-2008 M.A.Sc. The University of Western Ontario London, Ontario, Canada 2008-2014 Ph.D.
Honours and Awards:	Ontario Graduate Scholarship 2008-2009 Alexander Graham Bell Canada Graduate Scholarship 2010-2012 Ontario Graduate Scholarship Science and Technology 2009-2010, 2012-2013
Related Work Experience	Teaching Assistant The University of Western Ontario 2008-2012

Publications:

Grenier, D. and Bartlett, F. M. 2011. Contribution of Drywall Sheathing to Stiffness and Capacity of Axially Loaded Sheathed Walls. GC-197, CSCE General Conference, Ottawa, Ontario, June 14-17, 10 p.

Grenier, D. and Bartlett, F. M. 2012. Load-Slip Response of Gypsum Board-to-Stud Fastener Connections in Shear. STR-1236, 3rd International Structural Specialty Conference, Edmonton, Alberta, June 6-9, 10 p.